

Contents

Section		Page
1	Radiometric Quantities and Units	9
1.1	Symbols, Names, and Units	9
1.2	Other Radiometric Definitions.	12
1.3	Radiation Conversion Chart	13
1.4	Electromagnetic Spectrum	13
2	Photometric Quantities, Units, and Standards.	15
2.1	Symbols, Names, and Units	15
2.2	Photometric Standards	15
2.3	Illuminance, Luminous Exitance, and Luminance .	17
2.4	The Tungsten Lamp as a Luminous Intensity Standard	19
3	Physical Constants, Angle Conversion Factors, and Commonly Used Units	23
3.1	Physical Constants	23
3.2	Angle Conversion Factors	25
3.3	Symbols and Definitions Commonly Used in Electra-Optics	26
3.4	Prefixes for Metric System Units.	33

Section	Page	
4	Blackbody Radiation	35
4.1	Equations	35
4.2	Wavelength of Maximum Spectral Power (Wien's Displacement Law)	36
4.3	Values of Constants in Radiation Equations	37
4.4	Blackbody Radiation Curves	37
4.5	Blackbody References	42
5	Eye Response and Luminous Efficacy	45
5.1	Human Eye Response	45
5.2	Thresholds of Human Eye Response	46
5.3	Color and the Human Eye	47
5.4	Spectral Luminous Efficacy and Spectral Luminous Efficiency	53
5.5	Luminous Efficacy and Luminous Efficiency	55
5.6	Sample Calculations Involving Luminous Efficacy	55
6	Source of Radiation.	61
6.1	The Sun	61
6.2	The Moon	63
6.3	The Stars.	65
6.4	The Sky	68
6.5	Summary of Natural Illuminance Levels	72
6.6	Time Variation of Natural Illuminance	72
6.7	Lamp Sources	72
7	Atmospheric Transmittance	81
7.1	Entire Atmosphere.	82
7.2	Horizontal-Path Transmittance.	82
7.3	Horizontal Visibility	87
7.4	Calculation of Atmospheric Transmittance in the 0.4- μm to 4- μm Region	87
7.5	Calculation of Atmospheric Transmittance in the 8- μm to 14- μm Infrared Region	91
7.6	Effects of Atmosphere on Imaging Sensor Performance	93
7.7	Atmospheric Backscatter - Artificial Illumination	97

Section	Page
8	Detection, Resolution, and Recognition. 109
8.1	Pulse Detection in White Noise. 109
8.2	Pulse Detection in Quantum Noise 113
8.3	MTF (Modulation Transfer Function) and CTF (Contrast Transfer Function) 114
8.4	Display Interpretation 119
8.5	Target Detection/Recognition Model. 121
9	Lasers 127
9.1	Crystalline Lasers 128
9.2	Glass Lasers 128
9.3	Gas Lasers 128
9.4	Dye Lasers 132
9.5	Second Harmonic Generation and Parametric Down-Conversion 133
9.6	P-N Junction Light Sources 135
9.6a	P-N Junction Lasers 139
9.6b	Light-Emitting Diodes (LED's). 145
10	Detector Characteristics 146
10.1	Fundamental Photodetector Relationships and Definitions 146
10.2	Spectral Responsivity and Specific Spectral Detectivity 15 1
10.3	Noise 160
10.4	Time Characteristics of Photodetectors 167
10.5	Source-Detector Matching 170
11	Image and Camera Tubes 173
11.1	Image Tubes. 173
11.2	Characteristics of Image Tubes. 176
11.3	Television Camera Tubes. 180
11.4	Responsivity 185
11.5	Signal-to-Noise Ratio. 190
11.6	Lag 191
11.7	Modulation Transfer Function and Contrast Transfer Function 193
11.8	Limitations to Low-Light-Level Viewing. 195
11.9	Recognition Statistics 196

Section	Page
11.10	Lens and Sensor Limitations 199
11.11	Practical Detection and Recognition Parameters . . . 202
12	Optics. 209
12.1	Thin-Lens Characteristics and Formulae 209
12.2	Thick-Lens Characteristics 212
12.3	Lens Aberrations. 212
12.4	MTF Characteristics of Lenses 213
12.5	Diffraction Limits 214
12.6	Illuminance and Irradiance Formulae. 216
12.7	Properties of Optical Glasses 217
12.8	Spectral Transmittance of Materials 217
12.9	Corner Reflectors 217
13	Photographing E-O Displays 225
13.1	Sensitometry 225
13.2	Film Selection for Cathode-Ray Tube Recording. . . 233
13.3	Photographing Cathode-Ray Tube Images 236
13.4	Lens-Aperture and Exposure-Meter-Setting Formulae. , 236
14	Contributors . . , , 241
	Index , 243

Section 1

Radiometric Quantities and Units

1.1 SYMBOLS, NAMES, AND UNITS

Figure 1-1 gives the standard quantities of physical measurements which are basic to the definitions of the radiometric and photometric terms given in this Handbook.

Quantity	Symbol	SI unit	Symbol
Length	l, r, s	meter	m
Area	A	square meter	m^2
Volume	V	cubic meter	m^3
Solid Angle	ω	steradian	sr
Frequency	ν	hertz	Hz
Wavelength	λ	meter	m
Time	t	second	S

Fig. 1-1 Basic quantities of physical measurements.

Figures 1-2 and 1-3 summarize the basic radiometric and spectroradiometric quantities, definitions, units, and symbols. In accord with current international standardization, in these figures only the International System of Units (SI units) are shown. Their counterparts in other systems are shown in Figures 2-2, 2-3, 2-4, and 3-3.

The units for wavelength deserve special mention. In all of the figures, the **unit of wavelength (λ) is either micrometer or nanometer. In equations such as Planck's spectral radiation formula, wavelength is given in meters.**

Quantity	Symbol	Defining Equation*	SI Unit Symbol
Radiant energy	Q, Q_e		joule J
Radiant density	w, w_e	$w = \partial Q / \partial V$	joule per cubic meter $J m^{-3}$
Radiant flux	Φ, Φ_e	$\Phi = \partial Q / \partial t$	watt W
Radiant flux density at a surface : Radiant exitance (Radiant emittance) Irradiance	M, M_e E, E_e	$M = \partial \Phi / \partial A$ $E = \partial \Phi / \partial A$	watt per square meter $W m^{-2}$ watt per square meter $W m^{-2}$
Radiant intensity	I, I_e	$I = \partial \Phi / \partial \omega$ (ω = solid angle through which flux from point source is radiated)	watt per steradian $W sr^{-1}$
Radiance	L, L_e	$L = \partial^2 \Phi / \partial \omega (\partial A \cos \theta)$ $= \partial I / (\partial A \cos \theta)$ (θ = angle between line of sight and normal to emitting surface considered)	watt per steradian and square meter $W sr^{-1} m^{-2}$

* For symbols A, V, ω , and t, see Fig. 1-1.

Note: The symbols for photometric quantities (Section 2) are the same as those for corresponding radiometric quantities. When it is necessary to differentiate between the two quantities, the subscripts **v** should be used for photometric quantities and **e** for radiometric quantities, e.g., Q_v and Q_e .

Table adapted from U.S.A. Standard Letter Symbols for Illuminating Engineering (USAS Y 10.18-1967) published by the American Society of Mechanical Engineers, United Engineering Center, 345 East 47th Street, New York, New York 10017.

Fig. 1-2 Radiometric quantities and units.

Quantity [▲]	Symbol [▲]	Description	SI Unit	Symbol
Spectral radiant flux	Φ_λ	$\partial\Phi/\partial\lambda$ Radiant flux per unit wavelength interval	watt per micrometer	$\text{W } \mu\text{m}^{-1}$
Spectral radiant flux	Φ_ν	$\partial\Phi/\partial\nu$ Radiant flux per unit frequency interval	watt second or watt per hertz	W s or W Hz^{-1}
Spectral radiant exitance	M_λ	$\partial M/\partial\lambda$ Radiant exitance per unit wavelength interval	watt per square meter and micrometer	$\text{W m}^{-2} \mu\text{m}^{-1}$
Spectral irradiance	E_λ	$\partial E/\partial\lambda$ Irradiance per unit wavelength interval	watt per square meter and micrometer	$\text{W m}^{-2} \mu\text{m}^{-1}$
Spectral radiant intensity	I_λ	$\partial I/\partial\lambda$ Radiant intensity per unit wavelength interval	watt per steradian and micrometer	$\text{W sr}^{-1} \mu\text{m}^{-1}$
Spectral radiance	L_λ	$\partial L/\partial\lambda$ Radiance per unit wavelength interval	watt per square meter, steradian, and micro- meter	$\text{W m}^{-2} \text{sr}^{-1} \mu\text{m}^{-1}$

▲ The terms shown in this figure specify radiometric quantities per unit wavelength (λ) or per unit frequency (ν) by the introduction of the word spectral to the radiometric quantities given in Figure 1-2 and the introduction of the subscript λ or ν .

Fig. 1-3 Spectroradiometric quantities and units.

1.2 OTHER RADIOMETRIC DEFINITIONS (See Figure 1-4)

Quantity	Symbol	Defining Equation	Unit
Absorptance [•]	a	$a = \frac{(*) \text{ absorbed}}{(*) \text{ incident}}$	(numeric)
Reflectance	ρ	$\rho = \frac{(*) \text{ reflected}}{(*) \text{ incident}}$	(numeric)
Transmittance	τ	$\tau = \frac{(*) \text{ transmitted}}{(*) \text{ incident}}$	(numeric)
Emissivity	ϵ	$\epsilon = \frac{(*) \text{ specimen}}{(*) \text{ blackbody at same temperature as specimen}}$	(numeric)

where (*) represents the appropriate quantity Q, Φ , M, E, I, or L.

- Radiant absorptance should not be confused with absorption coefficient (mentioned in Section 7.2).

Fig. 1-4. Other radiometric quantities and units.

The processes of absorption, reflection (including scattering), and transmission account for all incident radiation in any particular situation, and the absorptance, reflectance, and transmittance must add up to one:

$$a + \rho + \tau = 1 \quad (1-1)$$

If a material transmits no radiation, $\tau = 0$ and

$$a + \rho = 1 \quad (1-2)$$

A Lambertian surface is a perfectly diffuse surface which has a constant radiance L independent of viewing direction; constant radiance is given by the formula

$$L = \frac{M}{\pi} \quad (1-3)$$

where the units of L are $W m^{-2} sr^{-1}$
 and the units of M the radiant exitance are $W m^{-2}$

1.3 RADIATION CONVERSION CHART

Figure 1-5 presents a useful nomograph for quick conversion of radiation quantities. Note that the μm scale appears at both margins to permit aligning a straight edge across the other scales.

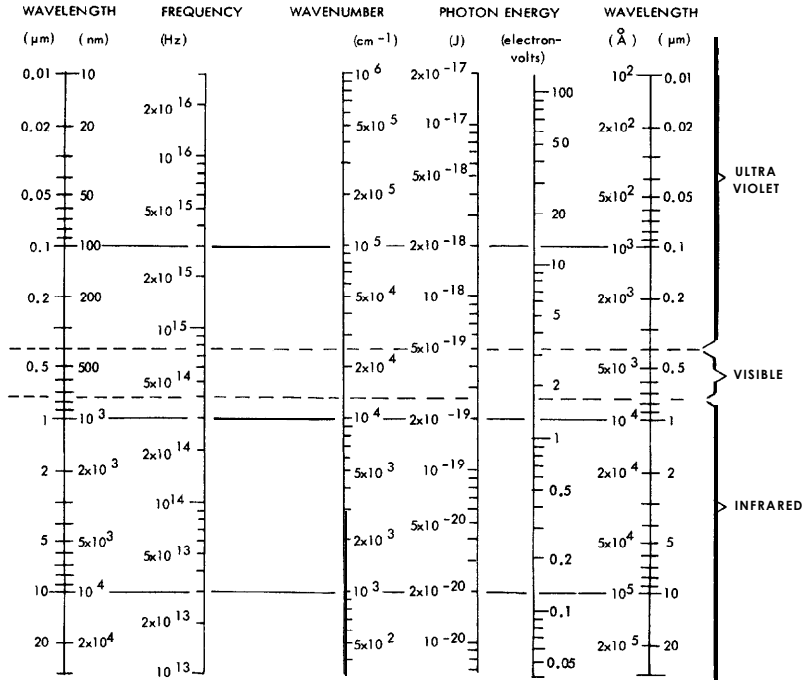


Fig. 1-5 Radiation conversion chart (Adapted from Reference 1).

1.4 ELECTROMAGNETIC SPECTRUM

Figure 1-6 shows the entire electromagnetic spectrum for wavelengths from $10^{-10} \mu m$ to $10^5 km$. The UV, visible, and IR portion has been separately expanded for greater definition.

Reference

- Blattner, D., "Radiation Nomograph," ELECTRONIC DESIGN, Vol. 14, No. 22, Sept. 27, 1966

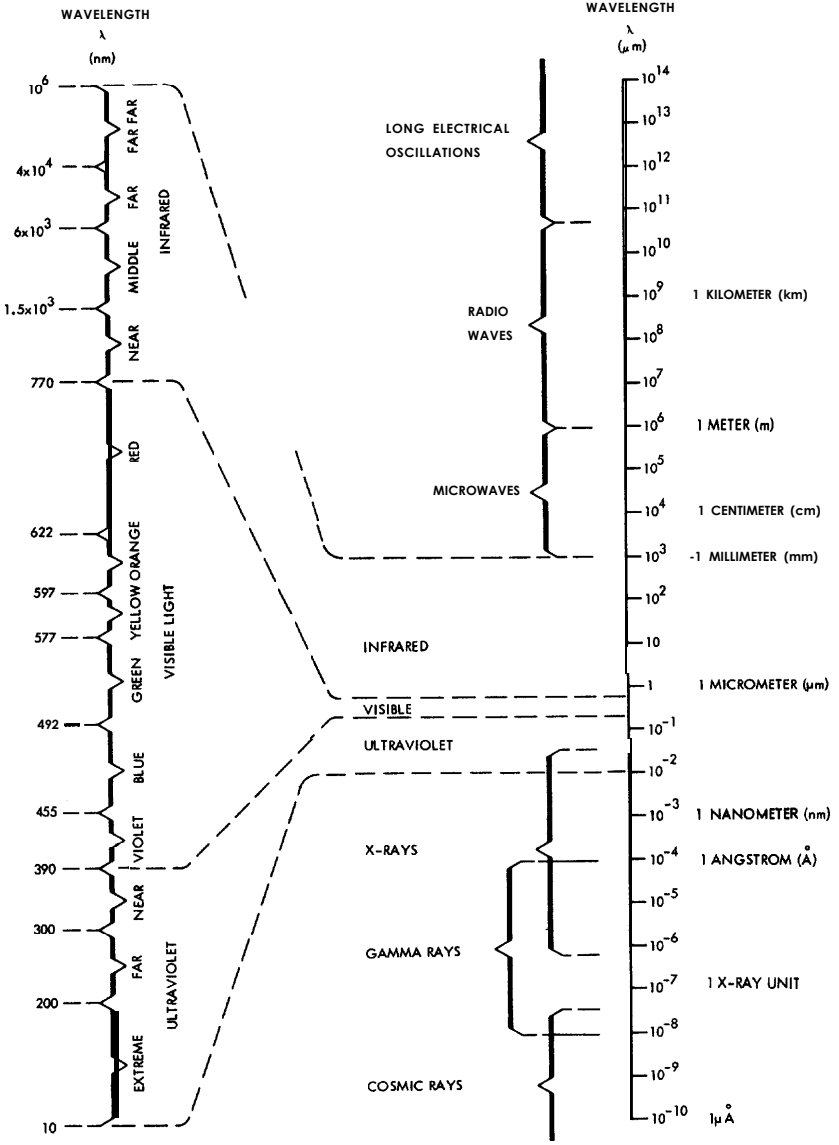


Fig. 1-6 Electromagnetic spectrum.

Section 2

Photometric Quantities, Units, and Standards

2.1 SYMBOLS, NAMES, AND UNITS

Figure 2-1 summarizes the basic photometric quantities, definitions, units, and symbols. This table parallels that of Figure 1-2.

Whereas the radiometric quantities Φ_e , M_e , I_e , L_e , and E_e have meaning throughout the entire electromagnetic spectrum, their photometric counterparts Φ_v , M_v , I_v , L_v , and E_v are meaningful only in the visible portion of the spectrum ($0.38 \mu\text{m} < \lambda < 0.77 \mu\text{m}$).

2.2 PHOTOMETRIC STANDARDS

The candela-The standard candle has been redefined as the new candle or candela (cd). One candela is the luminous intensity of $1/60$ of 1 cm^2 of the projected area of a black body radiator operating at the temperature of the solidification of platinum (2045 K). The candela emits one lumen per steradian (1 lm sr^{-1}).

Note that the luminous intensity emanating from a source with a spectral distribution that differs from that of the standard candle may be evaluated by using a sensor whose relative spectral response is identical to that standardized for photopic vision. See Section 5.

The lumen-The lumen (lm) is defined in terms of the candela. The luminous flux per steradian from a source whose luminous intensity is 1 candela is 1 lumen.

Quantity	Symbol	Defining Equation*	SI Unit	Symbol
Luminous energy (quantity of light)	Q, Q_v	$Q_v = \int K(\lambda) Q_e \lambda d\lambda$ where $K(\lambda)$ = spectral luminous efficacy	lumen second (talbot)	lm s
Luminous density	w, w_v	$w = \partial Q / \partial V$	lumen second per cubic meter	lm s m ⁻³
Luminous flux	Φ, Φ_v	$\Phi = \partial Q / \partial t$	lumen	lm
Luminous flux density at a surface Luminous exitance (formerly luminous emittance)	M, M_v	$M = \partial \Phi / \partial A$	lumen per square meter	lm m ⁻²
Illuminance (formerly illumination)	E, E_v	$E = \partial \Phi / \partial A$	lux (lumen per square meter)	lx
Luminous intensity (formerly candlepower)	I, I_v	$I = \partial \Phi / \partial \omega$ (ω = solid angle through which flux from point source is radiated)	candela (lumen per steradian)	cd
Luminance (formerly photometric brightness)	L, L_v	$L = \partial^2 \Phi / \partial \omega (\partial A \cos \theta) = \partial I / (\partial A \cos \theta)$ (θ = angle between line of sight and normal to emitting surface considered)	nit (candela per square meter or lumen per steradian and square meter)	nt
luminous efficacy	K	$K = \Phi_v / \Phi_e$	lumen per watt	lm W ⁻¹
spectral luminous efficacy	$K(\lambda)$	$K(\lambda) = \Phi_v \lambda / \Phi_e \lambda$	lumen per watt	lm W ⁻¹
Luminous efficiency	$V(\lambda)$	$V = K(\lambda) / K(\lambda_{\max})$ $K(\lambda_{\max})$ = maximum value of $K(\lambda)$ function	(numeric)	

*For symbols A, V, ω , and t, see Fig. 1-1.

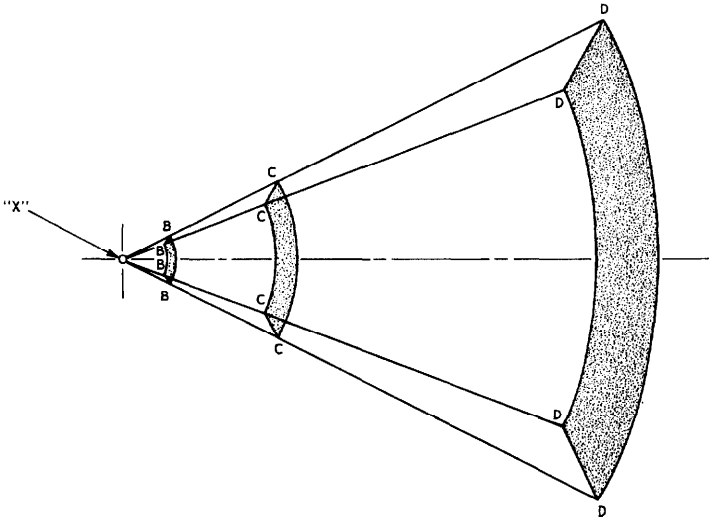
Note: The symbols for photometric quantities are the same as those for corresponding radiometric quantities, shown in Section 1. When it is necessary to differentiate between the two quantities, the subscripts v should be used for photometric quantities and e for radiometric quantities, e.g., Q_v and Q_e .

Table adapted from U.S.A. Standard Letter Symbols for Illuminating Engineering (USAS Y published by the American Society of Mechanical Engineers, United Engineering Center, 345 East 47th Street, New York, New York 7.

Fig. 2-1 Photometric quantities and units.

2.3 ILLUMINANCE, LUMINOUS EXITANCE, AND LUMINANCE

A schematic representation depicting the relationships of commonly employed photometric units is shown in Figure 2.2.



X represents point source having a linear intensity of one candela. Solid angle shown represents one steradian.

Point "X" to any point "B" is 1 cm; the surface represented by "BBBB" is 1 cm².

Point "X" to any point "C" is 1 ft; the surface represented by "CCCC" is 1 ft².

Point "X" to any point "D" is 1 m; the surface represented by "DDDD" is 1 m².

Fig. 2-2 Schematic representation of various photometric units (Courtesy of National Bureau of Standards).

Units of illuminance—Illuminance, $E = d\Phi/dA$, is sometimes called illumination. (Note the distinction that dA in the definition for E is the differential area that receives the flux $d\Phi$ whereas dA in the definition for M (luminous exitance) is the differential area that emits the flux $d\Phi$). The lux (SI unit) is the unit of illuminance resulting from the flux of 1 lumen falling on the surface represented by "DDDD" from "X" = 1 candela.

The footcandle is the unit of illuminance resulting from the flux of 1 lumen falling on the surface represented by “CCCC” from “X” = 1 candela. The phot is the unit of illuminance resulting from the flux of 1 lumen falling on the surface represented by “BBBB” from “X” = 1 candela.

Conversion factors for these units are shown in Figure 2-3.

		lux (lx)	footcandle (fc)	phot (ph)
1 lux (lm m ⁻²) (lx)	=	1	0.0929	1 x 10 ⁻⁴
1 footcandle (lm ft ⁻²) (fc)	=	10.764	1	0.001076
1 phot (lm cm ⁻²) (ph)	=	1 x 10 ⁴	929	1

Fig. 2-3 Conversion factors for commonly used illuminance quantities

Units of luminous exitance – $M = d\Phi/dA$, denotes the luminous flux output per unit surface area. It applies for either self-luminous or reflective bodies.

Referring to Figure 2-2 and assuming 100% of the luminous flux from “X” (1 candela in all directions) is reflected by surfaces represented by “DDDD”, “CCCC”, or “BBBB”, then:

1. “DDDD” will have an exitance of 1 lumen/m²
2. “CCCC” will have an exitance of 1 lumen/ft²
3. “BBBB” will have an exitance of 1 lumen/cm²

Figure 2-4 gives conversion factors for commonly used luminous exitance quantities.

Units of luminance—Luminance, often called brightness, $L = dI/dA \cos \theta$, is the luminous intensity per projected area normal to the line of observation. Referring to Figure 2-2 and assuming 100% of the luminous flux from “X” (1 candela in all directions) is reflected in a perfectly diffuse manner (Lambert’s Cosine Law) by the surface represented by “DDDD”, “CCCC”, or “BBBB”, then:

1. "DDDD" will have a directionally uniform luminance of 1 apostilb or $(1/\pi)$ candela/m² which is $(1/\pi)$ nit (SI unit).
2. "CCCC" will have a directionally uniform luminance of 1 footlambert or $(1/\pi)$ candela/ft².
3. "BBBB" will have a directionally uniform luminance of 1 lambert or $(1/\pi)$ candela/cm² which is $(1/\pi)$ stilb.

	1 m m ⁻²	1 m ft ⁻²	1 m cm ⁻²
1 lm m ⁻² =	1	0.0929	1 x 10 ⁻⁴
1 lm ft ⁻² =	10.764	1	0.001076
1 lm cm ⁻² =	1 x 10 ⁴	929	1

Fig. 2-4 Conversion factors for commonly used luminous exittance quantities.

The factor π in these expressions results from an integration of the flux per unit area and unit solid angle from a Lambertian emitter over a solid angle of 2π steradians. Thus:

$$M = \int_0^{\pi/2} (L \cos \theta) 2\pi \sin\theta \, d\theta = \pi L$$

where M is the exittance in lm m⁻² and L is the luminance in lm sr⁻¹ m⁻².

Figure 2-5 gives conversion factors for commonly used luminance units.

2.4 THE TUNGSTEN LAMP AS A LUMINOUS INTENSITY STANDARD

Although the candela is defined in terms of a blackbody at 2045 K, use of such a source is inconvenient in most laboratories. In the electro-optic industry, the tungsten-filament light source or lamp is commonly employed to evaluate electro-optic devices. These lamps are calibrated for candlepower and are maintained at a standard color temperature, usually 2856 K. Even though the spectral distribution of radiation from such a tungsten source differs considerably from that of a blackbody at 2045 K, this source has the practical advantages of being simple to operate and calibrate, is relatively stable, and provides radiation over a broad spectral band.

	nit (nt)	stilb (sb)	apostilb (asb)	lambert (L)	milli- lambert (mL)	foot- lambert (fL)	candela per square foot (cd ft ⁻²)
1 nit (cd m ⁻² , or lm sr ⁻¹ m ⁻²) (nt)	= 1	1 x 10 ⁻⁴	3.1416	3.1416 x 10 ⁻⁴	0.31416	0.2919	0.0929
1 stilb (cd cm ⁻²) (sb)	= 1 x 10 ⁴	1	3.1416 x 10 ⁴	3.1416	3141.6	2919	929
1 apostilb (π ⁻¹ cd m ⁻²) (asb)	= 0.3183	3.183 x 10 ⁻⁵	1	1 x 10 ⁻⁴	0.1	0.0929	0.02957
1 lambert (π ⁻¹ cd cm ⁻²) (L)	= 3183	0.3183	1 x 10 ⁴	1	1000	929	295.7
1 millilambert (mL)	= 3.183	3.183 x 10 ⁻⁴	10	0.001	1	0.929	0.2957
1 footlambert (π ⁻¹ cd ft ⁻²) (fL)	= 3.426	3.426 x 10 ⁻⁴	10.764	0.0010764	1.0764	1	0.3183
1 candela per square foot (cd ft ⁻²)	= 10.764	0.0010764	33.82	0.003382	3.382	3.1416	1

Fig. 2-5 Conversion factors for commonly used luminance quantities

If a source such as a tungsten lamp is to be rated against the standard blackbody source, it is important that the sensor used in the comparison have a spectral response closely equivalent to that of the standard photopic eye. Otherwise, significant errors could result because of radiation differences outside the visible range. When such a standard tungsten lamp is used to rate the responsivity of a detector, it must be understood that the luminous rating of the lamp is only a measure of its radiance in the visible region. A major part of the radiation from a tungsten lamp is actually in the infrared region. Misinterpretation can result from the quoting of luminous responsivity of a sensor, particularly if the sensor has infrared sensitivity. Photometers with characteristics comparable to the human eye are available from many manufacturers.

A preferred method of specifying sensor responsivities which avoids all ambiguities is to provide spectral radiant measurements over the entire spectral range of the sensor. From these measurements, luminous **responsivities** can be calculated for sources of any color distribution. Because radiant measurements require elaborate equipment and are time consuming, most photosensor manufacturers take 100% luminous responsivity measurements and make only spot measurements of spectral response. Even if the responsivities are defined in terms of total incident flux from the source in watts instead of lumens, the ambiguity resulting from different possible spectral radiation distributions still exists, although the inconsistency of rating an infrared sensitive sensor in terms of luminous responsivity is eliminated.

Section 3

Physical Constants, Angle Conversion Factors, and Commonly Used Unit Symbols

3.1 PHYSICAL CONSTANTS

Figure 3-1 lists some useful physical constants often encountered in **electro-optics**.

3.2 ANGLE CONVERSION FACTORS

Figure 3-2 provides a table of angle conversion factors.

3.3 SYMBOLS AND DEFINITIONS COMMONLY USED IN **ELECTRO-OPTICS**

Figure 3-3 lists the symbols and definitions for the units most commonly encountered in radiometry and photometry. This Figure, as well as Figure 3-4 is adapted from American National Standard Letter Symbols for Units Used in Science and Technology, (ANSI Y 10.19-1969), with the permission of the publisher, The American Society of Mechanical Engineers, United Engineering Center, 345 East 47th Street, New York, New York 10017.

3.4 PREFIXES AND METRIC SYSTEM UNITS

Figure 3-4 gives the multiplying prefixes and associated symbols for metric units.

References

2. Taylor, B.N., Parker, W.H., and Langenberg, D.N., "Determination of e/h , Using Macroscopic Quantum Phase Coherence in Superconductors: Implications for Quantum Electrodynamics and the Fundamental Physical Constants," REVIEW OF MODERN PHYSICS, Vol. 41, No. 3, July 1969.

Physical constant	Symbol	Value	Unit
Avogadro's number	N	6.022169×10^{23}	mol ⁻¹
Boltzmann's constant	k	1.380622×10^{-23}	J K ⁻¹
Electron charge	e	$1.6021917 \times 10^{-19}$	C
Electron charge to mass ratio	e/m	1.7588028×10^{11}	C kg ⁻¹
Energy of 1 electron volt	eV	$1.6021917 \times 10^{-19}$	J
Voltage-wavelength conversion factor	hc/e	1.2398541×10^{-6}	V m
First radiation constant ($8\pi hc$)	C_1	4.992579×10^{-24}	J m
kT value at room temperature	—	0.0259	eV
Luminous efficacy at 555 nm	$K(\lambda)_{\max}$	673	lm W ⁻¹
Mass of electron in free space	m	9.109558×10^{-31}	kg
Permittivity of free space	ϵ_0	8.86×10^{-12}	F m ⁻¹
Planck's constant	h	6.626196×10^{-34}	J s
Second radiation constant (hc/k)	C_2	0.01438833	m K
Speed of light in vacuum	c	2.9979250×10^8	m s ⁻¹
Stefan-Boltzmann constant	σ	5.66961×10^{-8}	W m ⁻² K ⁻⁴

Fig. 3-1 Useful physical constants (Adapted from Reference 2).

ANGLE CONVERSIONS							
	Degree	Minute	Second	Radian	Milliradian	Circumference	Quadrant
1 degree (°)	= 1	60	3600	0.017453	17.453	0.0027778	0.011111
1 minute (')	= 0.016667	1	60	2.9089 $\times 10^{-4}$	0.29089	4.6296 $\times 10^{-5}$	1.8519 $\times 10^{-4}$
1 second (")	= 2.7778 $\times 10^{-4}$	0.016667	1	4.8481 $\times 10^{-6}$	0.0048481	7.71605 $\times 10^{-7}$	3.0864 $\times 10^{-6}$
1 radian (rad)	= 57.2958	3437.75	2.06265 $\times 10^5$	1	1000	0.159155	0.63662
1 milliradian (mrad)	= 0.0572958	3.43775	206.265	0.001	1	1.59155 $\times 10^{-4}$	6.3662 $\times 10^{-4}$
1 circumference	= 360	2.16 $\times 10^4$	1.296 $\times 10^6$	6.28319	6283.19	1	4
1 quadrant	= 90	5400	3.24 $\times 10^5$	1.5708	1570.8	0.25000	1

Fig. 3-2 Angle conversion factors (Source: Optical Industries Inc., Costa Mesa, Ca., Catalog B, copyright 1971; used with permission).

Unit	Symbol	Notes
ampere	A	SI unit of electric current
ampere (turn)	A	SI unit of magnetomotive force
ampere per meter	A/m	SI unit of magnetic field strength
angstrom	Å	$1 \text{ Å} = 10^{-10} \text{ m}$
apostilb	asb	$1 \text{ asb} = (1/\pi) \text{ cd m}^{-2}$ A unit of luminance. One lumen per square meter leaves a surface whose luminance is one apostilb in all directions within a hemisphere. Use of the SI unit of luminance, the candela per square meter, is preferred.
atmosphere, standard	atm	$1 \text{ atm} = 101,325 \text{ N m}^{-2}$
atomic mass unit (unified)	U	The (unified) atomic mass unit is defined as one-twelfth of the mass of an atom of the ^{12}C nuclide. Use of the old atomic mass (amu), defined by reference to oxygen, is deprecated.
bar	bar	$1 \text{ bar} = 100,000 \text{ N m}^{-2}$
barn	b	$\text{b} = 10^{-28} \text{ m}^2$
baud	Bd	In telecommunications, a unit of signaling speed equal to one element per second. The signaling speed in bauds is equal to the reciprocal of the signal element length in seconds.
bel	B	A dimensionless unit for expressing the ratio of two values of power, the number of bels being the logarithm to the base 10 of the power ratio.
bit	b	A unit of information. The capacity in bits of a storage device is expressed as the logarithm to the base two of the number of possible states of the device.

Fig. 3-3 Units commonly used in radiometry and photometry.
Part 1 of 7

Physical Constants, Angle Conversion Factors, and Unit Symbols 27

unit	Symbol	Notes
bit per second	b/s	
calorie (International Table calorie)	cal _{IT}	1 cal _{IT} = 4.1868J The 9th Conference Generale des Poids et Mesures adopted the joule as the unit of heat. Use of the joule is preferred.
calorie (thermochemical calorie)	cal	1 cal = 4.1840 J (See note for International Table calorie.)
candela	cd	SI unit of luminous intensity
candela per square meter	cd/m²	SI unit of luminance. The name nit is sometimes used for this unit.
candle	cd	The unit of luminous intensity has been given the name candela; use of the name candle for this unit is deprecated.
circular mil	cmil	1 cmil = $(\pi/4) 10^{-6} \text{ in}^2$
coulomb	C	SI unit of electronic charge
curie	Ci	1 Ci = 3.7×10^{10} disintegrations per second. Unit of activity in the field of radiation dosimetry.
cycle per second	Hz	See Hertz. The name hertz is internationally accepted for this unit; the symbol Hz is preferred to <i>c/s</i> .
decibel	dB	One tenth of a bel
degree (temperature)		
degree Celsius	°C	The use of the word centigrade for the Celsius temperature scale was abandoned by the Conference Generale des Poids et Mesures in 1948. Note there is no space between the symbol ° and the letter.
degree Fahrenheit	°F	
degree Kelvin	K	See kelvin
degree Rankine	°R	
dyne	dyn	The CGS unit of force
electronvolt	eV	The energy received by an electron in falling through a potential difference of one volt.

Fig. 3-3 Units commonly used in radiometry and photometry.
Part 2 of 7

Unit	Symbol	Notes
erg	erg	The unit of energy in the CGS system of units
farad	F	SI unit of capacitance
foot	ft	
footcandle	fc	$fc = lm\ ft^{-2}$ The name lumen per square foot is recommended for this unit. Use of the SI unit of illuminance, the lux (lumen per square meter), is preferred.
footlambert	fL	$1\ fL = (1/\pi)\ cd\ ft^{-2}$ A unit of luminance. Use of the SI unit, the candela per square meter, is preferred.
gauss	G	The gauss is the electromagnetic CGS unit of magnetic flux density. Use of SI unit, the tesla, is preferred.
gilbert	Gb	The gilbert is the electromagnetic CGS unit of magnetomotive force. Use of the SI unit, the ampere (or ampere turn), is preferred.
gram	g	
henry	H	SI unit of inductance
hertz	Hz	SI unit of frequency
inch	in	
joule	J	SI unit of energy
joule per kelvin	J/K	SI unit of heat capacity and entropy
kelvin	K	In 1967 the CGPM gave the name kelvin to the SI unit of temperature which had formerly been called degree Kelvin and assigned it the symbol K (without the symbol °).
kilogram	kg	SI unit of mass

Fig. 3-3 Units commonly used in radiometry and photometry.
Part 3 of 7

Physical Constants, Angle Conversion Factors, and Unit Symbols 29

Unit	Symbol	Notes
kilogram-force	kg _f	In some countries the name kilopond (kp) has been adopted for this unit.
knot	kn	kn = nmi hr ⁻¹
lambert	L	$1L = (1/\pi) \text{ cd cm}^{-2}$ A CGS unit of luminance. Use of the SI unit of luminance, the candela per square meter, is preferred.
liter	l	1l = 10 ⁻³ m ³
lumen	lm	SI unit of luminous flux
lumen per square foot	lm/ft ²	A unit of illuminance and also a unit of luminous exitance. Use of the SI unit, lumen per square meter, is preferred.
lumen per square meter	lm/m ²	SI unit of luminous exitance.
lumen per watt	lm/W	SI unit of luminous efficacy.
lumen second	lm s	SI unit of quantity of light, also known as the talbot.
lux	lx	lx = lm m ⁻² SI unit of illuminance
maxwell	Mx	The maxwell is the electromagnetic CGS unit of magnetic flux. Use of the SI unit, the weber, is preferred.
meter	m	SI unit of length
mho	mho	CIPM has accepted the name siemens (S) for this unit and will submit it to the 14th CGPM for approval.
micrometer	μm	
micron	μm	See micrometer. The name micron was abrogated by the Conference Generale des Poids et Mesures, 1967.

Fig. 3-3 Units commonly used in radiometry and photometry.
Part 4 of 7

Unit	Symbol	Notes
mil	mil	1 mil = 0.001 in
mile (statute)	mi	1 mi = 5280 ft
mile per hour	mi/h	Although use of mph as an abbreviation is common, it should not be used as a symbol.
millimeter	mm	
conventional millimeter of mercury	mmHg	1 mmHg = 133.322 N m ⁻²
millimicron	nm	Use of the name millimicron for the nanometer is deprecated.
minute (time)	min	Time may also be designated by means of superscripts as in the following example, 9 ^h 46 ^m 30 ^s .
mole	mol	SI unit of amount of substance.
nautical mile	nmi	1 nmi = 1852 m
neper	Np	The natural logarithm of the scalar ratio of two currents or voltages.
newton	N	SI unit of force
newton meter	N m	Unit of energy equal to one joule.
newton per square meter	N/m ²	SI unit of pressure or stress. See pascal
newton second per square meter	N s / m ²	SI unit of dynamic viscosity
nit	nt	nt = cd m ⁻² The name nit is given to the SI unit of luminance, the candela per square meter.
oersted	Oe	The oersted is the electromagnetic CGS unit of magnetic field strength. Use of the SI unit, the ampere per meter, is preferred.
ohm	Ω	SI unit of resistance

Fig. 3-3 Units commonly used in radiometry and photometry.
Part 5 of 7

Unit	Symbol	Notes
ounce (avoirdupois)	oz	
pascal	Pa	$\text{Pa} = \text{N m}^{-2}$ SI unit of pressure or stress. This name accepted by the CIPM in 1969 for submission to the 14th CGPM.
phot	ph	$\text{ph} = \text{lm cm}^{-2}$ CGS unit of illuminance. Use of the SI unit, the lux (lumen per square meter), is preferred.
poise	P	$\text{P} = \text{dyn s cm}^{-2}$ Unit of coefficient of viscosity.
rad	rd	Unit of absorbed dose in the field of radiation dosimetry.
radian	rad	SI unit of plane angle
rem	rem	Unit of dose equivalent in the field of radiation dosimetry.
roentgen	R	Unit of exposure in the field of radiation dosimetry.
second (time)	s	SI unit of time
siemens	S	$\text{S} = \Omega^{-1}$ SI unit of conductance. This name and symbol were accepted by the CIPM in 1969 for submission to the 14th CGPM. The name mho is also used for this unit in the USA.
steradian	sr	SI unit of solid angle
stilb	sb	$\text{sb} = \text{cd cm}^{-2}$ A CGS unit of luminance. Use of the SI unit, the candela per square meter, is preferred.
stokes	St	Unit of viscosity

Fig. 3-3 Units commonly used in radiometry and photometry
 Part 6 of 7

Unit	Symbol	Notes
tesla	T	$T = N A^{-1} m^{-1} = Wb m^{-2}$ SI unit of magnetic flux density (magnetic induction)
tonne	t	1 t = 1000 kg
var	var	IEC name and symbol for the SI unit of reactive power
volt	V	SI unit of voltage
volt per meter	V/m	SI unit of electric field strength
voltampere	VA	IEC name and symbol for the SI unit of apparent power
watt	W	SI unit of power
watt per meter kelvin	W/(m.K)	SI unit of thermal conductivity
watt per steradian	W/sr	SI unit of radiant intensity
watt per steradian and square meter	W/(sr.m ²)	SI unit of radiance
watthour	Wh	
weber	Wb	Wb = V s SI unit of magnetic flux

- CGPM Conference Generale des Poids et Mesures (General Conference on Weights and Measures)
- CGS Centimeter-Gram-Second
- CIPM Comite International des Poids et Mesures (International Committee for Weights and Measures)
- IEC International Electrotechnical Commission
- MKS Meter-Kilogram-Second
- SI Systeme International d'Unites (International System of Units)

Fig. 3-3 Units commonly used in radiometry and photometry.
Part 7 of 7

Prefix (Multiple)	Symbol
tera (10^{12})	.T
giga (10^9)	.G
mega (10^6)	.M
kilo (10^3)	.k
hecto (10^2)	.h
deka (10)	.da
deci (10^{-1})	.d
centi (10^{-2})	.c
milli (10^{-3})	.m
micro (10^{-6})	.μ
nano (10^{-9})	.n
pico (10^{-12})	.p
femto (10^{-15})	.f
atto (10^{-18})	.a

Fig. 3-4 Metric unit prefixes and symbols.

Section 4

Blackbody Radiation**4.1 EQUATIONS***

The equation for spectral radiant exitance (Planck's) is

$$M_{\lambda} = \frac{2\pi c^2 h}{\lambda^5 (e^{hc/\lambda kT} - 1)} \quad (\text{in } W \text{ m}^{-2} \text{ m}^{-1}), \quad (4-1)$$

where

λ = wavelength (m)

h = Planck's constant (J s)

c = velocity of light in a vacuum (m s^{-1})

k = Boltzmann's constant (J K^{-1})

T = absolute temperature (K)

Spectral radiance L_{λ} is equal to $M_{\lambda}\pi^{-1}$ according to equation 1-3 because blackbodies are Lambertian sources; hence,

$$L_{\lambda} = \frac{2c^2 h}{\lambda^5 (e^{hc/\lambda kT} - 1)} \quad (\text{in } W \text{ m}^{-2} \text{ sr}^{-1} \text{ m}^{-1}) \quad (4-2)$$

*See Section 1 for further definition of symbols.

Equation 4-2 gives the spectral radiance per unit of wavelength increment. A useful alternative to equation 4-2 gives the spectral radiance in number of photons per second rather than watts ($\eta_\lambda = L_\lambda/h\nu$ where ν is radiation frequency);

$$\eta_\lambda = \frac{2c}{\lambda^4 (e^{hc/\lambda kT} - 1)} \quad (\text{in number of photons } s^{-1} \text{ m}^{-2} \text{ sr}^{-1} \text{ m}^{-1}) \quad (4-3)$$

Another useful alternative is the expression,

$$L_\nu = \frac{2h}{c^2} \frac{\nu^3}{(e^{h\nu/kT} - 1)} \quad (\text{in W m}^{-2} \text{ sr}^{-1} \text{ Hz}^{-1}) \quad (4-4)$$

which gives the spectral radiance per frequency increment.

For $h\nu \ll kT$, the Rayleigh-Jeans approximation leads to

$$L_\nu \cong \frac{2kT\nu^2}{c^2} \quad (\text{in W m}^{-2} \text{ sr}^{-1} \text{ Hz}^{-1}) \quad (4-5)$$

Radiant exitance, M , is given by the Stefan-Boltzmann equation:

$$M = \int_0^\infty M_\lambda d\lambda = \sigma T^4 \quad (\text{in W m}^{-2}) \quad (4-6)$$

where σ , the Stefan-Boltzmann constant, is given by

$$\sigma = \frac{2\pi^5 k^4}{15c^2 h^3} \quad (\text{in W m}^{-2} \text{ K}^{-4}) \quad (4-7)$$

4.2 WAVELENGTH OF MAXIMUM SPECTRAL POWER (WIEN'S DISPLACEMENT LAW)

It can be shown from equations 4-1 and 4-2 that blackbodies at temperature T emit maximum power per unit wavelength at that wavelength λ_m determined from

$$\frac{ch}{k\lambda_m T} = 4.96512$$

or

(4-8)

$$\lambda_m T = 2898 \mu\text{m K}$$

The number of photons per second, however, based on equation 4-3, is found to be a maximum at a longer wavelength λ'_m by solving

$$\frac{ch}{k\lambda'_m T} = 3.9207$$

or

(4-9)

$$\lambda'_m T = 3670 \mu\text{m K}$$

4.3 VALUES OF CONSTANTS IN RADIATION EQUATIONS

$$2\pi c^2 h = 3.7418 \times 10^{-16} \text{ W m}^2$$

$$2c^2 h = 1.1911 \times 10^{-16} \text{ W m}^2 \text{ sr}^{-1}$$

$$2c = 5.9958 \times 10^8 \text{ photons sr}^{-1} \text{ m s}^{-1}$$

$$2h/c^2 = 1.4745 \times 10^{-50} \text{ W Hz}^{-4} \text{ m}^{-2} \text{ sr}^{-1}$$

$$ch/k = 0.014388 \text{ m K}$$

c, h, k (See Figure 3-1)

4.4 BLACKBODY RADIATION CURVES

Figure 4-1 – L_λ as a function of λ and T

$L_{\lambda(\text{max})}$ as a function of λ_m and T

Figure 4-2 – n_λ as a function of λ and T

$n_{\lambda(\text{max})}$ as a function of λ_m and T

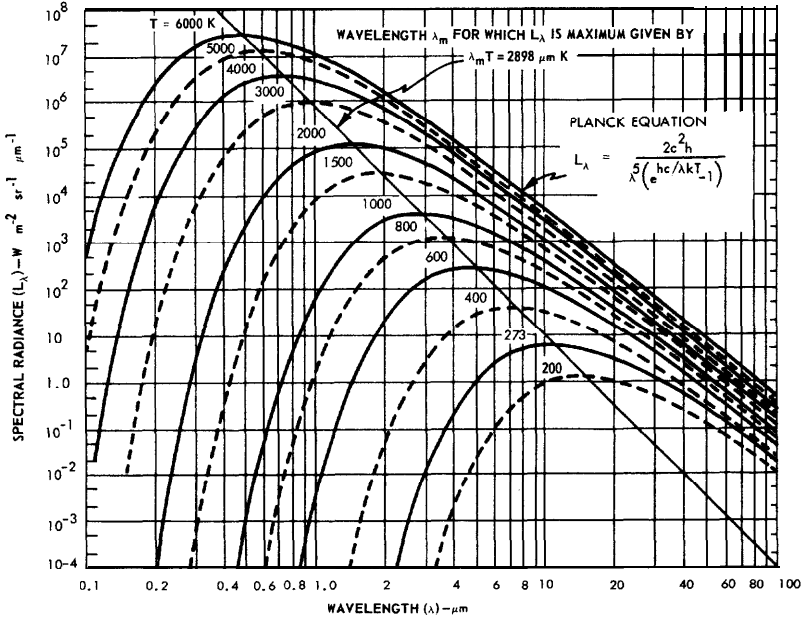


Fig. 4-1 Spectral radiance L_λ of a blackbody at the absolute temperature T shown on each curve. The diagonal line intersecting the curves at their maxima shows Wien's displacement law. Subdivisions of the ordinate scale are at 2 and 5. (Adapted from Reference 8 with permission).

Figure 4-3 — $\frac{M_\lambda(T)}{M_{\lambda\max}(T)}$ or $\frac{L_\lambda(T)}{L_{\lambda\max}(T)}$ as a function of λT

$$\frac{\int_0^\lambda M_\lambda d\lambda}{\int_0^\infty M_\lambda d\lambda} \quad \text{or} \quad \frac{\int_0^\lambda L_\lambda d\lambda}{\int_0^\infty L_\lambda d\lambda} \quad \text{as a function of } \lambda T$$

$$\frac{\int_{\frac{\lambda}{T}}^\infty M_\lambda d\lambda}{\int_0^\infty M_\lambda d\lambda} \quad \text{or} \quad \frac{\int_{\frac{\lambda}{T}}^\infty L_\lambda d\lambda}{\int_0^\infty L_\lambda d\lambda} \quad \text{as a function of } \lambda T$$

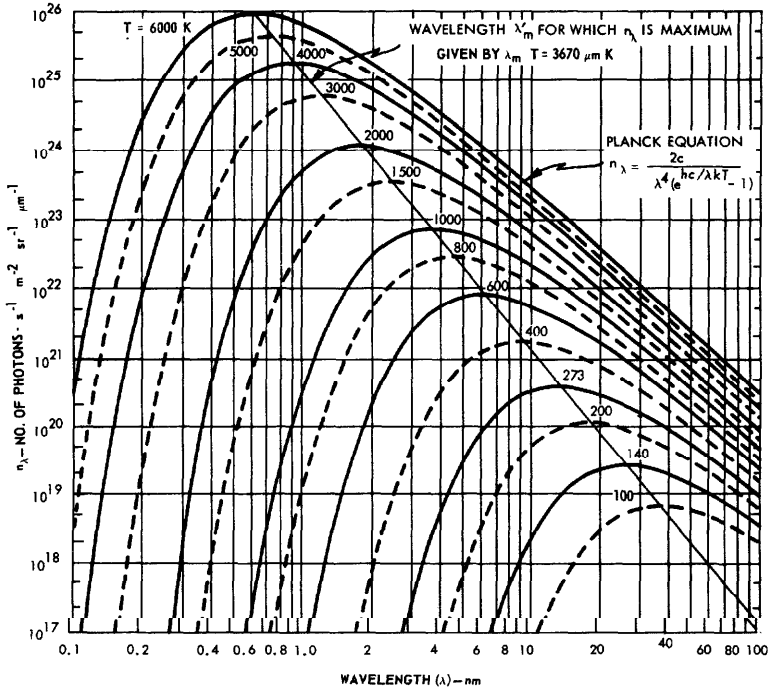


Fig. 4-2 Number of photons per second emitted per square meter per steradian per micrometer by a blackbody at various absolute temperatures. The diagonal line intersecting the curves at their maxima shows Wien's displacement law. (Adapted from Reference 8 with permission).

Figure 4-4 — The fraction of total blackbody radiant exitance that is luminous (i.e., visible) as a function of absolute temperature T . See Section 5.5

Figure 4-5 — Spectral radiance contrast $\alpha L_\lambda / \alpha T$ of a blackbody at the absolute temperature T from 250 K to 500 K.

Figure 4-6 — Spectral-band radiance contrast for the spectral bands 8-14 μm , 8-13 μm , and 8-11.5 μm .

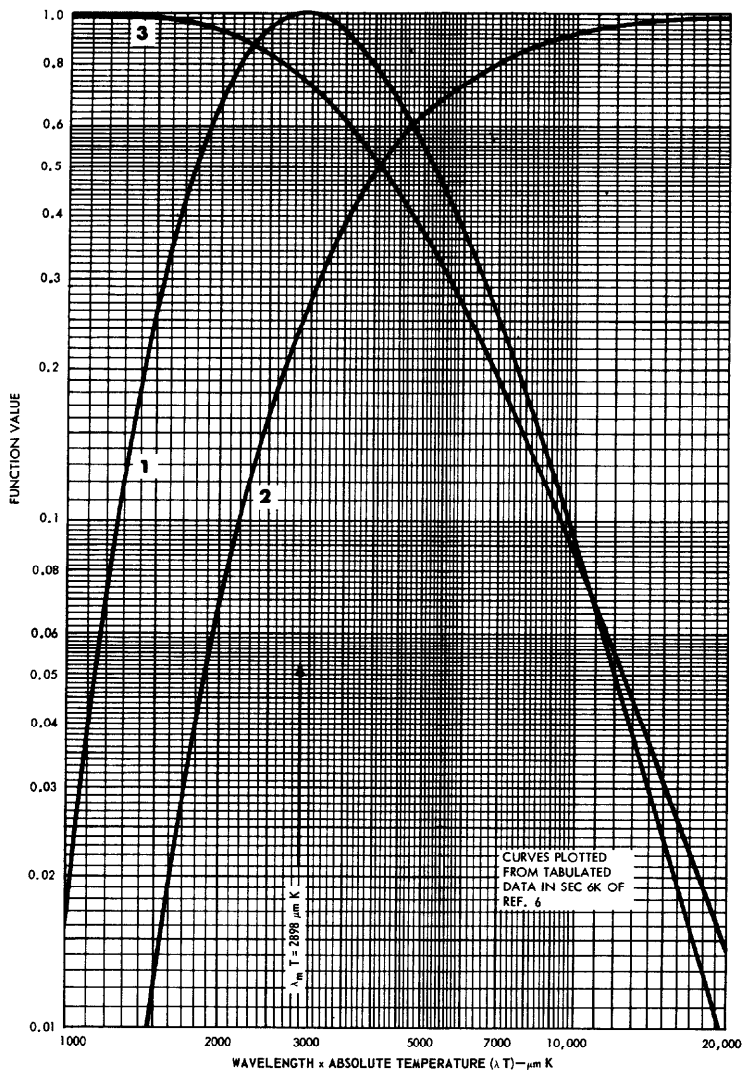


Fig. 4-3 Blackbody functions of λT : (1) Ratio of spectral exitance or radiance at wavelength λ to maximum spectral exitance or radiance (at wavelength λ_m). (2) Fraction of total radiant exitance or radiance in the wavelength interval 0 to λ . (3) Fraction of total radiant exitance or radiance in the wavelength interval λ to ∞ .

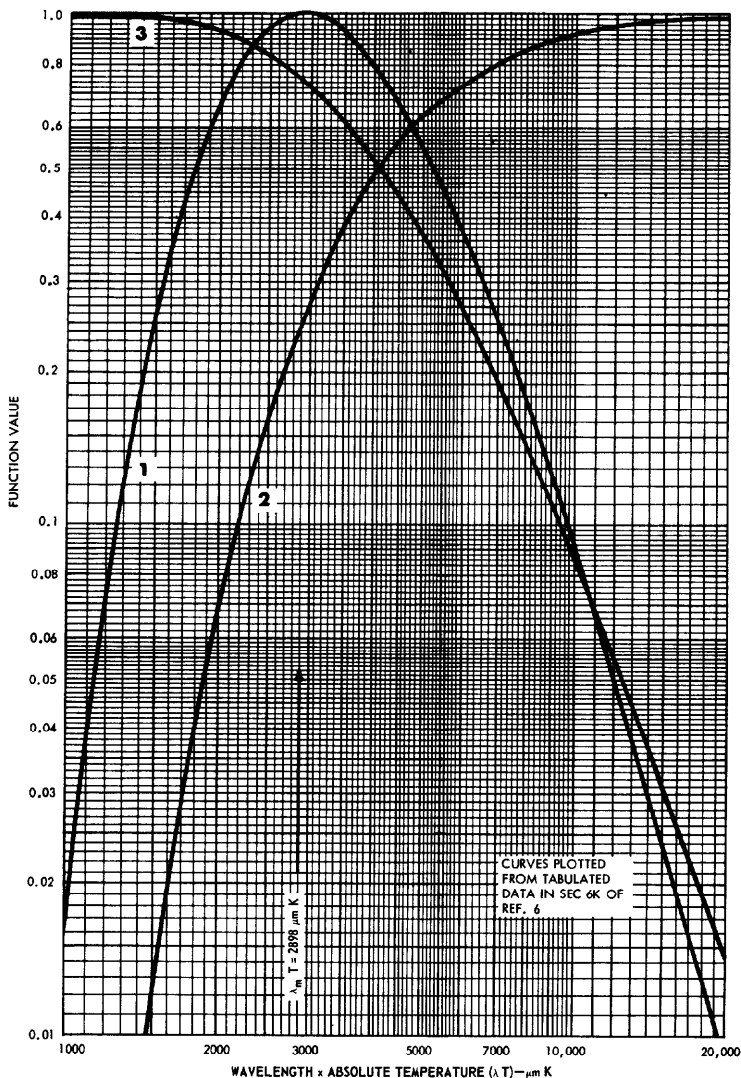


Fig. 4-3 Blackbody functions of **IT**: (1) Ratio of spectral exitance or radiance at wavelength λ to maximum spectral exitance or radiance (at wavelength λ_m). (2) Fraction of total radiant exitance or radiance in the wavelength interval 0 to λ . (3) Fraction of total radiant exitance or radiance in the wavelength interval λ to ∞ .

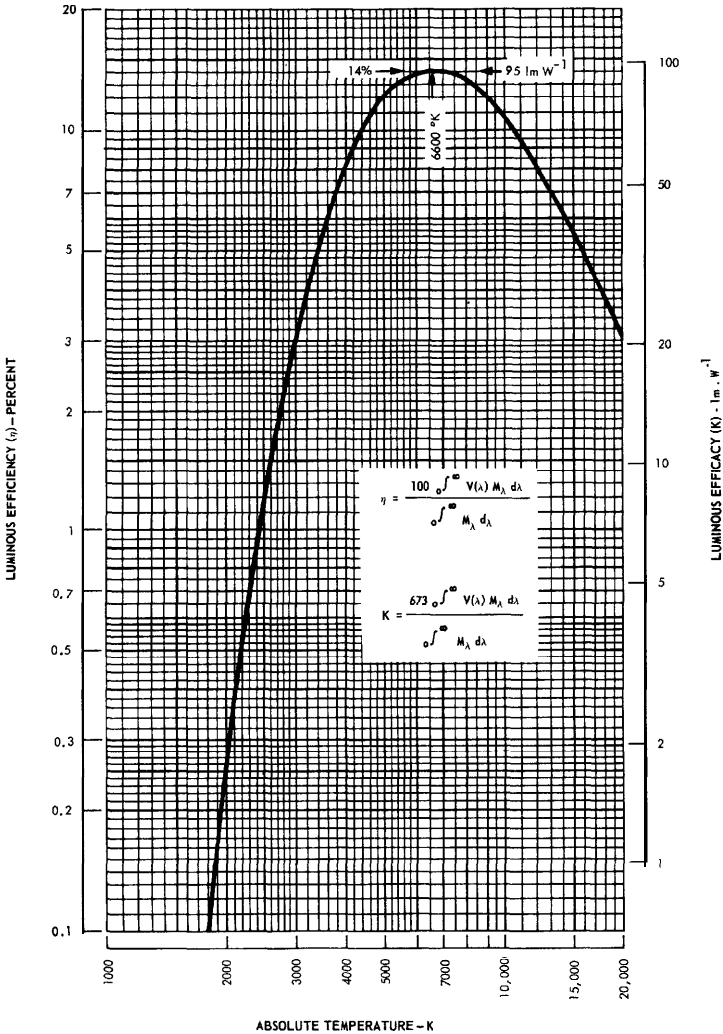


Fig. 4-4 Luminous efficiency η and luminous efficacy K of blackbody as a function of its absolute temperature where M_λ is the spectral radiant exitance of the blackbody and V_λ is the relative spectral response of the average human eye (Adapted from Fig. 11-15 of Reference 7 with permission).

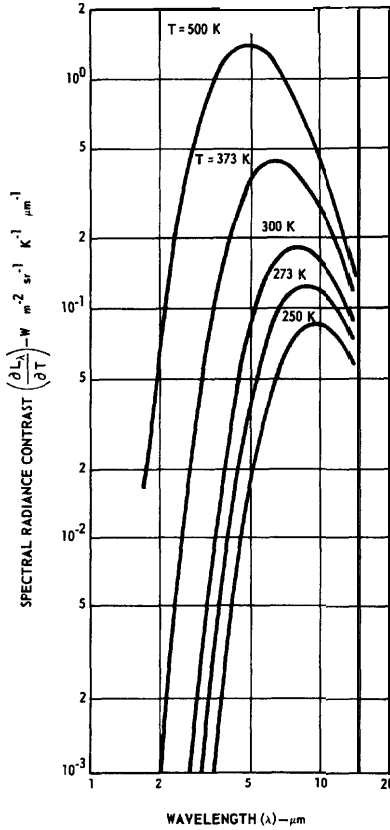


Fig. 4-5 Spectral radiance contrast $\partial L_{\lambda}/\partial T$ of a blackbody at the absolute temperature T shown on each curve (Plotted from tables in part 5 of Reference 9).

4.5 BLACKBODY REFERENCES

Theory, Radiation Slide Rules -- Reference 3, Chapter 2

Theory -- Reference 4

Tables — Reference 5
 Reference 6, Section 6k
 (page 6-153)

Curves — Reference 7, pages 43 - 57
 Reference 8, Appendix B

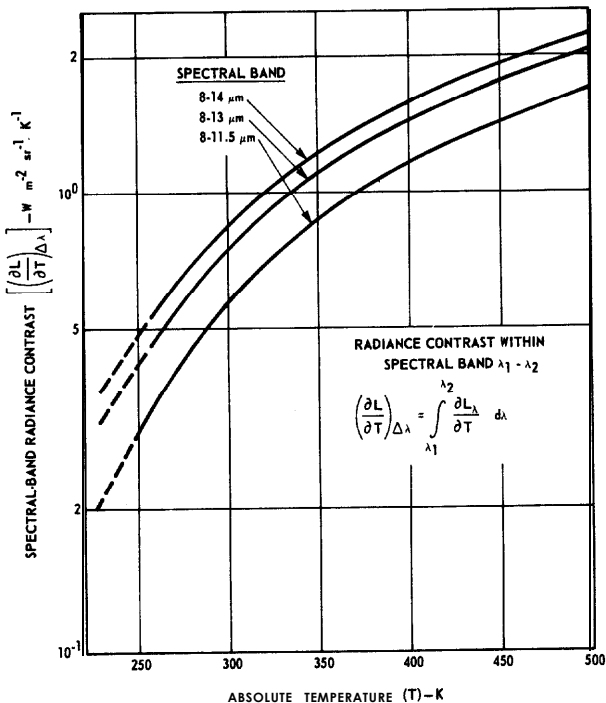


Fig. 4-6 Spectral-band radiance contrast for three spectral bands as a function of absolute temperature (Plotted from tables in part 5 of Reference 9).

References

3. Wolf, W.L., Editor, HANDBOOK OF MILITARY INFRARED TECHNOLOGY, Office of Naval Research, Dept. of the Navy, Washington, D.C., 1965.

4. Merritt, T.P. and Hall, F.F. Jr., "Blackbody Radiation," PROC. IRE, Sept. 1959.
5. Pivovonsky, M. and Nagel, M., TABLES OF BLACKBODY RADIATION FUNCTIONS, Macmillan, New York, N.Y., 1961
6. AMERICAN INSTITUTE OF PHYSICS HANDBOOK, Second edition, McGraw-Hill Book Co., Inc. New York, N.Y., 1962.
7. Mauro, J.A., Editor, OPTICAL ENGINEERING HANDBOOK, General Electric Co., Syracuse, N.Y., 1966.
8. Valley, S.L., HANDBOOK OF GEOPHYSICS AND SPACE ENVIRONMENTS, Air Force Cambridge Research Laboratories, Office of Aerospace Research. U.S. Air Force, 1965. Also published by McGraw-Hill Book Co., New York, N.Y., 1965.
9. Bramson, M.A., INFRARED RADIATION, A HANDBOOK FOR APPLICATIONS, Plenum Press, New York, N.Y., 1968.

Section 5

Eye Response and Luminous Efficacy

5.1 HUMAN EYE RESPONSE

Receptors of the Human Eye-The human eye contains two types of retinal receptors, rods and cones.

Photopic Eye Response (Cone Vision) - Photopic response is that of the cones in the retina and occurs after the eye has been adapted to a field luminance equal to or greater than about 3 nt (cd m^{-2}) (light-adapted state). After being dark adapted, the eye requires 'about two or three minutes to become light adapted when the luminance is raised.

Scotopic Eye Response (Rod Vision) - Scotopic response is that of the rods in the retina and occurs after the eye has been adapted to field luminance equal to, or less than, about 3×10^{-5} nt (cd m^{-2}). After being light adapted, the eye requires considerable time to become dark adapted when the luminance is lowered. See Figure 5-1. The rate of adaption depends on the initial luminance of the starting field with nearly complete dark adaption being approached in about 45 minutes. See Reference 10. Because the rods and not the cones function in the dark-adapted state and because color vision is entirely a function of the cones, the increased responsivity of the eye in the dark-adapted state is accompanied by a loss in color vision. The central part of the retina known as the fovea contains only cones.

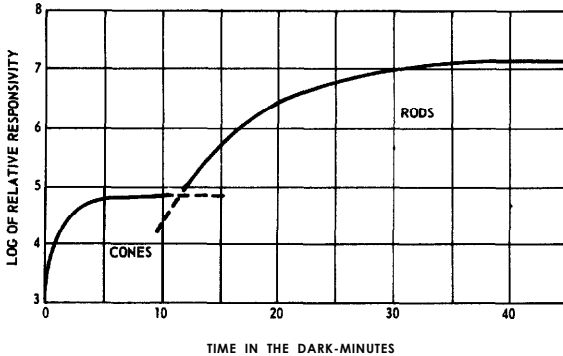


Fig. 5-1 Adaption of the eye to complete darkness after exposure to a bright field. Light incident 12° above fovea. (Adapted from Wald et al, Reference 10, with permission).

The spectral **responsivity** of the eye in the dark-adapted (scotopic) state differs considerably from the light-adapted (photopic) state. Between these two states, the spectral response of the eye is continuously variable; this condition is known as the mesopic state.

Mesopic Eye Response-As field luminance is lowered from about 3 nt to 3×10^{-5} nt (cd m^{-2}), the luminous efficacy curve of the eye shifts progressively from that of photopic vision to that of scotopic vision. See Reference 11, pp 5 through 8. Table II of this reference gives mesopic values of relative luminous efficacy corresponding to nine different values of luminance between the photopic and scotopic states.

5.2 THRESHOLDS OF HUMAN EYE RESPONSE

Hecht, Schlaer and Pirenne (1942) established that the minimum detectable visual stimulus is produced by 58 to 145 quanta of blue-green light (510 nm) impinging on the cornea. This stimulus, it was estimated, provides only from 5 to 14 quanta actually reaching and acting on the retinal sensors (see page 154 of Reference 12).

Experimental determinations have been made by Blackwell (1946) of the minimum contrast $(L_o - L_b)/L_b$ of an object with luminance L_o against a background with luminance L_b for a 50% probability of detection when both eyes are used and when unlimited time of exposure is available (Reference

13). The results are given in Figure 5-2. Note the discontinuity in all the curves on Figure 5-2 at about 2×10^{-3} nt (cd m^{-2}). This point marks the transition from photopic to scotopic vision.

Figure 5-3 gives the threshold illuminance E_t at the eye produced by a fixed barely detectable achromatic point source against a background luminance L_b as determined experimentally by a number of observers. The Tiffany data are for a 50% probability of detection; the other curves are for a practical certainty of detection. For convenient reference, an illuminance scale is also given in units of stellar magnitude (defined in Section 6). The discontinuity between photopic and scotopic vision is again evident on the curves.

Studies have been made by Griffin, Hubbard, and Wald to determine the spectral characteristics of the fully dark-adapted eye. See Reference 15. Figure 5-4 is a composite spectral response characteristic for the dark-adapted fovea and the peripheral retina based on the referenced work and on data from previous work. Because only the rods function in the dark-adapted state, faint signals are seen better in darkness when viewed indirectly. This characteristic is particularly true at the extremities of the visual spectral range.

5.3 COLOR AND THE HUMAN EYE

Trichromatic Response Theory of the Human Eye-The exact mechanics of human color vision are unknown but it has been determined that the response is shared by the eye and the brain.

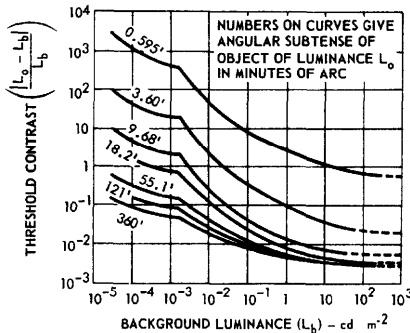


Fig. 5-2 *Thresholds of brightness contrast for 50% probability of detection of objects brighter than their backgrounds. Unlimited exposure time (Adapted from Blackwell, Reference 13, with permission).*

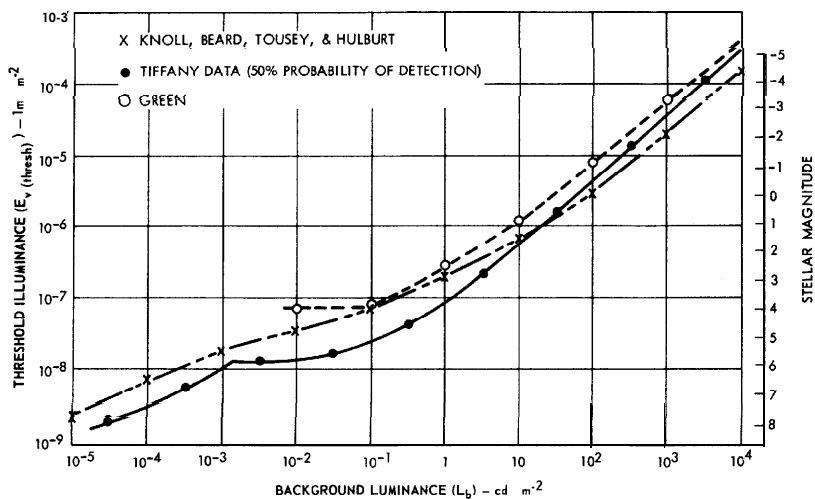


Fig. 5-3 Threshold illuminance for human eye from a fixed achromatic point source as a function of background luminance (Adapted from Middleton, Reference 14, with permission).

The trichromatic theory holds that the retina of the eye consists of a mosaic of three different receptor elements. Each element responds to specific wavelengths corresponding to blue, green, and red light. These three elements, which appear to overlap considerably in responsivity, are separately connected through nerves to the brain where the sensation of color is derived by the brain's analysis of the relative stimulus from the three elements.

Color is perceived as a conscious sensation in terms of three major subjective attributes, luminance, hue, and saturation; primary among these attributes is luminance (often called brightness). The second major attribute, hue, which is the most characteristic of color, is the distinction between redness, yellowness, blueness, etc. The hue of pure colors of the physical spectrum, relates directly to wavelength. The third attribute, which distinguishes strong colors from pale ones, is saturation or chroma. Saturation is related to physical purity, i.e., freedom from dilution by white.

Although the eye is not suitable for measuring color directly, it is a highly efficient color-matching instrument. This property of vision is utilized in colorimetry in which any color stimulus may be specified by finding a known

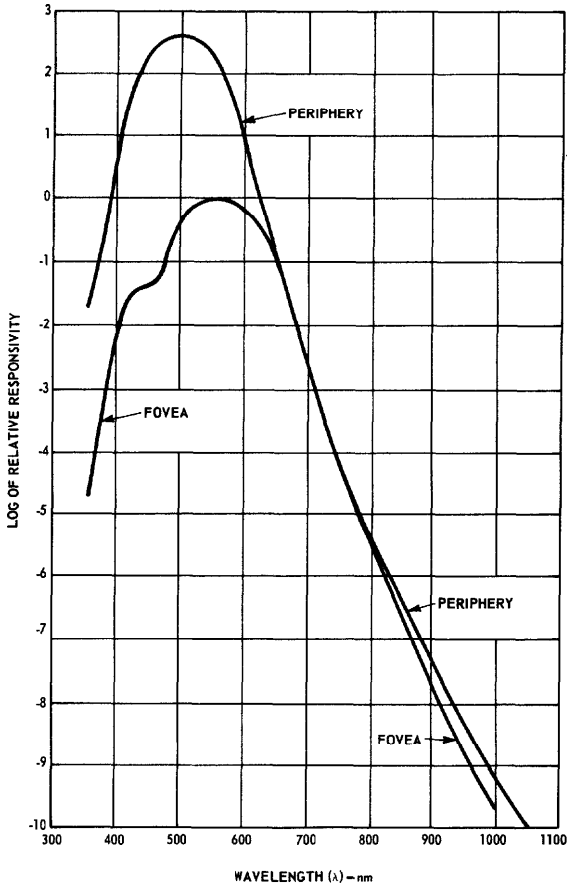


Fig. 5-4 Relative spectral responsivity of the dark-adapted fovea and peripheral retina (Adapted from Griffin et al, Reference 15, with permission).

second stimulus that the eye establishes as equivalent. In modern **colorimetry**, the second stimulus is usually a combination of red, green, and blue light; however, any three monochromatic (single color) colors can be used as primaries providing no two colors can be mixed in any proportion to match the third color.

Standard Color-Mixture Curves-Most color sensations can be matched by the mixture of three primary colors in suitable quantities. The three primaries may be but are not necessarily monochromatic. Typical primaries may be red, green, and blue. In using such a set of colors for matching, it may be necessary sometimes to use negative amounts of one of the primaries; "negative" implies the addition of that primary to the color sensation being matched by the other two primaries. To avoid the use of negative amounts of color and to provide a standard for calorimetric use, the Commission Internationale de l'Eclairage (CIE) proposed a set of idealized supersaturated primaries not physically realizable.

The three curves marked $\bar{x}(\lambda)$, $\bar{y}(\lambda)$, and $Z(\lambda)$ in Figure 5-5 represent the amounts of the idealized primaries required to match any of the pure spectral colors in the visible range indicated on the abscissa. These particular curves were selected so that \bar{y} represents the relative spectral luminous efficiency curve for the photopic eye (see Figure 5-8) and, thus, provides the luminance information in the matching function. The luminances of the (\bar{x}) and (\bar{z}) primaries are zero; these two primaries provide only chrominance information.

Consider a sample of monochromatic green light of wavelength 520 nanometers. The "tristimulus" values, determined from Figure 5-5, for a particular luminance level might be $X = 0.0633$, $Y = 0.7100$, and $Z = 0.0782$. Chroma coordinates are now defined in terms of the tristimulus values by the ratios as follows:

$$\begin{aligned}x &= X/(X + Y + Z) \\y &= Y/(X + Y + Z) \\z &= Z/(X + Y + Z)\end{aligned}$$

so that $x + y + z = 1$. In the example considered, the chroma coordinates are $x = 0.0633/0.8515 = 0.0743$; $y = 0.7000/0.8515 = 0.8338$; and, $z = 0.0782/0.8515 = 0.0918$.

If the color to be matched is not monochromatic, a summation or an integration process must be utilized:

$$\begin{aligned}X &= \int \phi_{\lambda} x(\lambda) d\lambda \\Y &= \int \phi_{\lambda} y(\lambda) d\lambda \\Z &= \int \phi_{\lambda} z(\lambda) d\lambda\end{aligned}$$

where ϕ_{λ} is the spectral radiant flux from the source to be matched. The integration or summation covers the entire visible spectrum. The chroma coordinates are determined by the ratios as previously defined.

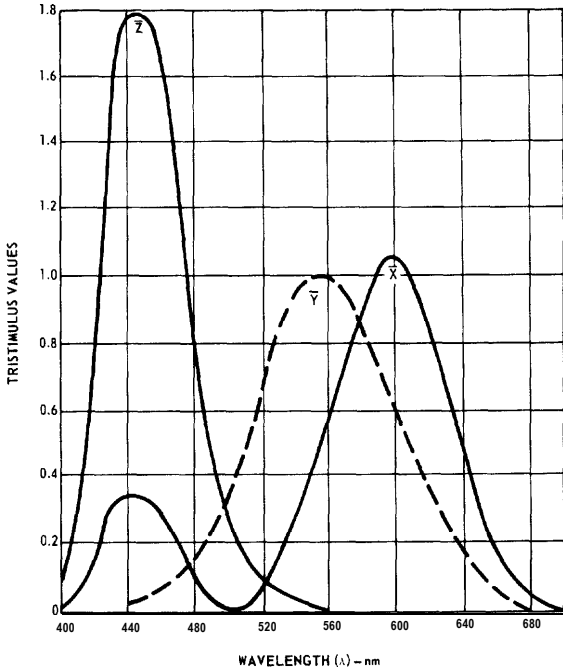


Fig. S-5 International Commission on Illumination (CIE) standard color-mixture curves.

Chromaticity Diagram-Each of the three chroma coefficients defines the relative proportion of the three CIE primaries required to match the color of the sample. Because the sum of the three chroma coefficients is unity, it is only necessary to specify two of them, x and y ; the third, z , may then be obtained by subtracting x and y from 1. The color may then be specified by a point on a two-dimensional graph as given in Figure 5-6, where x and y each run from 0 to 1.

Each point on the chromaticity diagram specifies chromaticity (hue and saturation) independent of luminance. The locus of all spectral colors (identified in nanometers) is plotted on this diagram. The open end of the spectral locus is closed by a nonspectral magenta. The standard CIE primaries are represented by the points $x = 0, y = 1$; $x = 0, y = 0$; and, $x = 1, y = 0$. The locus of black bodies at various temperatures (in degree **K**) is shown by the

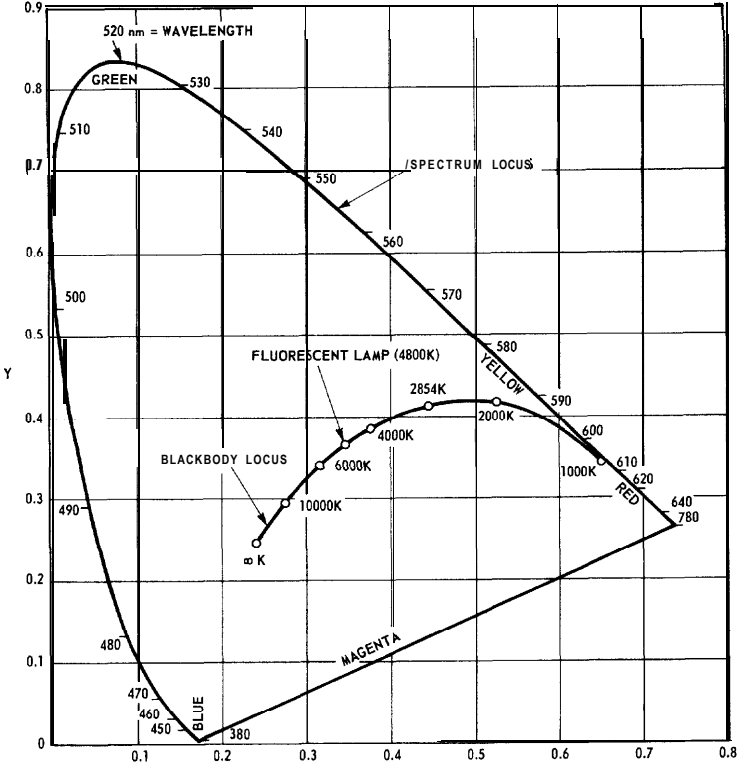


Fig. 5-6 CIE chromaticity diagram of spectral colors closed by non-spectral colors.

arched curve in the center of the diagram. Those points located in the central region of the diagram, including the segment of the blackbody locus between 2500 K and 12,000 K, are recognized as “white” depending upon the particular adaptation conditions of the observer.

Although color matching was originally done by human observers, **colorimetry** today is generally done indirectly. Spectroradiometric data are obtained for the sample to be matched and specifications are computed using the tristimulus curves of Figure 5-5 and the chromaticity diagram of Figure 5-6. Classification of ordinary colors by this technique provides matching that provides close correspondence for over 90% of the population.

5.4 SPECTRAL LUMINOUS EFFICACY AND SPECTRAL LUMINOUS EFFICIENCY

Spectral Luminous Efficacy (Photopic Vision)-Spectral luminous efficacy (formerly luminosity factor) of radiant flux $K(\lambda)$ is the quotient of the luminous flux at a given wavelength by the radiant flux at that wavelength. Hence,

$$K(\lambda) = \Phi_{v\lambda} / \Phi_{e\lambda} \quad (\text{in } \text{lm W}^{-1}), \tag{5-1}$$

The maximum value of the $K(X)$ function occurs at a wavelength of about 555 nm and has a value of 673 lm W^{-1}

Spectral Luminous Efficiency (Photopic Vision)-Spectral luminous efficiency of radiant flux $V(\lambda)$ is the ratio of the luminous efficacy at a given wavelength to the value of the luminous efficacy (673 lm W^{-1}) at the wavelength of maximum luminous efficacy. Accordingly,

$$V(\lambda) = K(\lambda) / 673 \tag{5-2}$$

Spectral Luminous Efficacy and Spectral Luminous Efficiency (Scotopic Vision)-The corresponding quantities for scotopic vision are spectral luminous efficacy $K'(\lambda)$ and spectral luminous efficiency $V'(\lambda)$ are related by the expression

$$V'(\lambda) = K'(\lambda) / 1725 \tag{5-3}$$

The value 1725 lm W^{-1} is the maximum of the spectral luminous efficacy function for scotopic vision and occurs at a wavelength of about 510 nm.

Tabulated values for $\zeta(\lambda)$ and $\zeta'(\lambda)$ are given in Figure 5-7. Graphical presentations of $V(\lambda)$, $V'(\lambda)$, $K(\lambda)$, and $K'(\lambda)$ are shown in Figures 5-8 and 5-9.

It should be noted that all photometric measurements are based on the spectral luminous efficacy and spectral luminous efficiency for photopic vision.

The difference in peak values between luminous efficacy for photopic vision and scotopic vision is not attributable to their responsivity differences but is due to the fact that the standard candela radiates less energy in the blue-green region (where scotopic vision peaks) than in the yellow-green region (where photopic vision peaks). Moreover, scotopic vision covers a narrower region of the spectrum than photopic vision.

Wavelength nm	Photopic $V(\lambda)$ $L \geq 3\text{nt (cd m}^{-2}\text{)}$	Scotopic $V'(\lambda)$ $(L \leq 3 \times 10^{-5} \text{ nt (cd m}^{-2}\text{)})$
380	0.00004	0.00059
390	0.00012	0.00221
400	0.0004	0.00929
410	0.0012	0.03484
420	0.0040	0.0966
430	0.0116	0.1998
440	0.0230	0.3281
450	0.0380	0.4550
460	0.0600	0.5672
470	0.0910	0.6756
480	0.1390	0.7930
490	0.2080	0.9043
500	0.3230	0.9817
510	0.5030	0.9966
520	0.7100	0.9352
530	0.8620	0.8110
540	0.9540	0.6497
550	0.9950	0.4808
560	0.9950	0.3288
570	0.9520	0.2076
580	0.8700	0.1212
590	0.7570	0.0655
600	0.6310	0.03325
610	0.5030	0.01593
620	0.3810	0.00737
630	0.2650	0.003335
640	0.1750	0.001497
650	0.1070	0.000677
660	0.0610	0.0003129
670	0.0320	0.0001480
680	0.0170	0.0000716
690	0.0082	0.00003533
700	0.0041	0.00001780
710	0.0021	0.00000914

Fig. 5-7 Relative spectral luminous efficiency values (from Table II, Chapter 1 of Kingslake, Reference 11 and Table 6j-1, page 6-1 40 of American Institute of Physics Handbook, Reference 6, with permission) (Part 1 of 2)

Wavelength nm	Photopic V (λ) L ≥ 3 nt (cd m ⁻²)	Scotopic V' (λ) (L ≤ 3 × 10 ⁻⁵ nt (cd m ⁻²))
720	0.00105	0.00000478
730	0.00052	0.000002546
740	0.00025	0.000001379
750	0.00012	0.000000760
760	0.00006	0.000000425
770	0.00000	0.000000241
780	0.000000139

Fig. 5-7 Relative spectral luminous efficiency values (from Table II, Chapter 1 of Kingslake, Reference 11 and Table 6j-1, page 6-140 of American Institute of Physics Handbook, Reference 6, with permission) (Part 2 of 2)

5.5 LUMINOUS EFFICACY AND LUMINOUS EFFICIENCY

In addition to $K(\lambda)$ and $\zeta(\lambda)$ which relate to a specific wavelength, the **luminous efficacy K** and **luminous efficiency η** functions have been developed which define the overall effectiveness of a given light source in producing luminous flux.

Luminous efficacy K, which may be defined for any radiant source, is the ratio of the total luminous flux to the total radiant flux. Its dimensions are lm W^{-1} and it may be used to convert flux in watts to flux in lumens.

Luminous efficiency η, usually expressed in per cent, is related to K by a constant factor

$$\eta = \frac{K}{673} 100 \% \tag{5-4}$$

Accordingly, η is the ratio of luminous flux from a given source to the luminous flux from a monochromatic source of the same radiant power at a wavelength of 555 nm.

Values for luminous efficacy K and luminous efficiency η for a blackbody as a function of temperature are shown in Figure 4-4.

5.6 SAMPLE CALCULATIONS INVOLVING LUMINOUS EFFICACY

1. Let $L_{e\lambda}$ represent the spectral radiance in $\text{W m}^{-2}\text{sr}^{-1} \mu\text{m}^{-1}$ of a blackbody at 2045 K. See Figure 4-1. The luminance L_v of this body, using the preceding relations, is calculated as follows:

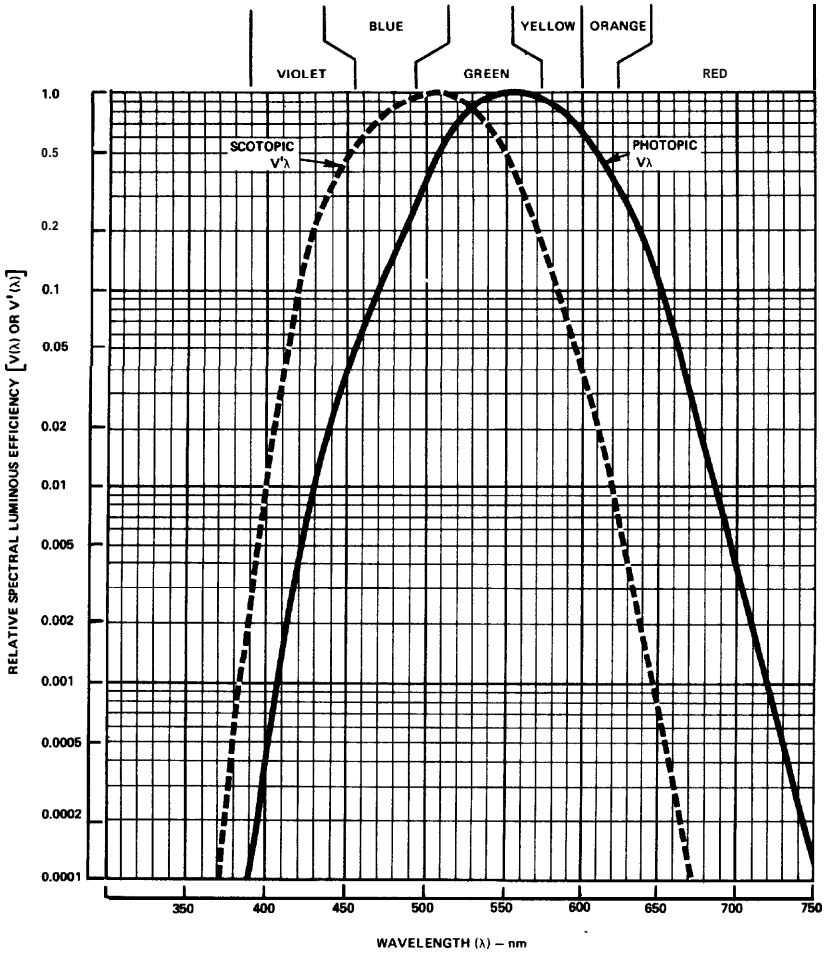


Fig 5-8 Relative spectral luminous efficiency as a function of wavelength. The relative response of the human eye to radiation of a given wavelength.

$$L_v = \int_0^{\infty} L_{v\lambda} d\lambda$$

$$L_v = \int_0^{\infty} K(\lambda) L_{e\lambda} d\lambda$$

$$L_v = 673 \int_0^{\infty} V(\lambda) L_{e\lambda} d\lambda$$

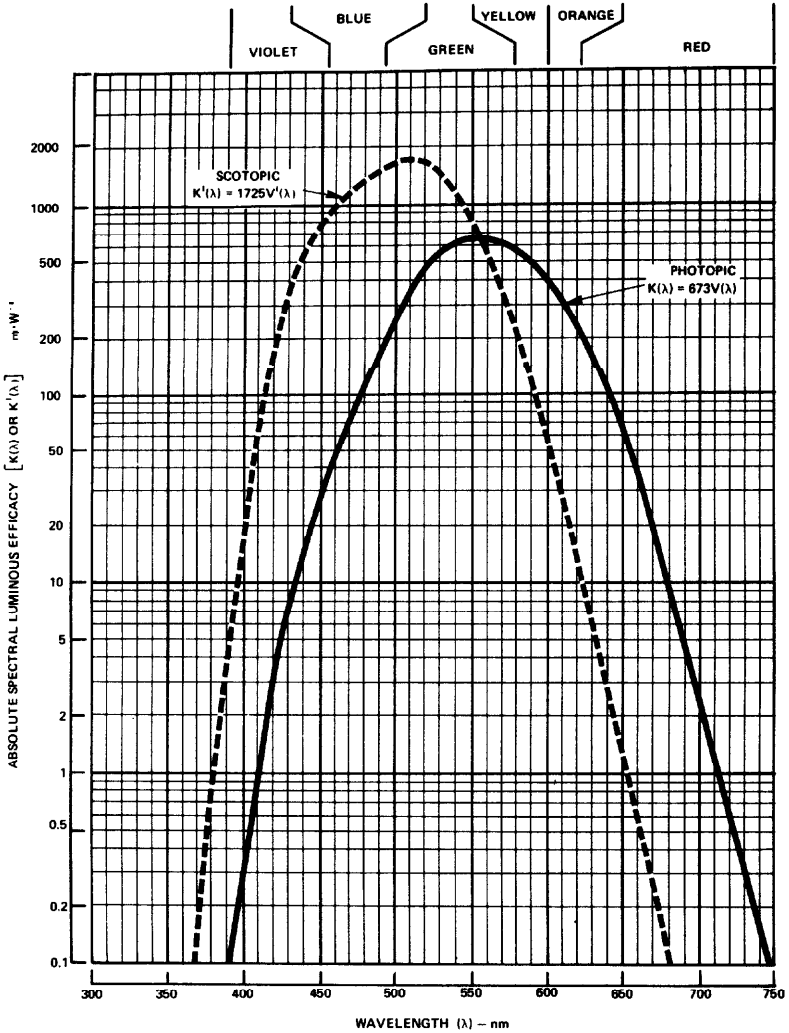


Fig. 5-9 Absolute spectral luminous efficacy as a function of wavelength. The response of the human eye to radiation of a given wavelength,

or,

$$L_v = 1725 \int_0^{\infty} V(\lambda) L_{e\lambda} d\lambda$$

$$L_v = 60 \times 10^4 \text{ c d m}^{-2}$$

2. Assume photopic vision and radiant flux having the following spectral radiant flux.

$$\Phi_{e\lambda} \begin{cases} = \text{constant, } 400 \text{ nm} < \lambda < 760 \text{ nm} \\ = 0, \text{ elsewhere in the spectrum} \end{cases}$$

The value of luminous efficacy K is calculated as follows:

$$K = \frac{\Phi_v}{\Phi_e}$$

$$K = \frac{\int_0^{\infty} \Phi_{v\lambda} d\lambda}{\int_0^{\infty} \Phi_{e\lambda} d\lambda}$$

$$K = \frac{\int_0^{\infty} K(\lambda) \Phi_{e\lambda} d\lambda}{\int_0^{\infty} \Phi_{e\lambda} d\lambda}$$

$$K = \frac{673 \int_0^{\infty} V(\lambda) \Phi_{e\lambda} d\lambda}{\int_0^{\infty} \Phi_{e\lambda} d\lambda}$$

Using the values for $V(\lambda)$ given in Figure 5-8 yields $K \cong 200 \text{ lm W}^{-1}$

3. The luminous efficacy K for a blackbody at a temperature of 2045 K (freezing point of platinum) is calculated as follows:

$$K = \frac{M_v}{M_e}$$

where

M_v = the luminous exitance lm m^{-2}

M_e = the radiant exitance W m^{-2}

For a blackbody, the Stefan-Boltzmann law gives

$$M_e = \sigma T^4$$

where $\sigma = 5.67 \times 10^{-8} \text{ W m}^{-2} \text{ K}^{-4}$ is the Stefan-Boltzmann constant. Thus:

$$M_e = 5.67 \times 10^{-8} (2045)^4 = 9.92 \times 10^5 \text{ W m}^{-2}$$

If one assumes equal luminance L in all directions, namely $6 \times 10^5 \text{ nt (cd m}^{-2}\text{)}$ using the definition given in Section 2.2 for the candela, then (because a blackbody is a Lambertian source),

$$M_v = \pi L_v = \pi \times 60 \times 10^4 = 1.885 \times 10^6 \text{ lx (lm m}^{-2}\text{)}$$

Therefore,

$$K = \frac{1.885 \times 10^6}{9.992 \times 10^5} = 1.9 \text{ lmW}^{-1}$$

Note that this result is consistent with the data on Figure 4-4.

References

6. AMERICAN INSTITUTE OF PHYSICS HANDBOOK, Second edition, McGraw-Hill Book Co., Inc. New York, N.Y., 1962.
10. Wald, G., Brown, P.K., and Smith, P.L., "Iodopsin," JOURNAL OF GENERAL PHYSIOLOGY, Vol. 38, No. 5, 623-681, 1955.
11. Kingslake, R., APPLIED OPTICS AND OPTICAL ENGINEERING, Vol. 1 "Light: Its Generation and Modification," Academic Press, New York, N.Y., 1965.
12. Graham, C.H., Editor, VISION AND VISUAL PERCEPTION, John Wiley and Sons, Inc., New York, N.Y., 1965.
13. Blackwell, H.R., "Contrast Thresholds of the Human Eye," J.O.S.A., Vol. 36, No. 11, 624-643, 1946.
14. Middleton, W.E.K., VISION THROUGH THE ATMOSPHERE, University of Toronto Press, Toronto, Canada, 1958.
15. Griffin, D.R., Hubbard, R., and Wald, G. "The Sensitivity of the Human Eye to Infrared Radiation," J.O.S.A., Vol. 37, No. 7, 546, 1947.

Section 6

Sources of Radiation

This section concerns radiation from the most important natural sources (sun, moon, stars and sky) and from lamps. Lasers and light-emitting diode sources are discussed in Section 9.

6.1 THE SUN

The sun's irradiance E just outside the earth's atmosphere is

- = 1390 W m⁻² at mean earth-sun distance
- = 1438 W m⁻² at perihelion (3 January 1965)
- = 1345 W m⁻² at aphelion (3 July 1965)

See page 16-1 of Reference 8.

In terms of E_λ the sun's spectral irradiance outside the atmosphere is

$$E = \int_0^{\infty} E_\lambda d\lambda. \quad (6-1)$$

Figure 6-1 gives E_λ for mean earth-sun separation and also shows an average effect of atmospheric attenuation and absorption on E_λ at sea level with the sun at the zenith.

An extensive series of solar-illuminance measurements at the earth's surface, made by D.R.E. Brown (see page 165 of Reference 16), indicates an

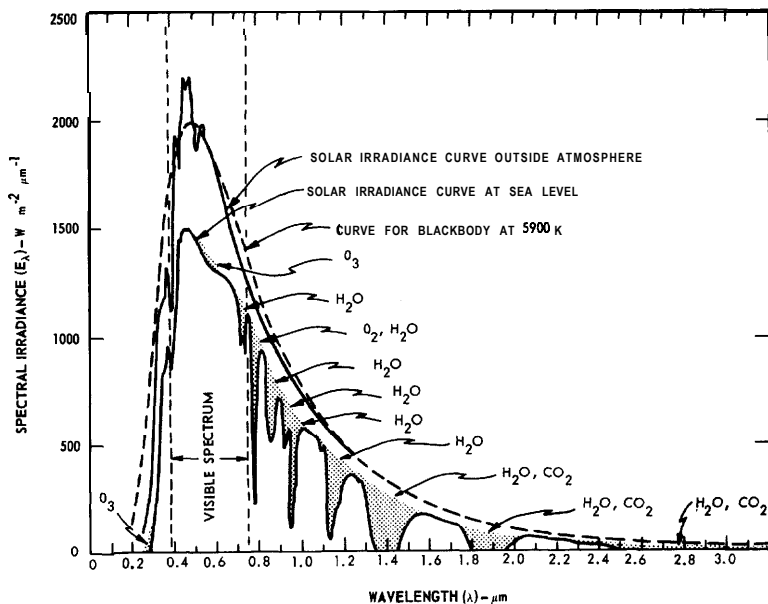


Fig. 6-1 Spectral radiance E_{λ} of the sun at mean earth-sun separation. Shaded areas indicate absorption at sea level due to the atmospheric constituents shown (Adapted from Reference 8 with permission).

illuminance on a horizontal surface at sea level, with the sun at its zenith in a “comparatively clear” sky of

$$E = 1.24 \times 10^5 \text{ lux (1mm}^{-2}\text{)} \quad (6-2)$$

As was noted in equation (6-1), the maximum variation from this average caused by the yearly changes in distance of the earth from the sun is less than $\pm 3.5\%$. Solar irradiance on the earth’s surface depends on the altitude angle of the sun above the horizon, on the observer’s altitude above sea level, and upon the amount of dust, haze, and clouds in the sky. Figure 6-2 summarizes the results obtained by Brown for various angles of the sun above the horizon. (The altitude angle of the sun at any time and point on the earth’s surface may be calculated by a method given in Appendix C of Reference 16.)

True Altitude Angle of Center of Sun degrees	Illuminance On Horizontal Surface E lux (or lm m^{-2})	Remarks
- 18	6.51×10^{-4}	Lower limit of astronomical twilight
- 12	8.31×10^{-3}	Lower limit of nautical twilight
- 6	3.40	Lower limit of civil twilight
- 5	10.8	
- 0.8	453	Sunrise or sunset
0	732	
5	4760	
10	1.09×10^4	
15	1.86×10^4	
20	2.73×10^4	
25	3.67×10^4	
30	4.70×10^4	
35	5.70×10^4	
40	6.67×10^4	
45	7.59×10^4	
50	8.50×10^4	Total change 2.64 magnitudes
55	9.40×10^4	(see Section 6.3)
60	10.2×10^4	
65	10.8×10^4	
70	11.3×10^4	
75	11.7×10^4	
80	12.0×10^4	
85	12.2×10^4	
90	12.4×10^4	

Fig. 6-2 Illuminance levels on the surface of the earth due to the sun (Reference 16).

6.2 THE MOON

The illuminance E at the earth's surface caused by sunlight reflected from the moon is affected by the following factors:

1. By the phase of the moon (phase may be expressed by its elongation, i.e., its angular distance from the sun). The relative effect of moon's phase on the illuminance E is shown in Figure 6-3.

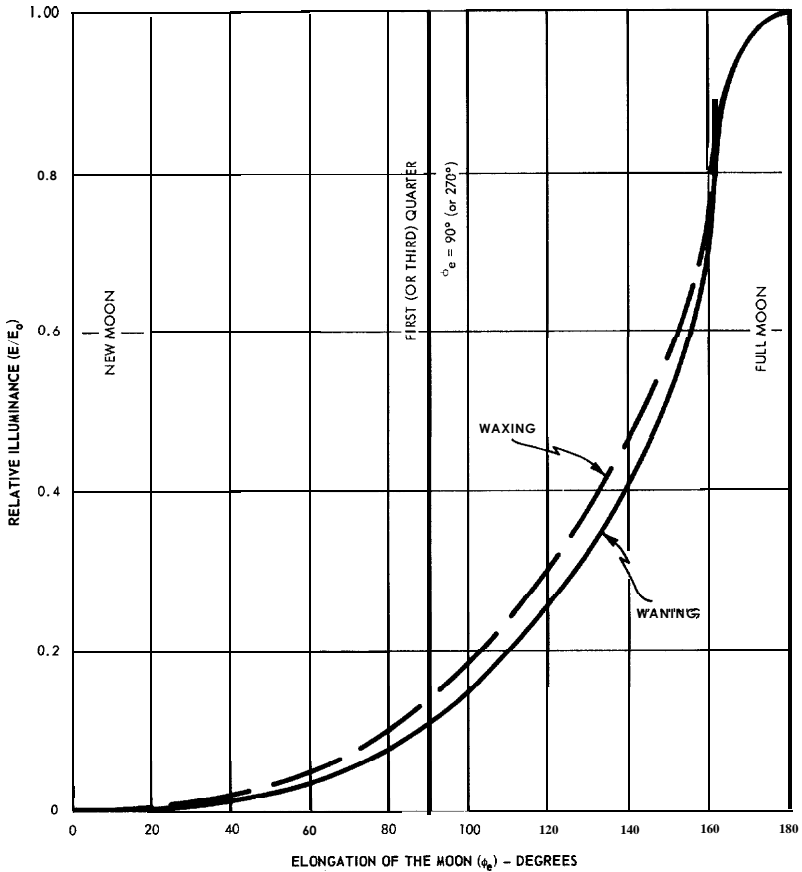


Fig. 6-3 Relative lunar illuminance as a function of the moon's angular distance Φ_e from the sun – elongation (Reference 16).

- By the variation in earth-moon distance during the lunar cycle. There is a total variation of about 26% from this effect.
- By the differences in reflectance (albedo) of the different portions of the moon surface that are illuminated during the lunar cycle. The moon is about 20% brighter at first quarter (waxing) than at third (waning) due to differences in the lunar surface. See Figure 6-3.

4. By the altitude angle of the moon above the earth's horizon and by atmospheric effects.

Figure 6-4 gives the computed variation of lunar illuminance E on a horizontal exposed surface at sea level as a function of the moon's altitude angle. These values assume a comparatively clear sky, mean earth-moon separation, and the mean of the waxing and waning curves in Figure 6-3. Values are omitted in Figure 64 for cases where the sun is above the horizon.

6.3 THE STARS

The apparent visual magnitude of stars (stellar magnitude) or of other sources is determined by the illuminance that source produces at a point outside the earth's atmosphere. (See page 107 of Reference 3.) The ratio of the illuminances produced by two sources differing by one magnitude is defined to be

$$\sqrt[5]{100} = 2.512.$$

True Altitude of Center of Moon	Illuminance on Horizontal Surface, E , At Elongation ϕ_e – lux (or lm m^{-2})			
	$\phi_e = 180^\circ$ (Full Moon)	$\phi_e = 120^\circ$	$\phi_e = 90^\circ$ (1st or 3rd quarter)	$\phi_e = 60^\circ$
(moonrise) -0.8° or moonset)	9.74×10^{-4}	2.73×10^{-4}	1.17×10^{-4}	3.12×10^{-5}
0°	1.57×10^{-3}	4.40×10^{-4}	1.88×10^{-4}	5.02×10^{-5}
10°	2.34×10^{-2}	6.55×10^{-3}	2.81×10^{-3}	7.49×10^{-4}
20°	5.87×10^{-2}	1.64×10^{-2}	7.04×10^{-3}	1.88×10^{-3}
30°	0.101	2.83×10^{-2}	1.21×10^{-2}	3.23×10^{-3}
40°	0.143	4.00×10^{-2}	1.72×10^{-2}	4.58×10^{-3}
50°	0.183	5.12×10^{-2}	2.20×10^{-2}	5.86×10^{-3}
60°	0.219	6.13×10^{-2}	2.63×10^{-2}
70°	0.243	6.80×10^{-2}	2.92×10^{-2}
80°	0.258	7.22×10^{-2}	3.10×10^{-2}
90°	0.267	7.48×10^{-2}

Fig. 6-4 Illuminance levels on the surface of the earth due to the moon (Reference 16).

Therefore, two sources having magnitudes m and n , respectively, would produce illuminances having a ratio given by

$$\frac{E_m}{E_n} = (2.512)^{n-m} \quad (6-3)$$

or

$$\log_{10} E_m - \log_{10} E_n = 0.400 (n-m)$$

Figure 6-5 contains values of the illuminance E computed in this way from the stellar magnitudes given for a number of sources. The illuminance for a zero magnitude star was taken as the reference for all the calculations to be $2.65 \times 10^{-6} \text{ lm m}^{-2}$.

The spectral distributions of stellar radiation is treated in Reference 3, pages 110 to 115.

The stars provide approximately $2.2 \times 10^{-4} \text{ lux (lm m}^{-2}\text{)}$ ground illuminance on a clear night. This illuminance is equivalent to about one-quarter of the actual light from the night sky with no moon. The greater portion of the natural light of the night sky, the **airglow** that originates in the upper

source	Stellar Magnitude	Calculated Illuminance lux (or lm m^{-2})
Candela at 1 meter	-13.9	1.00
Venus (at brightest)	-4.3**	1.39×10^{-4}
Sirius	-1.42+	9.80×10^{-6}
Zero Mag. Star	0	2.65×10^{-6} *
1st Mag. Star	1	1.05×10^{-6}
6th Mag. Star	6	1.05×10^{-8}

* Reference illuminance for calculations (page 191 of Reference 17)

** Reference 18, page 27

+ Reference 18, page 74

Fig. 6-5 Illuminance calculated from stellar magnitudes of various sources outside of the earth's atmosphere. The transmission of the atmosphere for an object observed at the zenith is approximately 79%.

atmosphere, is produced by the emission from various atoms and molecules. Other minor sources of night illuminance are the aurora and zodiacal light caused by the scattering of sunlight from interplanetary particulate matter.

Blackbody radiation characteristics of a number of stars and planets are shown in Figures 6-6 and 6-7. These curves were calculated from temperature and visual magnitude data. The curves peak at the wavelength derived from Wien's Displacement Law. See Section 4.2, equation 4-8. Each curve intersects the ordinate at $\lambda = 555$ nanometers (the wavelength of peak visual response) at an approximate value of the visual magnitude of the star.

The spectral irradiance from a typical aggregate of stars is shown in Figure 6-8.

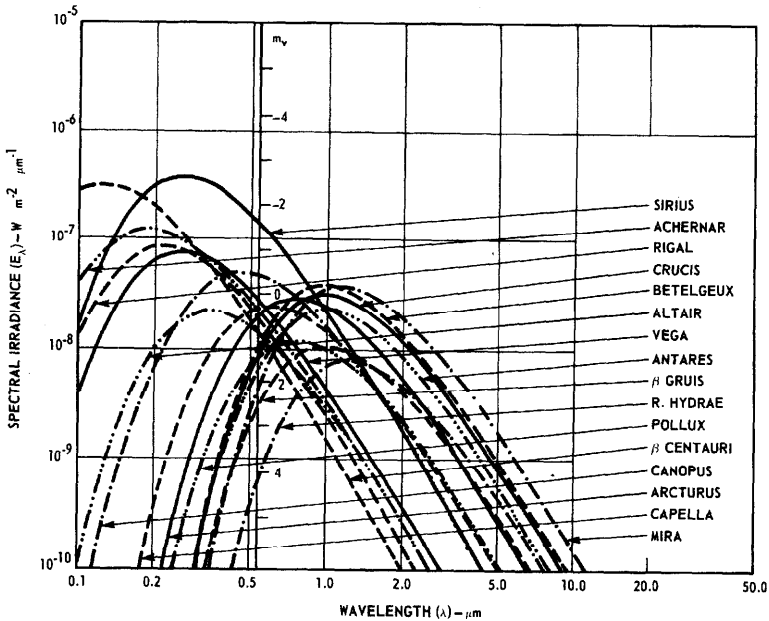


Fig. 6-6 Calculated spectral irradiance from the brightest stars outside of the earth's atmosphere; m_v = visual magnitude at maximum spectral irradiance (Reference 19).

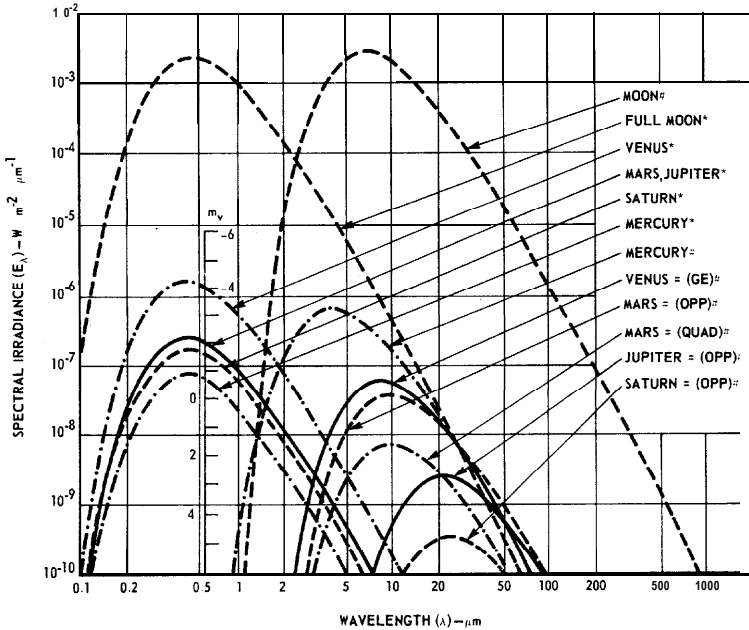


Fig. 6-7 Calculated spectral irradiance from planets at the top of the atmosphere; * = calculated irradiance from planets at brightest due only to sun reflectance; GF = inferior planet at greatest elongation; OPP = superior planet at opposition; QUAD = superior planet at quadrature; # = calculated irradiance from planets due only to self emission; m_v = visual magnitude at maximum spectral irradiance (Reference 19).

6.4 THE SKY

On a clear day, about one-fifth of the total illuminance E at the earth's surface is from the sky, that is, from sunlight scattered by the earth's atmosphere. Figure 6-9 lists some approximate levels of scene illuminance from the day and night sky under various conditions.

Figure 6-10 gives approximate values of the luminance L of the sky near the horizon under a variety of conditions. The concept of luminance when applied to the sky may not be readily apparent with respect to the location of the area implied by m^2 or the location of the apex of the solid angle implied

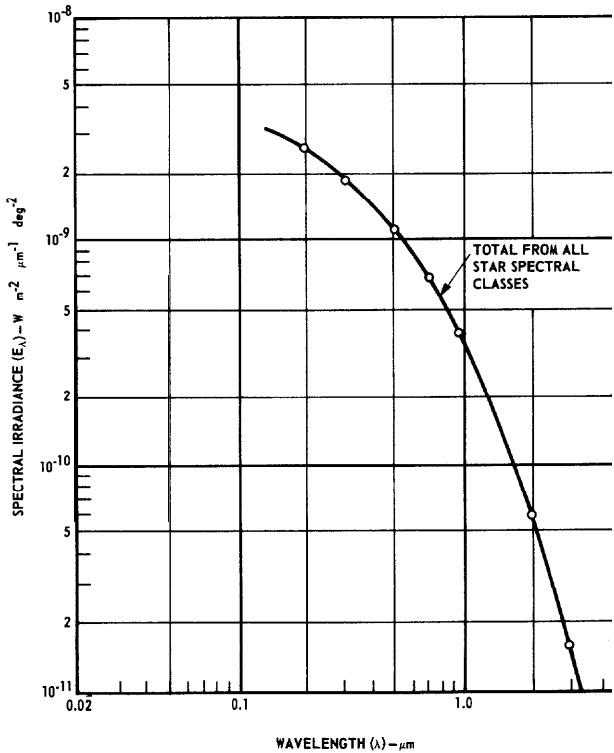


Fig. 6-8 Probable spectral irradiance from one-square-degree starfield in or near the galactic plane (Reference 20).

by the use of the unit candela. This difficulty may be resolved by considering the method used to measure the luminance of the sky.

Assume a photometer on earth which measures illuminance. Restrict the photometer with a suitable aperture such that a point on its sensitive area can see only a relatively small solid angle ω . Consider a sky area A_s located at a distance s from the observer such that the solid angle $A_s/s^2 = \omega$. If the luminance of the sky is L nits (cd m^{-2}), the total luminous intensity of the area A_s is $A_s L$ and the illuminance at the point of observation in a plane normal to the line of sight is $E = A_s L/s^2 = L\omega$. Thus $L = E/\omega$. Because the solid angle is measured from the point of observation, the distance to the sky is not required; only the measurement of E and ω is needed. See Reference 14, p 10.

Sky Condition	Approx. Levels of Illuminance – lux (lm m^{-2})
Direct sunlight..	$1-1.3 \times 10^5$
Full daylight (Not direct sunlight).	$1-2 \times 10^4$
Overcast day	10^3
Very dark day.	10^1
Twilight	10
Deep twilight	1
Fullmoon	10^{-1}
Quartermoon	10^{-2}
Moonless, clear night sky	10^{-3}
Moonless, overcast night sky	10^{-4}

Fig. 6-9 Natural scene illuminance.

Sky Condition	Approx. Values of Luminance – nit (cd m^{-2})
Clear day* -----	10^4
Overcast day -----	10^3
Heavily overcast day -----	10^2
Sunset, overcast day -----	10
¼ hour after sunset, clear -----	1
½ hour after sunset, clear -----	10^{-1}
Fairly bright moonlight -----	10^{-2}
Moonless, clear night sky -----	10^{-3}
Moonless, overcast night sky -----	10^{-4}

*The upper surface of a fog or cloud in sunshine may also have this value.

Fig. 6-10 Approximate values of the luminance of the sky near the horizon under various conditions (Adapted from Reference 14 with permission).

On a clear day the color temperature of the sky is approximately 20,000 K to 25,000 K. The intensity of the scattered sky light varies inversely as the fourth power when the size of the particles in the atmosphere causing the

scattering is in the order of magnitude of the light wave. Because the short waves, which correspond to the blue and violet colors, are scattered more than the longer waves of red light, the color of the sky is predominately blue. Figure 6-11 shows the spectral distribution of the clear sky and that of a blackbody at 25,000 K.

The irradiance from the night sky is due to the following sources (see page 141 of Reference 11):

Zodiacal	15%
Galactic	5%
Luminescence of night sky (fluctuates)	40% (avg.)
Scattering from the above	10%
Direct and scattered starlight	30%
Extra-Galactic sources	<1%

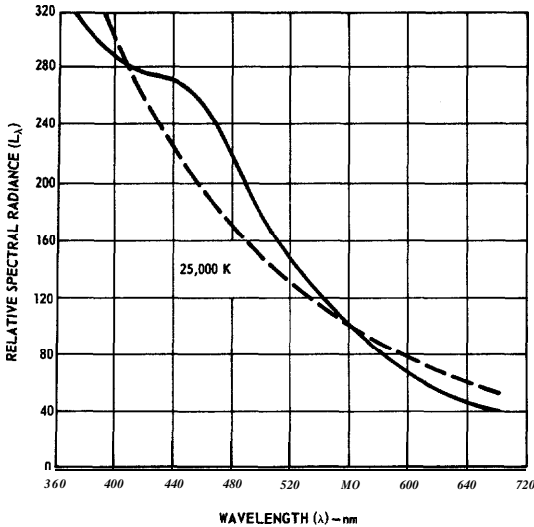


Fig. 6-11 Spectral distribution of sky light on a clear day. Dashed curve shows the spectral distribution of radiation from a blackbody at 25,000 K (Reference 7).

An estimate of the average spectral distribution of the night-sky irradiance is plotted in Figure 6-12. This result in photons per second is on a horizontal surface of one square meter at sea level in wavelength intervals of $0.05 \mu\text{m}$. Curves giving radiant exitance of blackbodies at 300 K and 400 K have been added for comparison. It is noteworthy that the lower atmosphere emits thermal radiation whose level may be approximated by blackbody radiation at ambient ground temperature. This effect is limited mostly to the far infrared region. If the spectral reflectance $\rho(\lambda)$, spectral emissivity $\epsilon(\lambda)$, and temperatures of objects within the scene are known, then data like that given in Figure 6-12 permit estimation as a function of wavelength of the photons available for low-light-level image formation. Note that Figure 6-12 indicates a greater abundance of photons at infrared than at visible wavelengths.

6.5 SUMMARY OF NATURAL ILLUMINANCE LEVELS

Figures 6-13 and 6-14 provide a summary of the ambient light levels presented in this section. Curves to indicate illuminances under cloudy moonlight may be drawn by displacing downward the given moonlight curves by the same amounts as for cloudy sun curves (compared to the unobscured sun).

More data on spectral distribution of sky and earth background radiance is available in the literature to augment that presented in this section. Examples are the following:

Reference 11, page 141 to 145

Reference 8, chapter 10

6.6 TIME VARIATION OF NATURAL ILLUMINANCE

Figure 6-15 shows the fraction of the time (averaged over a year) that the illuminance on the earth's surface due to natural light sources exceeds any given value E at three latitudes. It is assumed that the atmosphere is clear.

6.7 LAMP SOURCES

Figure 6-16 lists some of the optical parameters of a variety of continuous light sources. Spectral curves for some of these sources are referenced in the table, and appear in Figures 6-17 to 6-24. Lamps are available in much more variety than can be covered in this table, with various flux levels, spectral characteristics, mechanical dimensions, cooling requirements, etc. Some of these sources can be modulated.

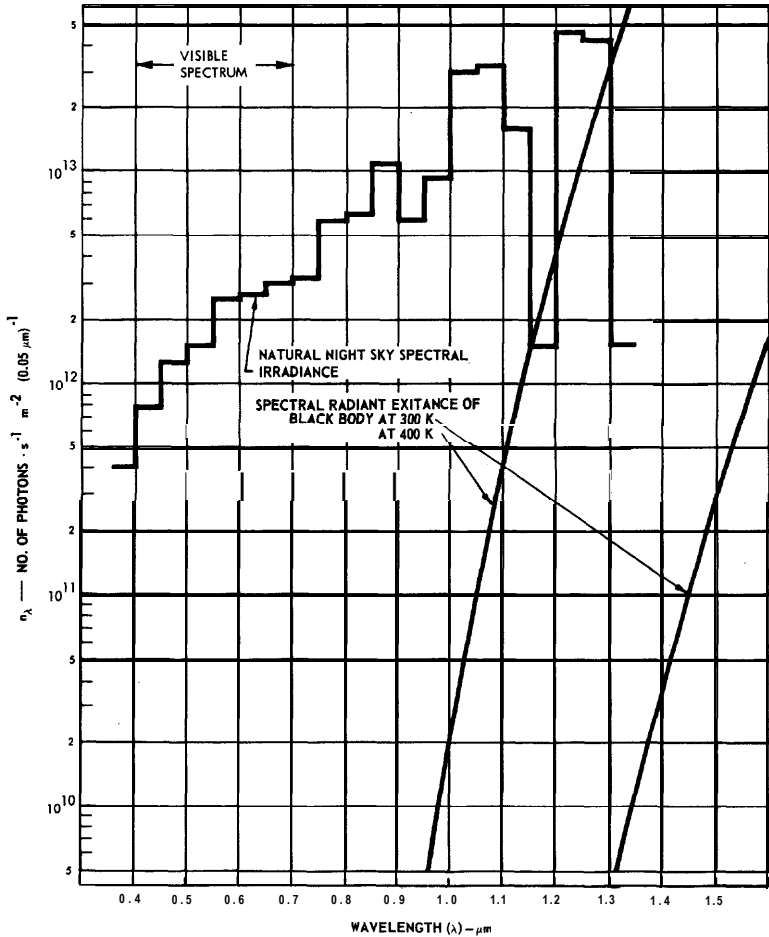


Fig. 6-12 Natural night-sky spectral irradiance on horizontal earth's surface and the spectral radiant exitance of blackbodies at 300 K and 400 K.

Figure 6-24 gives an example of a fluorescent lamp spectrum of the "daylight" type. Various spectral distributions are available for these lamps depending on their phosphor and gas filling.

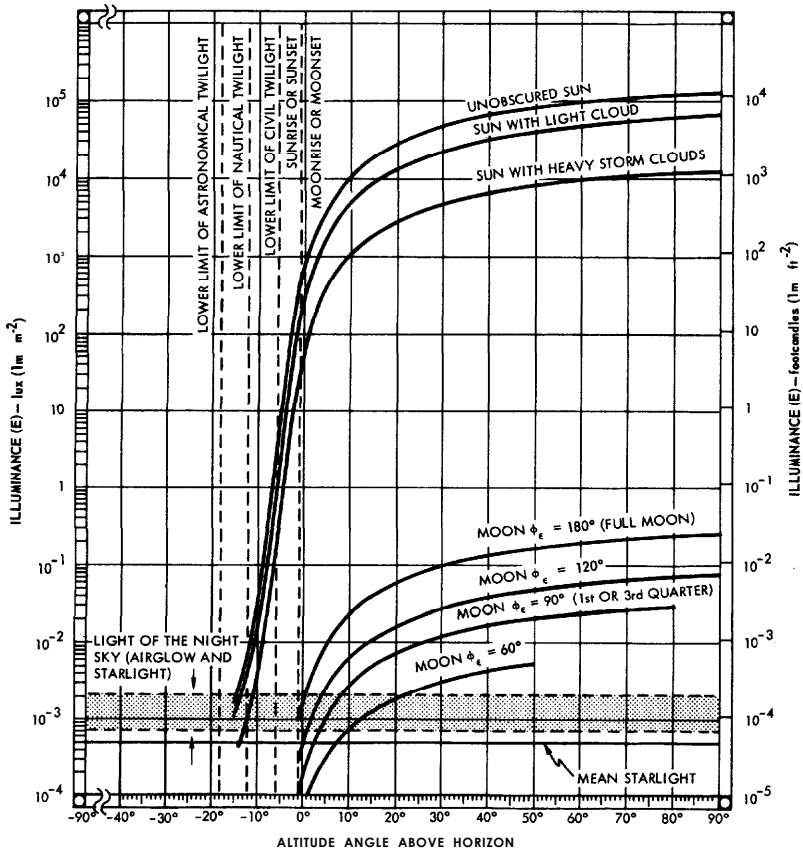


Fig. 6-13 Illuminance levels on the surface of the earth due to the sun, the moon, and the sky (Reference 16).

References

3. Wolf, W.L., Editor, HANDBOOK OF MILITARY INFRARED TECHNOLOGY, Office of Naval Research, Dept. of the Navy, Washington, D.C., 1965.
7. Mauro, J.A. Editor, OPTICAL ENGINEERING HANDBOOK, General Electric Co., Syracuse, N.Y., 1966.

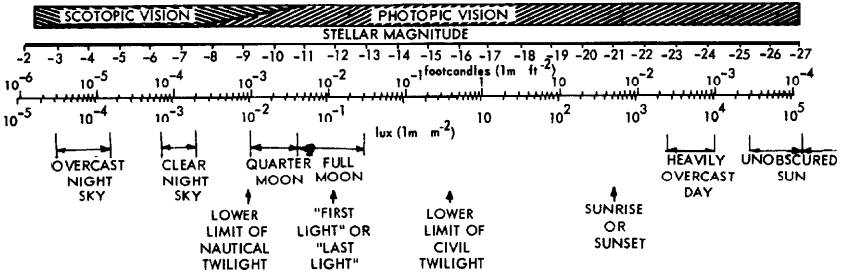


Fig. 6-14 Range of natural illuminance levels (Reference 16).

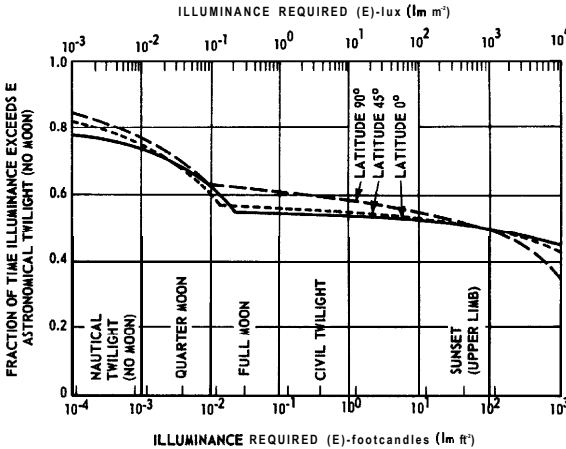


Fig. 6-15 Fraction of time natural illuminance exceeds a specified level E .

8. Valley, S.L., HANDBOOK OF GEOPHYSICS AND SPACE ENVIRONMENTS, Air Force Cambridge Research Laboratories, Office of Aerospace Research, U.S. Air Force, 1965. Also published by McGraw-Hill Book Co., New York, N.Y., 1965.

11. Kingslake, R., APPLIED OPTICS AND OPTICAL ENGINEERING, Vol. 1 "Light: Its Generation and Modification," Academic Press, New York, N.Y., 1965.

References continued on page 79.

Lamp Type	DC Input Power (W)	Arc Dimensions (mm)	Luminous Flux (lm)	Luminous Efficacy (lm W ⁻¹)	Average Luminance (cd. mm ⁻²)	Temperature (K) (Fig. No.)
Mercury Short Arc* (high pressure)	200	2.5 x 1.8	9500	47.5	250	Fig. 6-17
Xenon Short Arc*	1.50	1.3 x 1.0	3200	21	300	Fig. 6-18
Xenon Short Arc*	2 x 10 ⁴	12.5 x 6	1.15 x 10 ⁶	57	3000 (in 3 mm x 6mm)	Fig. 6-19
Zirconium Arc**	100	1.5 (diam.)	250	2.5	100	Fig. 6-20
Vortex-Stabilized Argon Arc**	2.48 x 10 ⁴	3 x 10	4.22 x 10 ⁵	17	1400	7000 K Fig. 6-21
Tungsten Light Bulbs	10	—	79	7.9	10 to 25	2400 K 2850 K Fig. 6-22 3000 K
	100	—	1630	16.3		
	1000	—	2.15 x 10 ⁴	21.5		
Fluorescent Lamp Standard Warm White	40	—	2560	64	—	—
Carbon Arc Non-Rotating	2000	≈ 5 x 5	3.68 x 10 ⁴	18.4	175 to 800	Fig. 6-23
Rotating	1.58 x 10 ⁴	≈ 8 x 8	3.5 x 10 ⁵	22.2		
Sun	—	—	—	—	1600	≈ 5900 K

* Courtesy, PEK, Inc., Sunnyvale, Calif. ** Adapted from Reference 21 *** Adapted from Reference 22 page 38

Fig 6-16 Typical lamp parameters.

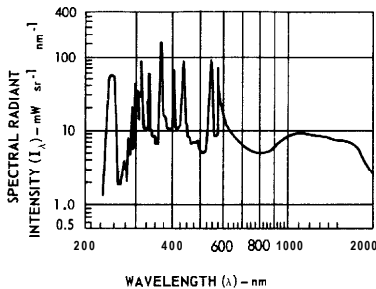


Fig. 6-17 Spectral distribution of 200 -watt mercury short arc.

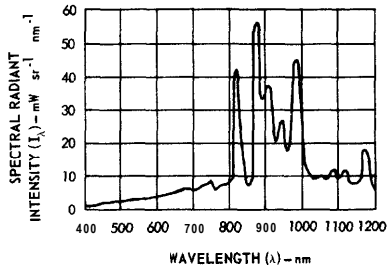


Fig. 6-18 Spectral distribution of 150-watt xenon short arc.

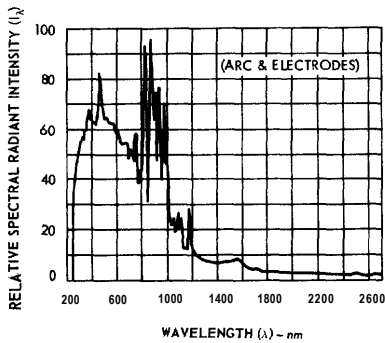


Fig. 6-19 Spectral distribution of 20-kilowatt xenon short arc.

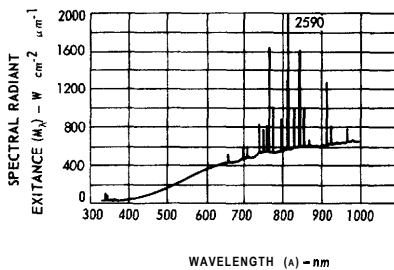


Fig. 6-20 Spectral distribution of 100-watt zirconium concentrated-arc lamp.

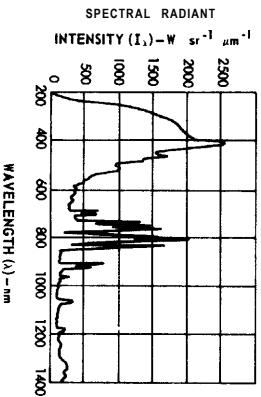


Fig. 6-21 Spectral distribution of 24.8-kilowatt vortex stabilized argon arc.

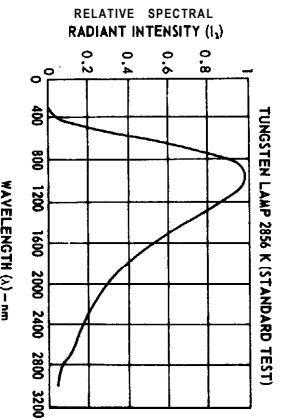


Fig. 6-22 Spectral distribution of 2856 K tungsten lamp.

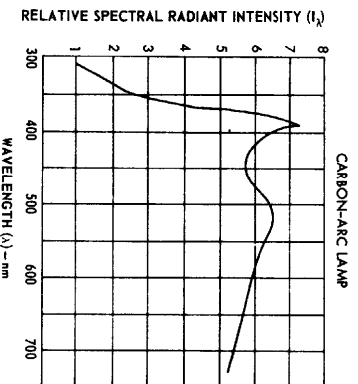


Fig. 6-23 Spectral distribution of carbon arc lamp.

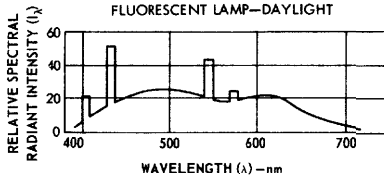


Fig. 6-24 Spectral distribution of fluorescent daylight lamp.

(References continued from page 75)

14. Middleton, W.E.K., VISION THROUGH THE ATMOSPHERE, University of Toronto Press, Toronto, Canada, 1958.
16. Bond, D.S. and Henderson, F.P., THE CONQUEST OF DARKNESS, AD 346297, Defense Documentation Center, Alexandria, Va., 1963.
17. Allen, C.W., ASTROPHYSICAL QUANTITIES, Second Edition, The Athelone Press, University of London, London, England.
18. THE OBSERVER'S HANDBOOK 1963, The Royal Astronomical Society of Canada.
19. Ramsey, R.C., "Spectral Irradiance from Stars and Planets, above the Atmosphere from 0.1 to 100.0 Microns," APPLIED OPTICS, Vol. 1, No. 4, July 1962.
20. Soule, H.V., ELECTROOPTICAL PHOTOGRAPHY AT LOW ILLUMINATION LEVELS, John Wiley and Sons, Inc., New York, N.Y., 1968.
21. Buckingham, W.D. and Diebert, C.R., "Characteristics and Applications of Concentrated-Arc-Lamps," J.S.M.P.E., Vol. 47. No. 5, Nov. 1946.
22. PLASMA JET TECHNOLOGY, SP-5033, NASA, Washington, DC., For sale by U.S. Government Printing Office, Oct. 1965.

Section 7

Atmospheric Transmittance

When a source emits radiation having an intensity I , and its path is through a vacuum, the irradiance E at some distance R from the source may be calculated according to the inverse square law. Thus

$$E = \frac{I}{R^2} \text{ W sr}^{-1} \text{ m}^{-2} \quad (7-1)$$

If, however, the path is through a gaseous atmosphere, some of the radiation is lost by scattering and some by absorption. Therefore

$$E = T_a \frac{I}{R^2} \text{ W sr}^{-1} \text{ m}^{-2} \quad (7-2)$$

where

T_a = the atmospheric transmittance over a designated path
(T_a has a value of less than unity)

Atmospheric transmittance T_a is a function of many variables: wavelength, path length, pressure, temperature, humidity, and the composition of the atmosphere. The factor T_a defines the decrease in radiant intensity due to absorption and scattering losses along the atmospheric path.

7.1 ENTIRE ATMOSPHERE

Figure 7-1 shows the spectral transmittance (in per cent) through the entire atmosphere (from sea level to outer space) along paths inclined to the zenith by angles of 0° , 60° , and 70.5° . These inclinations provide paths within the atmosphere that traverse air masses of ratios 1, 2, and 3, respectively. These curves indicate the net loss from all scattering mechanisms in a fairly clear atmosphere. Besides scattering by air molecules (Rayleigh scattering) there is scattering by the larger aerosol particles (Mie scattering). **Rayleigh scattering may be differentiated from Mie scattering by the following relationships; Rayleigh scattering applies when $2\pi a/\lambda < 1$ and Mie scattering when $2\pi a/\lambda \geq 2$** , where a is the radius of the scattering particle and λ is the wavelength of the radiation. See Reference 24.

Various regions of absorption are indicated on Figure 7-1. The most important are due to water vapor (H_2O), carbon dioxide (CO_2), and ozone (O_3). For most applications, the absorption by the other constituents is negligible.

7.2 HORIZONTAL-PATH TRANSMITTANCE

Figure 7-2 shows the atmospheric spectral transmittance over a 1000-foot horizontal path at sea level for the wavelength interval between $0.5 \mu\text{m}$ and $25 \mu\text{m}$. The atmospheric constituents responsible for the most prominent absorption effects are shown on this figure.

The transmittance of the atmosphere T_a over a path length R for radiation of wavelength λ may be expressed by

$$T_a = \exp(-\sigma R) \quad (7-3)$$

where σ is the spectral attenuation coefficient or "extinction coefficient". Equation 7-3 is valid only for very narrow wavelength bands, such as laser transmissions, and for transmission on a horizontal path through an atmosphere of uniform composition.

Sometimes the attenuation coefficient for each of several atmospheric constituents can be calculated separately and summed to obtain the total effect of transmittance. Figure 7-3 shows the sea level attenuation coefficient for a horizontal path in a model clear standard atmosphere (sea-level visibility approximately 23.5 kilometers). This coefficient is the sum of the ozone absorption coefficient, the **Rayleigh** scattering coefficient, and the aerosol scattering coefficient.

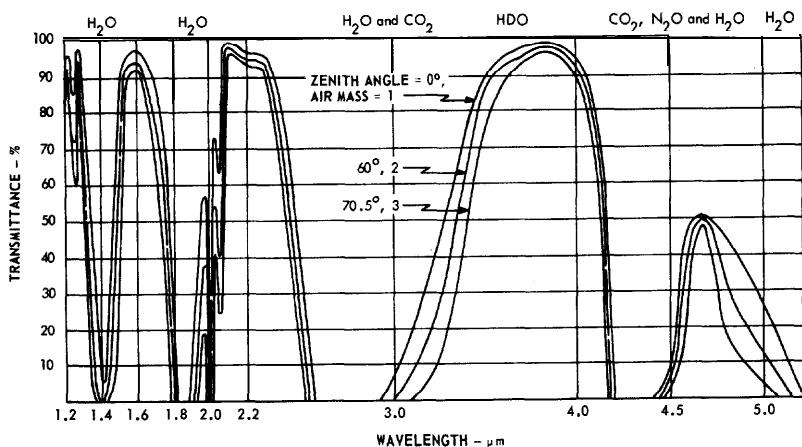
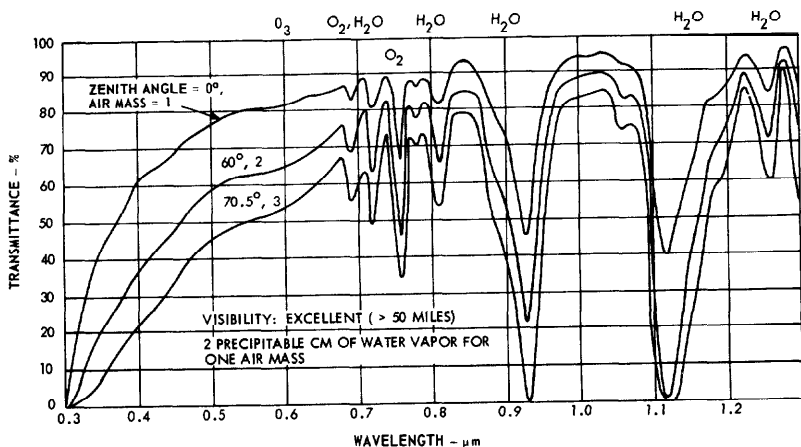


Fig 7-1 Spectral transmittance of the earth's atmosphere for varying optical air masses (Adapted from Reference 23 pp 25 and 26 with permission).

$$\sigma = \sigma_{\text{ozone}} + \sigma_{\text{Rayleigh}} + \sigma_{\text{aerosol}} \tag{7-4}$$

The effects of ozone absorption are most pronounced in the ultraviolet region of the spectrum and become negligible at longer radiation wavelengths. The

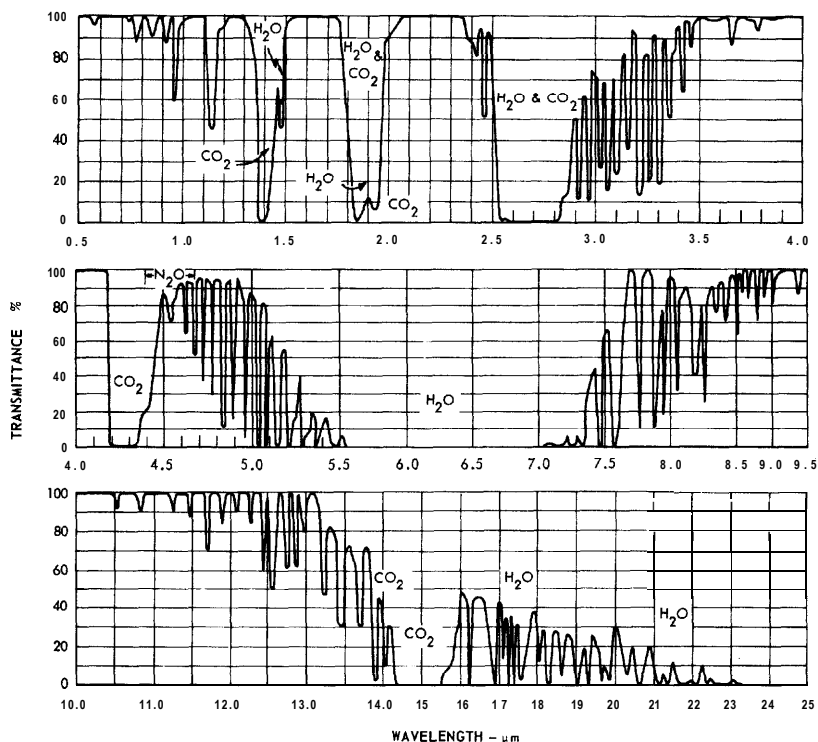


Fig. 7-2 Transmittance of 1000-ft horizontal air path at sea level containing 5.7-mm precipitable water at 79° F (From Reference 2.5 with permission).

Rayleigh scattering coefficient, σ_{Rayleigh} , is proportional to $(1/\lambda)^4$. The aerosol coefficient, σ_{aerosol} , is a complex function of particle size, shape, refractive index, scattering angle, and wavelength.

Absorbers other than O_3 , such as water vapor and carbon dioxide, are not included in the model of Figure 7-3. The absorption effects, which are highly dependent upon wavelength and absorber concentrations, may be determined by methods such as the one given in Section 10.2 of Reference 8. These effects, however, are generally negligible for narrow band radiation at the specific wavelengths plotted in Figure 7-3.

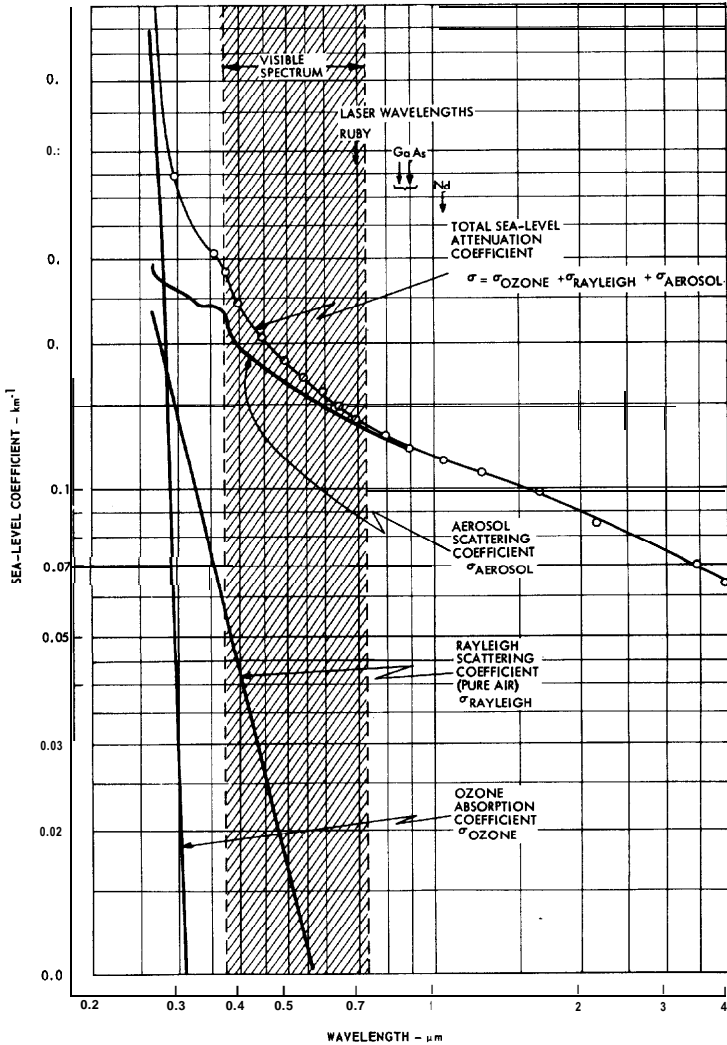


Fig. 7-3 Calculated atmospheric attenuation coefficients for horizontal transmission at sea level in a model clear standard atmosphere. Points are plotted from data in Table 7-4 of Reference 8. Absorption by H_2O and CO_2 , not included, may be appreciable at wavelengths other than those at plotted points.

Figure 7-4 shows how each of the three horizontal attenuations of equation 7-4 and the sun σ varies with altitude for ultraviolet radiation at $\lambda = 0.27 \mu\text{m}$ and $\lambda = 0.28 \mu\text{m}$ in a clear standard atmosphere. Two measured values of σ taken from Reference 26 are included in Figure 7-4 for comparison.

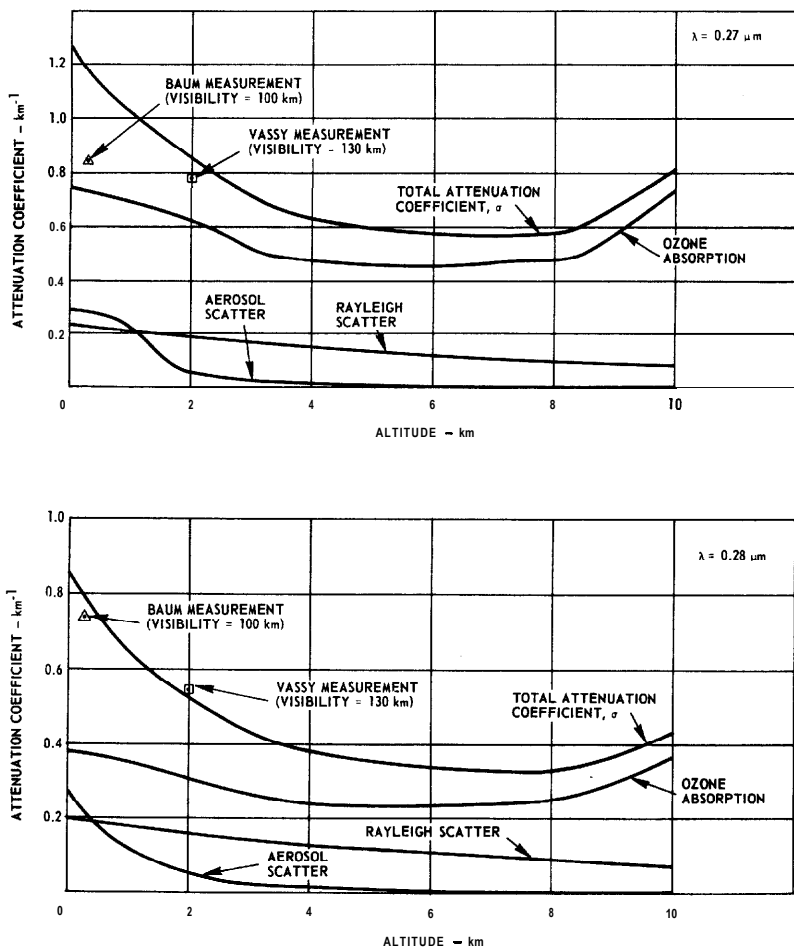


Fig. 7-4 Atmospheric attenuation coefficients for horizontal transmission of ultraviolet radiation at $0.27 \mu\text{m}$ and $0.28 \mu\text{m}$ as a function of altitude. Curves are plotted from model clear standard atmosphere data in Table 7-4 of Reference 8.

Scattering by water droplets (rain, fog, and snow) is treated by Gilbertson on pages 87 through 91 of Reference 27. According to Gilbertson, the scattering coefficient in rainfall is independent of wavelength in the visible to far infrared region of the spectrum and may be estimated by the equation

$$\sigma_{\text{rain}} = 0.248 r^{0.67} \tag{7-5}$$

where

and σ_{rain} = the scattering coefficient in km^{-1}

r = the rainfall rate in mm hr^{-1}

7.3 HORIZONTAL VISIBILITY

“Visibility range”, “visibility”, and “meterological range” are all names given for the horizontal distance R_v for which the contrast transmission of the atmosphere in daylight (C_R/C_0) is two per cent. C_0 is the inherent contrast of an object against the horizon sky and C_R is the apparent contrast at range R . Middleton (Reference 14, pps 68, 103 through 105) shows that the apparent contrast C_R reduces exponentially with range R according to $e^{-\sigma_v R}$. As indicated by the equations on Figure 7-5, the effective value of σ_v (the average attenuation coefficient for the visible spectrum— $0.38 \mu\text{m}$ through $0.72 \mu\text{m}$) depends as follows on the visibility range R_v

$$\sigma_v = 3.912/R_v \tag{7-6}$$

where the units of σ_v are determined by the units of R_v . Figure 7-5 provides a plot of equation 7-6 and also indicates approximately how R_v is affected by different kinds of weather.

7.4 CALCULATION OF ATMOSPHERIC TRANSMITTANCE IN THE 0.4- μm to 4- μm REGION

This section gives a simplified method for calculating the transmittance of the atmosphere over various path lengths at various altitudes for both horizontal and slant paths. Following this simple method are some calculated results for a standard model of a clear atmosphere.

The simplified calculation procedure uses Figures 7-6 and 7-7. Figure 7-6 gives the attenuation coefficient σ at sea level, the desired wavelength, and the condition of the atmosphere — the latter being identified either by the visibility range or by a general descriptive phrase on the figure. It will be noted that Figure 7-6 follows directly from the “total sea level” curve in

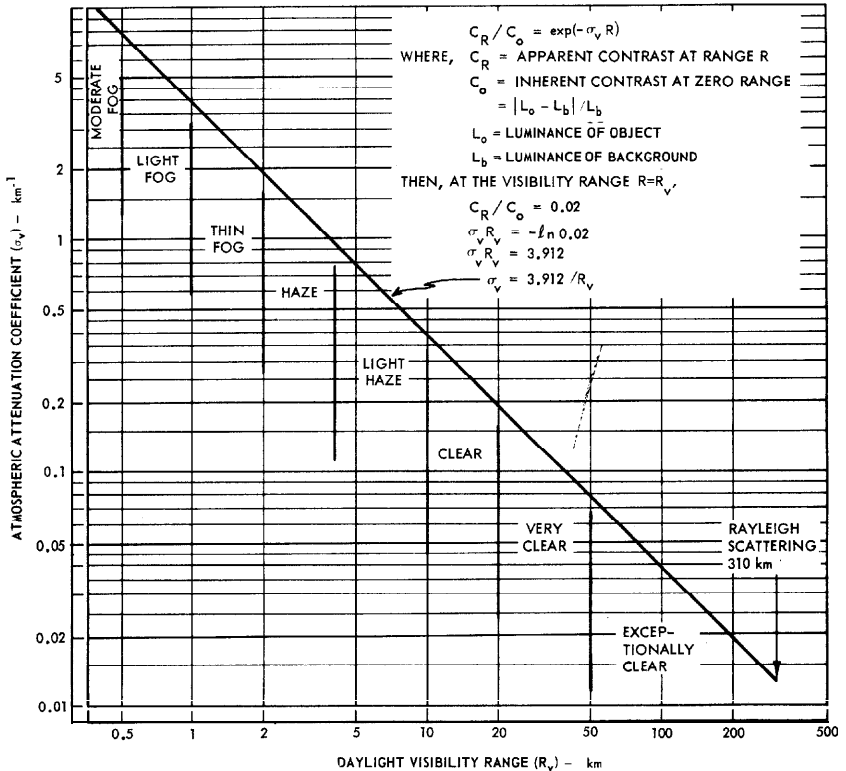


Fig. 7-5 Atmospheric attenuation coefficient for visible light-extinction coefficient-as a function of daylight visibility range-sometimes called "visibility" or "meteorological range."

Figure 7-3 (which applies to the standard clear atmosphere with a visibility of 23.5 km) corrected for the different visibilities by the factor $(\sigma_v R_v) / \sigma_v$ (23.5) which may be obtained from Figure 7-5. The line structure of atmospheric absorption due to water vapor, carbon dioxide, and other absorbers such as those shown in Figure 7-2 is therefore not accounted for in the simplified method.

Figure 7-7 provides a correction factor for σ as a function of altitude for either of two cases. The lower curve gives the correction factor for horizontal paths at specified altitudes, and the upper curve gives the correction factor

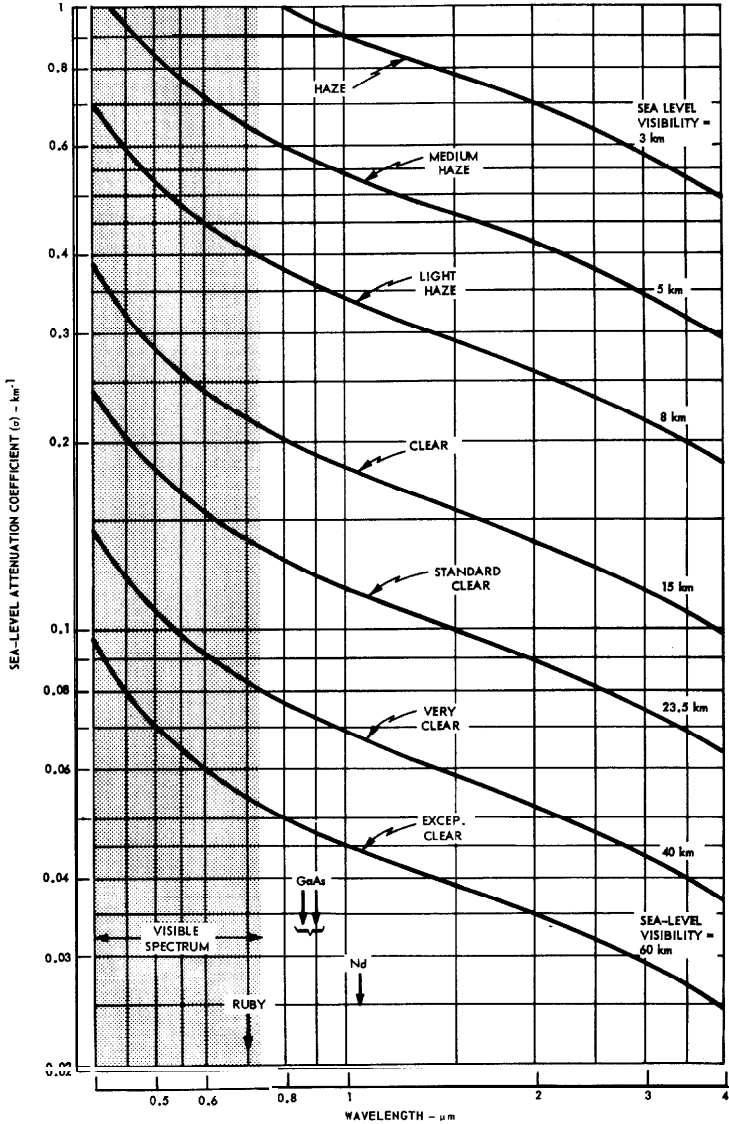


Fig. 7-6 Approximate variation of attenuation coefficient with wavelength at sea level for various atmospheric conditions. Neglects absorption by water vapor and carbon dioxide.

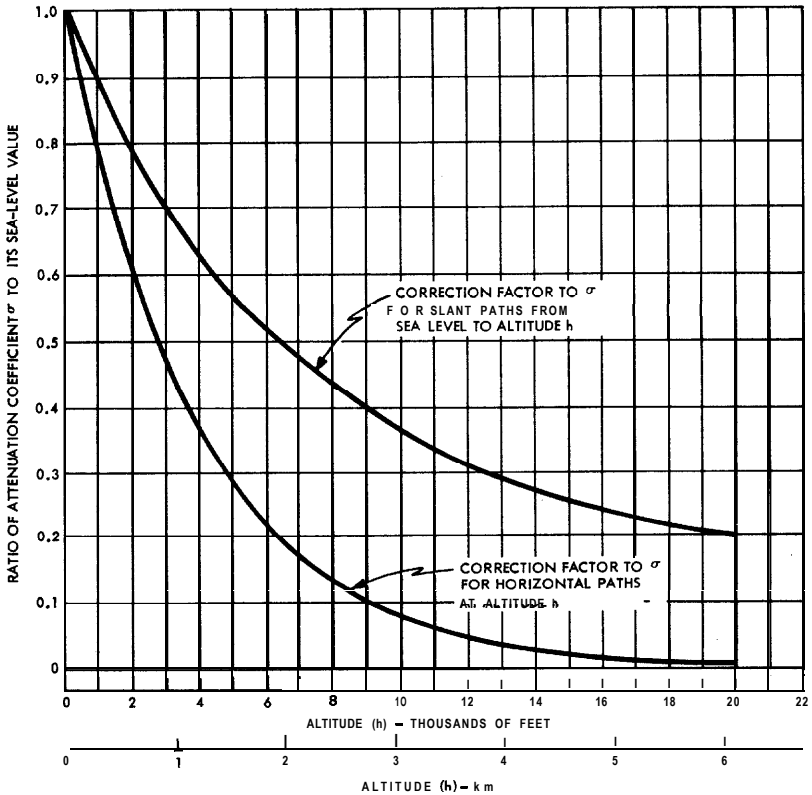


Fig. 7-7 Approximate ratio of attenuation coefficient to sea-level value for slant paths and horizontal paths. Neglects absorption by water vapor and carbon dioxide.

for slant paths from sea level to a specified altitude. The horizontal-path curve is taken from the standard clear atmosphere model of Table 7-4 in Reference 8 assuming that non-clear atmospheres have similar profiles. The slant-path curve is obtained by integrating an exponential approximation of the standard atmosphere over the appropriate paths and is presumably less accurate than the horizontal-path curve.

A better calculation for slant-path transmittance through the atmosphere can be obtained by using the data of Table 7-4 of Reference 8. Values of the

“extinction optical thickness” from the table have been used to calculate the atmospheric transmittance from a point at sea level to points at various altitudes and horizontal ranges from that point. The results are given in Figures 7-8 through 7-13, each corresponding to a specific radiation wavelength. These figures show contours of constant transmittance. Thus, if the horizontal range and altitude of a given point is known, the transmittance corresponding to the slant path can be estimated directly from the contours.

7.5 CALCULATION OF ATMOSPHERIC TRANSMITTANCE IN THE 8- μm to 14- μm INFRARED REGION

Estimates of atmospheric transmittance within the 8- μm to 14- μm “window” of the atmosphere (See Figure 7-2) are of particular interest for thermal imaging applications because most terrestrial objects, at temperatures of about 300 K, exhibit a peak in their spectral radiance within that window. See Figure 4-1 and 4-2. Scattering in the 8- μm to 14- μm region is considerably less than in the visible region of the spectrum and the principal attenuation mechanism is molecular absorption, particularly that due to water vapor.

Estimates of atmospheric transmittance on horizontal and slant paths may be made for this window as follows: first the water vapor concentration at sea level, p_0 , in $\text{g cm}^{-2} \text{ km}^{-1}$ (i.e., the precipitable cm of water vapor per kilometer of horizontal-path length) is determined from Figure 7-14 for the particular temperature and relative humidity conditions that apply at sea level. A correction factor, which is a function of altitude h , is then applied to p_0 for either horizontal or slant paths. The correction factor is obtained from the curves shown on Figure 7-15. These correction factors are based on exponential approximations of water-vapor versus altitude profiles. The corrections are variable as shown in Figure 7-15 between extremes corresponding to empirical height constants, h' , of about 3 km (10,000 feet) and 2 km (6,700 feet). For example, Figure 7-15 indicates that any slant path from 1.8 km (6,000 feet) to sea level should have somewhere between 0.66 and 0.75 of the total water content of an equivalent length horizontal path at sea level. Finally, after estimating the total water content pR (precipitable cm) on the horizontal or slant path of length R , one may estimate T_a for that path using the curves of Figure 7-16. (The supposition presented is that T_a depends primarily on the value of the product pR regardless of the value of p even though the curves of Figure 7-16 are based on transmittance data for various paths lengths for which $p = 0.92 \text{ cm km}^{-1}$).

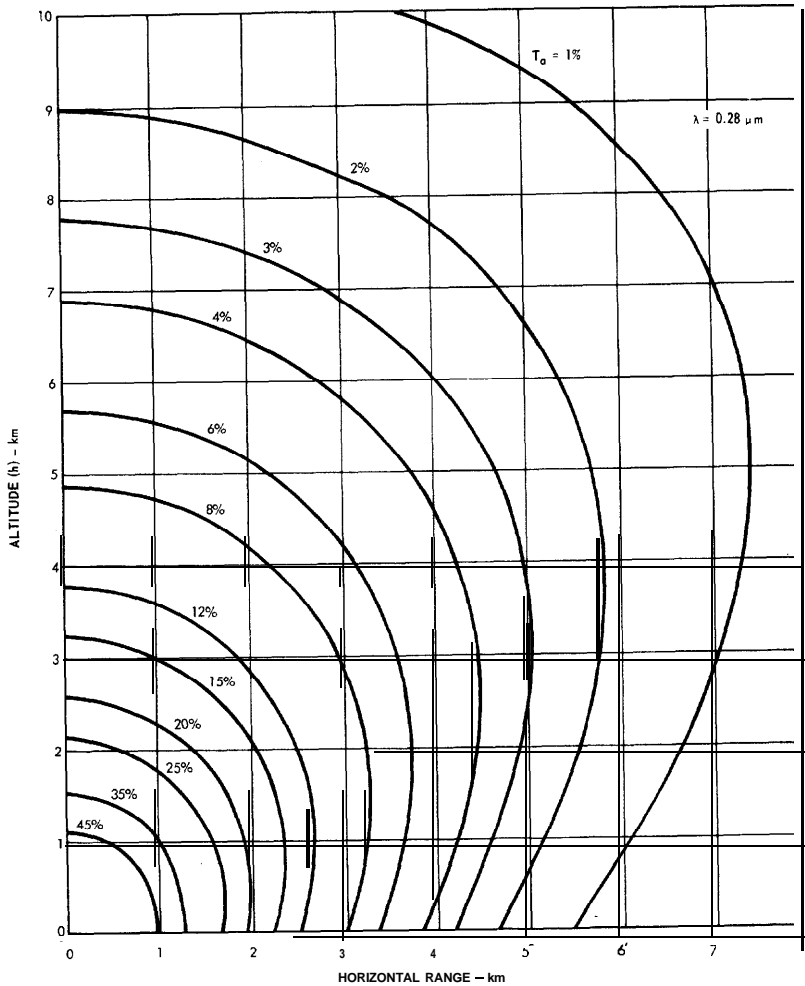


Fig. 7-8 Contours of constant atmospheric transmittance for radiation at $0.28 \mu\text{m}$ in a model clear standard atmosphere—visibility 23.5 km. Curves are plotted from data in Table 7-4 of Reference 8.

For comparison with the transmittance in the $8\text{-}\mu\text{m}$ to $14\text{-}\mu\text{m}$ band, values of transmittance for the $8\text{-}\mu\text{m}$ to $11.5\text{-}\mu\text{m}$ and the $8\text{-}\mu\text{m}$ to $13\text{-}\mu\text{m}$ bands are also shown on Figure 7-16.

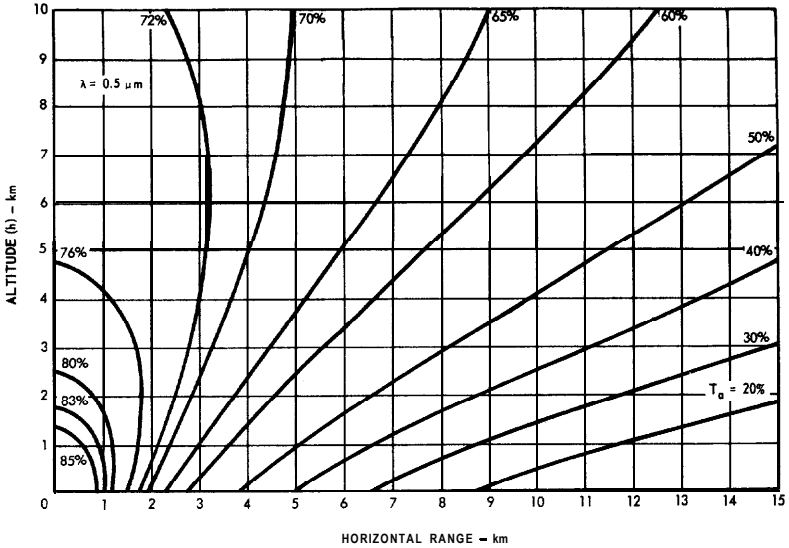


Fig. 7-9 Contours of constant atmospheric transmittance for radiation at 0.5 μm in a model clear standard atmosphere—visibility 23.5 km. Curves are plotted from data in Table 7-4 of Reference 8.

7.6 EFFECTS OF ATMOSPHERE ON IMAGING SENSOR PERFORMANCES

This section summarizes convenient analytical expressions derived by the Rand Corporation (Reference 28) for predicting the effects of atmospheric scattering and absorption on the performance of several optical sensors including the human eye, photographic systems, photoelectric devices, passive infrared sensors, and active gated-viewing systems.

The validity of these equations depends on the relation defined in equation 7-7 for the apparent radiance L' , of an object as observed at a horizontal range R .

$$L'_o = L_o T_a + L_q (1 - T_a) \tag{7-7}$$

where

L_o = the inherent zero-range radiance

T_a = the atmospheric transmittance of radiant flux over the path length R

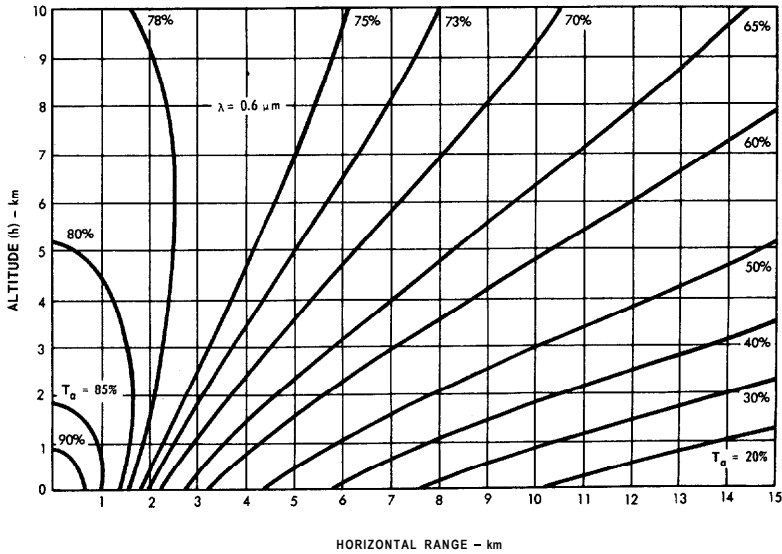


Fig. 7-10 Contours of constant atmospheric transmittance for radiation at $0.6 \mu\text{m}$ in a model clear standard atmosphere—visibility 23.5 km. Curves are plotted from data in Table 7-4 of Reference 8.

and L_q = the radiance of the horizon sky measured at an appropriate azimuth

The term $L_q(1-T_a)$ is an expression for the “path radiance” of the atmosphere that intervenes between the source and the sensor. Equation 7-7 is valid for cases of uniform h-radiance of the path and for a spatially homogeneous spectrum of particle sizes and types with negligible absorptions in the spectral band of interest. If the sensor is the human eye, or if sensor performance can be properly determined from photometric quantities, luminance values may be substituted for the radiometric values of L_o and L_q .

Not only is the apparent radiance of an object observed through the atmosphere different from its inherent radiance because of atmospheric transmittance and sky radiance effects but the apparent contrast of the object, and similar limits to visual preception, are also modified. The authors of Reference 28 urge the adoption of the term “**transference**” function

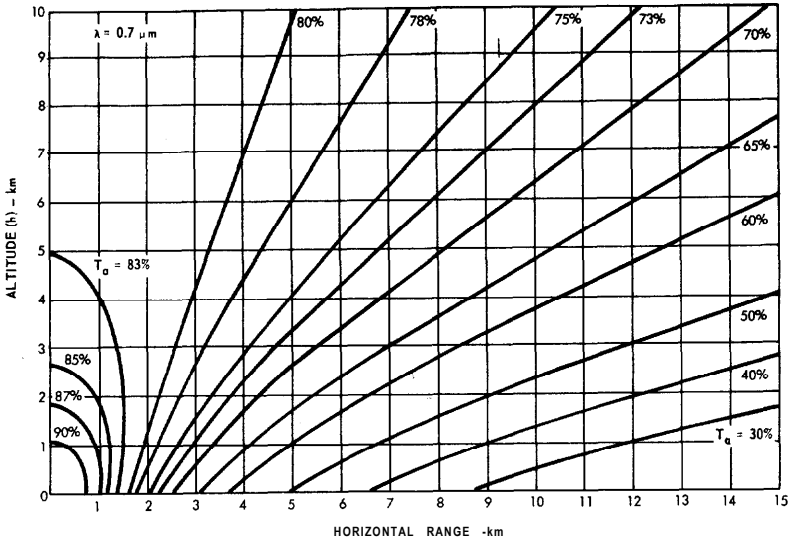


Fig. 7-11 Contours of constant atmospheric transmittance for radiation at $0.7 \mu\text{m}$ in a model clear standard atmosphere—visibility 23.5 km. Curves are plotted from data in Table 7-4 of Reference 8.

(symbol τ) to represent the ratio of an apparent optical property of an object (e.g., contrast) observed at some distance through the atmosphere to the same property observed at zero range.

The transference ratio, in certain cases, is simply equal to the transmittance of the atmosphere. For example, if the limiting noise in an observation is independent of path radiance, as is the case when the path radiance is time separated, the transference of the signal-to-noise ratio $\tau = T_a$. Similarly, if an object is viewed against the horizon sky, the transference of the contrast ratio is equal to T_a because the background is the same regardless of the range of the observation.

However, the transference of an optical property is in general a complicated function of the atmospheric transmittance and of the radiances of the object and of the background. For example, the transference of contrast (τ_c) can be developed as follows. Define the ratio of sky radiance to background radiance as

$$K = L_q/L_b \text{ radiometric or photometric units} \tag{7-8}$$

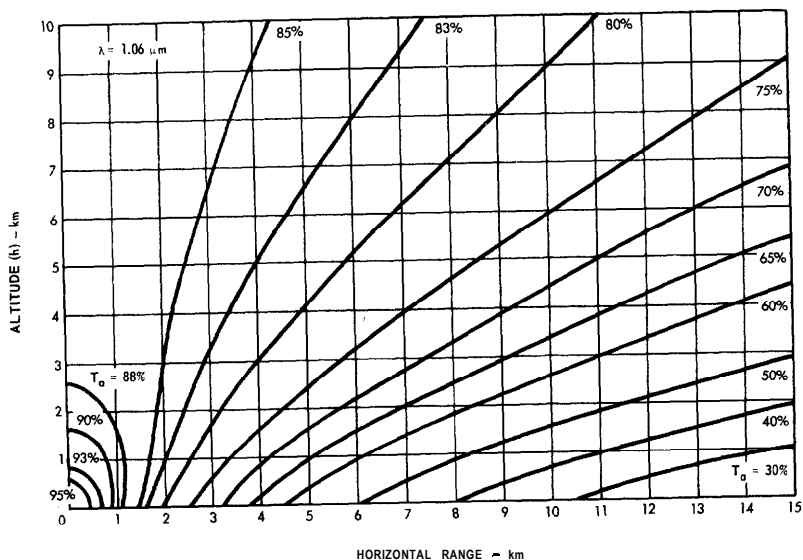


Fig. 7-12 Contours of constant atmospheric transmittance for radiation at $1.06 \mu\text{m}$ in a model clear standard atmosphere—visibility 25.0 km . Curves are plotted from data in Table 7-4 of Reference 8.

where

L_a = the radiance or luminance of the horizon sky measured at an appropriate azimuth

and

L_b = the inherent background radiance or luminance

Using equation 7-7, it may be shown that

$$\frac{|L'_o - L'_b|}{L'_b} = \tau_c \frac{|L_o - L_b|}{L_b}$$

where the transference of the contrast function τ_c is given by

$$\tau_c = \frac{1}{1 + \left(\frac{1 - T_a}{T_a} \right)} \quad (7-9)$$

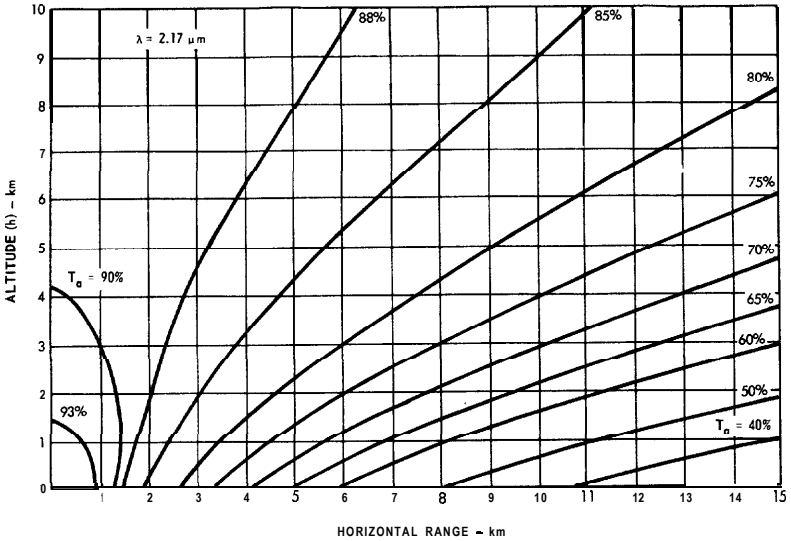


Fig. 7-13 Contours of constant atmospheric transmittance for radiation at $2.17 \mu\text{m}$ in a model clear standard atmosphere—visibility 23.5 km. Curves are plotted from data in Table 7-4 of Reference 8.

The primes (') on L_o and L_b indicate the observed radiances of the object and the background at the horizontal range R .

Figure 7-17 summarizes the expressions for the factors which limit the performance of each sensor type. The effect of the sky/background radiance or luminance ratio K on the transference τ_c for the contrast function is shown in Figure 7-18 for three values of T_a . The value of K for three types of terrain and a variety of atmospheric conditions is also shown on this figure. Figure 7-19 shows the transference τ_c as a function of T_a for three values of K .

7.7 ATMOSPHERIC BACKSCATTER – ARTIFICIAL ILLUMINATION

This section gives a convenient method for predicting the effects of atmospheric backscatter on image quality when an artificial source near the image sensor is used to illuminate a distant scene. The line-of-sight path through the atmosphere is taken to be horizontal so the atmospheric attenuation coefficient σ may be considered constant. It is also assumed that the separation between illuminator and imaging system is small compared to

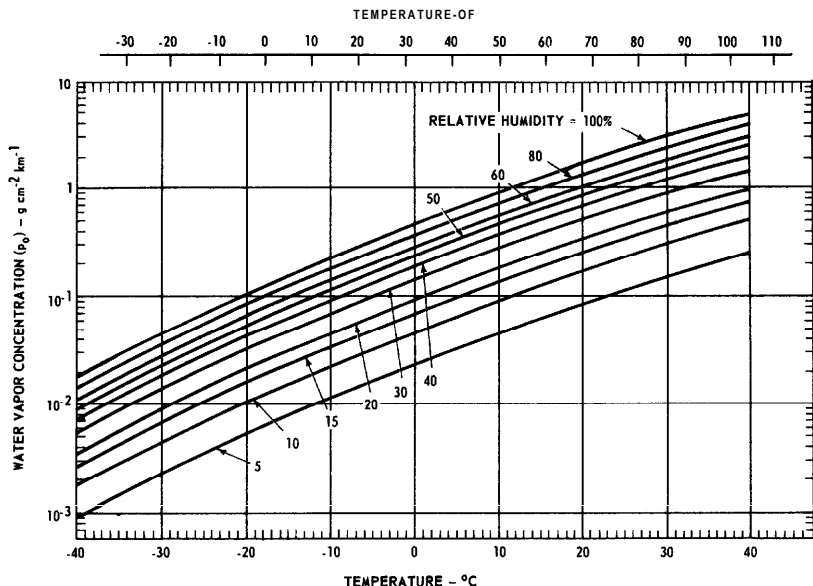


Fig. 7-14 Water vapor concentration per kilometer path length as a function of temperature and relative humidity.

the range to the nearest illuminated particles in the field of view. Then, the radiance of the atmosphere within the field of view is calculated by summing the backscatter contributions of all illuminated particles on the path between the sensor and the scene. The result is:

$$L_a = \frac{G \sigma^2 I}{2\pi} \int_{2\sigma R_{\min}}^{2\sigma R_{\max}} \frac{e^{-x}}{x^2} dx \quad (7-9)$$

where,

- L_a = radiance of atmospheric backscatter ($\text{W m}^{-2} \text{sr}^{-1}$)
- I = radiant intensity of illuminator (W sr^{-1})
- σ = atmospheric attenuation coefficient (m^{-1})
- G = backscatter gain of atmospheric particles relative to isotropic scatterers (dimensionless). A suggested value, for $0.4 \mu\text{m} < \lambda < 1 \mu\text{m}$, is 0.24 (Reference 29).

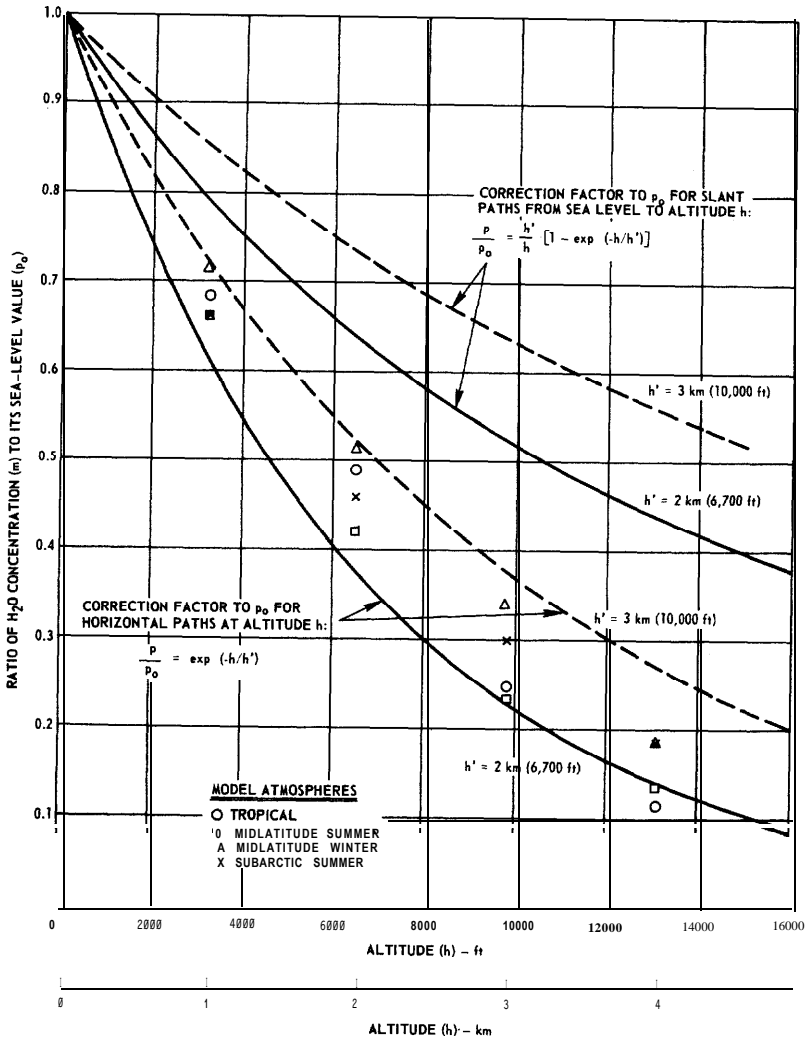


Fig. 7-15 Exponential approximations for the ratios of water vapor concentration p to sea-level values p_0 for slant paths and horizontal paths. Points shown are for the model atmospheres shown on the figure.

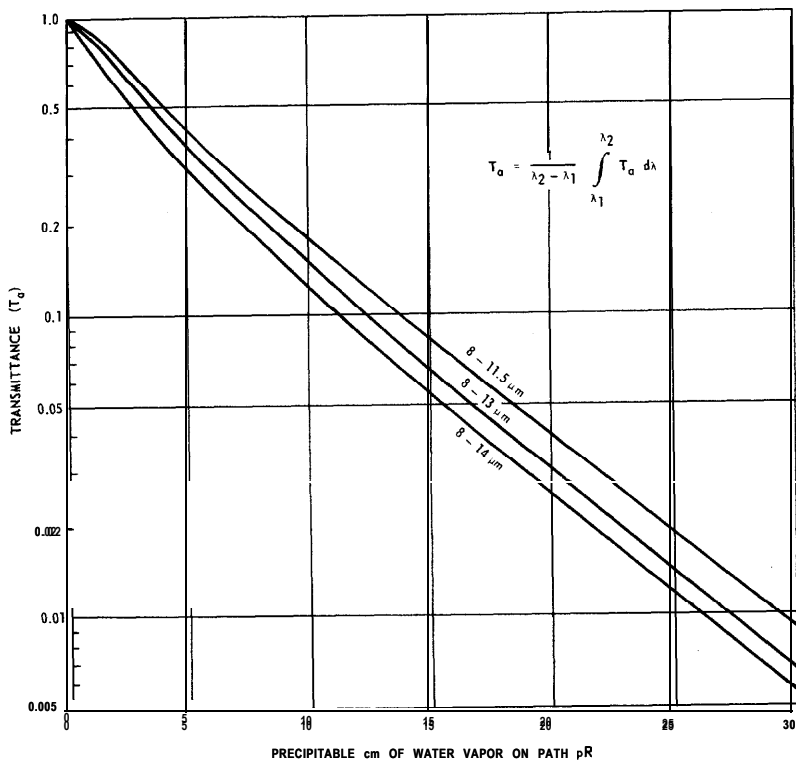


Fig. 7-16 Infrared band transmittances of the atmosphere as functions of the total number of precipitable cm of water vapor on the path.

- R_{\min} = range from imaging system (and from illuminator) to the nearest illuminated particles in the field-of-view (m).
 R_{\max} = range from imaging system (and from illuminator) to the scene being imaged (m)
 x = integration variable

The integral in equation 7-9 can be handled conveniently as follows. Make the substitution

$$\int_z^{\infty} \frac{e^{-x}}{x^2} dx = \frac{1}{z} E_2(z) \quad (7-10)$$

Factor	Definition and Equivalents	Application
T_a	Transmittance of radiant power in the spectral region of interest = Transference of signal-to-noise ratio when the limiting noise is independent of path radiance or when path radiance is time separated = Transference of contrast of object seen against the horizon sky (Sky/background ratio $K = 1$)	Passive infrared Gated viewing systems Aircraft spotter
τ_c	Transference of the contrast function (determines the performance of all contrast-limited sensors) $= \frac{1}{1 + K \left(\frac{1 - T_a}{T_a} \right)}$	$\frac{ L_o - L_b }{L_b}$ Vision at daylight levels Photographic systems

Fig. 7-1 7 Summary of atmospheric transmittance and transference factors (Adapted from Reference 28).

where, with the substitution $t = x/z$,

$$E_2(z) = \int_1^{\infty} \frac{e^{-zt}}{t^2} dt \tag{7-11}$$

is one of a family of “Exponential Integrals” (Reference 30). Combine equations 7-9 and 7-10 to obtain

$$L_a = \frac{G\sigma I}{4\pi} \left[\frac{E_2(2\sigma R_{min})}{R_{min}} - \frac{E_2(2\sigma R_{max})}{R_{max}} \right] \tag{7-12}$$

Equation 7-1 2 may be applied conveniently with the aid of the graph of $E_2(z)$ plotted in Figure 7-20 as a function of z .

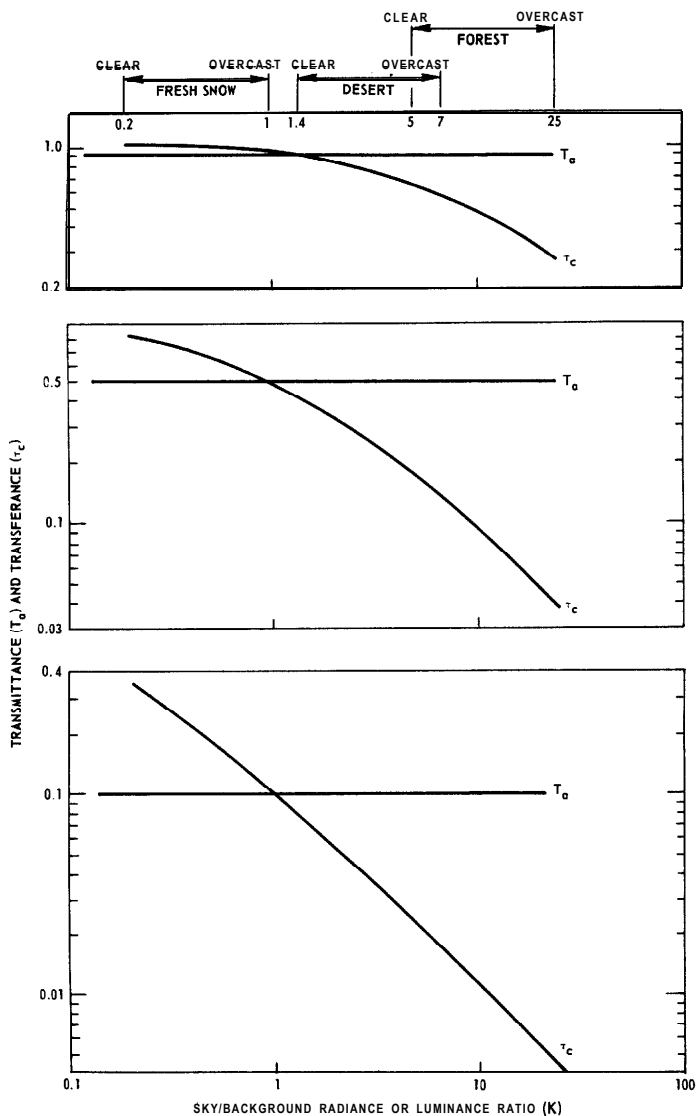


Fig. 7-18 Transmittance T_a and transference τ_c as a function of sky/background radiance or luminance ratio for three values of T_a (Adapted from Reference 28).

Factor	Definition and Equivalents	Application
T_a	Transmittance of radiant power in the spectral region of interest = Transference of signal-to-noise ratio when the limiting noise is independent of path radiance or when path radiance is time separated = Transference of contrast of object seen against the horizon sky (Sky/background ratio $K = 1$)	Passive infrared Gated viewing systems Aircraft spotter
τ_c	Transference of the contrast function (determines the performance of all contrast-limited sensors) $= \frac{1}{1 + K \left(\frac{1 - T_a}{T_a} \right)}$	$\frac{ L_o - L_b }{L_b}$ Vision at daylight levels Photographic systems

Fig. 7-1 7 Summary of atmospheric transmittance and transference factors (Adapted from Reference 28).

where, with the substitution $t = x/z$,

$$E_2(z) = \int_1^{\infty} \frac{e^{-zt}}{t^2} dt \tag{7-11}$$

is one of a family of “Exponential Integrals” (Reference 30). Combine equations 7-9 and 7-10 to obtain

$$L_a = \frac{G\sigma I}{4\pi} \left[\frac{E_2(2\sigma R_{min})}{R_{min}} - \frac{E_2(2\sigma R_{max})}{R_{max}} \right] \tag{7-12}$$

Equation 7-1 2 may be applied conveniently with the aid of the graph of $E_2(z)$ plotted in Figure 7-20 as a function of z .

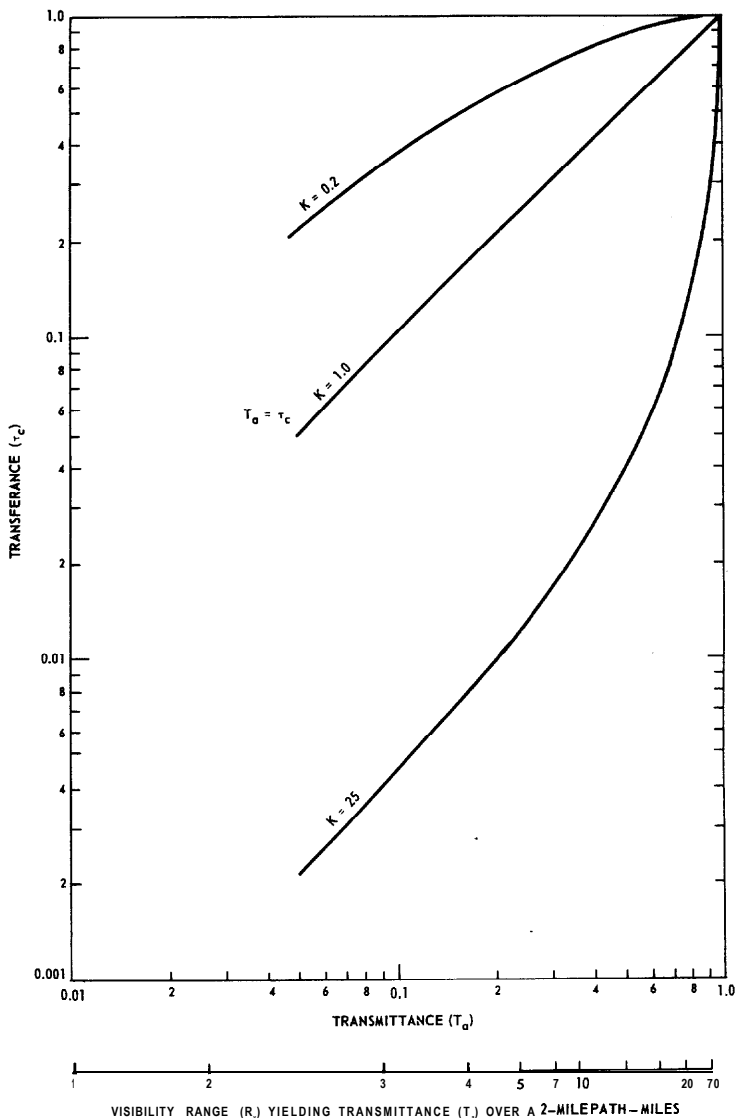


Fig. 7-19 Transference τ_c as a function of transmittance T_a for three values of sky/background radiance or luminance ratio K (Adapted from Reference 28).

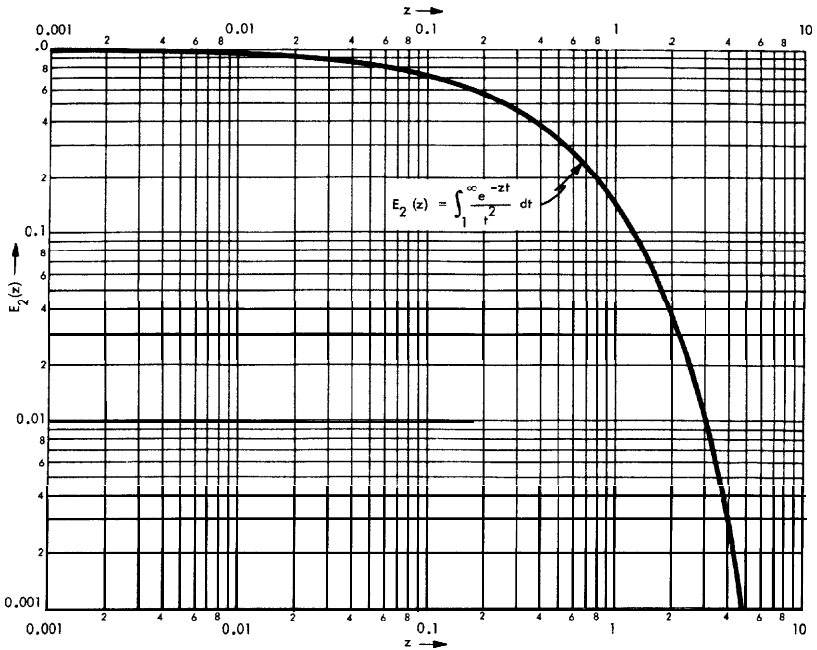


Fig. 7-20 Plot of the exponential integral $E_2(z)$ convenient for calculating atmospheric backscatter effects when artificial illuminators are used.

Example. An example is given of the use of equation 7-12 and Figure 7-20 in predicting some effects of atmospheric backscatter on image quality. Assume the following parameters apply:

- λ = illuminator wavelength = 850 nm
- σ = 0.126 km^{-1} (horizontal, path at sea level through standard clear atmosphere; see Figure 7-6)
- ρ_t = target reflectance = 0.4
- ρ_b = scene background reflectance = 0.6
- G = 0.24
- R_{\min} = 14.3 m
- R_{\max} = 1000 m

First, the radiance L_a due to the atmosphere backscatter alone is evaluated. The factor $I/\pi R^2_{max}$ is kept separate because in the final computation of contrast it will divide out. Use of equation 7-12 and Figure 7-20 gives

$$\begin{aligned}
 L_a &= \left[\frac{I}{\pi R^2_{max}} \right] \left[\frac{G \sigma R_{max}}{4} \right] \left[\frac{R_{max}}{R_{min}} E_2(2\sigma R_{min}) - E_2(2\sigma R_{max}) \right] \\
 &= \left[\frac{I}{\pi R^2_{max}} \right] \left[\frac{(.24)(.126 \times 10^{-3})(10^3)}{4} \right] \left[\frac{1000}{14.3} E_2(.0036) - E_2(.252) \right] \\
 &= \left[\frac{I}{\pi R^2_{max}} \right] (.00757) [70(.98) - .51] \\
 &= .515 \left[\frac{I}{\pi R^2_{max}} \right]
 \end{aligned}$$

Next, the following comparisons are made:

	<u>With No Atmosphere</u>	<u>With Atmosphere</u>
apparent target radiance	$L'_o = \frac{I\rho_t}{\pi R^2_{max}}$	$L'_o = L_a + \frac{I\rho_t e^{-2\sigma R_{max}}}{\pi R^2_{max}}$ $= \left[\frac{I}{\pi R^2_{max}} \right] [0.515 + (0.4)(0.6)]$
apparent background radiance	$L'_b = \frac{I\rho_b}{\pi R^2_{max}}$	$L_b = L_a + \frac{I\rho_b e^{-2\sigma R_{max}}}{\pi R^2_{max}}$ $= \left[\frac{I}{\pi R^2_{max}} \right] [0.515 + (0.4)(0.6)]$

apparent
target-to
background
contrast
(see Figure
7-21)

$$\begin{aligned}
 C &= \left| \frac{L'_o}{L'_b} - 1 \right| & C &= \left| \frac{L'_o}{L'_b} - 1 \right| \\
 &= \left| \frac{\rho_t}{\rho_b} - 1 \right| & &= \left| \frac{0.515 + 0.24}{0.515 + 0.36} - 1 \right| \\
 &= \left| \frac{0.4}{0.6} - 1 \right| & &= \left| \frac{0.755}{0.875} - 1 \right| \\
 &= 0.33 & &= 0.137
 \end{aligned}$$

One concludes for this **example** that, at a maximum range or 1000 m, the apparent target-to-background contrast is reduced to 41% of its value at the scene (0.33) by backscatter from the standard clear atmosphere. (Repeating the calculation for a range of 3000 m shows a reduction of apparent contrast to less than 6% of its value at the scene.)

References

8. Valley, S.L., HANDBOOK OF GEOPHYSICS AND SPACE ENVIRONMENTS, 'Air Force Cambridge Research Laboratories, Office of Aerospace Research, U.S. Air Force, 1965. Also published by McGraw-Hill Book Co., New York, N.Y., 1965.
14. Middleton, W.E.K., VISION THROUGH THE ATMOSPHERE, University of Toronto Press, Toronto, Canada, 1958.
23. Carpenter, R.O'B. and Chapman, R.M., EFFECTS OF NIGHT SKY BACKGROUNDS ON OPTICAL MEASUREMENTS, GCA Technical Report 61-23-A, Geophysics Corporation of America, Bedford; Mass., March 1959.
24. Van de Hulst, H.C., LIGHT SCATTERING BY SMALL PARTICLES, John Wiley and Sons, Inc., New York, N.Y., 1957.
25. INFRARED COMPONENTS, Brochure No. 67CM, Santa Barbara Research Center, Goleta, Ca., 1967.
26. Baum, W.A., ATTENUATION OF ULTRAVIOLET LIGHT BY THE LOWER ATMOSPHERE, **PhD** Thesis, California Institute of Technology, Pasadena, Ca., 1950.

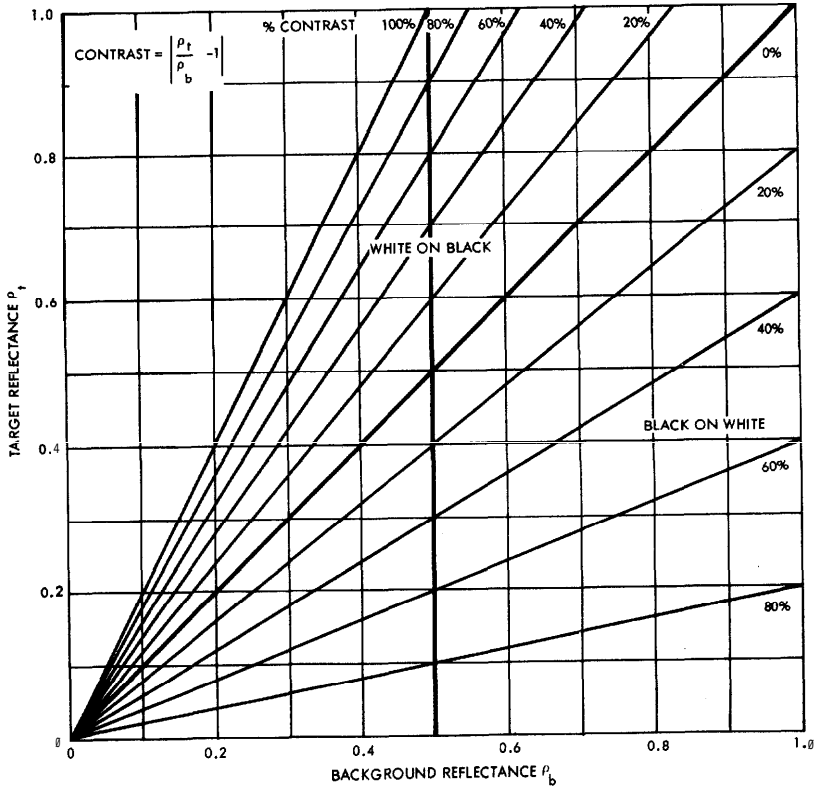


Fig. 7-21 Relationship of contrast to the reflectances of target and background.

27. Gilbertson, D.K., STUDY OF TACTICAL ARMY AIRCRAFT LANDING SYSTEMS (TAALS), Technical Report **ECOM-03367-4**, AD-477-727, Defense Documentation Center, Alexandria, Va., Jan. 1966.

28. Bailey, H.H. and Mundie, L.G., THE EFFECTS OF ATMOSPHERIC SCATTERING AND ABSORPTION ON THE PERFORMANCE OF OPTICAL SENSORS, Memorandum **RM-5938-PR**, RAND Corporation, Santa Monica, Ca., March 1969.

29. Deirmendjian, D., "Scattering and Polarization Properties of Water Clouds and Hazes in the Visible and Infrared," **APPLIED OPTICS**, Vol. 3, No. 2 Fig. 4, Feb. 1964.

30. HANDBOOK OF MATHEMATICAL FUNCTIONS, U.S. Dept. of Commerce, National Bureau of Standards, Applied Mathematics Series, 55, 1964; fifth printing, Aug. 1966. Contains a discussion of $E_2(z)$ and a tabulation of its values.
31. Tatarski, V.I., WAVE PROPAGATION IN A TURBULENT MEDIUM, McGraw-Hill Book Co., New York, N.Y., 1961.
32. Tatarski, V.I., THE EFFECTS OF THE TURBULENT ATMOSPHERE ON WAVE PROPAGATION, Translated for NOAA by Israel Program for Scientific Translations, Jerusalem, 1971 Available from U.S. Dept. of Commerce, NTIS, Springfield, Va.
33. Lawrence, R.S. and Strohbehn, J.W., "A Survey of Clear-Air Propagation Effects Relevant to Optical Communications," PROC. IEEE, Vol. 58, Oct. 1970.
34. Kerr, J.R., Titterton, P.J., Kraemer, A.R., and Cooke, CR., "Atmospheric Optical Communication Systems," PROC. IEEE, Vol. 58, Oct. 1970.
35. Brookner, E. "Atmospheric Propagation and Communication Channel Model for Laser Wavelengths," IEEE TRANS. COMM. TECHNOLOGY, Vol. COM-18, Aug. 1970.
36. Wyngaard, J.C., Izumi, Y., and Collins, S.A., "Behavior of the Refractive-Index-Structure Parameter near the Ground," J. OPT. SOC. AM., Vol. 60, Dec. 1971.
37. De Wolf, D.A., EFFECTS OF TURBULENCE INSTABILITIES ON LASER PROPAGATION, RCA Third Quarterly Report TR-72-119 to Rome Air Development Center, Griffiss AFB, N.Y., Apr. 1972.

Section 8

Detection, Resolution, and Recognition

A common problem in electro-optics is the detection and resolution of detail in the presence of noise. In Sections 8.1 and 8.2, two approaches are considered for detecting pulses in the presence of noise. The first analyzes detection of signal pulses in white noise. The second considers detection of signal pulses in quantum noise. The first approach is applicable when large numbers of photons are available and the fluctuations in the signal are small compared to the additive noise. The second approach is used when the signal and the noise are both characterized by low photo-electron generation rates. Section 8.3 relates image resolution to modulation transfer function (MTF) and to equivalent rectangular passband (Ne). Section 8.4 considers some aspects of visual interpretation of displays. In Section 8.5 the Rand Corporation's model for target detection/recognition is given.

8.1 PULSE DETECTION IN WHITE NOISE

The problem treated in this section is that of detecting a rectangular signal pulse of duration τ immersed in white noise. (See References 38 and 39). A threshold detector is used. The actual pulse shape is not critical. The signal plus noise is passed through a matched filter (or correlator) having a bandwidth $B = 1/2\tau$. For clarity, Figure 8-1 illustrates separately the effects of the matched filter on the rectangular signal pulse and on the white noise. At the filter output, the signal current component is denoted i_s , a triangular pulse of peak amplitude I_s (the same amplitude as the rectangular input

pulse). The filter output noise current i_n is gaussian with rms value I_n given by

$$\left. \begin{aligned} I_n &= \sqrt{i_n^2} \\ &= \sqrt{WB} \\ &= \sqrt{W/2\tau} \end{aligned} \right\} \quad (8-1)$$

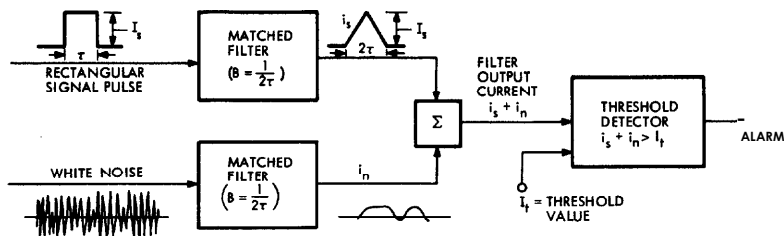


Fig. 8-1 Schematic representation of threshold detection process.

where,

$$\begin{aligned} W &= \text{spectral "power density" (A}^2 \text{ Hz}^{-1}\text{) of the input white noise.} \\ B &= 1/2\tau \\ &= \text{noise bandwidth of matched filter (Hz)} \\ \tau &= \text{input pulse duration(s)} \end{aligned} \quad (8-2)$$

The average false alarm rate $\overline{\text{FAR}}$ is the average number of times per second the output noise current i_n exceeds the threshold value I_t of the detector. This rate is given by Rice (equations 3.3-12 and 3.3-14 of Reference 40) as

$$\overline{\text{FAR}} = \frac{1}{2\tau\sqrt{3}} e^{-I_t^2/2I_n^2} \quad (8-3)$$

which decreases rapidly as the threshold value I_t is raised.

When a signal is present, the probability that it will be detected P_d is very nearly the probability that the signal plus noise exceeds the threshold I_t at the instant of signal peak, i.e.,

$$\left. \begin{aligned}
 P_d &= P(i_s + i_n > I_t) \\
 &\cong P(I_s + i_n > I_t) \\
 &\cong P(i_n > I_t - I_s)
 \end{aligned} \right\} \tag{8-4}$$

$$\cong \frac{1}{\sqrt{2\pi I_n}} \int_{I_t - I_s}^{\infty} \exp(-i_n^2 / 2I_n^2) di_n \tag{8-5}$$

$$P_d \cong \frac{1}{\sqrt{\pi}} \int_{\frac{I_t - I_s}{\sqrt{2} I_n}}^{\infty} \exp(-i_n^2 / 2I_n^2) d\left(\frac{i_n}{\sqrt{2} I_n}\right) \tag{8-6}$$

$$\cong \frac{1}{2} \left(1 + \operatorname{erf}\left(\frac{I_s - I_t}{\sqrt{2} I_n}\right) \right) \tag{8-7}$$

If the threshold I_t has been set according to equation 8-3 to achieve a given false alarm rate, then the peak-signal-to-rms-noise-current ratio I_s/I_n required to obtain a specified probability of detection P_d may be found from equation 8-7. The relations are shown graphically in Figure 8-2. Equation 8-7 is plotted in Figure 8-3 as a function of I_s/I_n for selected values of the parameters τ (FAR).

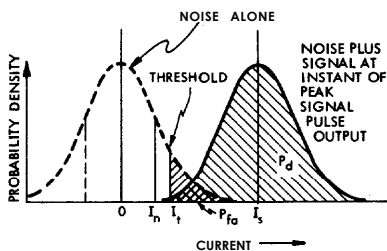


Fig. 8-2 Graphical relations between probability of detection P_d , probability of false alarm P_{fa} , and current threshold I_t .

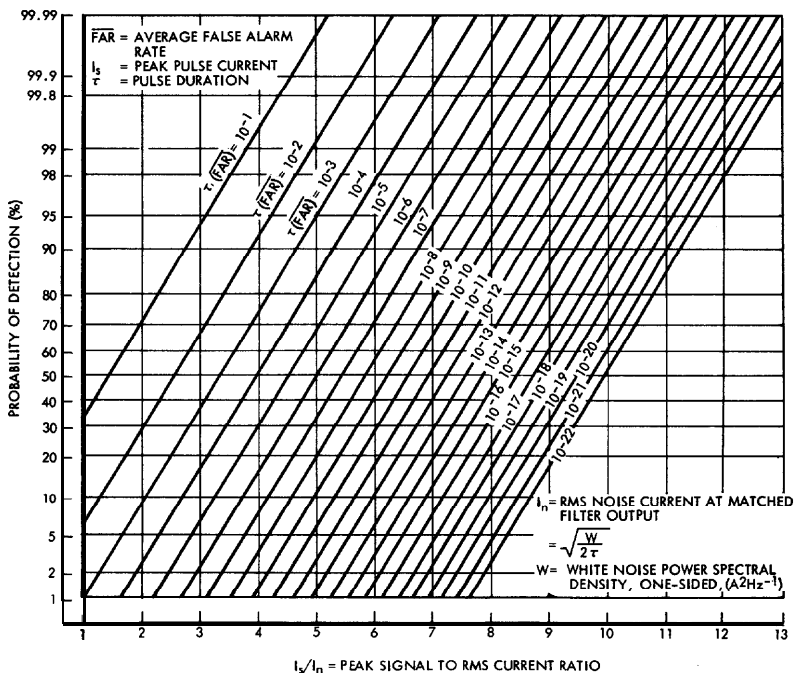


Fig. 8-3 Probability of detecting a rectangular pulse in white noise.

Example. A laser rangefinder has a pulse width τ of $0.1 \mu\text{s}$ and operates to a maximum range R_{max} of 10 km. If a matched filter and threshold detection are used, what signal-to-noise ratio and what threshold-to-noise ratio are required to obtain a probability of detection of 99.9% and a false detection no more than one time per thousand pulses?

In order to range to 10 km, the rangefinder must be gated open for a total interval of

$$\begin{aligned} \frac{2R_{\text{max}}}{c} &= \frac{2(10,000)}{3 \times 10^8} \\ &= 67 \times 10^{-6} \text{ s} \end{aligned}$$

where c is the velocity of light. The average false alarm rate $\overline{\text{FAR}}$ is thus established as once in a thousand of these $67\text{-}\mu\text{s}$ intervals, or

$$\begin{aligned} \text{FAR} &= \frac{1}{1000 \times 67 \times 10^{-6}} \\ &= 15 \text{ s}^{-1} \end{aligned}$$

Hence,

$$\begin{aligned} \tau(\overline{\text{FAR}}) &= (1 \times 10^{-7})(15) \\ &= 1.5 \times 10^{-6} \end{aligned}$$

With this value of $\tau(\overline{\text{FAR}})$ and a detection probability P_d of 99.9%, Figure 8-3 yields a peak-signal-to-rms-current ratio (I_s/I_n) of 8.1.

The required threshold-to-noise setting I_t/I_n is obtained from equation 8-3 and may be solved as follows:

$$\begin{aligned} I_t/I_n &= \sqrt{-2 \ln (2\sqrt{3} \tau(\overline{\text{FAR}}))} \\ &= \sqrt{-2 \ln (2\sqrt{3} \times 1.5 \times 10^{-6})} \\ &= 4.93 \end{aligned}$$

Note this latter ratio could also have been read directly from Figure 8-3 by realizing that $P_d = 50\%$ where $I_s/I_n = I_t/I_n$.

Note that the rms noise current I_n , dependent upon white noise power spectral density W and the filter noise bandwidth B , is found using equation 8-1.

8.2 PULSE DETECTION IN QUANTUM NOISE

When the signal and noise are small, the arrival of photons in a given small time interval is a small number and independent of the arrival of photons in any other small time interval. This condition is often the case, for example, when a photomultiplier detector is used in a laser range finder and there is low background noise. In such cases one may assume a Poisson distribution for evaluating the probability that in a certain time interval the number n of photons arriving or the number of photoelectrons generated or events occurring will be exactly equal to r ; namely

$$P(n = r) = \frac{e^{-r} (r)^r}{r!} \tag{8-8}$$

where \bar{n} is the expected (average) number for that time interval. If the actual number n of such events in that interval is counted, then a threshold number n_t can be established as a criterion for deciding whether a signal pulse is present or not. It follows from equation 8-8 that the probability of at least n_t events is

$$P(n \geq n_t) = \sum_{r=n_t}^{\infty} \frac{e^{-\bar{n}} (\bar{n})^r}{r!} \quad (8-9)$$

Equation 8-9 is plotted in Figures 8-4 and 8-5 in two parts (from data in Reference 41); Part I, shown in Figure 8-4, estimates the probability of detection $P(n \geq n_t)$ as a function of the threshold number n_t for expected counts n of signal plus noise events ranging between $0.2 < n < 35$ per time interval. Part 2, shown in Figure 8-5, estimates the probability of false alarm $P(n \geq n_t)$ as a function of the threshold number n_t for expected counts n of noise events only ranging between $10^{-7} < \bar{n} < 5$ per time interval.

Example. When no signal is present, an average of two events occurs per observation interval while sixteen occur on the average when a signal is present. If a false alarm rate of about one per ten thousand observations or less is allowable, where should the threshold be set and what is the detection probability?

From Figure 8-5, a threshold n_t of 9.5 events or higher will meet the false alarm rate specification. Setting n_t to 10 (next higher integer) and consulting Figure 8-4 shows that the detection probability is 0.955.

8.3 MTF (MODULATION TRANSFER FUNCTION) AND CTF (CONTRAST TRANSFER FUNCTION)

The MTF is a measure of the resolution of an imaging system sufficiently general to apply not only to the optics, but also to image intensifiers, camera tubes, video amplifiers and displays as well. The MTF is the sine-wave spatial-frequency amplitude response. It equals unity for sufficiently low spatial frequencies. Spatial frequency (N) refers to the number of cycles per unit length. The main usefulness of the MTF is that it permits cascading the effects of the several major components of a system in determining a measure of resolution of the overall system. The MTF of the overall system at a given spatial frequency is the product of the MTF's of the elements.

The CTF is the square-wave spatial-frequency amplitude response. Unlike MTF's, CTF's cannot be cascaded to evaluate overall system response. Amplitude response in this form, however, is frequently quoted because it is easier to measure. Either form of response can be converted to the other as shown in equations 8-10 and 8-11,

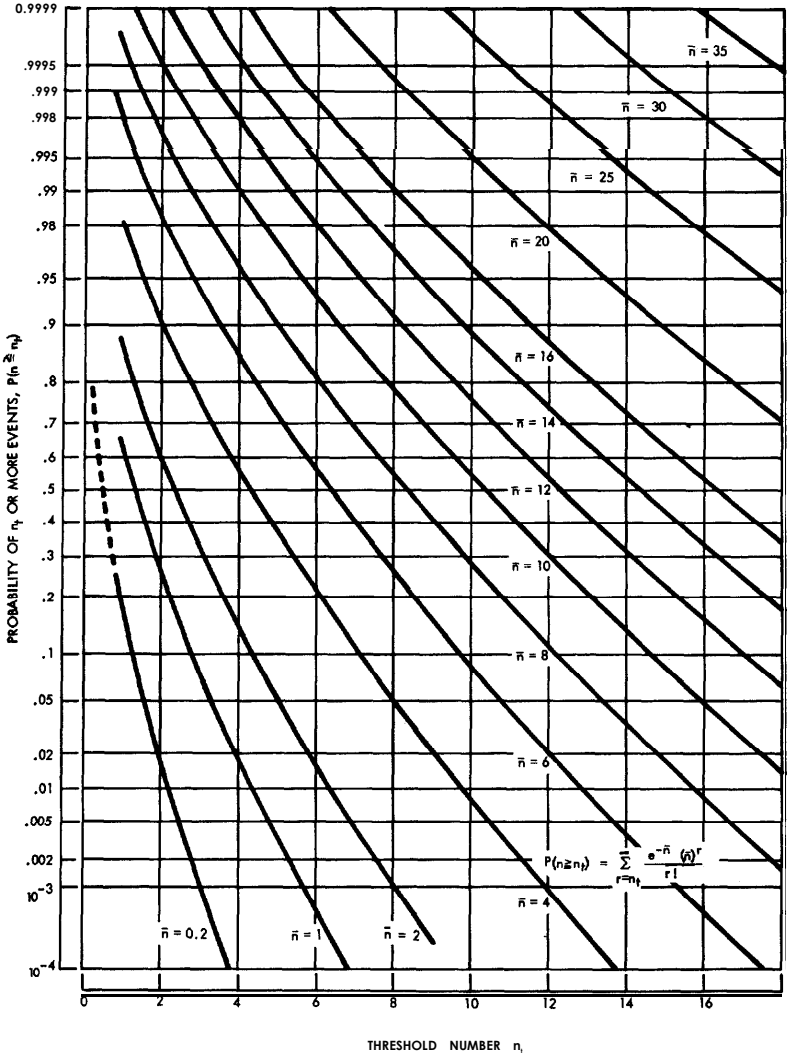


Fig. 8-4 Probability of n_t or more random events with Poisson distribution when the expected or mean number of events is \bar{n} as a function of the threshold number n_t (Part 1 of 2).

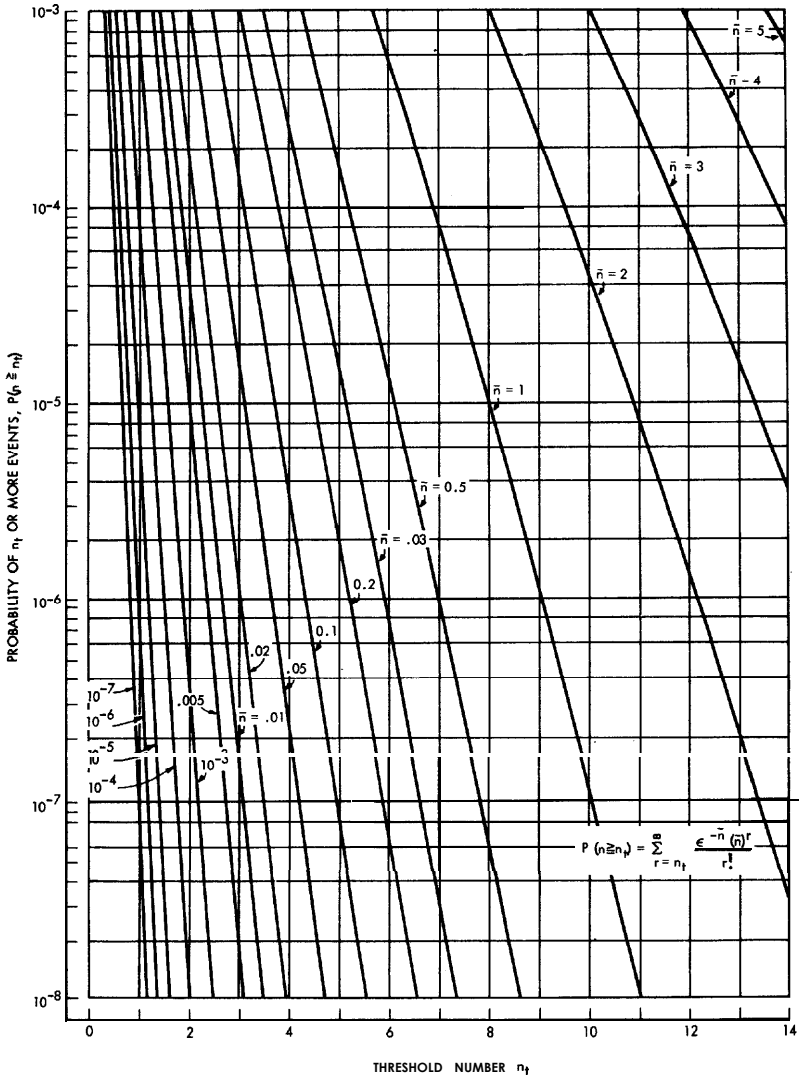


Fig. 8-5 Probability of n_t or more random events with Poisson distribution when the expected or mean number of events is \bar{n} as a function of the threshold number n_t . Curves for $10^{-7} < \bar{n} < 10^{-4}$ are approximate (Part 2 of 2).

$$MTF = M(N) = \frac{\pi}{4} \left[C(N) + \frac{C(3N)}{3} - \frac{C(5N)}{5} + \frac{C(7N)}{7} \dots \right] \quad (8-10)$$

The term involving C (9N) is omitted in equation 8-10 because it is zero.

$$CTF = C(N) = \frac{4}{\pi} \left[M(N) - \frac{M(3N)}{3} + \frac{M(5N)}{5} - \frac{M(7N)}{7} + \frac{M(9N)}{9} \dots \right] \quad (8-11)$$

Figure 8-6 presents a useful set of computations for a system with a Gaussian-shaped MTF. The MTF is normalized so that the response is 1% at a spatial frequency of 100. N_c is the equivalent rectangular **passband** (Reference 42) according to the formula definition given in Figure 8-6. The usefulness of the N_c measure is its ability to express the overall response by one number. A further advantage is that the subjective appearance of imagery from systems with equal N_c but differing limiting resolution tends to be very similar. N_c' is the equivalent rectangular **passband** for spatial frequencies from 0 to N as shown in Figure 8-6.

Degradation of MTF by Various Forms of Image Motion. Angular stabilization errors can produce smear and degrade camera resolution. The effects of four types of high-frequency (e.g. vibration) errors can be calculated from equation 8-12.

$$\bar{I}_x = \frac{1}{t_p} \int_0^{t_p} \sin \left(2\pi N \left[X + f(t) \right] \right) dt \quad (8-12)$$

where,

- \bar{I}_x = average intensity level at location X
- t_p = exposure time
- N = spatial frequency

$f(t)$ = a type of image-motion disturbance (periodic triangular, periodic sine wave, periodic square wave, Gaussian random displacement).

Normalized Spatial Frequency (N) See Note	Normalized MTF Sine-Wave * Response M(N)	Normalized CTF Square-Wave Response C(N)	N'_e Equivalent Rectangular Pass Band To Spatial Frequency N	$\frac{N}{N_e}$
0	100	100	0	0
2	99.8	100	2.0	0.0685
5	98.9	100	5.0	0.171
10	95.5	100	9.7	0.342
20	83.2	98.0	17.8	0.685
29.2	67.5	84.8	23.1	1
30	66.1	83.2	23.4	1.03
40	47.9	61.0	26.7	1.37
50	31.5	40.2	28.3	1.71
60	19.1	24.3	28.9	2.05
70	10.5	13.4	29.1	2.40
80		6.6	29.2	2.74
80.7	5.0	6.4	29.2	2.76
87.2	3.0	3.8	29.2	2.99
92.2	2.0	2.5	29.2	3.16
100	1.0	1.3	29.2	3.42

$$\text{MTF} = \exp(-4.605 \times 10^{-4} N^2)$$

$$N_e = \int_0^{\infty} (\text{MTF})^2 dN$$

$$N'_e = \int_0^N (\text{MTF})^2 dN$$

NOTE: Normalized spatial frequency (N) is usually expressed in units of cycles/unit length for MTF and in units of line-pairs/unit length for CTF.

Fig. 8-6 Various parameters related to a Gaussian-shaped MTF (Modulation Transfer Function).

Equation 8-12 can be solved for periodic triangular, sine or square-wave disturbances by making the exposure time, t_p , equal to one or more periods of the disturbance. The amplitude of I_x is shown in Figure 8-7 for several types of disturbances. A summary of the effects of these high-frequency errors is also provided in the table of Figure 8-8. The Gaussian random displacement-type disturbance can also be solved by appropriate analysis and the results are included in Figure 8-8.

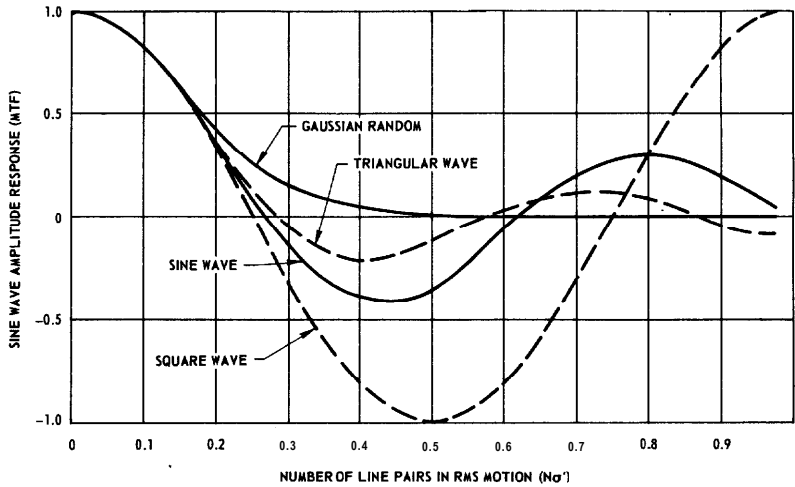

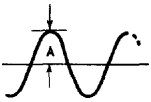
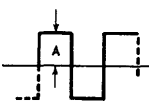
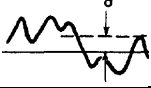


Fig. 8-7 MTF for several high-frequency image motions.

8.4 DISPLAY INTERPRETATION

Limiting Resolution. It is common practice to specify the resolving capability of an electro-optical imaging system in terms of the image of a black and white bar chart such as the **RETNA** television test pattern. The line limit represents the spatial frequency at which the observer's eye can no longer discriminate differences in the light and dark transitions in the bar image. It is assumed that the frequency response of the system is poorer than that of the eye, so that the line limit is truly a measure of the system's capability, and not that of the eye. (Reference 43).

Because the eye is normally considered to require an image contrast about three percent in order to appreciate the light-to-dark transitions in the bars, the limiting resolution in line-pairs/mm or in line-pairs per picture width can be considered as the spatial frequency at which the MTF (modulation transfer function) has fallen to a value of three percent. The limiting resolution measure of an electro-optical imaging system is therefore related to one point on the MTF. Contrast is here defined as the ratio of the imaged difference in luminance between the dark bar and its background to the luminance of the background. See Section 11.

Type of Image Motion	Error Waveform	rms Amplitude σ	Sine-Wave Response (MTF)	N_e in line pairs/unit length
Triangular Waveform		$A/\sqrt{3}$	$\frac{\sin(2\pi AN)}{2\pi N}$	$0.144/\sigma$
Sine Waveform		$A/\sqrt{2}$	$J_0(2\pi AN)**$	$0.128/\sigma^*$
Square Waveform		A	$\cos(2\pi AN)$	$0.125/\sigma^*$
Gaussian Random Displacement		σ	$\exp(-2(\pi N \sigma)^2)$	$0.141/\sigma$

*The values of N_e are obtained from $N_e = \int_0^{\infty} (MTF)^2 dN$; however, the integral is taken only to the first zero of the MTF for sine waveforms and square waveforms because the integrals do not converge for these two cases as the upper limit approaches.

**Zero-order Bessel function of first kind.

Fig. 8-8 Summary of the effects of high-frequency stabilization errors.

Line Resolution Requirements. Figure 8-9 summarizes conclusions from one set of measurements on the capability of humans to perceive single military targets (standing man to tank size) as a function of the limiting resolution per target minimum dimension (Reference 44).

Angular Threshold of Eye. The probability of seeing an object is influenced not only by the field luminance, the contrast of the object with respect to the scene background and the complexity of the scene, but also by the angular

Task	Line Resolution per Target Minimum Dimension
Detection	1.0 ± 0.25 line pairs
Orientation	1.4 ± 0.35 line pairs
Recognition	4.0 ± 0.8 line pairs
Identification	6.4 ± 1.5 line pairs

Fig. 8-9 Line resolution requirements.

subtense of that object at the eye of the observer. Under ideal conditions the eye can resolve about 30 seconds of arc. In most practical situations, however, the angular threshold of the eye is much larger than that. For example, it has been shown (Reference 45) that a target appearing in a complex field of confusion elements must subtend about 12 minutes of arc to enable a high (97 percent) probability of recognition. With a high resolution complex image, for which line resolution does not enter as a limiting and confounding factor, it appears that 6 to 12 minutes of arc are required for the typical visual acquisition and recognition tasks.

Visual Search Time. The time required to search a particular frame may be computed analytically from knowledge of the eye's fixation time and the angular size of the display, an approach discussed by Simon (Reference 46). Two assumptions are made:

- (1) a single fixation requires approximately three-tenths of a second
- (2) the circular field of clear vision subtends 5 degrees.

The length of time required to search an entire display field once through is computed by determining the number of nonoverlapping 5° fixations required to cover the field. A display subtending 16° x 16° at the eye would thereby be predicted to require:

$$16^{\circ}/5^{\circ} \times 16^{\circ}/5^{\circ} \times 0.3\text{s} = 3.1 \text{ s}$$

8.5 TARGET DETECTION/RECOGNITION MODEL

Imaging sensor performance may be estimated and/or evaluated by application of a target detection/recognition model such as that suggested by the Rand Corporation (Reference 47); namely:

$$P_r = P_1 P_2 P_3 \eta \quad (8-13)$$

where P_r is the probability that a target will be recognized on the display; P_1 is the probability that the observer, searching an area that is known to contain a target, looks with his foveal vision for a specified glimpse time ($1/3$ s) in the direction of the target; P_2 is the probability that if the displayed target image is viewed foveally for one glimpse period it will, in the absence of noise, have sufficient contrast and size to be detected; P_3 is the probability that if a target is detected, there will be enough detail shown for it to be **recognized (again during a single glimpse and in the absence of noise)**; and η is an overall degradation factor arising from noise.

The probability P_1 is difficult to estimate because it is affected (1) by the solid angle presented to the eye of the search field, (2) by the time available to search it, (3) by the number of confusing elements within the scene, and (4) by the availability of any "cues" or a priori information as to where to look on the display. The model employs the relation

$$P_1 = 1 - \exp \left[- \left(\frac{700}{G} \right) \left(\frac{a_t}{A_s} \right) t \right] \quad (8-14)$$

where,

a_t = area of target

A_s = area to be searched

= time

G = congestion factor, usually between 1 and 10, for most real imagery of interest.

The probability of detection, P_2 , at the threshold contrast C_t , is by definition 50%. A useful approximation for P_2 at other contrasts C available at the eye is given by

$$P_2 \cong \frac{1}{2} \pm \frac{1}{2} \sqrt{1 - \exp \left[-4.2 (C/C_t - 1)^2 \right]} \quad (8-15)$$

where the minus sign is used when $C < C_t$. A plot of equation 8-15 is given in Figure 8-10.

The other two factors in equation 8-13 are also plotted in Figure 8-10, being calculated respectively from

$$P_3 = \left\{ \begin{array}{ll} 1 - \exp \left[- (N_r/2 - 1)^2 \right] & N_r \geq 2 \\ 0 & N_r \leq 2 \end{array} \right\} \quad (8-16)$$

and

$$\eta = \left\{ \begin{array}{ll} 1 - \exp [- (\text{SNR}-1)] & \text{SNR} \geq 1 \\ 0 & \text{SNR} < 1 \end{array} \right\} \quad (8-17)$$

where,

$$N_r = \frac{L_{\min}}{\alpha R} \quad (8-18)$$

is the number of resolution cells contained in the minimum projected target dimension L_{\min} , α is angular resolution of the sensor, R is the target range, and SNR is the displayed signal-to-noise ratio. (A more complete treatment of the effect of noise in electro-optical displays is recent work reported in Reference 48).

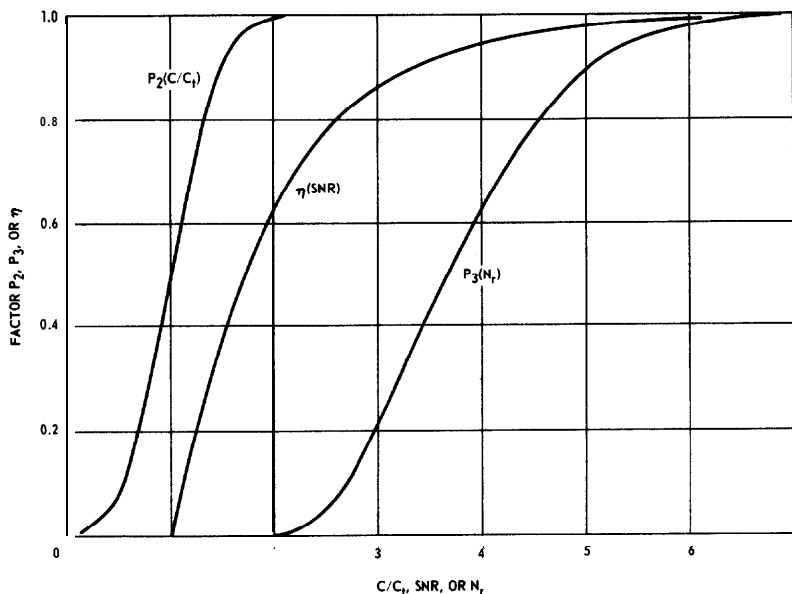


Fig. 8-10 Probability factors used in the Rand Corporation model (Reference 47) for target detection and recognition

Note that an expression for the probability of detection alone (without recognition) is obtained by considering only three of the factors in equation 8-13; namely

$$P_d = P_1 P_2 \eta \quad (8-19)$$

References

38. North, D.O., "An Analysis of the Factors which Determine Signal/Noise Discrimination in Pulsed-Carrier Systems," PROC IEEE, Vol. 51, July 1963.
39. Schwartz, M., INFORMATION TRANSMISSION, MODULATION, AND NOISE, McGraw-Hill Book Co., New York, N.Y., 1959.
40. Rice, S.O., "Mathematical Analysis of Random Noise," THE BELL SYSTEM TECHNICAL JOURNAL, Vol. 23, No. 3, July 1944 and Vol. 24, No. 1, Jan. 1945.
41. POISSON DISTRIBUTION, General Electric Co., Defense Systems Department, D. Van Nostrand Co., New York, N.Y., 1962.
42. Schade Sr., O.H., "A New System of Measuring and Specifying Image Definition," NATIONAL BUREAU OF STANDARDS CIRCULAR 526, 231-258, 1954.
43. SPECIFICATION FOR EIA(RETMA) RESOLUTION CHART 1956, Industrial Electronics Bulletin No. 2, Electronic Industries Association, Engineering Department, New York, N.Y., 1956.
44. Johnson, J., "Analytical Description of Night Vision Devices," PROCEEDINGS OF THE SEMINAR ON DIRECT-VIEWING ELECTRO-OPTICAL AIDS TO NIGHT VISION, Biberman, L., Editor, Institute for Defense Analyses Study S254, Oct. 1966.
45. Steedman, W., and Backer, C., "Target Size and Visual Recognition," HUMAN FACTORS, Vol. 2, Aug. 1960.
46. Simon, C., "Rapid Acquisition of Radar Targets from Moving and Static Displays," HUMAN FACTORS, Vol. 7, June 1965.
47. Bailey, H.H., "Target Detection Through Visual Recognition: A Quantitative Model," Rand Corporation, Santa Monica, Ca., Feb. 1970.

48. "Low Light Level Devices: A Designer's Manual," Report R-169, Institute for Defense Analysis, Science and Technology Division, Arlington, Va., Aug. 1971.
49. Coltman, J.W., and Anderson, A.E., "Noise Limitations to Resolving Power in Electronic Imaging," PROC. IRE, May 1960.
50. Rose, A., "The Sensitivity Performance of the Human Eye on an Absolute Scale," J.O.S.A., Vol. 38, No. 2, Feb. 1948.

Section 9

Lasers

Laser action has been observed in various media including crystalline solids, glasses, plastics, liquids, gases, organic dyes, and even jello (Reference 51). This section contains the current information concerning the characteristics of lasers. The emphasis is on those lasers that have either been proven to be practical or else are the only sources in a particular wavelength range. There are, in addition, indirect sources of coherent radiation such as frequency multiplication and parametric conversion. These indirect sources are discussed in separate parts of this section. For a detailed listing of all known laser transitions and of the nonlinear materials used for up and down conversion, see Reference 52.

The choice of a laser for a particular application involves consideration of the advantages and disadvantages of each type. The development of mode-locking and cavity dumping techniques, of high optical quality, damage-free nonlinear materials, of cw semiconductor lasers, and of the dye lasers has significantly increased the range of options available to the system designer. For high peak power applications the energy storage capacity of insulating solid crystal or glass lasers makes them the optimum choice. Due to their comparatively broad linewidth these lasers as well as the dye lasers are also the optimum **choice for the generation of ultra-short (~ten picosecond) pulses.** The gas lasers offer significant advantages for low power, reliable operation in the visible portion of the spectrum. In particular the He-Cd laser is the optimum choice for the exposure of photoresist materials. In the infrared the CO and **CO₂ lasers are efficient, high power sources which can be used directly in**

applications such as welding or as sources for parametric down conversion to longer wavelengths.

The reader is reminded that laser radiation may produce injury to the eyes or skin. Appropriate safety procedures for use with lasers of differing power and output wavelengths may be found in the American National Standards Institute Standard for the Safe Use of Lasers (2136.1).

9.1 CRYSTALLINE LASERS

Figure 9-1 is a list of useful crystalline lasers with their wavelength, mode of operation: pulsed (**p**) or continuous wave (**cw**), and typical operating temperature. The emphasis is on lasers that operate at room temperature. Those **dopants** listed in parentheses are additional impurities which absorb the pump radiation and transfer the energy to the active ion. Though the multiply doped lasers are not widely used at the present time, several of them are more efficient than the singly doped materials.

It is noticeable from Figure 9-1 that there are no lasers listed for wavelengths shorter than $0.690 \mu\text{m}$. Whereas crystalline lasers exist in this range they can not compete either in output power or in simplicity of operation with either gas lasers or up conversion of longer-wavelength crystalline lasers. The up-converted or tuned-output crystalline lasers will be discussed in Section 9-4.

As noted in the introduction, mode-locking and cavity dumping are two new modes of operation for crystalline lasers. The $\text{Y}_3\text{Al}_5\text{O}_{12}/\text{Nd}^{3+}$ laser is particularly adaptable to mode-locking techniques because of its comparatively broad spectral bandwidth ($\sim 0.1 \text{ nm}$).

9.2 GLASS LASERS

In addition to the crystalline lasers, lasing action can also be obtained in glass hosts. Two lasers of particular interest are the Nd^{3+} glass laser at $1.06 \mu\text{m}$ and the Er^{3+} glass laser at $1.54 \mu\text{m}$. In both cases the laser is operated in a pulsed mode at room temperature. The Nd^{3+} glass laser is of particular importance in high-power, pulsed-mode applications.

9.3 GAS LASERS

Figure 9-2 gives a list of gas lasers which are important at the present time. The table includes estimates of their output power for different modes of operation. The development of cavity dumping techniques has provided an

Host/Dopant	Wavelength μm	Mode of Operation	Operating Temperature (K)
$\text{Al}_2\text{O}_3/\text{Cr}^{3+}$	0.6929 0.6934	p p	350 350
$\text{CaWO}_4/\text{Nd}^{3+}$	1.0584 0.9145 1.3392	p, cw p p	300 77 300
$\text{CaMoO}_4/\text{Nd}^{3+}$	1.0673	p, cw	300
$\text{YA10}_3/\text{Nd}^{3+}$ (Polarized output)	1.0795 1.0645	p, cw p, cw	300 300
$\text{Y}_3\text{Al}_5\text{O}_{12}/\text{Nd}^{3+}$ $/\text{Nd}^{3+}, (\text{Cr}^{3+})$	0.946 1.0519 1.0613 1.0640 1.0736 1.319 1.338 1.358	p, cw p, cw p, cw p, cw p, cw p, cw p, cw p, cw	230 300 300 300 300 300 300 300
$\text{Y}_3\text{Al}_5\text{O}_{12}/\text{Er}^{3+}(\text{Yb}^{3+})$	1.6459	p	300
$\text{YA10}_3/\text{Er}^{3+}$	1.663	p	300
$\text{Y}_3\text{Al}_5\text{O}_{12}/\text{Tm}^{3+} (\text{Cr}^{3+})$	2.019	p	300
$\text{Ca}_2\text{MoO}_4/\text{Ho}^{3+}$	2.059	p	300
$\text{Y}_3\text{Al}_5\text{O}_{12}/\text{Ho}^{3+}(\text{Er}^{3+}, \text{Tm}^{3+})$	2.1288	p	300
$\text{CaF}_2/\text{U}^{3+}$	2.57 2.613	p p	300 300
$\text{CaF}_2/\text{Er}^{3+}$	2.69	p	300

Fig. 9-1 Crystalline laser systems.

additional output format which is usable with any of the gas lasers. The rapid advances in the area of "chemical" pumping of the molecular lasers and the variety of techniques used make the values given for the output power only a rough guide subject to careful qualification. See Reference 53.

Gas	Principal Wavelengths μm	Power Output		
		Typical	Maximum	Mode of Operation
Xe (ionized)	0.3454	15 mW	1 W	cw
	0.378 1	50 mW		cw
	0.4060	5mW		cw
	0.42 14-0.4272	50 mW		cw
	0.5419-0.627 1	10 mW		cw
Xe (Xe-He)	2.026		1 mW	cw
	3.507		1 mW	cw
	5.575		1 mW	cw
	9.007		1 mW	cw
N ₂ (ionized)	0.337 1		200 kW	P
			100 mW	cw
HeCd (ionized)	0.3250	4 mW	40 mW	cw
	0.4416	20 mW	200 mW	cw
Ne (ionized)	0.3324		10 mW	p, cw
Ne (neutral)	0.5401		1 kW	P
Cu (neutral)	0.5 106		40 kW	P
Ar (ionized)	0.3511	5mW	0.35 w	cw
	0.3638	5mW	0.35 w	cw
	0.4579	0.1 w	0.75 w	cw
	0.4658	0.1 w	0.3 w	cw
	0.4727	50 mW	0.4 w	cw
	0.4765	.3 w	1.5 w	cw
	0.4880	1.0 w	5.0 W	cw
	0.4965	.2 w	1.5 w	cw
	0.5 107	.1 w	.7 w	cw
	0.5 145	1.0 W	6.0 W	cw

Fig. 9-2 Some typical gas laser systems. (Part 1 of 2)

Gas	Principal Wavelengths μm	Power Output		
		Typical	Maximum	Mode of Operation
He-Se (ionized)	0.4605-0.6490 (24 lines) 0.5228		100 mW 20 mW	cw cw
Kr (ionized)	0.3507 0.3564 0.4762 0.4825 0.5208 0.5309 0.5682 0.647 1 0.6764 0.7525 0.793 1 0.7993	20 mW 20 mW 50 mW 30 mW 70 mW 200 mW 150 mW 500 mW 120 mW 100 mW 10 mW 30 mW		cw cw cw cw cw cw cw cw cw cw cw cw
He-Ne	0.6328 1.1523 3.3913	2 mW 2 mW 1 mW	150 mW 25 mW 10 mW	cw cw cw
HF (chemical)	2.6→3.5	4500 w 1 joule		cw p
CO	4.9→5.7		100 W	cw
CN	5.2		30 mW	p
CO ₂ (flowing)	10.6 } 9.6 }	{100 W 5 kW	200 kW	cw p
Transverse Excitation Atmospheric (TEA)	10.6	1000 w 50 kW		cw p
HCN	126→134 310 336 372	0.5 W 1 W 0.6 W 0.6 W	10 W	p p p p
H ₂ O	28		5 kW	p

Fig. 9-2 Some typical gas laser systems. (Part 2 of 2)

9.4 DYE LASERS

The active medium of a dye laser consists of a strongly fluorescing organic compound dissolved in an appropriate solvent. Included in this group are a number of commercial dyes. This medium is pumped with a flash lamp or a laser and is usually operated in the pulsed **mode**. Continuous operation has recently been obtained by circulating the active medium through the optical cavity and pumping with a cw laser.

The active molecule typically fluoresces over a bandwidth of 35 to 80 nm and lasing action can occur over most of this range. For a particular molecule, wavelength selection is accomplished with cavity mirrors (laser $\Delta\lambda \sim 20$ nm), an **intracavity grating** (laser $\Delta\lambda \sim 0.05$ nm), or a **combination of intracavity grating and etalon** ($\Delta\lambda \sim 0.001$ nm). **Tuning of the grating or grating plus etalon** allows one to scan across the fluorescent bandwidth of the active molecule. Use of several different dyes in succession can provide a **tunable** output from ~ 350 nm to 750 nm (**References 54 and 55**). **Beyond 750 nm** the available active molecules are unstable and as a result are not practical sources. A number of different materials which can provide a **tunable** output are listed in Figure 9-3. Solvents other than those listed may be used. It should be noted, however, that the fluorescent band position is solvent dependent.

Dye	Solvent	Tuning Range nm
Calcein Blue	Ethanol	449 - 490
1, 3 Diphenyliso-benzofuran	Ethanol	484 - 518
Fluorscein	Aqueous Alkaline	520 - 570
Rhodamine 6G	Ethanol	560 - 650
Rhodamine B	Ethanol	590 - 700
Cresyl Violet	Ethanol	630 - 690

Fig. 9-3 Some representative dye laser materials.

Typical output parameters for a pulsed visible dye laser include an energy output of 0.1 joule and peak powers of the order of 2 MW at a rate of 30 p/s. For cw operation with 1.0-watt Ar⁺ laser pumping at 488 nm or 514.5 nm, 50 mW can be obtained in a flowing dye system with a spectral bandwidth of less than 0.001 nm.

9.5 SECOND HARMONIC GENERATION AND PARAMETRIC DOWN-CONVERSION

Second harmonic generation (Reference 56) and parametric up- and down-conversion (References 57 and 58) provide alternative sources of coherent radiation in the ultraviolet to the infrared range. These effects occur in non-centrosymmetric materials for which the nonlinear polarization P_i can be written as

$$P_i = \sum_{jk} d_{ijk} E_j E_k.$$

where d_{ijk} is the nonlinear coefficient, and E_j , E_k are the optical electrical field amplitudes. In addition to this symmetry requirement, both energy and momentum must be conserved in the process. For second harmonic generation:

$$\omega_2 = 2\omega_1 \quad \hat{k}_2 = 2\hat{k}_1$$

and for parametric up- or down-conversion

$$\omega_{\text{pump}} = \omega_{\text{signal}} + \omega_{\text{idler}}$$

$$\hat{k}_{\text{pump}} = \hat{k}_{\text{signal}} + \hat{k}_{\text{idler}}$$

where ω is angular frequency and k is the momentum factor of the lightwave. These equations are the index of refraction matching conditions for the nonlinear processes. Figure 9-4 is a listing of commonly used nonlinear materials.

For second harmonic generation the nonlinear medium is usually placed within the laser cavity in low power applications and outside the cavity when the circulating power can damage it. Examples of frequency doubling are:

Material	Wavelength μm	Nonlinear Coefficients
$\text{Ba}_2\text{NaNb}_5\text{O}_{15}$	1.06	$d_{15}, d_{24}, d_{31}, d_{32}, d_{33} = 15 \times 10^{12} \text{ m/V}$
SiO_2	1.06	$d_{11} = 0.4 \times 10^{12} \text{ m/V}$
LiNbO_3	1.06	$d_{33} = 40 \times 10^{12} \text{ m/V}$
LiTaO_3	1.06	$d_{33} = 20 \times 10^{12} \text{ m/V}$
KDP	1.06	$d_{14}, d_{36} = 0.50 \times 10^{12} \text{ m/V}$
	0.6943	$d_{14}, d_{36} = 0.48 \times 10^{12} \text{ m/V}$
ADP	1.06	$d_{14}, d_{36} = 0.55 \times 10^{12} \text{ m/V}$
	0.6943	$d_{14}, d_{36} = 0.48 \times 10^{12} \text{ m/V}$
LiIO_3	1.06	$d_{31}, d_{33} = 5 \times 10^{12} \text{ m/V}$
Te	10.6	$d_{11} = 2000\text{-}5000 \times 10^{12} \text{ m/V}$
GaAs	0.8435-0.845	$d_{14} = 137 \times 10^{12} \text{ m/V}$
	1.06	$d_{14}, d_{36} = 250 \times 10^{12} \text{ m/V}$
	10.6	$d_{14} = 250 \times 10^{12} \text{ m/V}$
Ag_3AsS_3 } (Proustite)	1.15	$d_{31} = 15 \times 10^{12} \text{ m/V}$
	10.6	$d_{15}, d_{22} = 28 \times 10^{12} \text{ m/V}$

Fig. 9-4 Commonly used nonlinear materials in harmonic-generator lasers.

intracavity doubling of the Ar^+ 514.5 nm line to 257.2 nm and intracavity doubling of the Nd:YAG line at 1060 nm to 530 nm. This last example is the best source for high power repetitively Q-switched or repetitive short pulses (~ 50 ps) in the visible region. In principle, the same amount of power can be coupled out of a laser cavity at the harmonic as at the fundamental if the nonlinear coefficient is large enough. $\text{Ba}_2\text{NaNb}_5\text{O}_{15}$ is an example of such a material which is usable with the Nd:YAG laser.

In parametric conversion two signals are mixed to obtain sum or difference frequencies, or a single frequency (pump) is converted to two frequencies (signal and idler). Typically the optical parametric oscillator is a singly resonant cavity at the idler frequency and the signal frequency is the output of the oscillator. The output wavelength is varied by changing the index of

refraction of the nonlinear crystal. The index is changed by applied electric fields, change in the angle of incidence of the pump radiation, or by variation of the temperature of the nonlinear medium.

An example of a parametric oscillator is one pumped by a Q-switched Nd:YAG laser doubled into the visible by means of an intracavity LiIO_3 crystal. A lithium niobate crystal is temperature tuned to provide a variable output wavelength in the range from 620 nm to 3500 nm. The output is not continuous in wavelength but occurs in discrete ranges depending upon the particular pump wavelength and the mirrors used. Average output powers of several milliwatts and peak powers of 500 watts can be obtained. In the wavelength range beyond 750 nm, this device offers the only practical source of **tuneable** coherent radiation.

9.6 P-N JUNCTION LIGHT SOURCES

In a forward-biased p-n junction, the minority carriers injected across the p-n junction recombine either radiatively, with the emission of photons, or non-radiatively. The photon energy will depend on the nature of the atomic centers involved and the **bandgap** energy of the crystal. In so-called “direct **bandgap**” materials such as **GaAs**, the photon energy is close to the **bandgap** energy of the material. In “indirect **bandgap**” materials such as **GaP**, the luminescence frequently involves impurity levels which shift the photon energy of the emitted radiation to values substantially below the **bandgap** energy.

Recombination radiation has been observed over a wide range of efficiencies in most of those semiconductors in which p-n junctions can be fabricated. When the electro-luminescent radiation is incoherent, the diode source is described as a light-emitting diode (LED) type; when the radiation is coherent, the source is described as a laser type.

There are important differences in the nature of the materials needed and the construction of the device for the two types of application. The difference in **the radiant output is that at the threshold for lasing (I_{th})**, the laser diode emission becomes directional, the spectral width decreases to a few tenths of nanometers, and the differential efficiency increases sharply. This change in efficiency is shown in Figure 9-5.

9.6a P-N JUNCTION LASERS

A practical laser diode has three basic requirements: (1) it must be constructed from a direct **bandgap** semiconductor; (2) it must have a

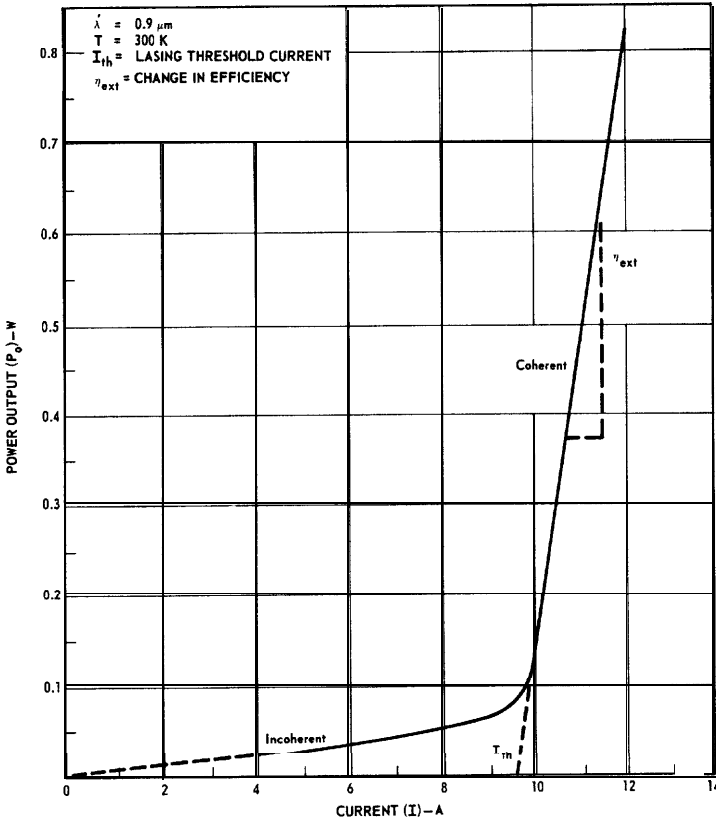


Fig. 9-5 Typical output curve of GaAs laser diodes.

Fabry-Perot cavity, which consists of two mirror-like surfaces defining the direction of photon flux; and (3) a region must be formed which confines the radiation and the injected carriers. The Fabry-Perot cavity is generally created by cleaving the material along parallel crystal planes either of which may be coated to a final reflectivity R_1 and R_2 , as shown in Figure 9-6. Radiation confinement to a waveguide region is achieved by structuring the dielectric constant ϵ (hence index of refraction) in the transverse direction during the growth of the crystal. Present-day commercial laser diodes are of the heterojunction type (also denoted "close-confinement") where the refractive index differences in the junction region are obtained by using layers of (AlGa)As and GaAs. The higher bandgap energy of the (AlGa)As which

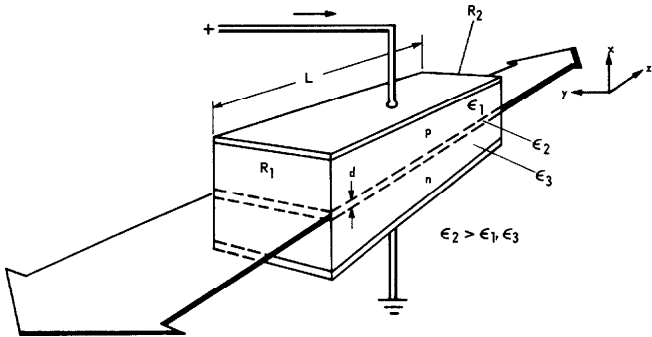


Fig. 9-6 Diagram including some essential features of a p-n junction laser: Fabry-Perot reflectivities R_1 and R_2 , dielectric waveguide d formed by dielectric constant $E_2 > E_1, E_3$.

adjoins the lasing region of **GaAs** also provides for carrier confinement thereby resulting in reduced threshold current densities and higher efficiencies than possible in older structures without the heterojunctions.

There are several types of heterojunction lasers with specific advantages peculiar to each. The most widely used commercially available diode (Reference 59) is the single heterojunction “close-confinement” device (SH-CC), Figure 9-7b, emitting at approximately 900 nm. It is capable of operating in the pulsed mode at relatively high duty cycle, about 0.1%, with peak power of several watts for single diodes and up to kilowatts for multidiode arrays. By lowering the operating temperature to 77K or less, the close-confined lasers can be operated continuously, provided adequate heat sinking is employed.

More recently, devices have been developed in which the radiation is confined by two **(AlGa)As-GaAs** heterojunctions (References 60, 61, and 62) as shown in Figure 9-7c. Such devices have improved radiation confinement compared to the single heterojunction type, and the width of the mode-guiding region can be adjusted by changing the spacing between the heterojunctions. By reducing the threshold current density to values below about 3000 A cm^{-2} , continuous wave operation can be obtained at room temperature. Due to the uncertain operating life of room temperature cw lasers, such devices are not yet commercially available.

The large optical cavity (LOC) laser diode, shown in cross section in Figure 9-7d, allows the construction of devices having rather wide well-controlled

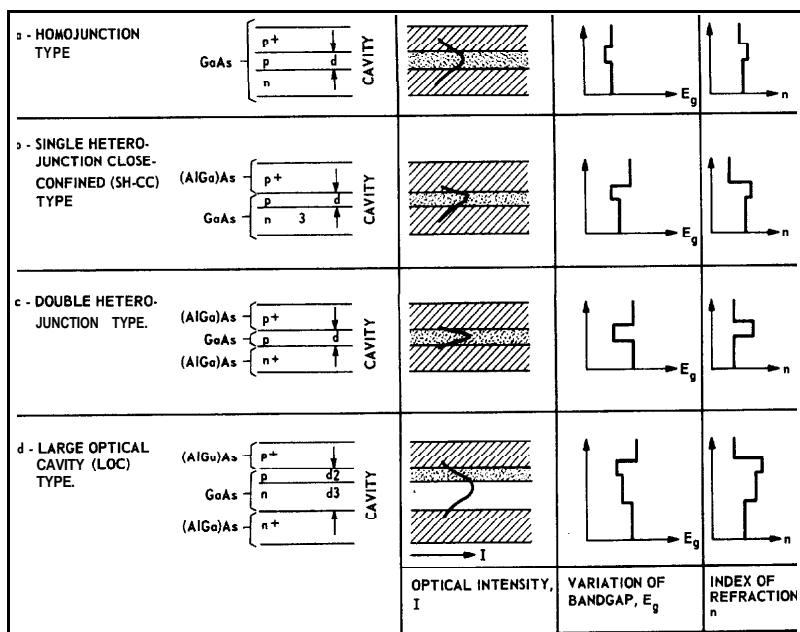


Fig. 9-7 Illustrations of various laser cross sections showing optical intensity I , variation of bandgap E_g , and index of refraction n .

mode-guiding regions. This diode can operate with higher efficiencies and at higher temperatures than possible with the single heterojunction type. Developmental devices of this type are capable of operation at a duty cycle of about 1 percent.

The wavelength of $\text{Al}_x\text{Ga}_{1-x}\text{As}$ lasers can be varied by varying the composition of the devices. Figure 9-8 indicates how the threshold current density J_{th} changes with lasing wavelength and shows the rapid increase in J_{th} as the visible region is approached.

Many other III-V, II-VI, and lead salt compounds have been operated as lasers (Reference 52) at wavelengths ranging from the near ultraviolet to the mid-infrared ($\sim 10 \mu\text{m}$). These devices, especially those emitting at wavelengths longer than $0.9 \mu\text{m}$, generally require operation at cryogenic temperatures and are not commercially available.

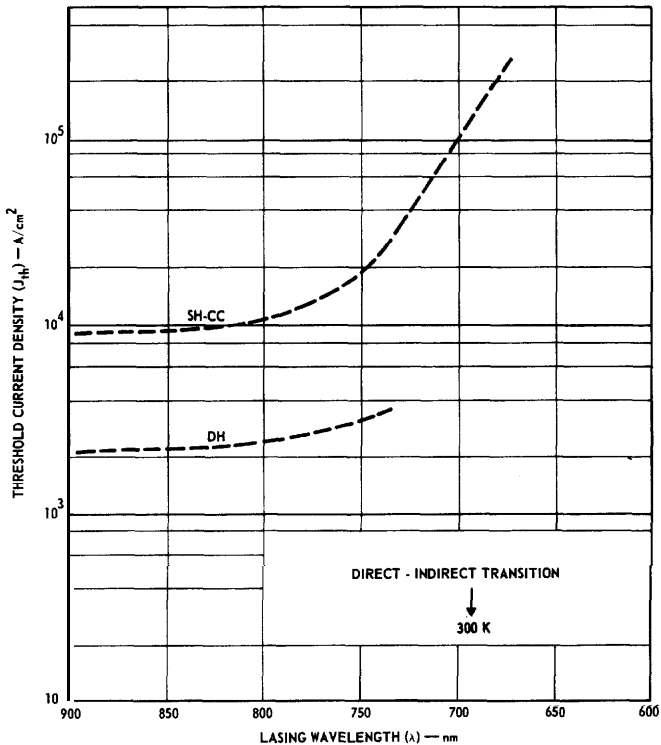


Fig. 9-8 Nominal dependence of threshold current density in single heterojunction close-confinement (SH-CC) and double heterojunction (DH) $Al_xGa_{1-x}As$ lasers as a function of lasing wavelength.

9.6b LIGHT-EMITTING DIODES (LEDs)

Incoherent or spontaneous emission devices (Reference 63) are available covering a broader range of the spectrum than laser diodes cover. Higher brightness sources in the visible portion of the spectrum (Reference 64) have been fabricated from $GaAs_{1-x}P_x$ (red), $InGa_{1-x}P_x$ (red), GaP (red, yellow, green), and GaN (blue, green and, yellow). See References 65, 66, 67, and 68. GaN has also produced near ultraviolet dc electroluminescence at room temperature (Reference 69). The $GaAs_{1-x}P_x$ and GaP LED's are currently in production and are commercially important as display devices.

Figure 9-9 lists many of the materials in which electroluminescence has been observed. The range shown for **GaP** is due to the incorporation of different impurities in the material which produces a range of colors from red to yellow (red plus green) to green.

Figure 9-10 indicates which of these materials has shown laser and light-emitting action and Figure 9-11 is a compilation of some of the important engineering parameters associated with the electroluminescent diodes commercially available.

References

51. Hansch, T.W., Pernier, M., Schawlow, A.L., "Laser Action of Dyes in Gelatin," J. QUANT. ELEC. Vol. QE-7, No. 1, Jan. 1971.
52. Pressley, R.J., Editor, HANDBOOK OF LASERS, Chemical Rubber Co., 1971.
53. Jeffers, W.Q., Editor, "Third Conference on Chemical and Molecular Lasers," J. QUANT. ELEC., Vol. QE-9, No. 1, Jan. 1973.
54. Furumato, H.W. and Cecon, H.L., "Ultraviolet Organic Liquid Lasers," J. QUANT. ELEC. Vol. QE-6, No. 5, May 1970.
55. Warden, J.T. and Gough, L., "Flashlamp-Pumped Laser Dyes: A Literature Survey," APPL. PHYS. LETT., Vol. 19, No. 9, Nov. 1971.
56. Kleinman, D.A., "Theory of Second Harmonic Generation of Light," PHYS. REV., Vol. 128, No. 4, Nov. 1962.
57. Oshman, M.K., and Harris, S.E., "Theory of Optical Parametric Oscillation Internal to the Laser Cavity," J. QUANT. ELEC., Vol. QE-4, No. 8, Aug. 1968.
58. Harris, S.E., "Tunable Optical Parametric Oscillators," PROC. IEEE, Vol. 57, No. 12, Dec. 1969.
59. Kressel, H. and Nelson, H., "Close-Confinement Gallium Arsenide PN Junction Lasers with Reduced Optical Loss at Room Temperature," RCA REVIEW, Vol. 30, No. 1, March 1969.

References continued on page 142

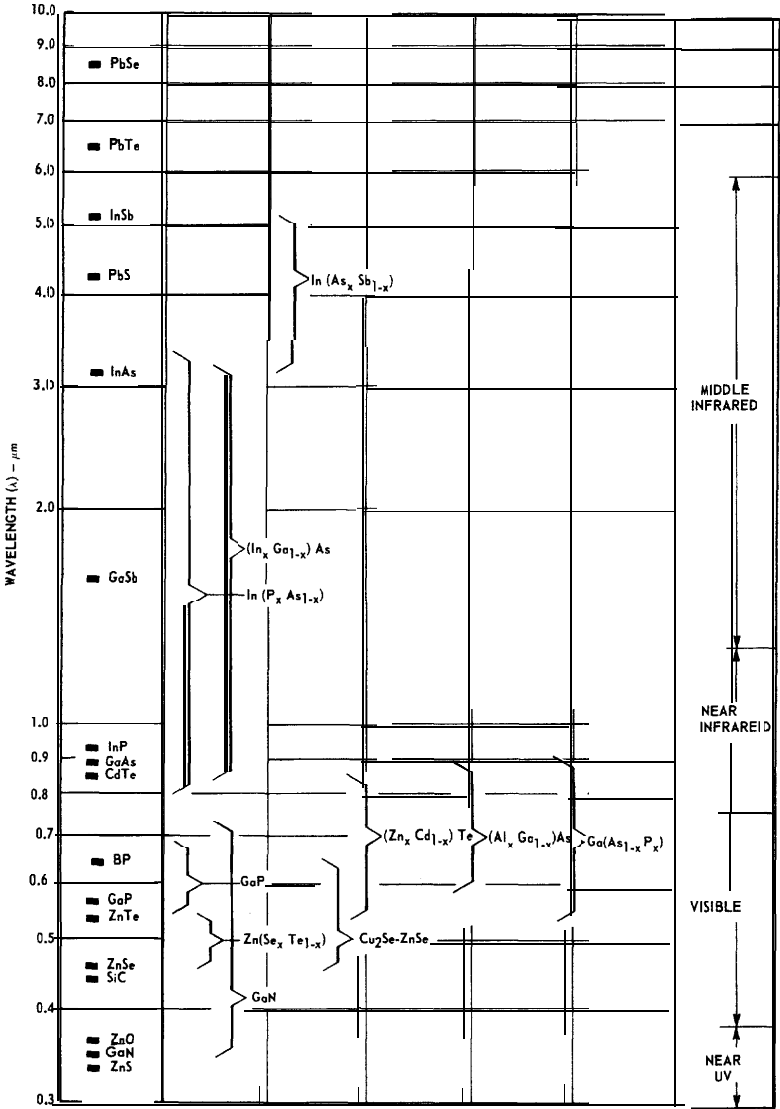


Fig. 9-9 Spectral range of some typical electroluminescent systems.

Crystal	Wavelength μm
INJECTION LASER SOURCES	
PbSe	8.5
PbTe	6.5
InSb	5.2
PbS	4.3
InAs	3.15
$(\text{In}_x\text{Ga}_{1-x})\text{As}$	0.85+3.15
$\text{In}(\text{P}_x\text{As}_{1-x})$	0.91+3.15
GaSb	1.6
InP	0.91
$\text{Al}_x\text{Ga}_{1-x}\text{As}$	0.90+0.62
$\text{Ga}(\text{As}_{1-x}\text{P}_x)$	0.55+0.90
LED SOURCES	
CdTe	0.855
$(\text{Zn}_x\text{Cd}_{1-x})\text{Te}$	0.53+0.83
BP	0.64
$\text{Cu}_2\text{Se-AnSe}$	0.40+0.63
$\text{Zn}(\text{Se}_x\text{Te}_{1-x})$	0.627
ZnTe	0.62
GaP	0.565
	0.68
SiC	0.456
GaN	0.34+0.7

Fig. 9-10 Partial listing of injection laser and LED sources.

References continued from page 140

60. Hayashi, I., Panish, M.B., Foy, P.N., Sumski, S., "Junction Lasers which Operate Continuously at Room Temperature," APPL. PHYS. LETT., Vol. 17, No. 3, Aug. 1970.

61. Kressel, H., Lockwood, H.F., Hawrylo, F.Z., "Low-Threshold LOC GaAs Injection Lasers," APPL. PHYS. LETT., Vol. 18, No. 2, Jan. 1971.

62. Kressel, H., Lockwood, H.F., Ettenberg, M., "Progress in Laser Diodes," IEEE SPECTRUM, Vol. 10, No. 5, May 1973. (A review of all laser types).

References continued on page 144

	LED			Laser		
				SH-CC		LOC
Crystal	GaAs	GaAsP	GaP	GaAs	GaAs	GaAs
Temperature (K)	300	300	300	77	300	300
Emission Wavelength (μm)	0.94	0.66, 0.61	0.69, 0.55	0.85	0.9	0.9
Spectral Bandwidth (μm)	0.05	0.03	0.09, 0.03	0.015	0.015	0.015
Typical Drive Current	<50mA	10-20mA	10-20mA	<5A	<30A	15A
Mode (pulsed or continuous)	p, cw	p, cw	p, cw	p	p	p
Maximum Pulse Duration	any	any	any	2 μs	0.2 μs	0.1 μs
Duty Factor (%)	any	any	any	<2	<0.1	<1
Rise Time (ns)	<300	10	300	<1	<1	<1
Typical Output (cw)	2.5mW	1700 nit (500fL)	600-3500 nit (175-1000fL)	–	–	–
Peak Pulse Power (W)	–	–	–	5	12	5
Power Efficiency (%)	3	<1	3, 0.1	20-40	3-5	5-10
Beam Spread	surface or edge 80°; dome 180°			15° x 25°		

CC – close confinement
LED – light-emitting diode

LOC – large optical cavity
SH – single heterojunction

Fig. 9-11 Typical parameters for some commercially available electroluminescent diodes.

References continued from page 142

63. Bergh, A.A. and Dean, P.J., "Light-Emitting Diodes," PROC. IEEE, Vol. 60, No. 2, Feb. 1972.
64. Nuese, C.J., Kressel, H., **Ladany, I.**, "Solid State: The Future for LED's," IEEE SPECTRUM, Vol. 9, No. 5, May 1972.
65. Maruska, H.P., Stevenson, D.A., Pankove, J.I., "Violet Luminescence of Mg-Doped **GaN**," APPL. PHYS. LETT., Vol. 22, No. 6, March 1973.
66. **Pankove, J.I., Miller, E.A., Berkeyheiser, J.E., "GaN Blue Light-Emitting Diodes," J. LUMINESCENCE, Vol. 5, No. 1, March 1972.**
67. **Pankove, J.I., Miller, E.A., Berkeyheiser, J.E., "GaN Electroluminescent Diodes," RCA REVIEW, Vol. 32, No. 3, Sept. 1971.**
68. Pankove, J.I., Miller, E.A., Berkeyheiser, J.E., "**GaN** Yellow-Light Emitting Diodes," J. LUMINESCENCE, Vol. 6, No. 1, Jan. 1973.
69. Pankove, J.I., "**UV** dc Electroluminescence from **GaN**," J. LUMINESCENCE, Vol. 5, No. 6, Dec. 1972.

Section 10

Detector Characteristics

There are two general classes of photodetectors; photoemissive devices in which photoelectrons are emitted into a vacuum or gas, and solid-state devices in which the excited charge is transported within the solid by holes or electrons. Detectors utilizing photoemission are principally vacuum **photo**-diodes, gas-filled phototubes, and photomultipliers. Solid-state detectors are available in a wide variety. These devices may be classified as **photoconduc**-tive or photovoltaic types. Typical solid-state detectors are p-n junction photocells, p-n-p phototransistors, avalanche photodiodes, p-i-n photo-detectors, and Schottky-barrier devices.

Although most non-critical applications can use any of these photodetectors there are some applications in which certain devices are particularly suitable. Vacuum photodiodes are used in applications where a relatively large sensitive area may be required, oil burner flame monitoring being a typical example. Vacuum photodiodes are also used as the sensor in spectrophotometers. Some vacuum photodiodes which have been specially designed to have a rise time in the order of 30 ps are of use in laser applications where the radiation level is quite high. Gas-filled phototubes were originally used in large numbers as the detectors of motion-picture sound. The gas filling provides an amplification factor of 5 to 10 but limits the speed of response to that just adequate for the audio range.

Photomultiplier tubes are manufactured in a wide variety of designs. This type of detector, utilizing either conventional secondary-emission dynodes or microchannel plates, is generally most useful in applications where radiation levels are very low and high speed of response is required. The secondary-emission gain factor of a photomultiplier may be as high as 10^7 . This high gain permits the signal to exceed the noise components of the output and amplifier circuit so that the limitation to detection becomes the statistical variation in the photocathode current. Photomultiplier tubes are widely used in scintillation counting applications, including the medical "gamma" camera, and in astronomy, laser ranging, and spectroscopy.

Solid-state photodetectors are used in a variety of applications. Inexpensive **CdS** photoconductive cells are used in street-light controls, oil-burner controls, and exposure controls in photography. The silicon photovoltaic cell is well known for its use as a solar energy converter. Other types of silicon p-n junction photocells are used in sound-on-film pickup, card reading, and in a variety of industrial controls. The silicon photodetector is small, reliable, and has high quantum efficiency through the visible to near infrared. Silicon avalanche detectors are characterized by high gain and fast speed of response; they find use in laser ranging. A number of solid-state photocells have been developed for detection of radiation in the near and far infrared. In the near infrared, materials such as **PbS** and **Si** are useful. Photodetectors for use in the far infrared must be cooled. Cells of this type are **(HgCd)Te**, **InSb**, **PbSe**, **Ge:Au**, **Ge:Hg**, and **Ge:Zn**.

10.1 FUNDAMENTAL PHOTODETECTOR RELATIONSHIPS AND DEFINITIONS

Because of the differing nature of the various types of photodetectors, it is not possible to characterize all of them in identical terminology. Although the units of measurement may differ, there are some characteristics that are common to all devices: spectral response, speed of response, and limits of detectivity.

Figure 10-1 is a glossary of the more common parameters, symbols, and units.

Incident Flux – The response of a photodetector is evaluated in terms of the flux incident on the sensitive area of the detector. The flux may be specified as the number of quanta per second at some wavelength, the radiant flux in a narrow wavelength band, the radiant flux over a wide band of wavelengths, luminous flux, and in some cases as a density, flux per unit area, in the plane of the device aperture or surface.

Parameter	Symbol	Units
Signal Response (the symbol S is commonly used as a lower case subscript to denote signal current, signal voltage, etc.)	S	V, A
Responsivity	R	A W ⁻¹ , V W ⁻¹ , A lm ⁻¹
Quantum Efficiency	η	
Dark Current	I _d	A _{av}
Noise	N	A _{rms} , V _{rms}
Signal-to-Noise Ratio	S/N	
Equivalent Noise Input	ENI	W, lm
Noise Equivalent Power	NEP	W
Detectivity	D	W ⁻¹
Specific Detectivity	D*	cm Hz ^{1/2} W ⁻¹

Fig. 10-1 Detector parameters, symbols, and units.

Relationship Between Quanta and Radiant Flux Units – The energy of a single quantum is $h\nu = hc/\lambda$ where **h** is Planck’s constant, ν and λ are the frequency and wavelength of the radiation, and **c** is the speed of light. The radiant flux per unit wavelength is Φ_λ and the radiant flux in a small increment of wavelength $d\lambda$ is $\Phi_{e\lambda} d\lambda$ watts. The radiant flux in this narrow wavelength band may be converted to a rate of flow of quanta

$$N = \frac{\lambda \Phi_{e\lambda} d\lambda}{hc} \quad (\text{in quanta per second}) \tag{10-1}$$

Equivalent Luminous Flux – As noted in Section 5, the ratio of luminous flux ($\Phi_{v\lambda}$) to radiant flux ($\Phi_{e\lambda}$) at a given wavelength is the spectral luminous efficacy, $K(\lambda)$.

Thus

$$\Phi_{\nu\lambda} d\lambda = K(\lambda) \Phi_{e\lambda} d\lambda \quad (\text{in lumens}) \quad (10-2)$$

Responsivity and Signal Current – The term responsivity (R) is used to describe the sensitivity of the photosensor and is the ratio of the output current or voltage to the input flux in watts or lumens. When the responsivity is indicated at a particular wavelength [$R(\lambda)$ in amperes/watt], it connotes the spectral response of the device. If $R(\lambda)$ and the radiant flux in the interval $d\lambda$ are known, the signal current (I_S) is given by

$$I_S = R(\lambda) \Phi_{e\lambda} d\lambda \quad (\text{in amperes}) \quad (10-3)$$

If R is given in amperes per lumen, the signal current is given by

$$I_S = R\Phi_v \quad (\text{in amperes}) \quad (10-4)$$

where Φ_v is the total incident luminous flux.

Sometimes, the radiant flux is shown for a band of wavelength, viz.,

$$\Phi_e = \int_{\lambda_1}^{\lambda_2} \Phi_{e\lambda} d\lambda \quad (\text{in watts}) \quad (10-5)$$

In this case the responsivity has a different value in terms of amperes/watt although the form of the equation remains

$$I_S = R\Phi_e \quad (\text{in amperes}) \quad (10-6)$$

Quantum Efficiency – A quantum efficiency (η) of unity implies that one photoelectron is emitted (or one electron-hole pair is generated) for each incident quantum. (Note: In a consideration of the fundamentals of the reaction between radiation and photodetector, quantum efficiency is sometimes defined in terms of absorbed rather than incident quantum; however, from the standpoint of the user, it is the incident quantum that is of interest). Quantum efficiency is usually defined at a particular wavelength.

Thus,

$$\eta(\lambda) = \frac{\text{Number of photoelectrons per second}}{\text{Number of incident quanta at wavelength } \lambda \text{ per second}} \quad (10-7)$$

The number of photoelectrons per second is given by

$$I_S/e = \frac{R(\lambda) \Phi_{e\lambda} d\lambda}{e}$$

where e is the charge of the electron and the number of quanta per second is given by equation 10-1. Therefore, the quantum efficiency is given by

$$\eta(\lambda) = \frac{R(\lambda) hc}{e\lambda} \quad (10-8)$$

When the values of Figure 3-1 are used, the value of the constant hc/e is

$$hc/e = 1.23985 \times 10^{-6} \text{ (in W m A}^{-1}\text{)} \quad (10-9)$$

Accordingly,

$$\eta(\lambda) = \frac{1.23985 R(\lambda)}{\lambda}$$

with λ in μm .

It is to be noted that quantum efficiency generally refers to the primary process in the device; i.e., the interaction of the incident radiation and the primary photosensor. In some cases where the responsivity is recorded, a gain mechanism is included in the device between the prime photosensor and the output as, for example, in a photomultiplier or avalanche photodiode. However, very little advantage is achieved by referring to a quantum efficiency which includes the gain and which, therefore, may be many times unity.

Dark Current — Dark current is that current that flows in a photodetector in the absence of signal and background radiation. The average or DC value of this current is identified by the symbol I_d .

Noise Current – There are various sources of noise or current fluctuation which interfere with the precise measurement of the signal current. Dark current has a random fluctuation as does signal current. When the individual pulse can be observed, these fluctuations are manifest in the random arrival of the dark or signal pulses. Sometimes, the noise in the associated components, such as thermal (or Johnson) noise in the coupling resistor or amplifier noise, is dominant.

Signal-to-Noise Ratio – Usually the signal-to-noise ratio (S/N) is expressed in terms of the noise in a particular bandwidth. It may be expressed in decibels or, in photoelectron counting applications, as the ratio of a number to the standard deviation of the number in a particular count duration.

Equivalent Noise Input – The Equivalent Noise Input (**ENI**) is defined as that value of input flux that produces an rms signal current that is just equal to the rms value of the noise current in a specified bandwidth (usually 1 Hz). Other parameters such as frequency, the type of light modulation, and temperature should also be specified. Equivalent noise input characteristics are useful in determining the threshold of detection in equivalents of the input flux in watts or lumens.

Noise Equivalent Power – Noise equivalent power (NEP) is essentially the equivalent of ENI except the units are always in watts. ⁺ NEP is the radiant flux in watts incident on the detector which gives a signal-to-noise ratio of unity. The frequency bandwidth and the frequency at which the radiation is chopped must be specified as well as the spectral content of the radiation. The two most common spectral specifications are for total radiation from a black body whose temperature is 500 K or monochromatic radiation at the peak of the detector response.

Detectivity – **Detectivity (D)** is the reciprocal of NEP; it is expressed in W^{-1} . Detectivity is a figure of merit providing the same information as NEP but describes the characteristics such that the lower the radiation level to which the photodetector can respond, the higher the detectivity.

⁺Some detector manufacturers rate their detectors in terms of an NEP having units of watts $Hz^{-1/2}$. Assuming that the noise spectrum is flat within the range of the specification and that NEP is normally specified for a bandwidth of one hertz, the two forms of NEP are numerically equal. However, in this handbook, NEP is taken as originally defined by R. Clark Jones (References 70 and 71); it has no bandwidth in its units although NEP may be a function of noise bandwidth as well as temperature and test frequency.

Specific Detectivity – Because the NEP for many types of IR photodetectors is proportional to the square root of the sensitive area (A) and to the square root of the bandwidth (B) of the measuring system, a specific **detectivity (D*)** has been defined which permits a comparison of sensors of different areas measured in different bandwidths.

$$D^* = \frac{A^{1/2} B^{1/2}}{(NEP)} \text{ (in cm Hz}^{1/2} \text{ W)} \tag{10-10}$$

or

$$D^* = D A^{1/2} B^{1/2} \text{ (in cm Hz}^{1/2} \text{ W)}$$

10.2 SPECTRAL RESPONSIVITY AND SPECIFIC SPECTRAL DETECTIVITY

The relative spectral response characteristics of a number of photodetectors have been standardized by the EIA (Electronics Industries Association). These responses have been assigned S-designations, e.g., S- 1, S- 11, S-20.

Figure 10-2 lists some of the S-designation responses as well as many other spectral responses. Other typical characteristics in this figure have been taken mainly from References 72 and 73.

UV-Visible Spectral Responses for Photoemissive Devices— Figure 10-3 shows typical spectral response curves for photoemitters having good UV responsivity. Generally, the lower-limit cut-off wavelength of most photo-emitting cathodes is established by the transmission characteristics of the window material and to some extent by the thickness of the photocathode layer for transmission-type photocathodes. The spectral transmittance of several commonly used window materials is given in Section 12.

Visible Light Spectral Responses for Photoemissive Devices – Figure 10-4 gives the spectral responsivity curves for photoemitters that are most useful for detecting radiant flux in the visible region of the spectrum. Other responses having good sensitivity to visible light are shown in Figure 10-3 and 10-5.

Near-Infrared Spectral Responses for Photoemissive Devices – Figure 10-5 shows those photoemitters having responsivity that extends usefully into the near infrared (to approximately 1.2 μm).

Spectral Response Designation	Photo-sensitive Material	Type of Sensor	Window Material	Mode* of Operation T or R	Wavelength of Maximum Response (λ_{max}) - nm	Typical Luminous Responsivity - $\mu\text{A lm}^{-1}$	Typical Radiant Responsivity at λ_{max} - mA W^{-1}	Typical Quantum Efficiency at λ_{max} - %	Photocathode Dark Emission at 25°C - fA cm^{-2}
S-1	Ag-O-Cs	Photo-emitter	Lime Glass	T,R	800	30	2.8	0.43	900
S-3	Ag-O-Rb	Photo-emitter	Lime Glass	R	420	6.5	1.8	0.53	-
S-4	Cs-Sb	Photo-emitter	Lime Glass	R	400	40	40	12.4	0.2
S-5	Cs-Sb	Photo-emitter	9741 Glass	R	340	40	50	18.2	0.3
S-8	Cs-Bi	Photo-emitter	Lime Glass	R	365	3	2.3	0.78	0.13
S-9	Cs-Sb	Photo-emitter	7052 Glass	T	480	30	20.5	5.3	0.3
S-10	Ag-Bi-O-Cs	Photo-emitter	Lime Glass	T	450	40	20	5.5	70
S-11	Cs-Sb	Photo emitter	Lime Glass	T	440	70	56	15.7	3
S-13	Cs-Sb	Photo-emitter	Fused Silica	T	440	60	48	13.5	4
S14	Ge	P-n Alloy Junction	Lime Glass	-	1,500	12,400▲	520▲	43▲	-
S-16	CdSe	Poly-crystalline Photoconductor	Lime Glass	-	730	-	-	-	-

S-17	Cs-Sb	Photo-emitter with Reflective Substrate	Lime Class	R	490	125	83	21	1.2
S-19	Cs-Sb	Photo-emitter	Fused Silica	R	330	40	65	24.4	0.3
S-20	Na-K-Cs-Sb	Photo-emitter	Lime Glass	T	420	150	64	18.8	0.3
↓ Not Standardized ↓	Na-K-Cs-Sb	Photo-emitter with Reflective Substrate	Lime Glass	R	530	300	89	20.8	—
	Na-K-Cs-Sb (ERMA III)	Photo-emitter	7740 Pyrex	T	565	230	45	10	1.4
	S-21	Cs-Sb	Photo-emitter	9741 Glass	T	440	30	23.5	6.6
S-23	Rb-Te	Photo-emitter	Fused Silica	T	240	—	4	2	0.001
S-24	K-Na-Sb	Photo-emitter	7056 Glass	T	380	45	67	21.8	0.0003
S-25	Na-K-Cs-Sb	Photo-emitter	Lime Glass	T	420	200	43	12.7	1 —
↓ Not Standardized ↓	K-Cs-Sb	Photo-emitter	Lime Glass	T	380	85	97	31	0.02
	K-Cs-Sb	Photo-emitter	Lime Glass	R	400	65	54	17	—
	Cs-Te	Photo-emitter	Fused Silica	T	250	—	15	7.4	—

* T = Transmission Mode R = Reflection Mode

▲ With 45 volts polarizing voltage

Fig. IO-2 Spectral response designations and related characteristics. (Part I of 2)

Spectral Response Designation	Photo-sensitive Material	Type of Sensor	Window Material	Mode* of Operation T or R	Wavelength of Maximum Response (λ_{max}) nm	Typical Luminous Responsivity – $\mu\text{A lm}^{-1}$	Typical Radiant Responsivity at λ_{max} – mA W^{-1}	Typical Quantum Efficiency at λ_{max} – %	Photo-cathode Dark Emission at 25°C – fA cm^{-2}
↑ Not Standardized ↓	Ga-As	Photo-emitter	9741 Glass	R	830	300	68	10	0.1
	Ga-As-P	Photo-emitter	9741 Glass	R	400	160	45	14	0.01
	Ga-In-As	Photo-emitter	9741 Glass	R	400	100	57	17.6	–
	Cd-S	Poly-crystalline Photoconductor	Lime Glass	–	510	–	–	–	–
	Cd(S-Se)	Poly-crystalline Photoconductor	Lime Glass	–	615	–	–	–	–
	Si	N-on-p Photo-voltaic	No Window	–	860	7,650●	580.	83.5●	–
	Si	P-i-n Photoconductor	Lime Glass	–	900#	620#	620#	85#	–

* T = Transmission Mode R = Reflection Mode

● . Photovoltaic short-circuit responsivity

For a wafer thickness of approximately 150 μm

Fig. 1 O-2 Spectral response designations and related characteristics. (Part 2 of 2)

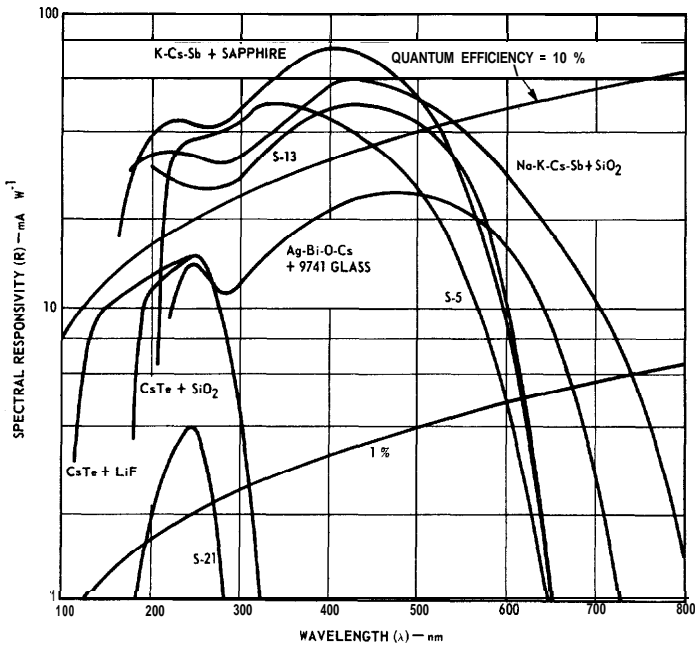


Fig. 10-3 UV-visible photoemitter characteristics. Absolute spectral responsivity of various photocathode-window combinations useful in the ultraviolet-visible region of the spectrum

Long-Wave Threshold Variation with Temperature for Photoemissive Devices—The long-wavelength threshold of certain photoemitters is a function of temperature and decreases as the temperature of the photoemitter decreases. Figure 10-6 shows this effect for four typical photoemitting materials (See Reference 74). These photocathodes, which extend into the near infrared, are normally cooled to reduce dark current and noise. Note that no decrease in long wavelength threshold was observed for the S-1 spectral response.

Visible and Near-Infrared Spectral Responses for Solid-State Devices — Figures 10-7a and 10-7b show spectral responsivity characteristics for a number of common photoconductive and photovoltaic cells. The n-on-p diffused silicon and Se photovoltaic characteristics represent typical responsivities under short-circuit conditions. The p-i-n silicon photoconductive responses in Figure 10-7a are shown for two different wafer thicknesses. Relative spectral response characteristics for CdS and CdSe are shown in Figure 10-7b; these cells can be characterized as photoresistive.

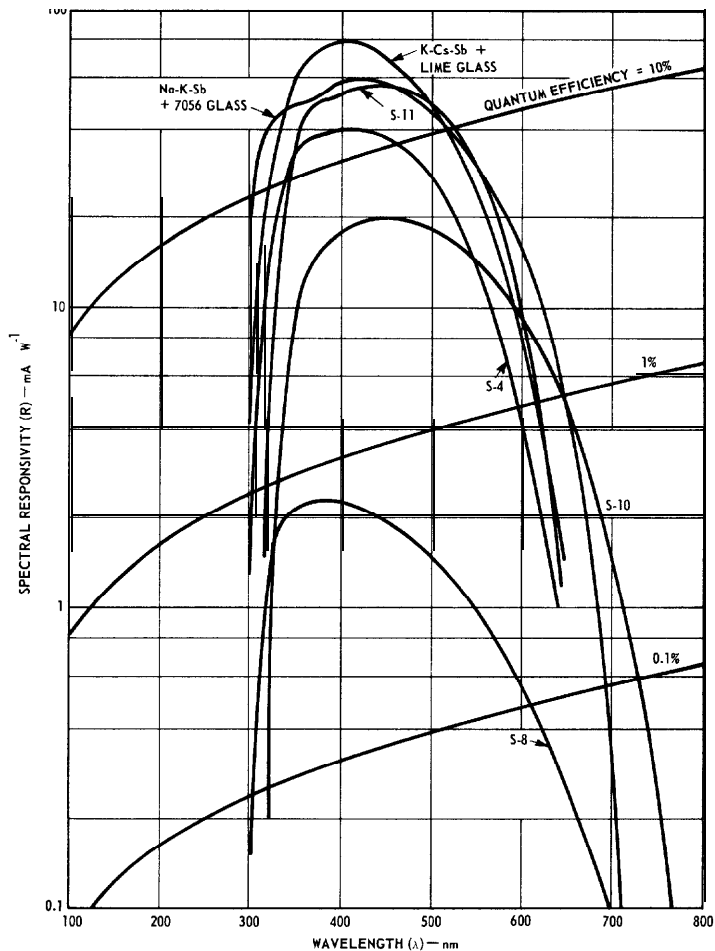


Fig. 10-4 Visible photoemitter characteristics. Absolute spectral responsivity of various photocathode-window combinations useful for the detection of visible light.

Far-Infrared Spectral Responses for Solid-State Devices — When a far-infrared response is required, solid-state detectors must be used. No photoemissive materials are currently available having responsivity much beyond 1.2 μm . Photoconductive materials can be made having excitation energies corre-

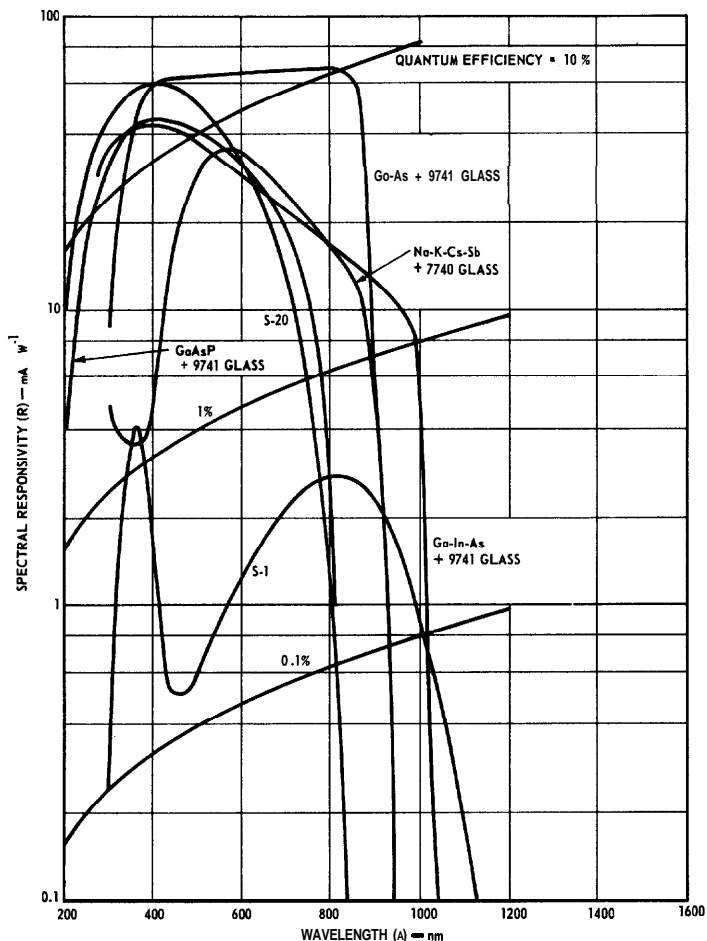


Fig. 10-5 Near infrared-visible photoemitter characteristics. Absolute spectral responsivity of various photocathode-window combinations useful for the detection of visible and near infrared radiant flux.

sponding to tenths and even hundredths of an eV. However, such materials require cooling to prevent thermal excitation from obscuring the signal.

The spectral response characteristics of the far-infrared solid-state detectors of Figures 10-8 and 10-9 are shown in terms of specific detectivity, D^* . The

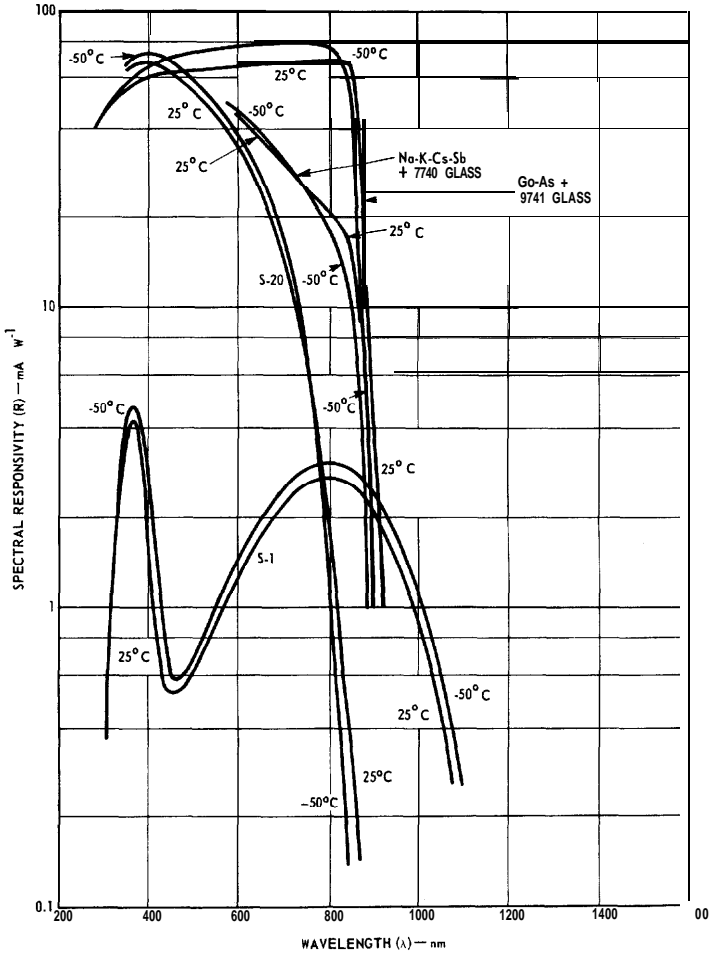


Fig. 10-6 Typical effect of photocathode cooling using four typical photocathode materials.

data are taken from references 25 and 75. The particular temperature at which each response characteristic was measured is indicated on the Figures. The dashed curves represent the limitation on specific detectivity imposed by the fluctuation of the background thermal radiation (assumed to be

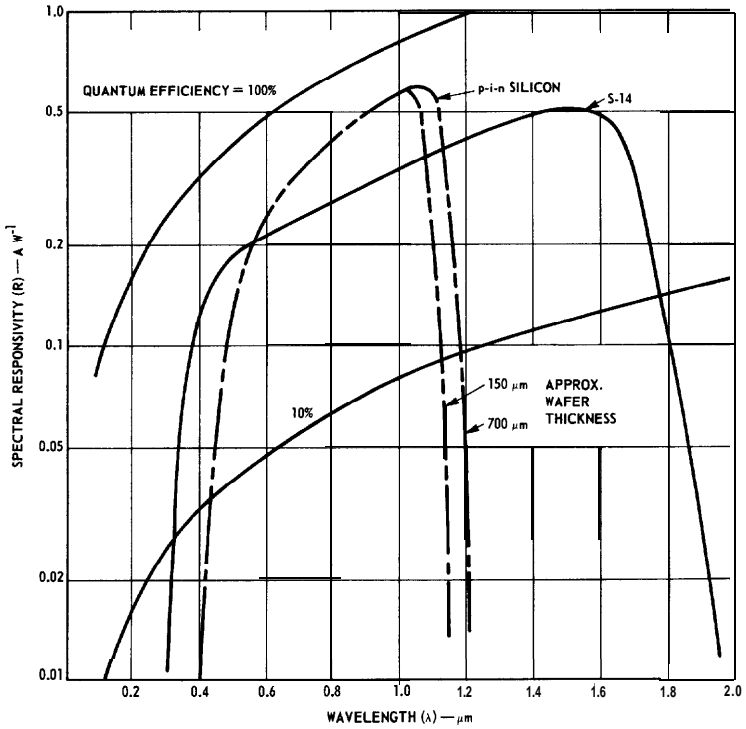


Fig. 10-7a Spectral response of p-i-n silicon and germanium (S-14) photo-detectors.

characteristic of 295 K and 2π steradian field of view). The ideal solid-state sensor can only equal these theoretical curves if each quantum received is detected.

Variation of D^* (λ_{max}) with Temperature and Modulation Frequency — Figure 10-10, which supplements the spectral response characteristics of Figures 10-7a and 10-7b, shows the temperature dependence of specific detectivity for various solid-state photodetectors. The particular value for D^* is taken at the wavelength of maximum spectral detectivity. Figure 10-11 shows D^* at λ_{max} as a function of radiant flux modulation (chop) frequency for PbS.

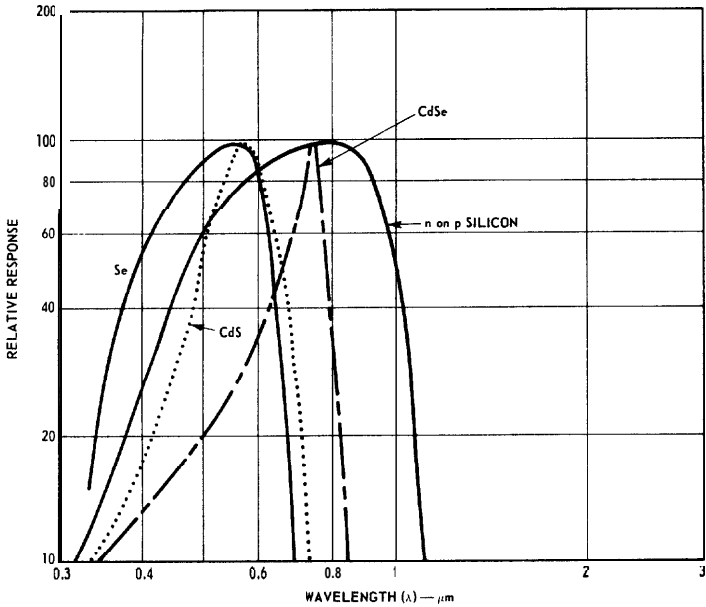


Fig. 10-7b Spectral response of CdS and CdSe photoconductive cells and Se and n on p silicon photovoltaic cells.

10.3 NOISE

Photodiodes — Devices such as a vacuum photodiode or a silicon p-n photodiode produce a noise current variation of the output current which ultimately limits the detectivity of the device in the absence of other interference. This current is the common rms shot noise current $(i_n^2)^{1/2}$ and may be defined as follows:

$$(i_n^2)^{1/2} = (2 e I B)^{1/2} \quad (\text{in amperes}) \quad (10-11)$$

where

e = the charge of the electron

I = the total average current from the device (the sum of the signal current I_s , the background current I_b , and the dark current I_d).

B = the bandwidth

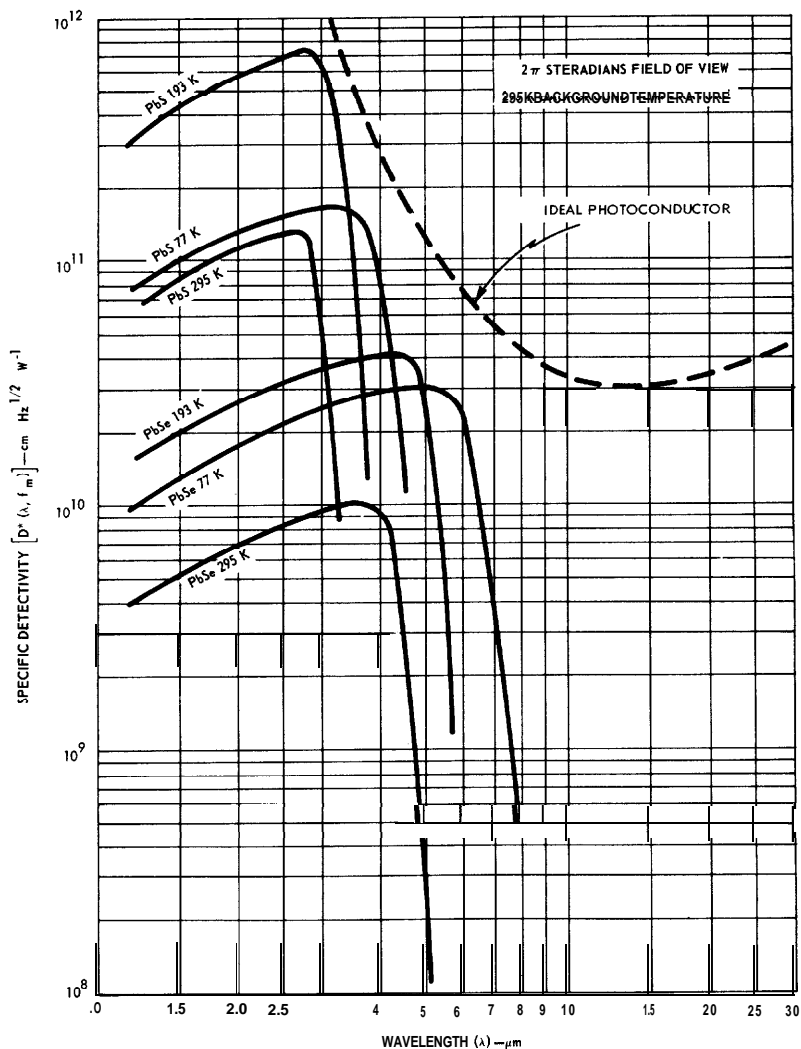


Fig. 10-8 Spectral detectivities for above-average thin-film detectors at frequency f_m (courtesy Santa Barbara Research Center).

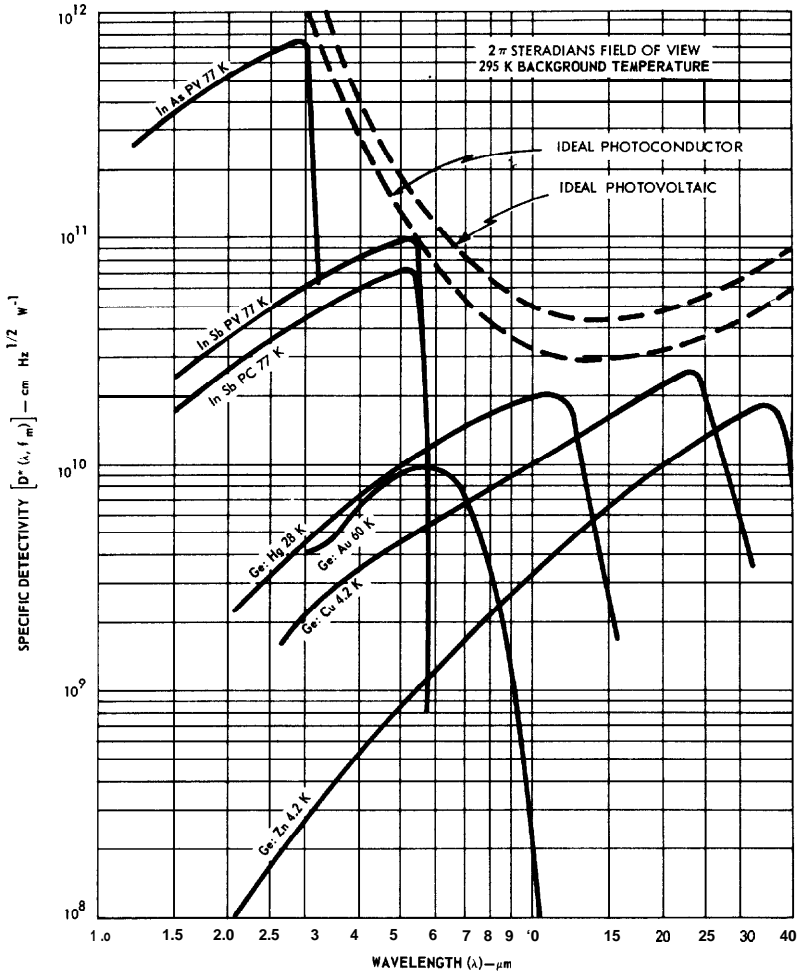


Fig. 10-9 Spectral detectivities for above-average crystal detectors at frequency f_m (courtesy Santa Barbara Research Center).

In summing the three components of the total average current I , it is assumed that each component is statistically independent of the other so that the noise components may be added by taking the square root of the sum of the squares.

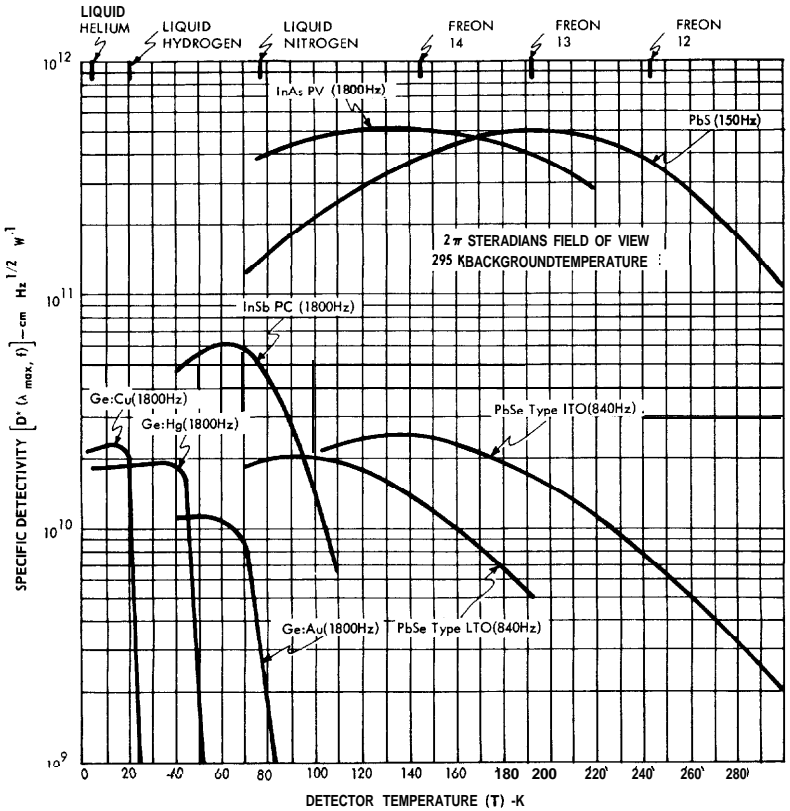


Fig. 1 O-1 0 Typical dependence of specific detectivity on operating temperature (courtesy Santa Barbara Research Center).

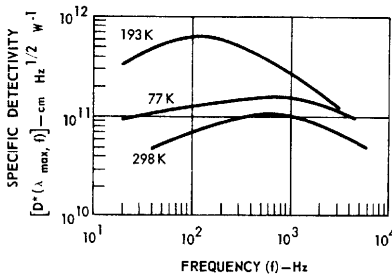


Fig. 10-11 Example of detectivity as a function of frequency for PbS detectors (courtesy Santa Barbara Research Center).

Photodetectors with Internal Amplification (**Photomultipliers**) – In applications involving low light levels, the noise in the photodiode output (equation 10-11) may be totally obscured by other sources of noise such as that of the amplifier used as the measuring instrument. In such a case, the total **detectivity** capability of the diode is not used. To overcome this difficulty, devices such as photomultipliers have been developed in which the primary photocurrent is amplified within the device itself. Although this amplification is not noise free, it adds in most cases only a small increment to the fundamental diode output noise compared to the amplified signal current. The rms shot-noise current at the output of a photomultiplier is given by

$$(i_n^2)^{1/2} = M_k \left[(2 e I B) \left(1 + \frac{1}{\delta_1} + \frac{1}{\delta_1 \delta_2} + \dots + \frac{1}{\delta_1 \delta_2 \delta_3 \dots \delta_k} \right) \right]^{1/2} \quad (\text{in amperes}) \quad (10-12)$$

where

I = the total average photocathode current

$\delta_1, \delta_2 \dots \delta_k$ = the secondary emission gain factors for each of the dynode stages

$M_k = \delta_1 \cdot \delta_2 \dots \delta_k$ = the total gain of the photomultiplier

B = the bandwidth

e = the charge of the electron

Note that the inherent noise in the photocathode is multiplied by the total gain of the photomultiplier as is the signal current.

An additional factor to be considered is the statistics of secondary emission of the dynodes. The major contributor is the secondary emission from the first stage. If δ_1 is large, the multiplier is essentially noise free because $1/\delta_1$ becomes negligible with respect to the 1. Equation 10-12 is developed assuming Poisson statistics for the secondary emission process. In general, noise values for photomultipliers are somewhat higher than those obtained from equation 10-12. See Reference 76. If the secondary emission of each stage is assumed to be the same, equation 10-12 may be simplified to the approximate expression

$$(i_n^2)^{1/2} = M_k \left[(2 e I B) \left(\frac{1}{1 - 1/\delta} \right) \right]^{1/2} \quad (\text{in amperes}) \quad (10-13)$$

For typical secondary emission gain of 4, the increase in rms noise current over that of a “perfect” amplifier is about 15%.

Photodetectors with Internal Amplification (Avalanche Photodiodes) – The avalanche photodiode is a p-n junction type photodetector that is operated at the high reverse bias voltages required for avalanche multiplication. Very high multiplication factors M can be achieved, but the process is noisy. The gain is a result of holes and electrons being accelerated within the depletion layer of the diode; ionization takes place and gain process may be repeated many times. McIntyre (See Reference 77) has analyzed this statistical process and has shown that when the ionization rates for electrons and holes are the same, then the rms noise current $(i_n^2)^{1/2}$ for the white noise part of the spectrum (at high frequencies) is given by the expression

$$(i_n^2)^{1/2} = M (2 e I B M)^{1/2} \text{ (in amperes)} \tag{10-14}$$

where

- M = the multiplication factor
- e = the charge of the electron
- I = the total average current before multiplication
- B = the bandwidth

Note that the noise increase factor over that of a noise-free amplification process varies as $M^{1/2}$.

Circuit Noise – When a photodetector is coupled to a circuit, the noise introduced by the circuit elements must be considered. For example, if the output current from a phototube flows through a resistor R_L , the thermal noise generated in the resistor must be added to the photoelectron shot noise. The adding process must be done using the equivalent expression of power, i.e., the sum of the squares of the noise currents or of the noise voltages. The total rms noise is then obtained by taking the square root of the sum. For a coupling resistor, the thermal rms noise voltage developed is given by

$$(v_n^2)^{1/2} = (4 k T B R_L)^{1/2} \text{ (in volts)} \tag{10-15}$$

where

- k = Boltzmann’s constant
- T = absolute temperature
- B = the bandwidth

The equivalent thermal noise current may be written

$$(i_n^2)^{1/2} = \left(\frac{4 k T B}{R_L} \right)^{1/2} \quad (\text{in amperes}) \quad (1016)$$

When the photodetector is coupled to an amplifier, the equivalent rms noise current expressed in terms of current through the coupling resistor is given by

$$(i_n^2)^{1/2} = \left(\frac{4 k T B}{R_L} \right)^{1/2} \left[\frac{(R_L + R_t)}{R_L} + \frac{4\pi^2}{3} C^2 R_L R_t B^2 \right]^{1/2} \quad (\text{in amperes}) \quad (10-17)$$

where

R_L = the resistance of the coupling resistor in ohms

R_t = the equivalent noise resistance of the amplifier input in ohms

C = the total capacitance of the tube and associated input in farads

(See Reference 77)

B = the bandwidth

If the coupling resistor has a large value and the bandwidth is narrow, equation 10-17 reduces to equation 10-16. For wide bandwidths, the equivalent rms noise current input reduces to

$$(i_n^2)^{1/2} = \left[4 k T \frac{4\pi^2}{3} C^2 R_t B^3 \right]^{1/2} \quad (10-18)$$

Pulse Counting Applications — Operation of the photomultiplier in a pulse counting mode is of growing importance. When the photomultiplier is used to count single electron pulses first with radiation incident on the photocathode and then with radiation excluded from the photocathode, it becomes important to determine the optimum time to be spent under each condition to provide the best signal-to-noise ratio.

Let N_Φ represent the count rate with radiation incident on the phototube and N_d represent the count rate of the tube in the dark. Also, let t_Φ and t_d

represent the respective count durations. With the tube irradiated, the total count is $N_{\Phi} t_{\Phi}$; with the tube in the dark, $N_d t_d$. The variance in this case in each of these counts is $N_{\Phi} t_{\Phi}$ and $N_d t_d$ (variance is equal to the square of the standard deviation). The variance for the whole measurement is $N_{\Phi} t_{\Phi} + N_d t_d$. The signal is the difference in the count rates, $N_{\Phi} - N_d$. The variance in the signal determination becomes

$$\frac{N_{\Phi}}{t_{\Phi}} + \frac{N_d}{t_d}$$

Accordingly, the expression for signal to noise for this counting process becomes

$$S/N = \frac{N_{\Phi} - N_d}{\left(\frac{N_{\Phi}}{t_{\Phi}} + \frac{N_d}{t_d}\right)^{1/2}} \tag{1049}$$

If the total time t of the measurement is assumed to be fixed ($t = t_{\Phi} + t_d$), and t_{Φ} is eliminated, the condition for maximum signal to noise may be obtained by differentiating the equation with respect to t_d .

$$\frac{t_d}{t} = \frac{\sqrt{\frac{N_{\Phi}}{N_d}} - 1}{\frac{N_{\Phi}}{N_d} - 1} \tag{10-20}$$

Figure 10-1 2, which is a plot of equation 10-20, shows the optimum fraction of the count time that should be spent for the dark count as a function of the ratio N_{Φ}/N_d . If the signal is small with respect to the dark count rate, i.e., $N_{\Phi} \simeq N_d$, the light count time and dark count time should be equal. However, if the signal count in the light dominates, then the time for measuring the dark count may be reduced significantly.

10.4 TIME CHARACTERISTICS OF PHOTODETECTORS

Time Response Characteristics of Photomultipliers – The three basic parameters which define a photodetector are its responsivity, noise, and temporal response characteristics. The limitation in speed of response for

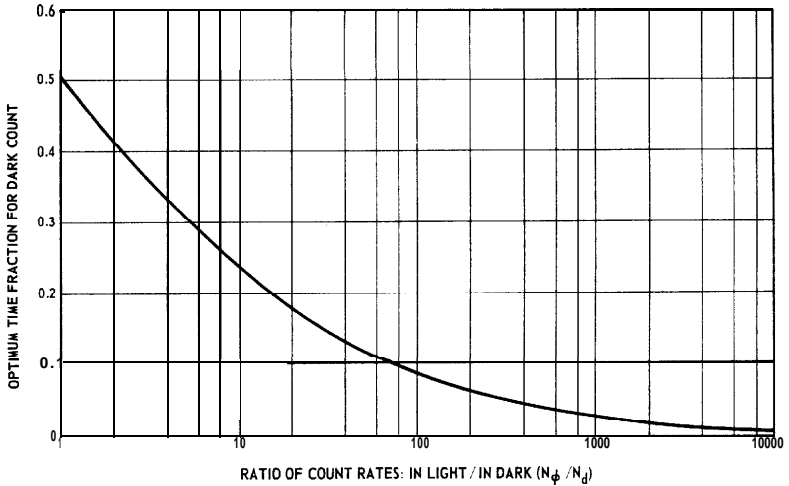


Fig. 10-12 Fraction of the count time to be used for the dark count to obtain the optimum signal-to-noise ratio for a fixed total time.

photomultipliers is principally one of design, i.e., the structural design of the “front end” (photocathode-to-first-dynode region), the electron multiplier, and the anode output structure. The time response capability of the photomultiplier is usually defined in terms of the anode output pulse characteristics for delta-function photocathode excitation. Scintillation and “photon” (properly photoelectron) counting systems are examples of natural occurrences of delta-function light excitations. In practical test measurements, pulsed LED’s, mode-locked lasers, and spark sources are often used to approximate the delta-function light source.

The most commonly specified anode pulse characteristics are rise time, fall time, and FWHM (Full Width at Half Maximum). These characteristics are shown in Figure 10-13. Measurement techniques on these and other time characteristics of photodetectors are contained in References 78, 79, and 80.

Time Response Characteristics of Solid-State Photodetectors — Rise time is the most commonly specified temporal figure of merit for solid-state detectors. The measurement is quite similar to that used for obtaining rise time of the photomultiplier except a step-function light excitation is employed.

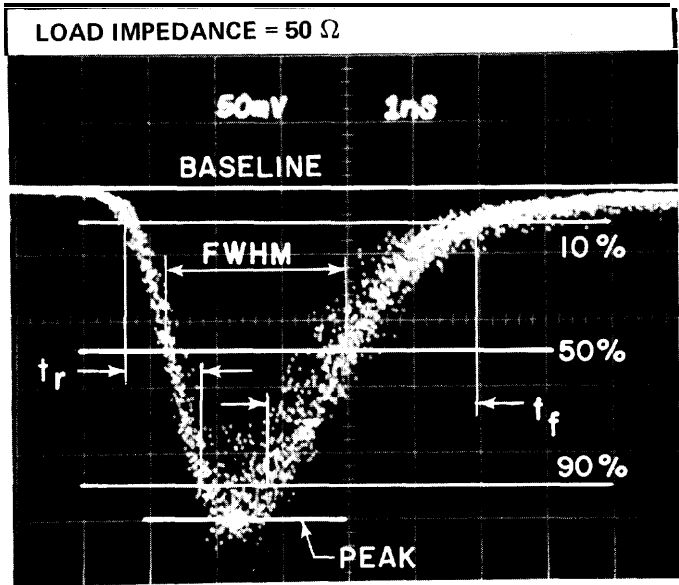


Fig. 10-13 Pictorial representation of anode pulse showing rise time t_r and fall time t_f characteristics and full width at half maximum points (FWHM).

The speed with which a solid-state photodetector responds to radiant signals is determined ultimately by the time it takes for the generated electrons and holes to be collected in the diode. Best time response is attained by using fully depleted detectors to eliminate any series resistance, and very small loads, e.g., 50 ohms. When higher value loads are used, the speed of response is limited by the RC time constant of the circuit. If the circuit is carefully constructed and the amplifier that follows it has negligible input capacitance, the capacitance of the photodiode limits the speed of response of the system.

The speed of response of the circuit may be described in two ways. First, the radiation can be modulated sinusoidally and the frequency of modulation increased until the output signal power falls to 1/2 of its low-frequency value (3 dB point). The frequency at which this happens is denoted f_o . Second, the

photodetector can be irradiated with a step input of radiant flux, and the rise time (t_r) of the detector can be measured. (Rise time is the time between the 10% and 90% points of the output waveform). These two methods are equivalent and are related to a first order of approximation as follows

$$t_r = \frac{0.35}{f_o} \quad (\text{in seconds}) \quad (10-21)$$

where

$$t_r = 2.2 R_L C_d \quad (\text{in seconds}) \quad (10-22)$$

and

$$f_o = (2\pi R_L C_d)^{-1} \quad (\text{in hertz}) \quad (10-23)$$

10.5 SOURCE-DETECTOR MATCHING

It is often desirable to determine the response of a photosensitive device to a particular source of radiation. Narrow spectral band sources (e.g. lasers) are easily accommodated using the spectral response data already presented. However, wide spectral band sources of radiation require evaluation of an integral like that shown in Figure 10-14. The responsivity values in that table are the results of such integrations carried out for several representative sources and for a variety of photoconductors and photoemitters.

References

25. INFRARED COMPONENTS, Brochure No. **67CM**, Santa Barbara Research Center, Goleta, Ca., 1967.

39. Schwartz, M., INFORMATION TRANSMISSION, MODULATION, AND NOISE, McGraw-Hill Book Co., New York, N.Y., 1959.

70. Jones, **R.C.**, "Phenomenological Description of Response and Detecting Ability of Radiation Detectors," PROC. IRE, Vol. 47, No. 9, Sept. 1959.

71. **Marton**, L., Editor, ADVANCES IN ELECTRONICS, Academic Press, New York, N.Y., 1953.

References continued on page 172.

Source	Source Luminous Efficacy (K) – lm W ⁻¹	ϕ Responsivity (R) – A W ⁻¹						
		Photoconductors		Photoemitters				
		Sb ₂ S ₃	Asos†	S-1	S-10	K-C _s -Sb BI-ALKALI	S-20	S-25
P-1 Phosphor	140	8.0 x 10 ⁻²	1.4 x 10 ⁻¹	5.1 x 10 ⁻⁴	1.9 x 10 ⁻²	6.7 x 10 ⁻²	5.7 x 10 ⁻²	4.1 x 10 ⁻²
P-20 Phosphor	476	9.0 x 10 ⁻²	2.5 x 10 ⁻¹	9.3 x 10 ⁻⁴	1.2 x 10 ⁻²	2.8 x 10 ⁻²	3.8 x 10 ⁻²	3.4 x 10 ⁻²
2854 K Tungsten	23	8.1 x 10 ⁻³	1.8 x 10 ⁻²	5.8 x 10 ⁻⁴	9.1 x 10 ⁻⁴	2.2 x 10 ⁻³	3.5 x 10 ⁻³	4.8 x 10 ⁻³
† 5500 K Blackbody	88	3.1 x 10 ⁻²	6.1 x 10 ⁻²	1.0 x 10 ⁻³	5.5 x 10 ⁻³	2.4 x 10 ⁻²	1.9 x 10 ⁻²	1.7 x 10 ⁻²

‡ Antimony sulfide oxysulfide.

† 5500 K blackbody radiation is approximately representative of sunlight.

ϕ Responsivity computed for each source from:

$$R = \frac{\int_0^{\infty} R_{\lambda} \Phi_{\lambda} d\lambda}{\Phi}$$

where

R = responsivity (A W⁻¹)

R_λ = spectral responsivity (A W⁻¹)

Φ = ∫₀[∞] R_λ dλ = radiant flux on photosensitive surface (W)

Φ_λ = spectral radiant flux (W μm⁻¹)

Fig. 10-14 Photocathode responsivity to various sources (A W⁻¹).

References continued from page 170

72. Engstrom, R.W., "Absolute Spectral Response Characteristics of Photosensitive Devices," RCA REVIEW, Vol. 21, No. 2, June 1960.
73. Engstrom, R.W., and Morehead, A.L., "Standard Test-Lamp Temperature for Photosensitive Devices – Relationship of Absolute and Luminous Sensitivities," RCA REVIEW, Vol. 28, No. 3, Sept. 1967.
74. Cole, M. and Ryer, D., "Cooling PM Tubes for Best Spectral Response," ELECTRO-OPTICAL SYSTEMS DESIGN, Vol. 4, No. 6, June 1972.
75. SBRC WALL CHART 3M67, Santa Barbara Research Center, Goleta, Ca., 1967.
76. RCA PHOTOMULTIPLIER MANUAL, Technical Series PT-6 1, 1970.
77. McIntyre, R.J., "Multiplication Noise in Uniform Avalanche Diodes," IEEE TRANS. ON ELECTRON DEVICES, Vol. ED-13, No. 1, Jan. 1966.
78. McHose, R.E., "Fast Photomultiplier Tube Techniques," RCA Application Note AN-4797, 1971.
79. McHose, R.E., "Time Characteristics of Photomultipliers – Some General Observations," RCA Application Note AN-4884, 1972.
80. METHODS OF TESTING PHOTOMULTIPLIERS FOR SCINTILLATION COUNTING, IEEE Standard No. 398, 1972.
81. Jamieson, J.A., et al, INFRARED PHYSICS AND ENGINEERING, McGraw-Hill Book Co., New York, N.Y., 1963.
82. RCA PHOTOTUBES AND PHOTOCELLS, Technical Series PT-60, 1963.
83. RELATIVE SPECTRAL RESPONSE DATA FOR PHOTOSENSITIVE DEVICES ("S" CURVES), JEDEC Publication No. 50, Oct. 1964.
84. TYPICAL CHARACTERISTICS OF PHOTOSENSITIVE SURFACES, JEDEC Publication No. 61, Dec. 1966.
85. IRE STANDARDS ON ELECTRON TUBES – METHODS OF TESTING, IEEE 62, IRE-7.S 1, 1962.

Section 11

Image and Camera Tubes

This section presents a basic comparison of the general characteristics of the different types of image and camera tubes. Guide lines for low-light-level operation and statistical limitations to viewing are also discussed.

11 .1 IMAGE TUBES

An image tube (often called an image-intensifier or image-converter tube) is an electron device that reproduces on its fluorescent screen an image of the radiation pattern focused on its photosensitive surface. These tubes are used when it is desired to have an output image that is brighter than the input image or to convert non-visible radiation from an image into a visible display. The image tube consists basically of a photocathode upon which a radiant image is focused, an electron lens, and a phosphor screen upon which the output is displayed. Image intensification results when the electrons emitted by the photocathode strike the phosphor screen after being accelerated by high voltage. Luminance gains in a single-stage image tube are usually in the order of 50 to 100. When image tubes are coupled, it is possible to obtain **luminance gains of 10^5 to 10^6** . With such gains it is possible to make observations that are limited by photoelectron statistics only.

The several different families of image tubes which have been developed can be categorized by the type of electron-optical focusing mechanism. In an electrostatic-type image tube, Figure 11-1, an electrostatic field directs the photoelectrons through an anode cone and focuses an inverted image on the

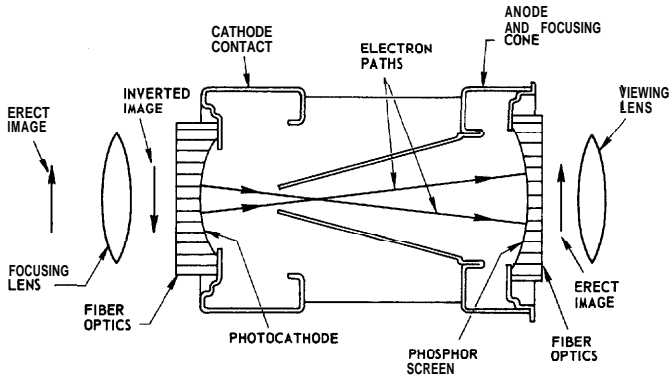


Fig. 11-1 Schematic diagram of an electrostatic-type image tube.

phosphor screen. Electrostatically focused image tubes are relatively simple to operate requiring only a suitable optical lens for focusing the scene on the photocathode, an ocular for viewing, and a power supply. These tubes frequently use a fiber optic faceplate to minimize the fall off in image resolution toward the edge of the tube. The fiber optics also permit efficient coupling to another image tube, to a camera tube, or to photographic film. Although image tubes have, at times, been coupled by conventional optics, the efficiency loss is quite severe.

Another class of image tube may be identified as a "proximity focus" type. In such a tube, the photocathode and the phosphor screen are in parallel planes spaced closely together. The photoelectrons are not actually focused in this arrangement but, because of the high field between the screen and cathode, do not deviate much from trajectories that are parallel to the tube's axis. The tube is small and the screen image is erect, but resolution is not as good as that for the electrostatic or magnetic types.

The magnetic-type image tube combines an electrostatic field with an axial magnetic field provided by either a solenoid or a permanent magnet. With a uniform magnetic field, the resolution is good over the entire screen and distortion effects are very low. Magnetic-type image stages are normally coupled by means of a thin mica or fiber-optic layer with a phosphor on one side and a photocathode on the other, all within the same vacuum. Figures 11-2 and 11-3 show the construction techniques of typical three-stage electrostatically focused and magnetically focused image intensifier tubes.

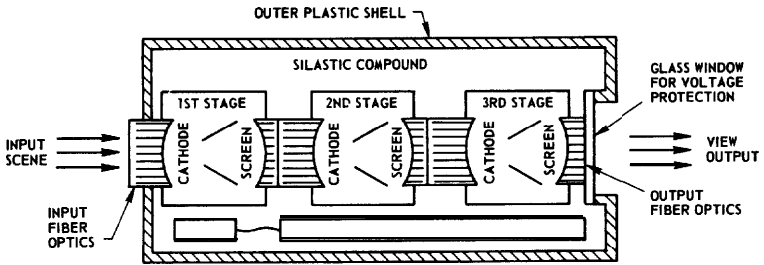


Fig. 11-2 Schematic diagram of typical three-stage electrostatically focused image tube.

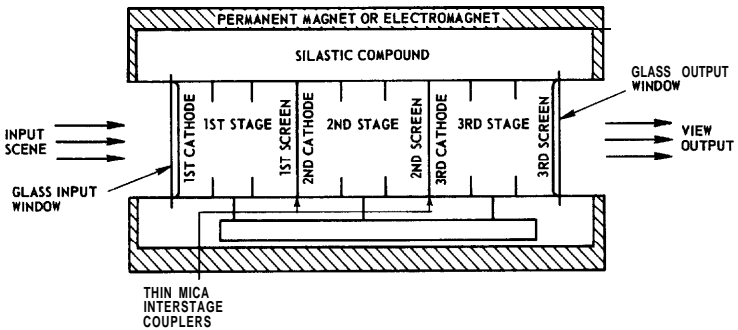


Fig. 11-3 Schematic diagram of typical three-stage magnetically focused image tube.

So-called “second generation” image tubes make use of microchannel plates (MCP’s) to achieve luminance gains in the order of 10^4 . Although high gain is achieved in a small space by means of the MCP structure, the pulse height statistics of the image are degraded by the inherent fluctuation of noise from the MCP. The MCP is essentially a thin secondary-emission current amplifier located between the photocathode and the phosphor screen. This amplifier makes possible a high-gain tube having not only minimum size and weight, but also a saturable-gain characteristic which minimizes blooming (or halation) effects. The microchannel plate itself consists of parallel array of hollow glass cylinders about $10\ \mu\text{m}$ in diameter and about 1 mm, or less, in length. The inside walls of the cylinders are coated with a secondary emitting material. Primary electrons strike the inside walls near the entrance end and cause secondary electrons to be emitted. These secondary electrons in turn

strike the wall further into the depth of the cylinder and create additional secondary electrons. This cascading mechanism produces the high gain. There are two distinct designs of image tubes utilizing the MCP's: the "wafer" design and the inverter design. These tubes are illustrated in Figures 11-4 and 11-5. Most image tubes are also differentiated by the nominal useful diameter of the photocathode. Typical diameter values are 18, 25, and 40 mm.

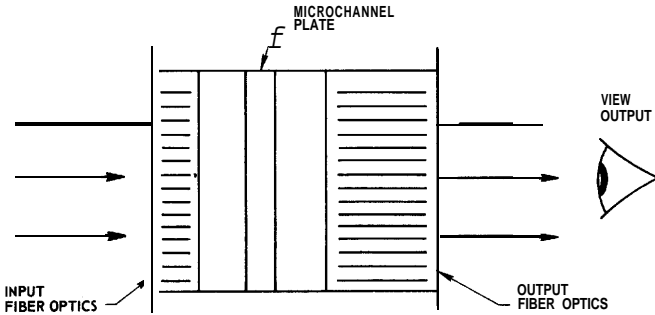


Fig. 11-4 Schematic diagram of proximity focus image tube of the wafer design utilizing an MCP to increase gain.

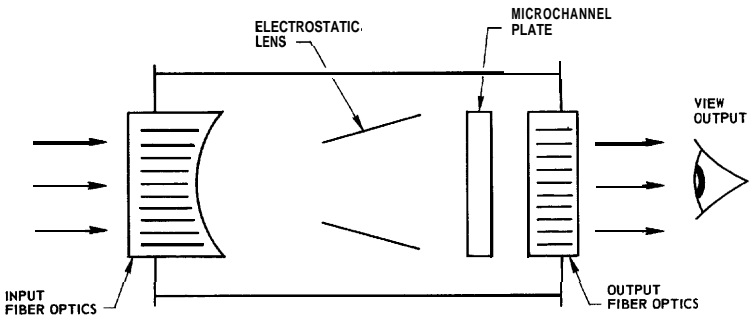


Fig. 11-5 Schematic diagram of electrostatic-focus type image tube utilizing an MCP to increase gain.

11.2 CHARACTERISTICS OF IMAGE TUBES

The resolution capability of magnetically and electrostatically focused single-stage image intensifiers is comparable to that of photographic films such as Royal-X Pan or Tri-X Pan. Figure 11-6 relates typical image tube

resolution ranges in limiting line-pairs per mm to equivalent TV lines per picture height and to the resolving power of photographic film.

Image Tube Limiting Resolution (line pairs/mm)	Equivalent TV line/picture height (25-mm Picture Height)	Comparable Photographic Film	Kodak Resolving Power Designation
25 - 40	1050-2000	—	—
45 - 55	2250 - 2750	—	—
60 - 70	3000 - 3500	Royal-X Pan	ML (Medium-Low)
75 - 90	3750 - 4500	Tri-X Pan	M (Medium)

Fig. 11-6 Image tube limiting resolution compared to that of photographic film.

The modulation transfer function (MTF) or the contrast transfer function (CTF) characteristics are preferable ways of specifying image tube resolution. Limiting resolution values, commonly specified in image tube data publications, provide only a single point on the MTF or CTF characteristic curve. The measured value of limiting resolution corresponds closely with spatial frequency in line pairs per mm at the 3% contrast point. Figure 11-7 gives the typical MTF characteristics of several image intensifiers.

Most image tube manufacturers measure MTF with a commercially available modulation transfer analyzer. The analyzer projects an image of a narrow slit (approximately 10 μm wide) onto the tube input surface. The value of the illuminance falling within the slit is adjusted to provide a fairly bright image on the image tube output screen that is a replica of the slit imaged on the photocathode. The analyzer has an internal optical system that refocuses the intensified slit from the tube screen onto a moving mask whose transmission varies sinusoidally along its length and whose frequency varies from very low (a fraction of a cycle per millimeter) to about 10 cycles per millimeter. The analyzer measures the amplitude of the spatial frequency components in the modulated output image. The input slit image is also analyzed in the frequency domain and the comparison between the output and input data determines the MTF of the image tube. See Section 8-3 for additional information on the modulation transfer function and on contrast transfer function characteristics.

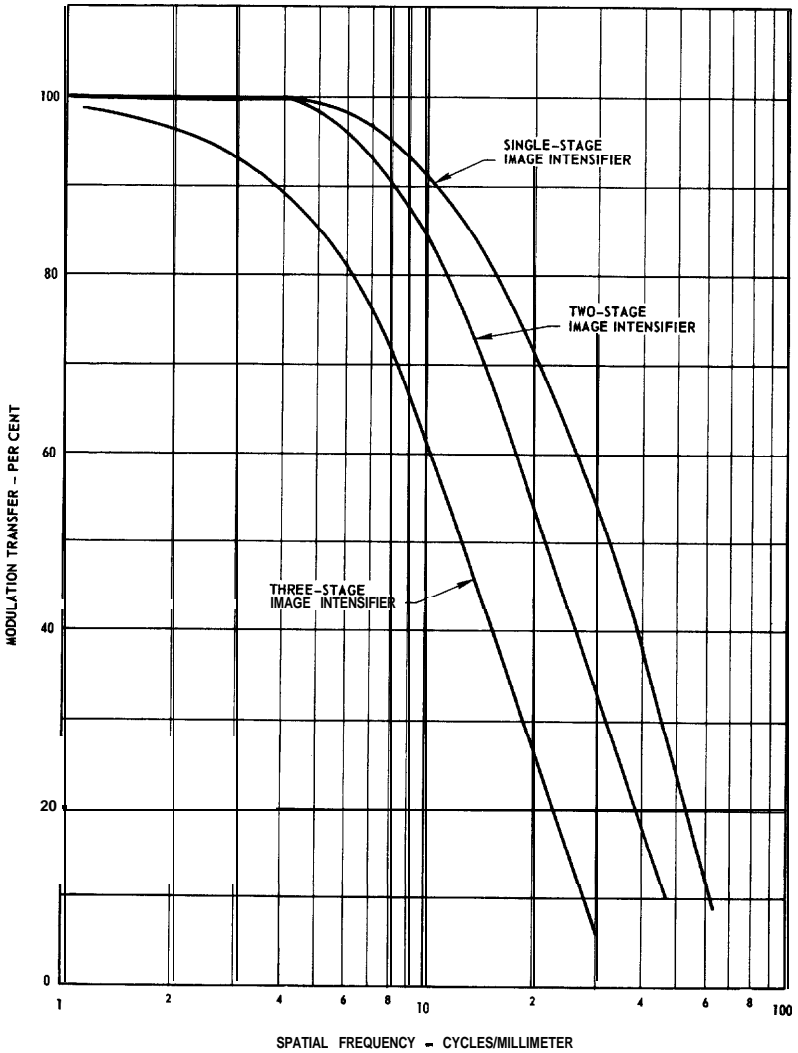


Fig. 1 l-7 Typical MTF characteristics of one-stage, two-stage, and three-stage electrostatically focused image tubes (useful screen diameter- 18 mm).

The gain of an image tube may be defined in a number of ways such as (1) radiant power output divided by radiant power input, (2) luminous flux output divided by luminous flux input, or (3) luminance output divided by illuminance input. The particular gain definition is usually chosen to meet the

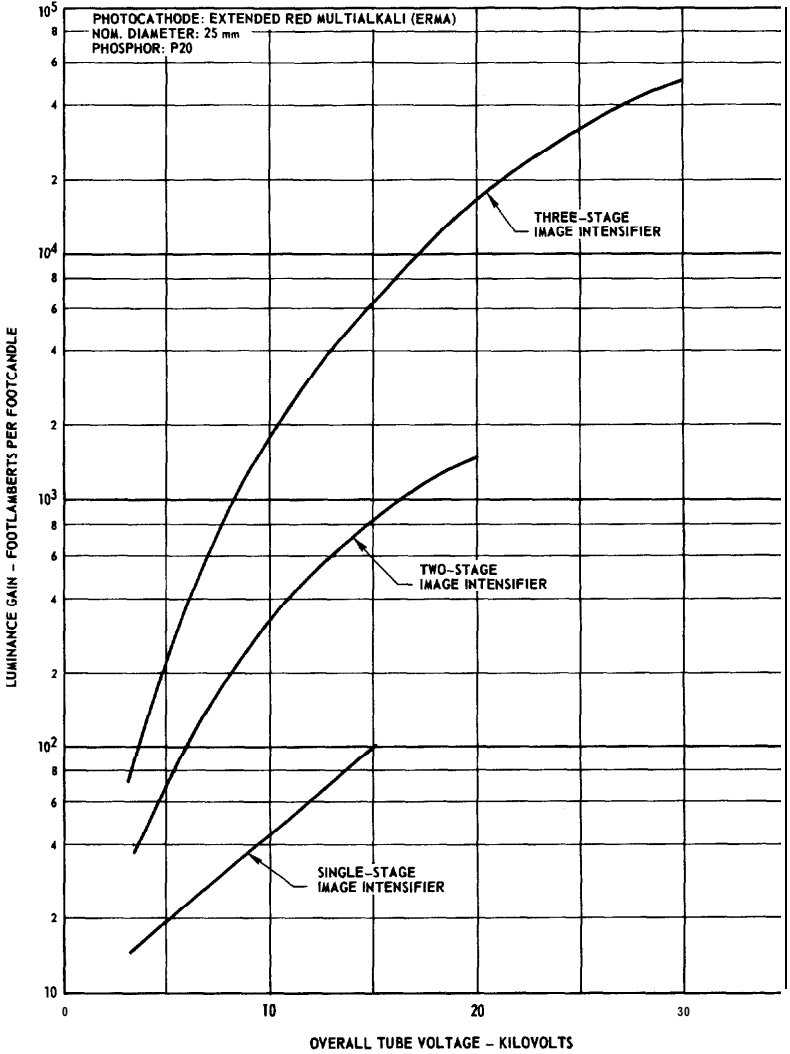


Fig. 11-8 Typical luminance gain characteristics of image tubes.

requirements of the application. Figure 1 1-8 shows luminance gain of single-stage, two-stage, and three-stage 25-mm image tubes as a function of applied voltage.

Image tubes are available with a number of different spectral responses. See Section 10. The S-1 spectral response has been widely used in image tubes for covert viewing at night with an auxiliary infrared radiation source (usually referred to as an active system). Image tubes having a S-20 spectral response and variations of the multialkali photocathode have been used for night viewing without auxiliary irradiation (usually referred to as a passive system) because of their higher quantum efficiency and good response in the red and near-infrared regions of the spectrum.

The output phosphor is usually selected to optimize the tube response by matching to a chosen mode of reception. For example, the P20 (yellow-green) phosphor is frequently used for direct viewing because its spectral output peaks close to the maximum sensitivity of the human eye. See Section 10 for the typical spectral emission characteristics of various phosphors. The P11 phosphor is used for photographic applications because its peak spectral output (about 460 nm) closely matches the characteristics of most photographic films. The P20 and P11 phosphors in single-stage tubes have a persistence in the order of 10 ms, from initial brightness to the 10 percent decay point, under normal image intensifier operating conditions. Coupled intensifier stages will, of course, have longer persistence. Because the persistence durations of P11 and P20 phosphors are not suitable for some applications, other phosphors such as P15 and P16 which have a faster decay characteristic are often used. However, these phosphors usually have lower efficiency and a lower resolution than the P11 or P20 phosphors.

11.3 TELEVISION CAMERA TUBES

The television camera tube is an electron device which converts an optical image into an electrical signal. Camera tubes are used to generate a train of electrical pulses which represent light intensities present in an optical image focused on the tube.

TV camera tubes are used in commercial TV broadcasting, closed-circuit monitor service, the conversion of motion picture into electrical signals, and low-light-level viewing for military and other surveillance applications. A description of each of the many different types of TV camera tubes follows.

The vidicon is the most widely used camera tube. Its small size and simplicity of operation and adjustment permit its use by relatively inexperienced

personnel. Vidicons have moderate sensitivity and are useable in many locations without auxiliary lighting. The speed of response of the vidicon, generally, is somewhat less than that of most other types of camera tubes. A schematic representation of a vidicon tube is given in Figure 11-9.

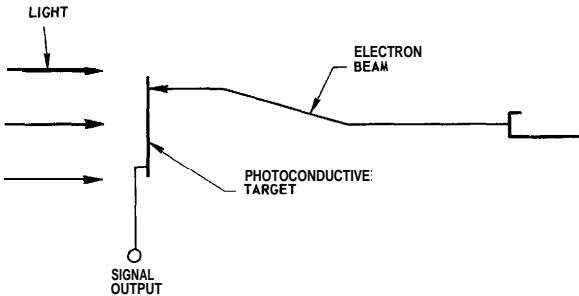


Fig. 11-9 Schematic representation of vidicon camera tube.

The vidicon utilizes an electron beam to scan a photoconductive target which is the light sensor. A transparent conductive layer applied to the front side of the photoconductor serves as the signal (target) electrode. The signal electrode is operated at a positive voltage with respect to the back side of the photoconductor which operates at the cathode (near zero) voltage. In operation, the scanning beam initially charges the back side of the target to cathode potential. When a light pattern is focused on the photoconductor, its conductivity increases in the illuminated areas and the back side of the target charges to more positive values. The electron beam then reads the signal by depositing electrons on the positively charged areas thereby providing a capacitively coupled signal at the signal electrode.

The image orthicon is a more intricate camera tube type than the vidicon. However, it has very high sensitivity and the ability to handle a wide range of light levels and contrasts. A disadvantage of the tube is that the return-beam mode of operation results in excessive noise in the dark areas of the image. For many years, the image orthicon was used almost exclusively for live pickup in studio and outdoor broadcast television cameras. In recent years the image orthicon has been replaced by certain vidicon types (e.g., the lead oxide types) in such applications.

A schematic representation of an image orthicon is given in Figure 11-10. The image orthicon utilizes a photocathode as the light sensor. The photoelectron image pattern developed at the photocathode is focused by an axial magnetic field producing one spiral loop onto a thin moderately insulating target

surface. When the photoelectrons from the photocathode strike the target, secondary emission occurs causing the establishment of net positive charges on the target. The electron beam scans the charged target pattern, deposits some electrons on the more positively charged areas, and the modulated beam returns to an electron multiplier surrounding the electron gun. The output signal is the amplified anode current of the electron multiplier.

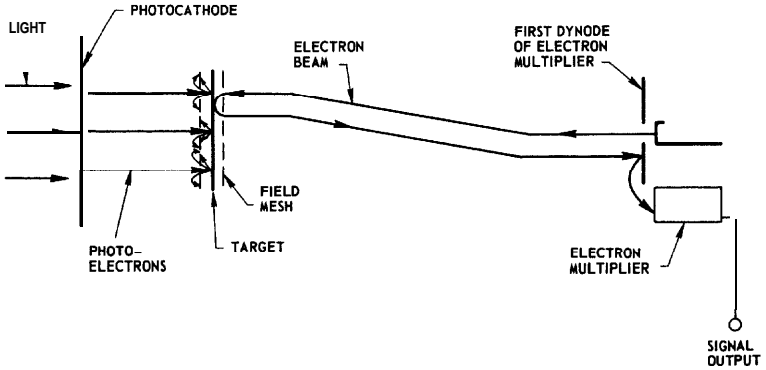


Fig. 11-10 Schematic representation of image orthicon camera tube.

The image isocon is a variant of the image orthicon in which an improved electron-optic system is used and in which the inherent beam-noise problem is largely overcome. The image isocon produces a higher signal-to-noise than the image orthicon, particularly in the dark areas of the picture, and it has equivalent or better resolution, sensitivity, and amplitude response. This tube finds use in low-light-level TV and as a pickup tube for monitoring the output of X-ray image intensifiers in medical applications.

A schematic representation of the image isocon is given in Figure 11-11. In operation, the image isocon is similar to the image orthicon, although the method of extracting the output signal from the return beam differs. When the electron scanning beam approaches the target, several events occur: electrons may enter the target and neutralize a positive charge, electrons may fail to land and be electrostatically reflected, or electrons may land on the target and be scattered back at various angles. The scattered electrons constitute the signal in the return beam. The reflected electrons are eliminated by means of a carefully aligned baffle positioned to assure separation of the return beam components caused by the different electron paths.

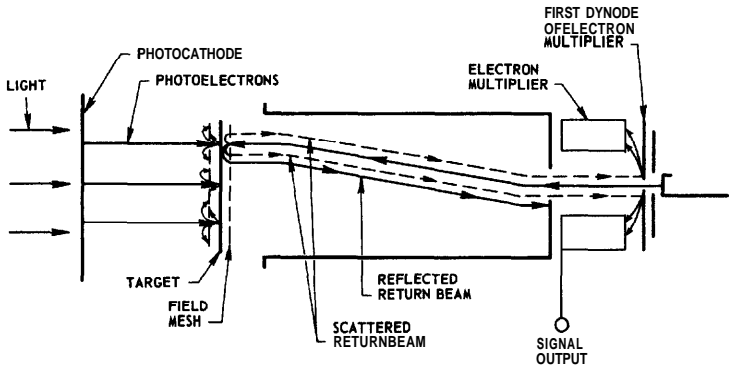


Fig. 11-11 Schematic representation of image isocon camera tube.

The SIT (silicon intensifier target) and the SEC (secondary electron conduction) camera tubes are similar to the image orthicon in that they both employ a photocathode as the image sensor, but the scanning and read-out methods are more like that of the vidicon. A schematic representation of the SIT tube and the SEC tube is given in Figure 11-12. In both tube types, the photoelectrons are focused onto a special target which provides relatively high gain before the scanning operation commences. For the SIT camera tube, the target is a very thin silicon wafer upon which a tightly spaced matrix of p-n junction diodes is formed. The center-to-center spacing of the diodes is approximately $14\ \mu\text{m}$. The gain mechanism is provided when a primary photoelectron, accelerated to perhaps $10\ \text{keV}$, impinges on the target and causes multiple dissociations of electron-hole pairs. Gains of 1000 or more may be achieved. The holes are collected at the p-side of the diode where the charge is neutralized by the scanning beam. The signal is read out on the backplate of the target.

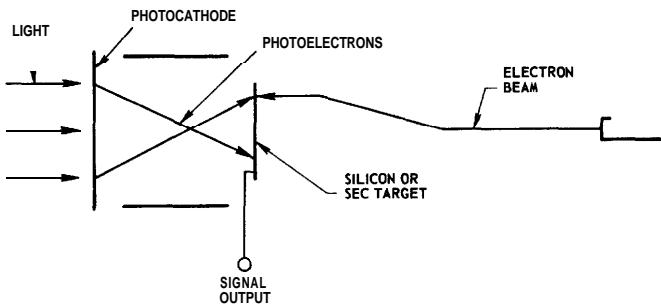


Fig. 11-12 Schematic representation of SIT and SEC camera tube.

The target of the SEC camera tube is a thin layer of semiporous KC1 which has the property of providing gain by internal secondary electron emission. Typical electron gain figures obtained are as high as 100. The signal is read out, like that of the SIT tube, from the backplate of the target.

Both the SIT and SEC tubes have been used extensively for low-light-level pickup. The SIT tube is capable of a very wide range of operation because of the flexibility of its gain mechanism. For example, a SIT tube was successfully used as the color camera tube in the last Apollo moon missions. When an image intensifier is coupled to the SIT tube, the combination is capable of photoelectron-noise-limited operation at the very lowest light levels.

The image dissector is a non-storage type of camera tube in which a photocathode is used as its light sensitive surface. This tube, illustrated schematically in Figure 11-13, does not employ a scanning beam. In the image dissector electron streams from the illuminated photosurface are focused onto an image plane. A set of deflection coils provides fields which sweep the entire electron image, in TV fashion, across an aperture positioned near the center of the image plane. An electron multiplier behind the aperture multiplies only those electrons passing through the hole. The electrons from the output of the multiplier are the output signal. Those electrons not passing through the aperture are discarded. Although the image dissector has low efficiency, because of its very rapid response it is used in application such as star trackers, photon counters, and document readers. If the number of picture elements is small, the lack of storage capability is not too important.

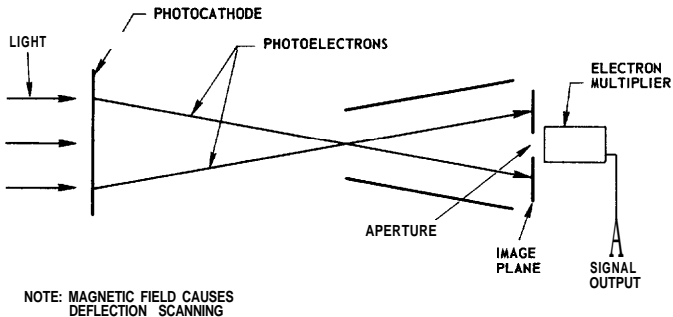


Fig. 11-13 Schematic representation of image dissector camera tube.

A charge-coupled device (CCD) is an MOS-type solid-state imaging device which requires no scanning beam. A schematic representation of the CCD is given in Figure 11-14. Individual cells are formed into a TV-type raster by an

array of parallel conducting strips in one direction and p+-type channel stops at right angles. Electron-hole pairs are created when light is incident on the p-type silicon. The charges, representing picture element signals, are stored in potential wells under depletion-biased electrodes. The charges are transferred by applying a positive pulse to the adjacent electrodes. The whole image is transferred, in this manner, to a storage raster during the vertical blanking period. Each horizontal line is then read out from the storage raster in sequence in a similar manner to provide the output TV signal.

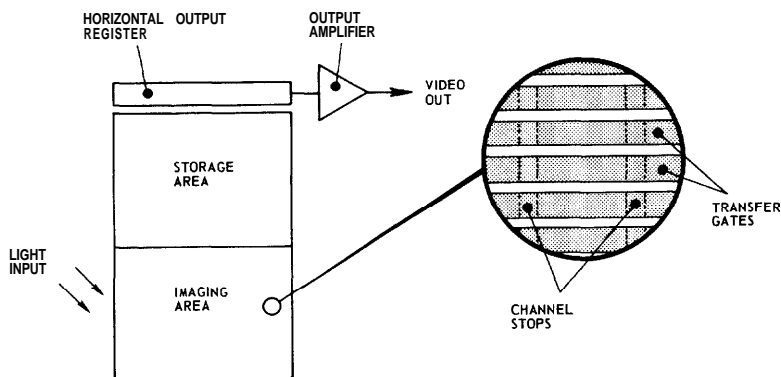


Fig. 11-14 Schematic representation of CCD (Charge-Coupled Device), a solid-state imager.

The foregoing material provides a basic description of the generic types of camera tubes and devices. Many of these tubes, however, are referred to by trade names. Figure 11-15 identifies the names of the various types currently in use in the camera tube industry.

Figure 11-16 is a comparison of some of the more common types of camera tubes and their more important characteristics.

11.4 RESPONSIVITY

Camera tubes are generally rated in terms of output current for a given light level or radiation input level. This quotient, output current divided by incident flux, is called responsivity and varies widely for the different types of camera tubes. The responsivity of vidicons is relatively low because there is no internal gain mechanism as there is in most other camera tube types. Figure 11-17 shows typical signal output characteristics as a function of faceplate illuminance (also known as a transfer characteristic). The slope of

Name	Generic Type	Description
EBIR	—	Electron Bombardment Induced Response. A recently proposed acronym describing target action in response to electron excitation (as opposed to photon). In general, this is the target action encountered in tubes of the image orthicon generic class.
Ebitron	Image Orthicon	Trade name for EM1 (England) camera tube described by them as an intensifier vidicon. It employs a photocathode, an "electron bombardment induced conductivity" (EBIC) target and the electron gun structure of a vidicon. As such it resembles the SIT or SEC type of tube.
EBS	Image Orthicon	Westinghouse Silicon-Intensifier Target (SIT) tube. (Electron Bombardment Silicon).
Epicon	Vidicon	Trade name for General Electric Silicon Target Tube.
Esicon	Image Orthicon	Trade name for a Thomson-CSF (France) tube similar to the SEC.
Image Isocon	Image Orthicon	A very low noise, high performance tube derived from the Image Orthicon.
ISEC	Image Orthicon	Westinghouse-a SEC tube (see SEC) coupled to an image tube.
Isocon	—	See Image Isocon.
ISIT	Image Orthicon	RCA Silicon-Intensifier Target tube (see SIT) with a coupled image tube.
IV	Vidicon	Vidicon with a coupled image tube.
I ² V	Vidicon	Vidicon with a 2-stage coupled image tube.

Fig. 1 1-15 Trade names and generic identification of various camera tubes. (Part I of 3)

Name	Generic Type	Description
Leddicon	Vidicon	Trade name for EEV (English Electric Valve) lead-oxide vidicon.
Oxycon	Vidicon	Trade name for GEC (General Electrodynamics Corp.) lead oxide vidicon.
Plumbicon	Vidicon	Registered trade name for Philips lead-oxide vidicon.
Proxicon	Image Orthicon	Trade name for Westinghouse proximity focus SEC tube (see SEC).
Rebicon	Vidicon	Trade name for RCA "return beam" vidicon (see Return Beam).
Resistron	Vidicon	Trade name for Siemens (Germany) vidicon.
Return Beam Vidicon	Vidicon	RCA-a vidicon in which the output signal is the returning scanning beam (present in any Vidicon) which has been amplified by a secondary emission (multiplier) structure within the tube.
SIEBIR	—	Silicon Electron Bombardment Induced Response. EBIR action involving a silicon target.
SEC	Image Orthicon	Westinghouse-Secondary Electron Conduction (referring to storage target mechanism). The SEC is generically an image orthicon using a target fabricated from KCl.
SEM	Image Orthicon	Toshiba-Silicon Electron Multiplication. The tube is similar to the RCA SIT tube.
Sidicon	Vidicon	Trade name for EEV (English Electric Valve) silicon target vidicon.

*Fig. 1 1-15 Trade names and generic identification of various camera tubes.
(Part 2 of 3)*

Name	Generic Type	Description
SIT	Image Orthicon	RCA-Silicon Intensifier Target. Generically an image orthicon. Electrons emitted by the photocathode are accelerated by high-voltage, focused on a silicon target where the high energy is translated into a large quantity of charged particle pairs and stored by the silicon diode array. Useful target gains of about 2000 are possible.
ST-Vidicon	Vidicon	Trade name for RCA Silicon Target vidicon.
Sivicon	Vidicon	Trade name for Amperex Silicon Target vidicon.
Spectraplex	Vidicon	Trade name for RCA color vidicon (three color tube).
Super Esicon	Image Orthicon	Trade name for Thomson-CSF (France) tube consisting of an Esicon coupled to an image intensifier. Similar to ISEC.
Tivicon	Vidicon	Trade name for Texas Instrument Silicon-Target vidicon.
Vistacon	Vidicon	Trade name for RCA lead-oxide vidicon.
	Charge Coupled Device (CCD)	A solid-state charge-coupled camera device.

*Fig. 1 l-1.5 Trade names and generic identification of various camera tubes.
(Part 3 of 3)*

Characteristic	Sb ₂ S ₃ Vidicon	PbO Vidicon	CdSe Vidicon	Silicon Vidicon	SIT Camera Tube	SEC Camera Tube	Image Orthicon	Isocon
Image Diagonal, mm	16	21	11	16	25	25	45	35
Typical faceplate illuminance, lux (1)	20	3	1	0.5	2×10^{-3}	0.035	0.2	0.02
Responsivity, $\mu\text{A}/\text{lm}$ (3)	250	350	2,750	4,350	2.9×10^5	1.35×10^4	4×10^4	9.2×10^5
Typical signal level, nA	300	300	200	300	300	150	8000	4000
Limiting center resolution, TV lines per picture height (Aspect Ratio—4:3)	1,100	600	700	700	750	600	750	1,100
Lag, 3rd field, % (4)	18	3	12	8	10	3	3	3
Output dark current, nA	20	0.5	1	8.5	10	0.001	(7)	(5)
Intrascene dynamic range (2)	350:1	60:1	60:1	50:1	50:1	50:1	100:1 (6)	1000:1 (6)
Photoconductor material or Spectral response	Sb ₂ S ₃	PbO	CdSe	Si	S-20	S-20	S-10	S-20

- (1) 1 lux = 0.0929 footcandle
 (2) Illuminance range on the faceplate for a 50: 1 (34dB) signal range. Details may be observed in the total range.
 (3) Illumination from a tungsten lamp, 2856 K color temperature.
 (4) Measured at the indicated typical signal level.

- (5) Dark current is equivalent to 10% of the signal current. Dark current is uniform and independent of temperature.
 (6) There is a useful compression of the signal above the knee for wide variations of scene luminance.
 (7) Larger than the signal current and increases with excess beam current.

Fig. 11-16 Important performance characteristics of typical camera tubes.

the characteristic on a log-log plot is referred to as the "gamma" of the tube type. In some cases, a low gamma has the advantage of providing an easier accommodation to a wide range of input light levels. The "saturation" characteristic of the image orthicon, referred to as the "knee", is useful in limiting high light overload situations in scenes, e.g., specular reflections from glass or jewelry. These curves allow the determination of the signal level to be expected from a given type of camera tube and hence the type of processing amplifier required.

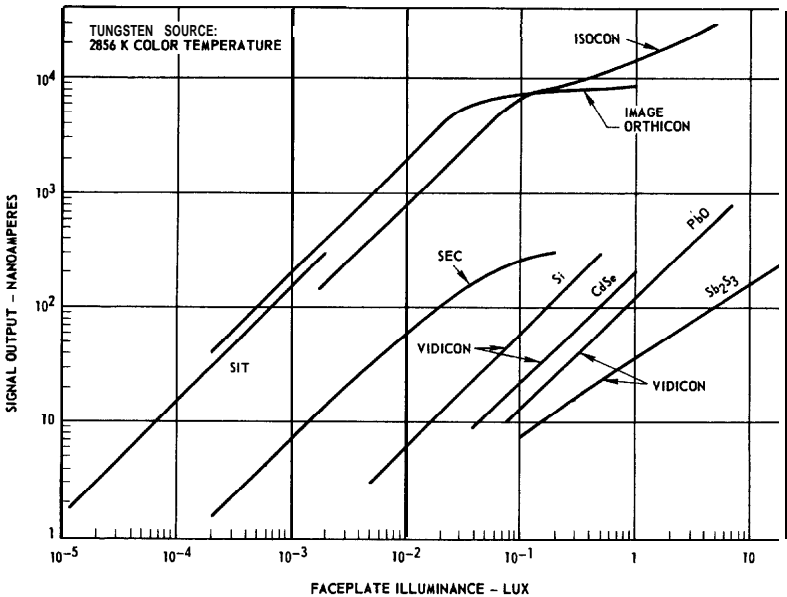


Fig. 11-17 Transfer characteristics of typical camera tubes.

11.5 SIGNAL-TO-NOISE RATIO

The signal-to-noise ratio (S/N) of a camera tube is ideally determined only by the signal-to-noise ratio associated with the photoemission or photoconductive current resulting from the image on the photosensor. In general, the limitation for vidicons results from amplifier noise. Thus, vidicons having the highest responsivity have the highest signal-to-noise ratio at a given light level. Figure 11-18, which shows the signal-to-noise ratio of the most common type camera tubes, is for guidance purposes only because individual types within a camera tube grouping have many varieties in size, responsivities, and internal electrode spacings. In the measurement of S/N it is assumed that the amplifier

bandwidth is 4 MHz and the input noise figure is 5 nA. However, it is to be noted that the signal current is not only dependent on the faceplate illuminance but also on the area of the active raster, with the larger-area devices providing higher signal currents. In the curves shown for the SIT and SEC tubes, which have substantial target gain, the S/N ratio was determined by taking the amplified photoelectron noise and the amplifier noise in quadrature. The electron scanning beam of the image orthicon and image isocon is an additional source of noise, but the multiplier gain is sufficiently high so that the amplifier noise is negligible. The curves shown in Figure 11-18 for these return-beam-type camera tubes were taken with the beam setting fixed at one stop above the knee.

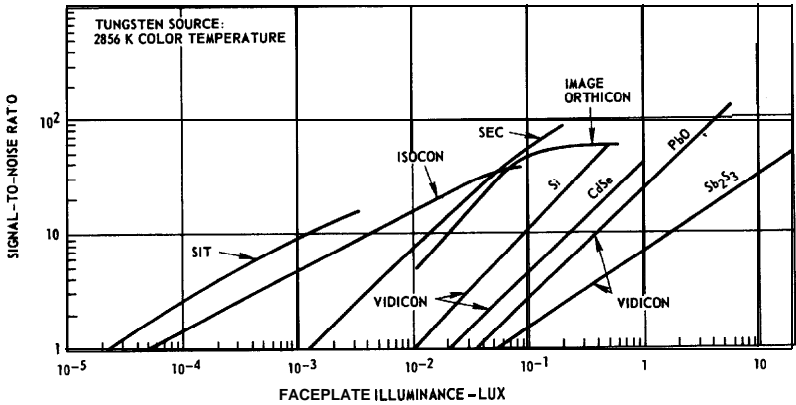


Fig. 11-18 Signal-to-noise ratio characteristics of typical camera tubes.

11.6 LAG

The lag characteristic is an important consideration in selecting a camera tube for a given application, especially at low signal levels. Figure 11-19 shows the range of lag observed or calculated for the different camera-tube types as a function of faceplate illuminance.

The lag shown is the "third field" lag, i.e., the residual signal that is observed three fields (3/60th second) after the light is removed from the tube. Lag is expressed as a percentage of the original signal. For the typical vidicon, which does not have unity gamma, corrections have been made to the measurements to show the lag percentage in terms of the light level. Because the gamma is of the order of 0.65, this correction lowers lag values by a substantial amount, as shown in Figure 11-19. The lower corrected curve can then be compared directly with the linear (unity gamma) devices.

Lag in camera tubes is associated with photoconductive and capacitive effects. Photoconductive lag occurs in certain vidicon types when charge carriers are trapped between the valence and conduction bands in states associated with impurities or imperfections. The time required for thermal excitation to occur and return the carrier to its role as a conductor depends upon the separation of the trap from the appropriate band. The time constant increases at low excitation levels because under this condition only the deeper traps are filled. Photoconductive lag occurs in photoconductive targets such as Sb_2S_3 , PbO , CdSe , but not in Si .

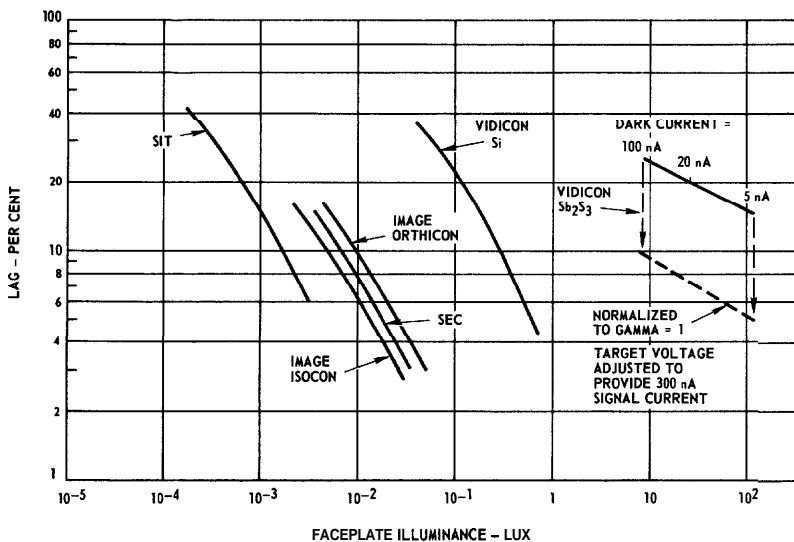


Fig. 1 I-19 Lag characteristics of typical camera tubes.

Capacitive lag occurs as a result of the finite time it takes the electron-scanning beam to remove the charge accumulated on the camera tube target. For a high-capacitance target, a longer time is required for discharge. For low target voltage, a longer time is required to discharge the target because of the exponential dependence of the beam-landing characteristic on target voltage. Thus, capacitive lag also increases as the light level decreases. The lag characteristic for the Sb_2S_3 photoconductive target vidicon shown in Figure 11-19 is a combination of both photoconductive and capacitive lag. The other lag characteristics shown in this figure result from capacitive lag only. Capacitive lag may be characterized by the quotient of the target capacitance and the target gain. Figure 1 I-20 presents data illustrating these characteristics which may be compared with the results of

Figure 11-19. The lower the value of C/μ , the less lag at a given initiating sensor current. Lag is also a function of target area; the smaller the area, the less the lag. The SIT tube has the lowest lag despite its relatively high target capacitance because of its higher gain and the reduced target size caused by demagnification by the image section electron optics. Data are shown only for the silicon-type vidicon where the lag is capacitive. The other types of vidicons, e.g., Sb_2S_3 , PbO , or $CdSe$, have lag characteristics that are dominated by photoconductive trapping effects. Lag values larger than 20 to 30 per cent result in objectionable smearing in scenes with motion; commercial broadcast requirements are in the range of 10 per cent, or less.

Tube type	Target	Capacitance per unit area (C) pF cm^{-2}	Target gain (μ)	C/μ , pF cm^{-2}
Image Orthicon	Electronically conducting glass. Target-to-mesh spacing, $50 \mu\text{m}$	15	3	5
Image Isocon	Glass, target-to-mesh spacing, $250 \mu\text{m}$	7.5	3	2.5
SEC	KCl	300	70	4
Si Vidicon	Si diode array	4500	1	4500
SIT	Si diode array	4500	1500	3

Fig. 11-20 Parameters affecting capacitive lag in typical camera tubes.

11.7 MODULATION TRANSFER FUNCTION (MTF) AND CONTRAST TRANSFER FUNCTION (CTF) CHARACTERISTICS

Although it is preferable to measure the resolution performance of camera tubes in terms of MTF, for practical purposes, the CTF characteristics—square-wave, black and white patterns, see Section 8—are frequently specified in data sheets. CTF and MTF values may be converted from one to the other as shown in Section 8.3.

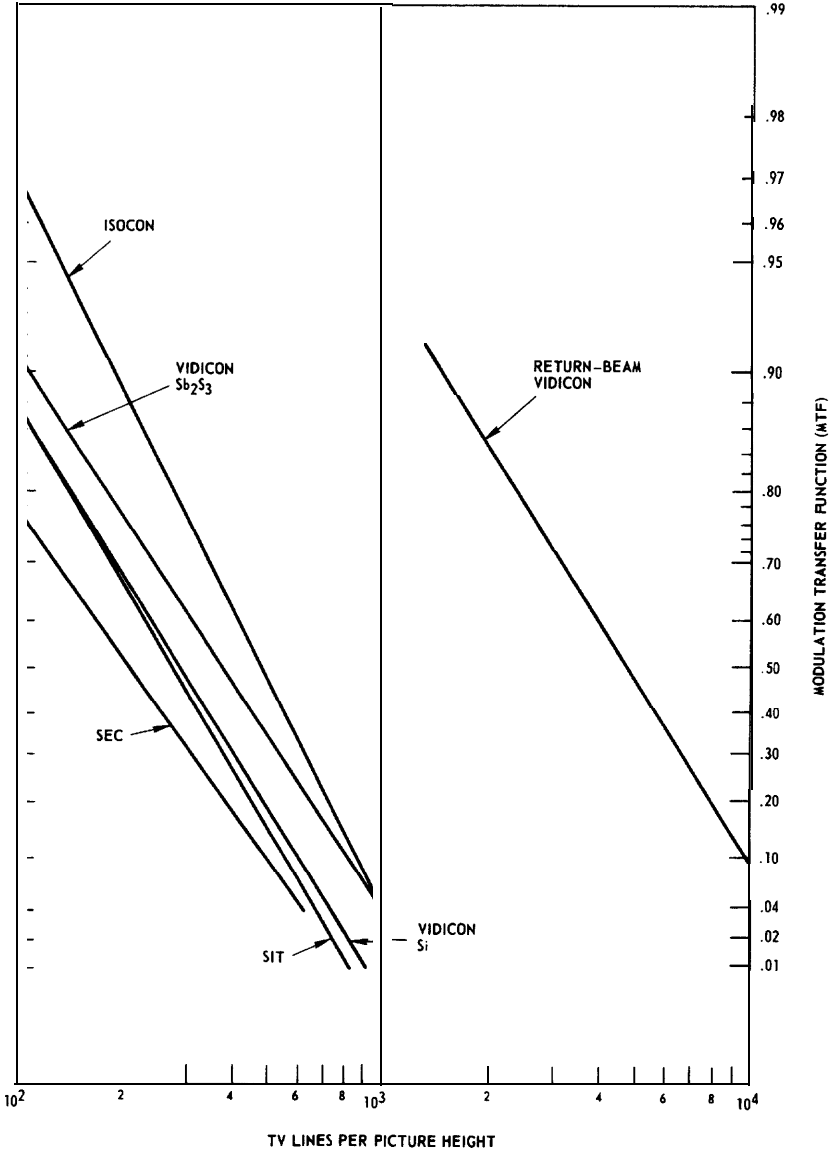


Fig. 11-21 Modulation transfer function (MTF) characteristics of typical camera tubes. (Based on reference 86).

It has been shown (Reference 86) that MTF values may be closely approximated by functions of the class $T(f) = \exp - (f/f_c)^n$, where f is the spatial frequency, f_c is the spatial frequency at which the MTF has a value of e^{-1} , and n is an index which depends on the particular device and may have a value from about 1.1 to 2.1. It is to be noted that if the line spread function for the device is gaussian in character, then $n = 2$. When the log-log of $T(f)$ is plotted as a function of the log of f , a straight line is obtained which permits extrapolation to other MTF values, such as the limiting resolution value (approx. 3%). Figure 11-21 shows MTF characteristics for a number of different camera tube types.

The MTF characteristics for the Sb_2S_3 , PbO, and CdSe type vidicons are principally limited by the electron-beam characteristic and for the same size format are essentially identical. The silicon vidicon is somewhat lower in response because of the finite size of the silicon diodes and the thickness of the target, in addition to the effects of the electron beam. The MTF of a return-beam vidicon (RBV) is also shown in Figure 11-21. In this type of tube, the scanning beam is returned to a multiplier section just as in the image orthicon. When a high resolution gun and a large-format photoconductive target are used, the RBV can provide very high resolution capability. O.H. Schade, Sr. has reported on the return beam vidicon (Reference 87), but the tube type is not generally available commercially and has only been mentioned to indicate the state of the art in high-resolution camera tube developments.

In addition to beam effects and target losses affecting MTF, some camera tube types have additional losses due to the electron-optic characteristics in the image section of the device, the finite fiber size in fiber-optic faceplates, and, in image-intensifier camera-tube combinations, the thickness and particle size of the phosphors.

11.8 LIMITATIONS TO LOW-LIGHT-LEVEL VIEWING

Under typical room luminance conditions, 10^9 photons per second are reflected from an area the size of a single typed letter and are focused by the lens of the eye onto the retina. However, on a dark night, the number of photons per second striking the retina from the same area may be less than 100. The quantum efficiency of the eye for "white" light is estimated to be of the order of 3 per cent. Thus, in a night scene the number of detected photons from a picture element can be very small. For night viewing, the statistical variation in the number of detected photons from a picture element during an observation time may actually exceed the differences to be expected because of the variation in contrast in the scene. The fundamental

statistical problem in picture element identification is examined first before considering the use of optical lenses and image and camera tubes to enhance recognition capability.

11.9 RECOGNITION STATISTICS

Figure 11-22 illustrates a scene composed of an array of square picture elements. One picture element, A, is assumed to have a higher luminance level than the background elements, B.

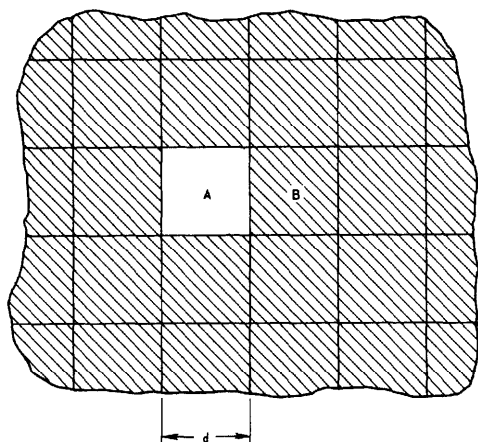


Fig. 11-22 Artificial pattern related to statistical detection of elements making up a scene.

The criterion for identifying picture element A as brighter than that of the background B may be established as follows: During a time of observation, it is assumed that on the average N_a photon events are detected from element A and that on the average N_b photon events are detected from a background element B. Contrast, C, may then be defined as:

$$C = \frac{N_a - N_b}{N_a} = \frac{AN}{N_a} \quad (11-1)$$

Therefore, $1/C$ contrast bands have also been defined.

Assuming gaussian statistics, the probability of a given measure of N_a being outside a one contrast band depends upon the width of the contrast band,

ΔN , compared with the standard deviation. Accordingly $\Delta N = N_a C$ can be compared with $\sqrt{N_a}$. If $\Delta N = \sqrt{N_a}$, the probability that a given measurement would exceed one contrast band from the true value is 31.7 per cent. (The normal distribution for 1σ).

To obtain a higher probability of success than that defined by 10 assume that

$$N_a C = k \sqrt{N_a} \quad (11-2)$$

where k is called the "certainty coefficient". By referring to tables of normal distribution (See Reference 88), one may tabulate the probability that a given measurement for a square is inaccurate by more than 1 contrast band.

k	Probability Measurement Error Will Exceed One Contrast Band
1	3.173×10^{-1}
2	4.55×10^{-2}
3	2.7×10^{-3}
4	6×10^{-5}
5	6×10^{-7}

The selection of the certainty coefficient depends on the complexity of the picture and the degree of certainty that is required. For example, in a TV picture there may be about 200,000 picture elements displayed per frame time of $1/30$ second. To faithfully reproduce all elements within one contrast band, the value for k should be at least 5. However, if the approximate location of a test-pattern picture element within a scene is known, a k value of 1 to 2 is probably satisfactory. The k value may be reduced by a factor of \sqrt{n} if a test pattern contains n picture elements because the average of the n elements is better determined by this factor. The same concept can be used when the detection of an object whose size and shape are known is attempted.

If the quantity, n_a , which corresponds to the white area A in Figure 1 1-22 but gives the density of detected photons per unit area per unit time, is introduced to equation 11-2 then

$$n_a = \frac{N_a}{d^2 t} \quad (11-3)$$

where

- d = the dimension of the resolution element
 t = the integration time for one observation

Changing the criterion of detection to terms of n_a , which is closely related to the illuminance on the scene, provides

$$n_a = \frac{k^2}{C^2 d^2 t} \quad (11-4)$$

Equation 11-4 indicates that the illuminance required for detection increases as the square of the number of contrast bands (gradations), $1/C^2$; increases directly as the number of picture elements per unit area, $1/d^2$; and decreases as the time of observation increases.

A different expression is often developed when the test pattern being observed consists of equal alternate bars of different contrast. In this case variances are added representing the noise in both bars. Thus,

$$N_a - N_b = k \sqrt{N_a + N_b} \quad (11-5)$$

By eliminating N_b and using the definition of C as specified by equation 11-1, the following equations are obtained

$$N_a C = k \sqrt{N_a} \sqrt{2 - C} \quad (11-6)$$

and

$$n_a = \frac{k^2 (2 - C)}{C^2 d^2 t} \quad (11-7)$$

Equation 11-6 may be compared with equation 11-2. Similarly equation 11-7 may be compared with equation 11-4. The equation 11-4 corresponds more closely to a real scene, not one having equal background and signal areas. When the background area is much larger than the signal object, the background variance term is reduced in proportion to the relative area of the background to the signal spot area and may be neglected. Because the U.S. Air Force 1951 three-bar test pattern has a substantially greater background area than the bar pattern area, a more accurate significant general expression probably lies between equations 11-4 and 11-7.

11.10 LENS AND SENSOR LIMITATIONS

Although the F/number of the lens system determines the angle of view, it has no significance in the relationship between the number of photons falling on a picture element in a scene and the number of photons directed by the lens from the element to the photosensor. Only the lens diameter, D , and the lens transmission, T , are needed to specify the flux associated with a particular picture element.

Assume an object picture element is located at some distance, s , from the lens and that it is located on the lens axis and in a plane normal to the lens axis. If n photons per unit time are incident on the picture element, then the corresponding rate of arrival of photons on the sensor which forms the image element is given by the following equation.

$$\text{Rate of arrival of photons} = \frac{n R D^2 T}{4 s^2} \quad (11-8)$$

where R = the scene reflectance. A Lambertian distribution of reflected photons in the scene is assumed. The number of detected photons per picture element at the sensor in an observation time t is, therefore, given by the expression

$$\frac{n R D^2 T t}{4 s^2} \eta \quad (11-9)$$

where η = the quantum efficiency of the sensor.

The expression 11-9 is helpful when comparing the relative advantage that image and camera tube systems have over the unaided eye in **very-low-light-level**, statistically limited viewing. Only three factors are involved in the comparison: the effective diameter of the lens, the quantum efficiency of the sensor, and the time of observation.

The time constant of the eye is often quoted as 0.2 second, but this time varies with light level and becomes longer as the light level decreases. The time constant of an image-intensifier system is a combination of the phosphor decay time and the time constant of the eye. In an image-intensifier camera-tube system, the lag of the camera tube at low signal levels must be considered. Target storage or photographic exposure techniques are often used to achieve very long integration times-providing the scene is stationary.

It is of interest to compare the effectiveness of the unaided eye with optical lenses (telescopes, binoculars), image intensifiers and intensifier-camera tubes for low light level detection capability. The effective diameter of the dark-adapted eye is about 6 mm. For a catadioptric-type lens which is used in night vision optical devices, the T/number may be 1.5 and have a focal length of 300 mm. The effective diameter is therefore 200 mm including the transmission losses. The use of this lens affords an improvement over the unaided eye of 1100 times in the number of photons collected. From equation 11-4, for a given light level, the optical lens thus reduces the smallest resolvable picture element in a scene by a factor of 33 when compared with the eye alone.

In order to compare the effective quantum efficiency of the eye with that of a photosensor element used in photoemissive imaging devices, account must be taken of the different numbers of photons across the spectrum wavelengths. **One must therefore integrate the product of n and η from expression 11-9 and divide by the integral of n over the involved band of wavelengths.** For the eye over a wavelength band of 300 nanometers, the effective quantum efficiency for "white" light is 3 per cent. See Reference 50. The 3 per cent value is calculated from Blackwell's data for eye performance assuming that vision is statistically limited at very low light levels.

For a typical photoemissive photocathode, the extended-red multialkali type, the ratio of detected photons in the total responsivity range of the photocathode to the number of photons in the visible range of the spectrum is 13 per cent for natural night sky irradiance. See Figure 6-12. This value is not quantum efficiency in the usual sense but is weighted to compare the advantage of the photocathode sensor over that of the unaided eye. The advantage of using the multialkali photocathode with a 200-mm lens is an approximate factor of 1.6×10^4 in the number of observed photon events, or a reduction factor of 125 in picture element size when compared with the eye alone.

A low-light-level viewing system thus requires a sensitive photocathode and a large lens to collect the radiation. However, a further requirement is that a relatively noise-free gain mechanism must be provided so that picture presented to the observer is statistically limited by the photoelectron arrival rate and not by noise in the gain mechanism. For a direct-view image-intensifier system, the luminance gain must be at least 2×10^4 . This gain is readily obtainable from three-stage image intensifiers and from second-generation (microchannel-plate) image tubes. In the TV camera system, a noise-free gain mechanism must be provided so that the amplified photoelectron noise in the signal exceeds that of any other noise source in the

system, e.g., electron beam or amplifier noise. This noise condition is approached by various camera-tube image-intensifier coupled devices.

The limiting resolution of a device at low light levels can be compared with the theoretical considerations implied by equation 11-4. Limiting resolution is generally measured with a bar pattern having 100 per cent contrast. For image tubes it is usually specified in terms of line-pairs per millimeter; for camera tubes, in terms of the number of TV lines (black and white) that can be resolved in a picture height. One black and white line is equivalent to one line pair. See equation 11-4. The limiting resolution value corresponds to an MTF of about 3 per cent at high light levels where picture noise is not a limitation. As the light level is reduced, the number of resolved lines decreases because of the obscuration caused by the noise in the picture. Limiting resolution varies approximately as the square root of the scene luminance at low light levels but is MTF limited at high light levels.

However, because the limiting resolution values are obtained using a 100 per cent contrast pattern, these values tend to give misleading information when compared to the performance capability in a real scene. With actual scene contrast values of 30 per cent, or less, the resolution is considerably reduced. Figure 11-23 shows a limiting resolution characteristic for a fiber-optic, three-stage, electrostatically focused image tube. The dashed line represents

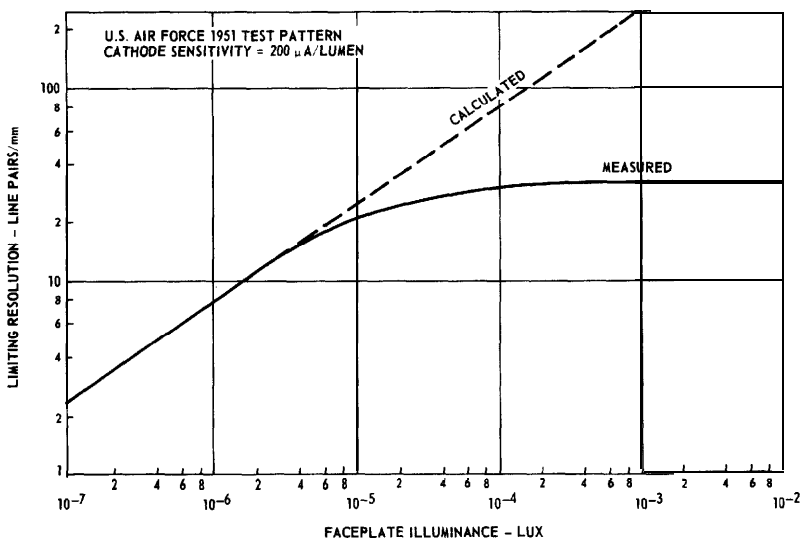


Fig. 11-23 Limiting-resolution characteristics of a three-stage electrostatically focused image tube with fiber-optic coupling.

calculated values from equation 11-4 for $t = 0.2$ second (the integration time of the eye), $C = 1$, and $k = 1$. This resolution measurement was made with the U.S. Air Force pattern which consists of groups of three white bars (each 5 x the width) separated by equal black spaces.

The small value of k seems to provide a good fit to the experimental data and its choice is justified because (1) the location of the minimum distinguishable pattern is quite well known from its relationship to other elements of the test pattern, and (2), the eye-brain combination uses a number of the 15 elements of the pattern in the process of decision and the value of k is reduced by the square root of this decision number.

11.1.1 PRACTICAL DETECTION AND RECOGNITION PARAMETERS

The probability of detection and recognition of specific objectives has been determined experimentally by the Night Vision Laboratory of the U.S. Army Electronics Command at Fort Belvoir, Virginia. Figure 11-24 shows the probabilities of detection and of recognition as a function of the number of cycles of limiting resolution equivalent to the critical target dimension (minimum height or width). From Figure 11-24 it can be seen that there is a 60 per cent possibility of recognizing a vehicle if three cycles of spatial information can be resolved (6 picture elements) in the height of the vehicle.

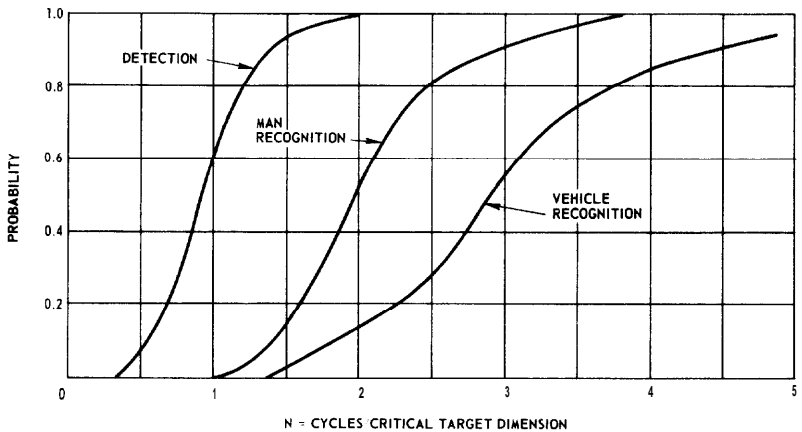


Fig 11-24 Probability of detection and recognition as a function of system resolution across critical target dimensions (Courtesy U.S. Night Vision Laboratory, Fort Belvoir, VA.)

The nomograph of Figure 11-25 relates those parameters which influence the performance of a low-light-level image-intensifier system. The nomograph is based on the detection and recognition probability data of Figure 11-24. The curves for the different contrast values are shifted from the 100 per cent contrast data in accordance with the theoretical concept illustrated by equation 11-4 and the implied definition of contrast.

The shapes of the limiting resolution curves are based on the combination of tube limiting resolution at high light levels and the square root relationship (resolution as a function of illuminance) at low light levels by the approximation:

$$\frac{1}{R^2} = \frac{1}{R_s^2} + \frac{1}{R_t^2} \quad (11-10)$$

where

- R** = the combined resolution limit
- R_s** = the statistical resolution
- R_t** = the inherent tube resolution

An example of the use of the nomograph follows. Assume an illuminance of 2×10^{-2} lux (which is equivalent to the illuminance provided by the moon at first quarter on a clear night in a remote country scene) and that the object viewed reflects 10 per cent of the incident light. A line drawn from the 2×10^{-2} lux point through the 10 per cent reflectance point intersects the scene exitance line at 2×10^{-3} lumen per square meter. For an F/1.5 lens which has an assumed transmission of 90 per cent, a line projected from this line intersects the photocathode illuminance scale at 2×10^{-4} lux. If the contrast of the object against the background is 30 per cent, then by extending a vertical line to the 30 per cent contrast curve, the limiting resolution is 24 line-pairs per millimeter. With this limiting resolution value, the number of picture element cycles required for recognition, the actual dimensions of the target object and the focal length of the lens, one can now determine the range at which the object may be recognized. For example, assume the object to be recognized is a vehicle whose minimum dimension is 2 meters. From the 24 lp/mm point on the vertical axis, extend a line through the 2-meter point to reference line B. Because a wide field of view is generally preferred for close-range observation over a relatively broad scene area, a 50-mm lens was chosen. A line is next extended through the 50-mm focal length point to intersect reference line A. For a vehicle, the N value as obtained from Figure 11-24 is 4 cycles per critical target dimension for an 80 per cent probability of recognition. By extending the line from reference line A through the N

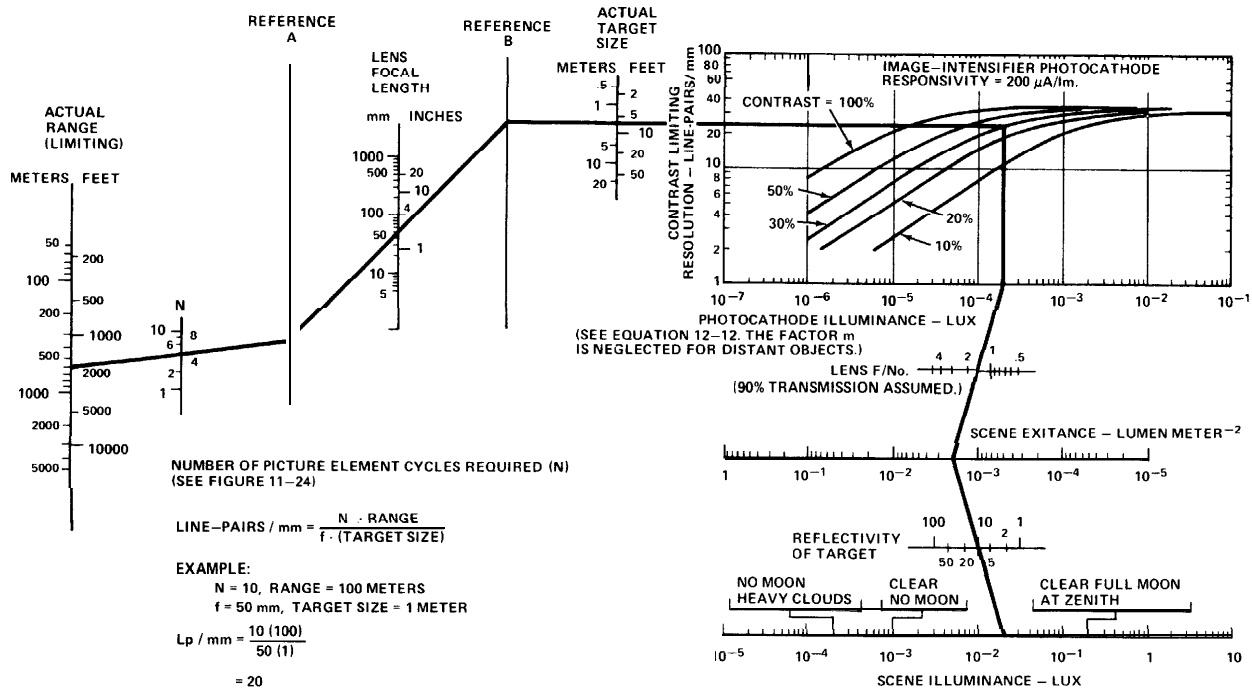


Fig. 11-25 Nomograph for determining performance parameters of a low-light-level image intensifier target detection or recognition system.

point, the maximum range is established as 600 meters. If the other parameters remained the same, the range could be extended by use of a lens having a larger focal length, but this implies a larger lens diameter and a smaller field of view.

Certain camera-tube types may also be operated near the photoelectron noise limit. However, image-intensifier stages must be coupled to the input of the camera tubes to reach the lowest illuminance levels. Limiting resolution characteristics for several different types of camera tubes, for a range of contrast from 30 to 100 per cent, as functions of faceplate illuminance are shown in Figure 11-26. Figure 11-27 shows the same characteristics for fiber-optic image-intensifier coupled camera tubes. The notation I^3V indicates that a three-stage image tube is coupled to a vidicon. The dashed line at the left of the curve in both Figures 11-26 and 11-27 is the limit to be expected for 100 per cent contrast and corresponds to the left side of the curve of Figure 11-23. The illuminance on the tube faceplates for various scene illuminances can be obtained from the nomograph of Figure 11-25. At the very lowest levels of illuminance, and especially for scenes having high contrast, the I-SIT camera tube provides best performance. At more realistic contrast values, however, and at somewhat higher illuminance levels, the image-intensifier isocon (I-Isocon) has a higher limiting resolution capability.

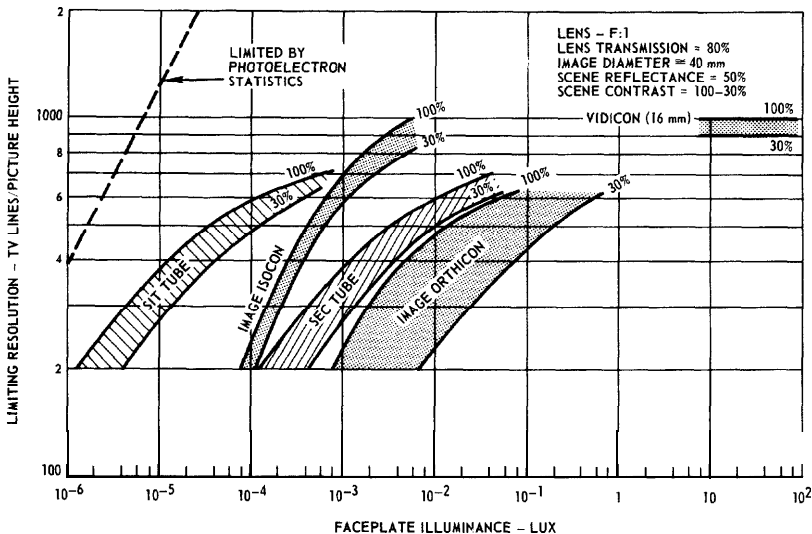


Fig. 11-26 Typical resolution characteristics of selected camera tubes.

Figure 11-28 tabulates comparative data for several different image-intensifier camera-tube combinations when operated under starlight lighting conditions.

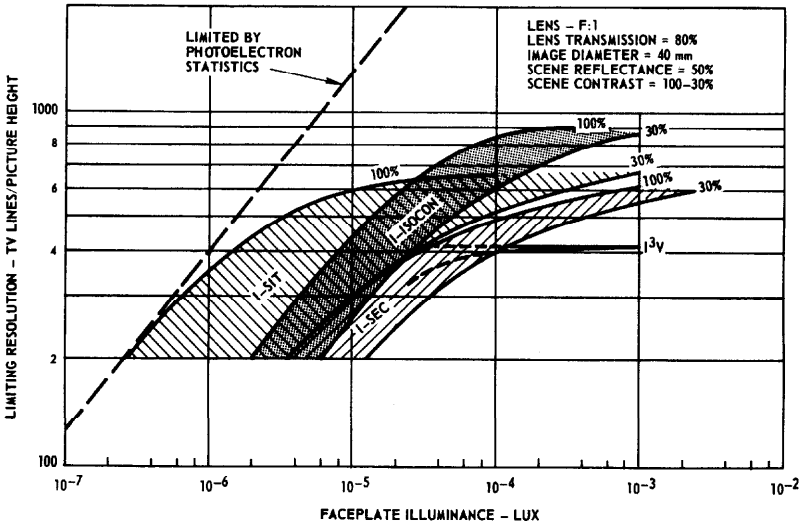


Fig. 11-27 Typical resolution characteristics of selected image and camera tube combinations.

References

50. Rose, A., "The Sensitivity Performance of the Human Eye on an Absolute Scale," J.O.S.A., Vol. 38, No. 2, Feb. 1948.
86. Johnson, C.B., "A Method for Characterizing Electro-Optical Device Modulation Transfer Functions," PHOTOGRAPHIC SCIENCE AND ENGINEERING, Vol. 14, No. 6, Nov.-Dec., 1970.
87. Schade, Sr., O.H., "Electron Optics and Signal Readout of High-Definition Return-Beam Vidicon Camera," RCA REVIEW, Vol. 31, No. 1, March 1970.
88. Dixon, W.J. and Massey, F.J., INTRODUCTION TO STATISTICAL ANALYSIS, McGraw-Hill Book Co., 1957.
89. Neuhauser, R.G., "Understanding the Vistacon," RCA Application Note AN-48 14.1972.

References continued on page 208.

Tube Type		SIT	ISOCON	SEC	I-SIT	I-ISOCON	I-SEC
GENERAL DATA							
Photocathode Diameter	mm	40	35	40	40	35	40
Responsivity	A lm ⁻¹	0.4	0.9	0.015	12	27	0.45
Intrascene Dynamic Range	(1)	50:1	1000:1	100:1	—	—	—
Usable Light Range of Illuminance	(2)	10,000:1	2000:1	200:1	10 ⁵ :1	20,000:1	2000:1
Exposure Damage Limit	lux s	10 ⁵	10 ⁶	10 ²	—	—	—
TYPICAL PERFORMANCE AT NORMAL HIGHLIGHT							
Output Current	nA	500	3000	150	500	3000	150
Faceplate Illuminance to Obtain Typ. Output Current	lux	2 x 10 ⁻³	1.5 x 10 ⁻²	3 x 10 ⁻²	7 x 10 ⁻⁵	5 x 10 ⁻⁴	1 x 10 ⁻³
Lag After 50 ms	%	10	4	2	10	4	2
Limiting Resolution 100% Contrast	TVL	1100	1100	600	1000	1000	500
400 Line Amplitude Response	%	56	75	20	41	56	13
PERFORMANCE AT 10⁻⁴ LUX FACEPLATE ILLUMINANCE							
Output Current	nA	35	20	Not Usable. Signal is very low. Picture would be very laggy and noisy.	500	600	25
Limiting Resolution 100% Contrast	TVL	700	250		900	900	300
Limiting Resolution 30% Contrast	TVL	600	175		550	600	250
Lag After 50 ms	%	30	Not Usable because of lag.		10	13	18
S/N (4 MHz Bandwidth)		3	2		3	3	3
PERFORMANCE AT 10⁻⁵ LUX FACEPLATE ILLUMINANCE							
Output Current	nA				100	60	
Limiting Resolution 100% Contrast	TVL	Not Usable. Low Signal.			800	450	Not Usable. Low Signal.
Limiting Resolution 30% Contrast	TVL	Very Laggy.			350	250	Very Laggy
Lag After 50 ms	%				25	Not Usable. Very Laggy.	

(1) Intrascene dynamic range is here defined as the range of illuminance in a single scene such that the output signal level has a range of 50: 1.

(2) Usable light range is the total range of illuminance which can be accommodated by variation of gain within the tube as well as by the inherent intrascene dynamic range capability.

Fig. I l-28 Typical performance data for selected camera tubes and image and camera tube combinations operated under low-light-level conditions

(References continued from page 206.)

90. Schade Sr., O.H., Resolving Power Functions and Integrals of High-Definition Television and Photographic Cameras-A New Concept in Image Evaluation," RCA REVIEW, Vol. 32, No. 4, Dec. 1971.

91. Rodgers III, R-L. "Beam-Scanned Silicon Targets for Camera Tubes," IEEE INTERCON PROC., March 1973.

92. Rodgers III, R.L., "Charge-Coupled Imager for 525-Line Television," IEEE INTERCON PROC., March 1974.

Section 12

Optics

This section provides simple formulae and definitions that are useful in understanding overall lens requirements for electro-optical systems. Also included are data on the optical properties of glass and on corner reflectors.

12.1 THIN-LENS CHARACTERISTICS AND FORMULAE

A thin lens can be described as either a converging lens or as a diverging lens which has negligible thickness compared with the object and image distances. These lens types have relatively small apertures. The convergent, or positive, lens which is thicker at the center than at its edges, will converge a beam of collimated or parallel light rays to a real focus. The divergent, or negative, lens which is thinner at its center than at its edges will diverge a beam of collimated light. See Figure 12-1.

Focal length, f , is the image distance when the object is infinitely distant.

Lens manufacturers normally determine f using a collimated light source. Focal length f is positive for a converging lens and negative for a diverging lens.

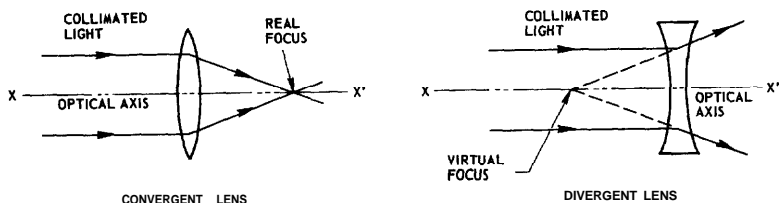


Fig. 12-1 Simple thin-lens types.

Thin-lens formula. The relationship between the focal length and the distances between the lens and the object and the lens and the image is given by

$$\frac{1}{f} = \frac{1}{a} + \frac{1}{b} \quad (12-1)$$

where

- a = the object distance (a is positive for real object)
- b = the image distance (b is positive for a real image, and negative for a virtual image)

Another formulation of this equation, attributed to Newton, is

$$f = \sqrt{(a - f)(b - f)} \quad (12-2)$$

Focal length and index of refraction, n . The relationship between focal length, f , and the index of refraction, n , is given by

$$\frac{1}{f} = (n - 1) \left[\frac{1}{r_1} - \frac{1}{r_2} \right] \quad (12-3)$$

where

- r_1 = the radius on the left lens surface
- r_2 = the radius on the right lens surface
- n = the index of refraction of the lens material

NOTE:

A convention of signs is observed such that both radii are considered positive if the center of curvature is to the right of the vertex (intersection of the surface of the lens with the optical axis).

Image Magnification, m is given by

$$m = \frac{b}{a} = \frac{\text{size of image}}{\text{size of object}} = \frac{\text{image distance from lens}}{\text{object distance from lens}} \quad (12-4)$$

Thin lenses in contact. When two thin lenses having different focal lengths are spaced closely together, the focal length of the combination (f_c) is given by

$$\frac{1}{f_c} = \frac{1}{f_1} + \frac{1}{f_2} \quad (12-5)$$

Lens Power is the reciprocal of the focal length and is expressed in terms of diopters when the focal length units are meters.

F/number or “speed” of a lens is a measure of the angular acceptance of the lens.

$$\text{F/number} = \frac{f}{D} \quad (12-6)$$

where

D = the entrance pupil diameter of the lens (assuming the lens has a circular cross section)

T/number is the effective F/number of the lens and includes the lens losses. Thus,

$$\text{T/number} = F / \sqrt{T_r} \quad (12-7)$$

where

T_r = the transmittance of the lens optics

Numerical Aperture (NA). The numerical aperture, like the F/number, is a measure of the acceptance angle of the lens. Numerical aperture is, however, more applicable to all types of lenses, especially for those having relatively large apertures.

$$NA = n_o \sin \alpha \quad (12-8)$$

where

- α = the maximum possible angle between the optical axis and an extreme ray from the object.
- n_o = the index of refraction in the object or image medium (for air, $n_o = 1$; actually 1.00029). If the image medium is air and the angle α is small, $NA = 1/2F$.

12.2 THICK-LENS CHARACTERISTICS

Principal Planes are the surfaces formed through the intersection points defined by extending the rays parallel to the optical axis entering the system until they intersect the backward extension of the corresponding emerging rays. See Figure 12-2.

Principal Points are the intersections of the principal planes with the optical axis. The primary focal point and the primary principal point are those defined by rays entering the lens from the right. The secondary focal point and the secondary principal point are defined by rays entering from the left.

Focal Lengths. The effective focal length (f_{eff}) for a thick lens is illustrated in Figure 12-2; this length is the distance from the secondary principal plane to the secondary focal point. The front focal length (f_f) is the distance between the primary principal plane and the primary focal point. The back focal length (f_b) is measured from the vertex of the last surface of the lens to the secondary focal point.

The advantage of defining the principal points is that thin lens formulae such as equations 12-1 and 12-2 may be applied to thick lenses provided the object distance is measured from the primary principal point and the image distance is measured from the secondary principal point.

12.3 LENS ABERRATIONS

Spherical Aberration: when various zones of the refracting surface focus the incident ray bundle at different points along the optical axis.

Coma: when an object point is off-axis, and the various zones of the refracting surface magnify images by different amounts and the images formed by the various zones are displaced from the axis by various amounts.

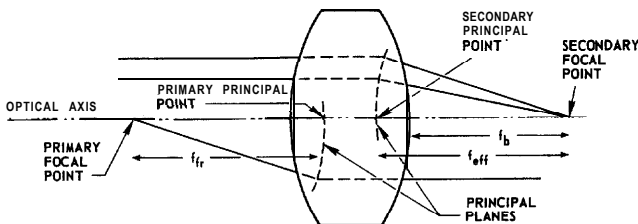


Fig. 12-2 Thick-lens characteristics.

Astigmatism : when light rays passing through the lens in a vertical plane focus at a different distance than light rays passing through the lens in a horizontal plane.

Field Curvature: when a plane surface normal to the optical axis is imaged by the lens not into a plane but into a curved surface.

Distortion: when the magnification of an object line segment varies with its distance from the optical axis of the lens. If the image of a rectangle appears with its sides curved inward, this aberration is called positive or pincushion distortion. If the sides curve outward, it is called negative or barrel distortion.

Chromatic Aberration (longitudinal): when light rays of different wavelengths focus at different distances from the lens.

The table of Figure 12-3 indicates how the different types of aberrations vary with image height, size of aperture, and field angle.

12.4 MTF CHARACTERISTICS OF LENSES

The modulation transfer function (MTF) of a perfect, diffraction-limited circular lens is a function of the wavelength and the F/number of the lens for incoherent radiation. MTF is given by the following equation.

$$\text{MTF} = \frac{2}{\pi} \left[\cos^{-1}(y) - y \sqrt{1 - y^2} \right] \quad (12-9)$$

where $y = \lambda F \nu$ and the spatial cutoff frequency is $\nu = \frac{1}{\lambda F}$

(See Reference 93).

Aberration	Image Height (h)	Aperture Size (d)	Field Angle (a)
Spherical	Independent	d^2	Independent
Coma	h	d^2	a
Astigmatism	h^2	Independent	a^2
Field Curvature	h^2	Independent	a^2
Distortion	h^2	Independent	a^3
Chromatic (Longitudinal)	Independent	Independent	Independent

Fig. 12-3 Relationship of lens aberrations to image height, aperture size, and field angle.

This function is shown in Figure 12-4 for “green” light ($\lambda = 0.5 \mu\text{m}$) and an F/number of 5.6. An experimentally measured curve for an El Nikkor lens is also shown for “white” light and F/5.6. The lens had an f_{eff} of 63 millimeters and a nominal F/number (fully opened) of 3.5.

Lenses may be corrected to achieve various objectives; for example, low-light-level TV systems require the highest possible MTF, especially in the low range of spatial frequencies, because of the limitations imposed by the photoelectron statistics. For photographic purposes lenses are designed to provide optimum performance at high spatial frequencies somewhat at the expense of performance at the lower frequencies.

12.5 DIFFRACTION LIMITS

The image of a distant point source appears, for an ideal lens, as a central bright region (called the Airy disk) surrounded by a series of rings separated by dark rings. The central bright region theoretically contains 83.8 per cent of the total energy. The radius of the first null is given by

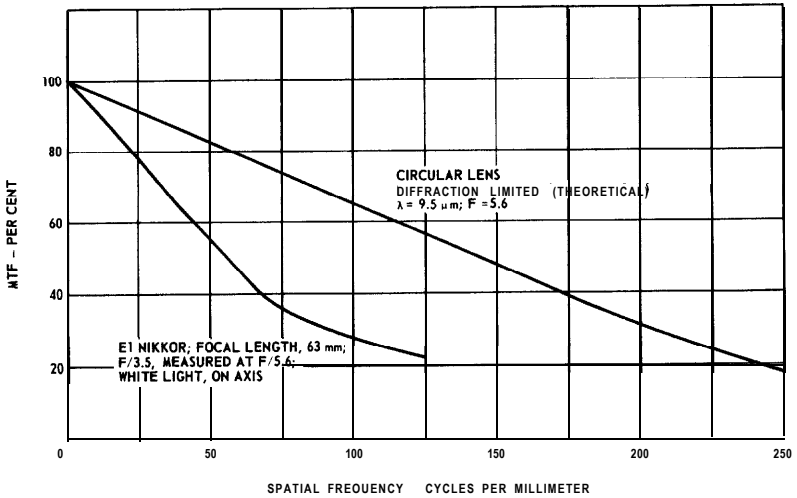


Fig. 12-4 MTF characteristic of a theoretical perfect lens and the measured MTF characteristic of a practical lens.

$$r = \frac{1.22 \lambda f}{D} \quad (12-10)$$

where

λ = the wavelength of the incident radiation

D = the diameter of the lens

f = the focal length of the lens

The resolving power of the lens for viewing distant objects may be expressed in terms of the angular separation of two points which can just be discerned. This minimum angle, a , follows from equation 12-10:

$$a = \frac{1.22 \lambda}{D} \quad (12-11)$$

Practical lenses have larger, more irregular diffraction patterns and, therefore, have somewhat less resolving power.

12.6 ILLUMINANCE AND IRRADIANCE FORMULAE

When an optical lens is used to image a scene on a detector faceplate or on film, the faceplate illuminance may be obtained from the following equation.

$$E_{fp} = \frac{E_{sc} R T_r}{4 F^2 (1 + m)^2} \quad (12-12)$$

where

- E_{fp} = detector faceplate or film illuminance in lx or fc
- E_{sc} = scene illuminance in lx or fc
- R = scene reflectance
- T_r = lens transmission
- F = F/number of the lens
- m = magnification from scene to detector faceplate or film

Equation 12-12 also applies if radiant units are used. In this case, E_{fp} and E_{sc} are expressed in units of watts per square meter ($W m^{-2}$).

Equation 12-12 can also be modified by substituting the T_r /number for the F /number and by substituting luminance, πL_{sc} , for $E_{sc} R$:

$$E_{fp} = \frac{\pi L_{sc}}{4 T^2 (1 + m)^2} \quad (\text{lux}) \quad (1243)$$

where

$$L_{sc} = \text{scene luminance in nits (lm m}^{-2} \text{sr}^{-1}\text{)}$$

If luminance units of footlamberts are used in equation 1-2-13, then E_{fp} is in units of footcandles but the π must be removed from the equation. Equation 12-13 may also be used for radiant units; in this case, E_{fp} is in watts per square meter ($W m^{-2}$) and L_{sc} is in watts per square meter per steradian ($W m^{-2} sr^{-1}$).

The power or radiant flux reaching the image plane from a distant object, Φ_{fp} , is given by

$$\Phi_{fp} = E_o \frac{\pi D^2}{4} T_r \quad (12-14)$$

where

E_o = the irradiance from a distant object at the lens aperture in watts per square meter ($W m^{-2}$)

D = the diameter of the lens aperture in meters (m)

When equation 12-14 is used with photometric units, Φ_{fp} is in units of lumens instead of watts and E_o is expressed in units of lux.

If the distant point source is described in terms of radiant intensity or luminous intensity, equation 12-14 becomes

$$\Phi_{fp} = I \frac{\pi D^2}{4s^2} T_r \text{ (lumens or watts)} \quad (12-15)$$

where

I = the intensity in candelas (cd), or watts per steradian ($W sr^{-1}$)

s = the distance from the lens to the source in meters (m)

Note that the F/number is not used in equations 12-14 and 12-15. Compare the expression for photons given in equation 11-9.

12.7 PROPERTIES OF OPTICAL GLASSES

Figure 12-5 gives the indices of refraction as a function of wavelength for various optical glasses.

The table of Figure 12-6 relates indices of refraction for various optical glasses to principal spectral lines.

12.8 SPECTRAL TRANSMITTANCE OF MATERIALS

Figures 12-7 and 12-8 give spectral transmittance data for materials used as optical windows.

12.9 CORNER REFLECTORS

The amount of energy which is returned toward a radiating source from a cooperating target can be greatly increased by installing a corner reflector or an array of corner reflectors on the target. These devices are capable of retroreflecting most of the radiant power they intercept even though the source is appreciably off the axis, as shown in Figure 12-9.

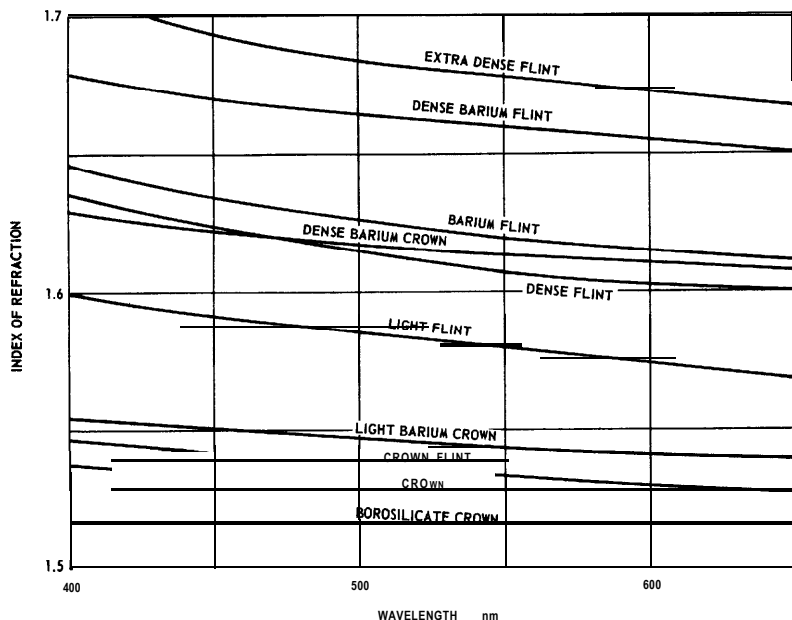


Fig. 12-5 Indexes of refraction as a function of wavelength for various optical glasses (Source: Optical Industries Inc., Costa Mesa, Ca, Catalog B, Copyright 1971; used with permission).

The total radiant power Φ_e that is retroreflected is given by

$$\Phi_e = EA_e(\theta) \text{ (watts)} \quad (12-16)$$

where

E = irradiance of the incident radiation at the corner reflector (W m^{-2})

$A_e(\theta)$ = area of effective aperture of corner reflector (m^2) assuming perfect reflecting surfaces.

θ = angle of incidence of transmitted energy with respect to corner reflector axis.

	589.3 nm n_D	$n_F - n_C^*$	V^{**}	656.3 nm n_C	546.1 nm n_e	486.1 nm n_F	434.1 nm n_G'	404.7 nm n_h	Critical angle at 589.3 nm Φ_c^{***}
Borosilicate Crown	1.51100	0.00804	63.5	1.50860	1.51300	1.51664	1.52112	1.52450	41° 26'
	1.51700	0.00802	64.5	1.51462	1.51901	1.52264	1.52712	1.53047	41° 14'
	1.50500	0.00760	66.5	1.50272	1.50688	1.51032	1.51455	1.51771	41° 38'
Crown	1.52300	0.00895	58.5	1.52035	1.52521	1.52930	1.53437	1.53822	41° 3'
	1.51300	0.00846	60.5	1.51050	1.51509	1.51897	1.52375	1.52737	41° 22'
	1.50800	0.00832	61.0	1.50551	1.51005	1.51383	1.51849	1.52201	41° 32'
Light Barium Crown	1.54100	0.00905	59.8	1.53832	1.54323	1.54737	1.55250	1.55638	40° 28'
	1.58800	0.01102	53.3	1.58477	1.59071	1.59579	1.60214	1.60698	39° 2'
Dense Barium Crown	1.61100	0.01039	58.8	1.60796	1.61359	1.61835	1.62425	1.62868	38° 22'
	1.61300	0.01030	59.5	1.60999	1.61557	1.62029	1.62614	1.63053	38° 19'
Crown Flint	1.53000	0.01022	51.8	1.52702	1.53251	1.53724	1.54316	1.54770	40° 49'
	1.50200	0.00885	56.7	1.49940	1.50417	1.50825	1.51327	1.51714	41° 45'
Light Flint	1.57300	0.01345	42.5	1.56912	1.57631	1.58257	1.59059	1.59686	39° 28'
	1.54900	0.01201	45.7	1.54556	1.55199	1.55757	1.56468	1.57020	40° 13'
Dense Flint	1.65400	0.01925	34.0	1.64857	1.65872	1.66782	1.67967	1.68908	37° 12'
Extra Dense Flint	1.72800	0.02572	28.3	1.72080	1.73430	1.74652	1.76276	1.77592	35° 22'
Barium Flint	1.61700	0.01605	38.5	1.61240	1.62095	1.62845	1.63815	1.64578	38° 12'
Dense Barium Flint	1.70000	0.01709	41.0	1.69509	1.70421	1.71218	1.72246	1.73054	36° 21'
	1.65700	0.01286	51.2	1.65326	1.66016	1.66612	1.67360	1.67934	37° 7'

*The "dispersion" of a material is the rate of change of the index of refraction with wavelength. The F and C lines are normally used to define the dispersion of a particular glass.

** $V = \frac{n_D - 1}{n_F - n_C}$. This is the Abbe Factor and is used in calculations to minimize chromatic aberrations.

***The critical angle is that angle where total reflection occurs. It depends on wavelength and index of refraction.

Fig. 12-6 Indexes of refraction for various glasses at selected spectral lines (Source: Optical Industries Inc., Costa Mesa, Ca., Catalog B, Copyright 1971; used with permission).

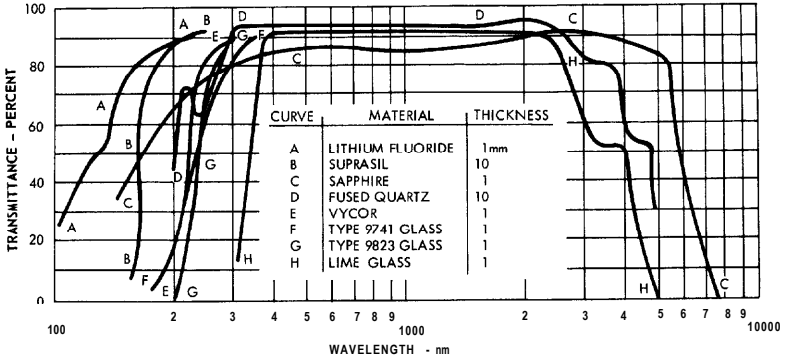


Fig. 12-7 Spectral transmittance of various window materials used in the UV-visible and near infrared.

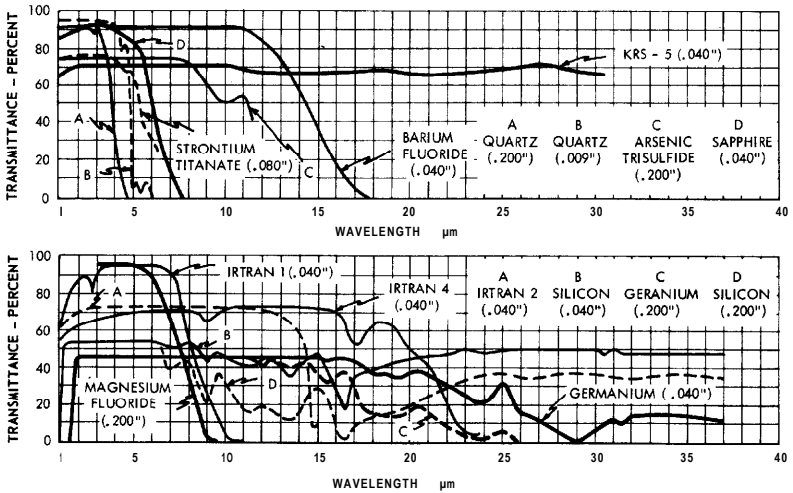


Fig. 12-8 Transmittance of optical materials used in infrared detection systems (Courtesy of Santa Barbara Research Center).

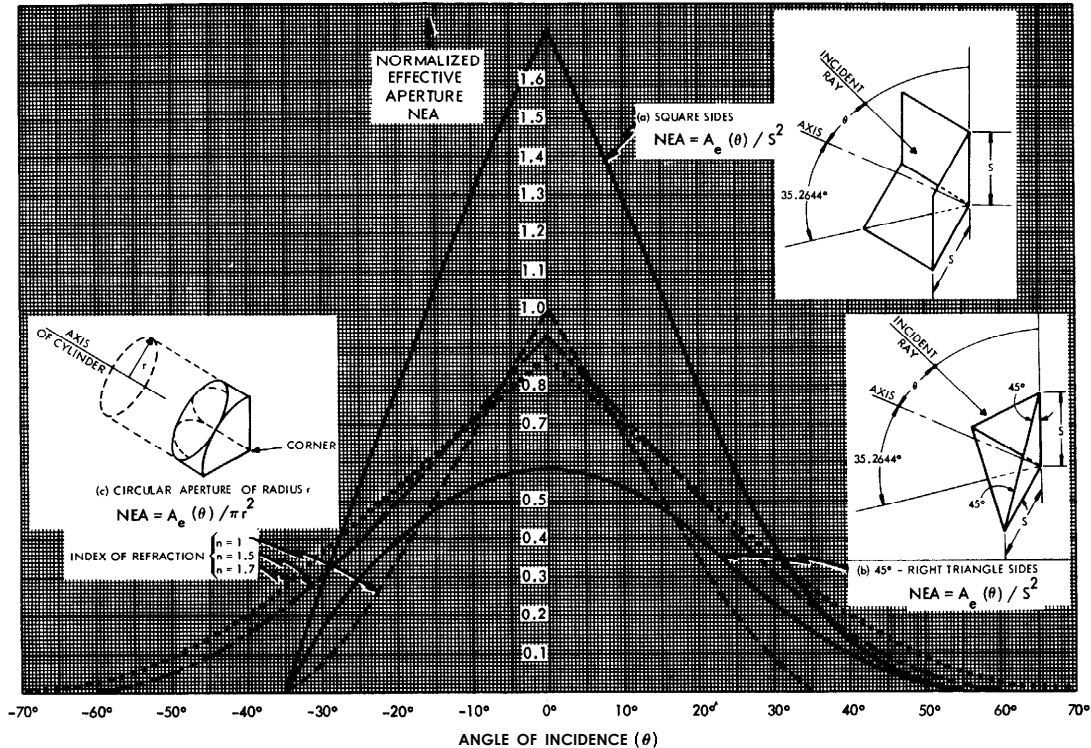


Fig. 12-9 Effective aperture area $A_e(\theta)$ of several kinds of cube corner retroreflectors as a function of the angle of incidence.

The variation of the effective aperture $A_e(\theta)$ is given in Figure 12-9 for three specific cube corner retroreflectors; namely:

- (1) the sides are squares with linear dimensions "S"
- (2) the sides are 45° right triangles (obtained by cutting each of the square sides of configuration (1) along its diagonal).
- (3) the aperture is circular. This retroreflector is a solid section obtained by making a cylindrical cut of maximum radius ($r = S/\sqrt{6}$) in the solid tetrahedron of (2).

The corner reflector of types (1) and (2) can also be made of solid materials as the type (3), in which case wider angular coverage is achieved due to bending of the light on entering and leaving the solid.

The effective aperture $A_e(\theta)$ is indicative of the effect of viewing angle on the energy retroreflected. The intensity at long range is determined also by the diffraction of the retroreflected beam. The following approximate relation applies for single corner reflectors with perfectly aligned reflecting surfaces, where I is the intensity at long range at the beam center and E_e is the irradiance in watts per square meter at the corner reflector (atmospheric loss is neglected):

$$I = \frac{E_e [A_e(\theta)]^2}{2} \quad (\text{W sr}^{-1}) \quad (12-17)$$

The performance of an array of corner reflectors can be formulated somewhat differently from the above because the energy reflected along the center of the beam is also proportional to the number of reflectors, or equivalently, the area used by the reflectors.

Performance parameters of several commercial retroreflectors are given in Figure 12-10, in accordance with the following explanations. The performance of a given corner reflector or a given array of corner reflectors can be defined by the ratios:

$$\text{specific intensity} = \frac{I_e \text{ (watts per steradian at long range)}}{E_e \text{ (watts per square meter illuminating the corner)}}$$

This relation is often expressed in photometric units as

$$\text{specific intensity} = \frac{I_v \text{ (lumens per steradian)}}{E_v \text{ (lumens per square meter)}}$$

which equals

$$\text{specific intensity} = \frac{I \text{ (candela)}}{E \text{ (lux)}}$$

Equation 12-17 gives the theoretical maximum for this performance, for single corner reflectors.

In the case of arrays of corner reflectors, the amount of performance per unit of target area A utilized is of interest and is defined by

$$\text{specific radiance} = \frac{I_e}{E_e A}$$

$$\text{specific luminance} = \frac{I_v}{E_v A}$$

in units of sr^{-1} if the same units of area are used in E and in A . A common usage, however, is to express A in square inches as in Figure 12-10 in which case the units are in mixed English photometric units, candela per foot candle per square inch ($\text{cd fc}^{-1} \text{in}^{-2}$).

When arrays are used as an extended reflecting area, it is convenient to know the gain which they have over more ordinary reflecting surfaces. Because for a perfectly reflecting plane diffuse surface of area A (Lambertian surface)

$$I_d = \frac{E_a}{\pi}$$

and for a perfectly reflecting isotrope of area A

$$I_i = \frac{EA}{4\pi}$$

the following formulas for the gain of a corner reflector array result.

$$\text{Gain over equal-area perfect diffuse reflector} = \pi \frac{I_e}{E_e A} \text{ or } \pi \frac{I_v}{E_v A}$$

$$\text{Gain over equal-area perfect isotrope} = 4\pi \frac{I_e}{E_e A} \text{ or } 4\pi \frac{I_v}{E_v A}$$

These two latter quantities also appear in Figure 12-10.

Model	Description	Area (in) ²	Beam-width	Peak Specific Intensity (cd fc ⁻¹)	Peak specific Luminana (cd fc ¹ in ²)	Gain Over Perfect Diffuse Surface	Gain Over Perfect Isotrope
Stimsonite* FOS-21	Plastic Array	3.839	0.7°	50	13	5850	23,400
Stimsonite* FOS-3111	Plastic Array	.67	0.3°	60	90	40,600	162,000
Hutson* * HCC-S	2½ in. dia. single glass corner	4.91	6 arc sec	5.1x10 ⁷	1.0x10 ⁷	4.7 x 10 ⁹	1.9 x 10 ¹⁰

*Courtesy Stimsonite Division of Elastic Stop Nut Corporation of America, Chicago, Ill.

**Courtesy Hutson Corporation, Optics Division, Arlington, Texas.

Fig. 12-10 Performance characteristics of several commercial retroreflectors.

References

93. Levi, L., APPLIED OPTICS, A GUIDE TO MODERN OPTICAL SYSTEM DESIGN, Vol. 1. John Wiley and Sons, Inc., New York, N.Y., 1968.
94. Catalog B, Optical Industries Inc., Costa Mesa, Ca., 1971.

Section 13

Photographing E-O Displays

This section is intended to assist those desiring to photograph electro-optic displays. Pertinent information is given on sensitometry, the science of measuring the sensitivity of photographic material (film speed) as applied to the control of operations in exposing and processing photographic materials. In addition, information is provided on film exposure definitions and units, film selection for recording cathode-ray tube images, and lens-aperture and exposure-meter settings.

13.1 SENSITOMETRY

Optical Density - The property of photographic film to absorb light (amount of blackening on the negative) is its optical density and is calculated from

$$D = \log \frac{1}{T} \quad (13-1)$$

where D = optical density

T = transmittance value of the film

(NOTE: Transmittance is the ratio of the amount of light that an object passes to the total light that falls upon the object; $1/T$ is defined as opacity.)

Figure 13-1, which is a graphical presentation of Equation 13-1, shows a typical relationship of optical density as a function of transmittance for a film negative.

Photographic Exposure – Photographic exposure E_m is defined as the product of the illuminance E on the film and the time of exposure, viz., $E_m = E \cdot t$. E is expressed in lux and t in seconds or in the customarily used equivalent meter-candle-seconds (m cd s).

Density-Exposure Characteristic – The characteristic curve showing a typical film response for monochrome, negative photographic film is given in Figure 13-2. In this figure, the density D of the developed film is shown as a function of the log exposure

Gamma (γ) – The slope of the straight line portion of the curve (between points B and C) in Figure 13-2 is the film's gamma and indicates how the film will record a scene (degree of contrast). Gamma (γ) can be expressed as:

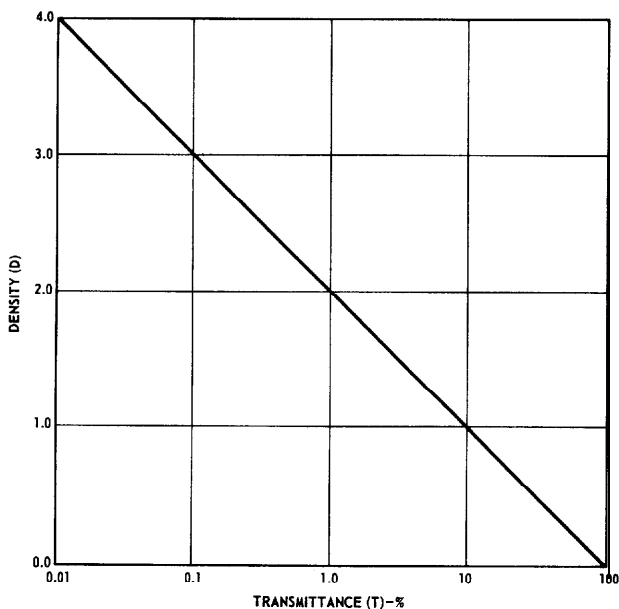


Fig. 13-1 Relationship of density and transmittance for a film negative.

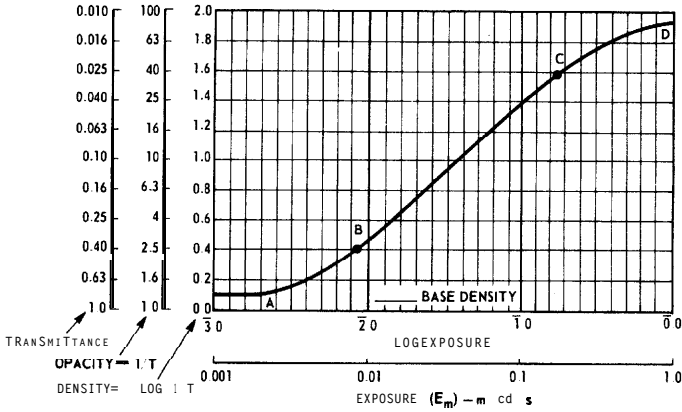


Fig. 13-2 Typical characteristic curve for monochrome negative photographic film (Adapted from Reference 9.5, with permission).

$$\gamma = \frac{D_C - D_B}{\log E_{m,C} - \log E_{m,B}} \tag{13-2}$$

where D_C and D_B = densities on straight line portion of plot produced by

$E_{m,C}$ and $E_{m,B}$ = respective exposures.

For certain types of films, controlling gamma by varying the development time can improve the reproduction of some scenes. Generally, low-contrast scenes can be improved by increasing the development time; high contrast scenes can usually be improved by reducing the development time. These controls, however, can be used only within the limits specified for that particular film. Because different types of developers may be recommended for a particular film, gamma-time curves, such as those shown in Figure 13-3, are provided by the film manufacturers to aid in obtaining a specific gamma during development.

Average Gradient – The value of the average gradient \bar{G} expresses the relationship between optical density and exposure (contrast) over the non-linear portions of the film’s characteristic curve. The two points of optical density between which the calculation is made are written as subscripts of G. For example:

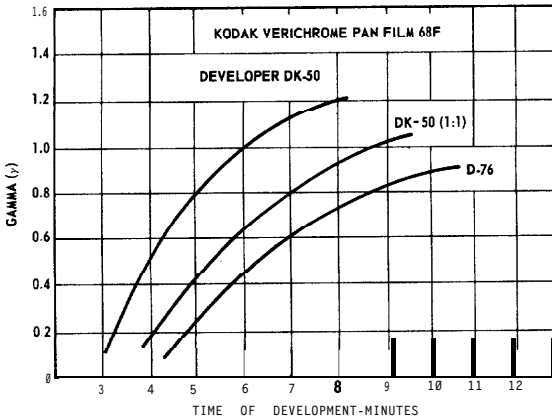


Fig. 13-3 Typical curve showing film gamma as a function of development time (Adapted from Reference 96, with permission).

$$G_{0.8, 0.2} = \frac{0.8 - 0.2}{2.4 - 1.63} = \frac{0.6}{0.77} = 0.78$$

Gross Fog – Gross fog is synonymous with a film's minimum density (D_{\min}) and results from (1) the base material of the film having some inherent density D_{base} , and (2) a spontaneous density that occurs with the development of an unexposed emulsion, referred to as net fog (F_{net}). Consequently,

$$\text{Gross Fog } (D_{\min}) = D_{\text{base}} + F_{\text{net}} \quad (13-3)$$

Exposure Latitude – The ability of a film to reproduce a scene over a range of several different exposure steps is called the exposure latitude and is usually expressed in terms of some number of lens stops.

The brightness range (the difference between the darkest and lightest objects in the scene) can be shifted on the characteristic curve by varying the exposure. Changing the exposure by one lens stop (a factor of 2) results in a corresponding shift of 0.3 log exposure unit along the curve. Most **black-and-white** films have an exposure latitude of 1 to 2 stops underexposure to 2 to 3 stops overexposure. A typical curve having a total exposure latitude of 4 stops is shown in Figure 13-4.

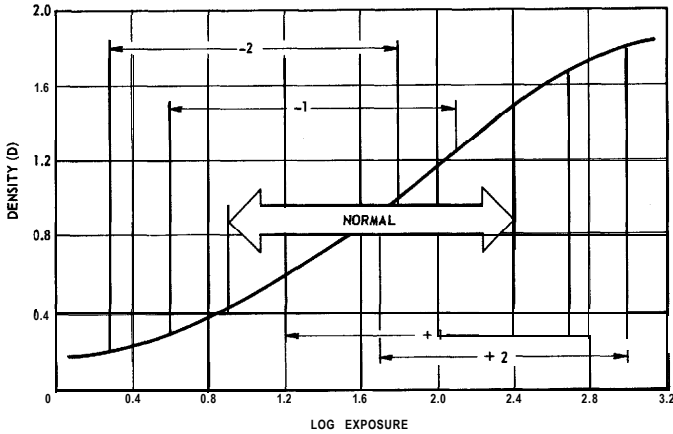


Fig. 13-4 Typical curve of exposure latitude (Adapted from Reference 96, with permission).

Film Speed (For Photographic Negative Materials – Monochrome and Continuous Tone) – In order to determine the correct exposure for a specific film, it is essential that the film speed be known. Film “speed” is another way of indicating the relative sensitivity of film. In the U.S.A., the standard designation of film speed is the ASA number (see reference 97). The ASA speed (arithmetic) is defined in relation to the characteristic curve of the film and its expected usage. Specifically, the ASA speed (S_x) is determined by the equation:

$$S_x = 0.8/E_m \tag{13-4}$$

where E_m is a particular exposure in meter-candle-seconds that corresponds to the point M of Figure 13-5. The point M has been established as that point where the density is 0.10 unit above the base plus fog density (gross fog).

To minimize the effects of different development processes, a development time has been established such that the point N of Figure 13-5, which lies 1.3 log exposure units from point M in the direction of greater exposure, represents a density interval $AD = 0.80$ above the density at point M. Figure 13-6 gives typical values of ASA arithmetic speed.

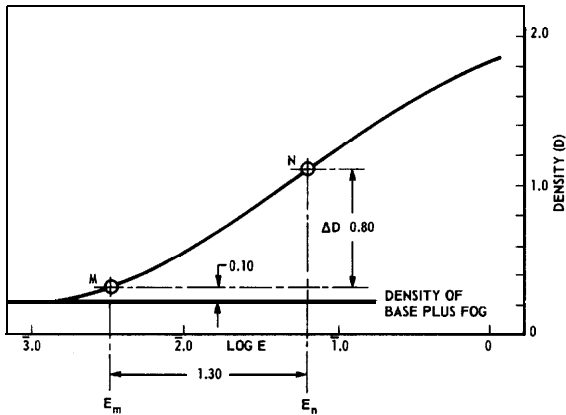


Fig. 13-5 Determining the speed of photographic negative materials (Adapted from Reference 97, with permission).

Black-and-White Reversal Processing – A film that gives the characteristics curve shown in Figure 13-7 is called a positive film, and is generally achieved by reversal processing. By this method, the negative silver image formed is destroyed with a bleach method and the remaining light-sensitive material is exposed and processed to produce a positive image. Reversal processing is often used when a positive image is desired on film. Examples are a motion-picture film when a single copy is sufficient or a black-and-white slide projection.

Speed of Reversal Color Films – For reversal color film intended for viewing on slide projectors, the definition of speed differs from that of photographic negative materials. With regard to the use of photographic exposure meters, however, the result is quite similar.

The arithmetic speed (ASA number) (see reference 98) is computed from the formula

$$S_x = 8/E_m \quad (13-5)$$

Figure 13-8 shows the density-log exposure curve for reversal color film. The value of E_m for reversal color film is determined as follows:

$$E_m = (E_h E_s)^{1/2} \quad (13-6)$$

For $\text{Log}_{10} E_m$ Values		American National Standard Speed
From	To	ASA
6.35-10	6.44-10	3200
6.45	6.54	2500
6.55	6.64	2000
6.65	6.74	1600
6.75	6.84	1250
6.85	6.94	1000
6.95	7.04	800
7.05	7.14	630
7.15	7.24	500
7.25	7.34	400
7.35	7.44	320
7.45	7.54	250
7.55	7.64	200
7.65	7.74	160
7.75	7.84	125
7.85	7.94	100
7.95	8.04	80
8.05	8.14	63
8.15	8.24	50
8.25	8.34	40
8.35	8.44	32
8.45	8.54	25
8.55	8.64	20
8.65	8.74	16
8.75	8.84	12
8.85	8.94	10
8.95	9.04	8
9.05	9.14	6

Fig. 13-6 ASA speed scale (Adapted from Reference 97, with permission).

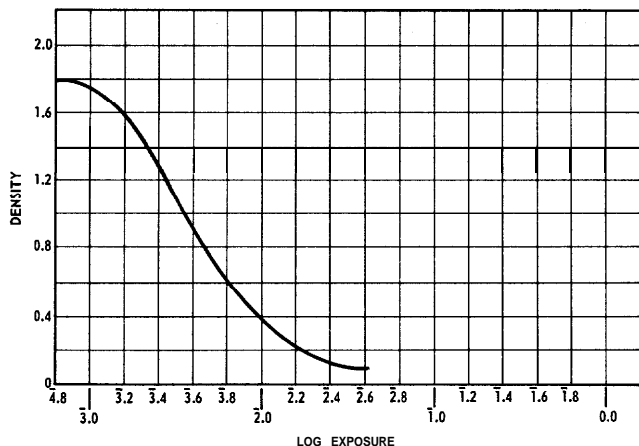


Fig. 13-7 Characteristic curve of a positive film plotted from a reversal processing (Adapted from Reference 96, with permission).

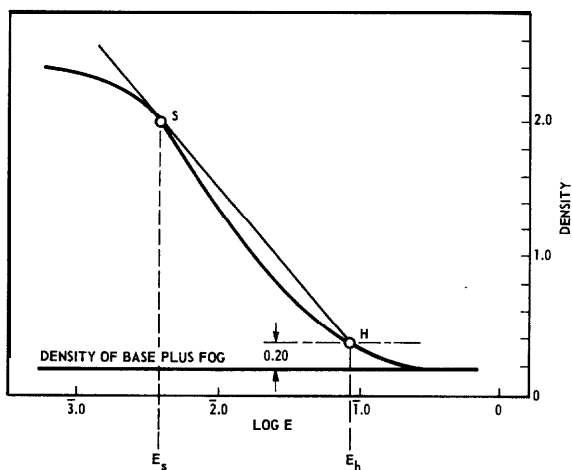


Fig. 13-8 Determining the speed of reversal color films (Adapted from Reference 98, with permission).

The value of E_h is defined as that exposure at a point H whose density is 0.20 unit above the base plus fog density (gross fog). The value of E_s is the exposure corresponding to point S of Figure 13-8. Point S is determined by drawing a line tangent to the curve and passing through point H. If the tangent to the curve occurs at a density greater than 2.0 units above the gross fog, then the point S is taken as that point on the curve where the density is 2.0 units above the gross fog.

Photographic Papers — The characteristic curves for photographic papers are the same as those for films. Gamma values for photographic papers, however, are generally higher than for films. Photographic papers are supplied in various paper-grade numbers which are related to the gamma of the characteristic curve. The higher paper-grade numbers (3, 4, 5) are intended for use with **low**-contrast negatives. Conversely, the lower paper-grade numbers (0, 1) are for use with high-contrast negatives. Grade 2 paper is used with negatives having a normal range of contrasts.

13.2 FILM SELECTION FOR CATHODE-RAY TUBE RECORDING

Film and Phosphor Spectral Characteristics — The most important consideration in selecting the proper film for CRT recording is the relationship of the spectral sensitivity of the emulsion to the spectral output of the phosphor. Because the spectral output of most phosphors is limited to a narrow spectral range, it is necessary to select a film having a spectral sensitivity that includes the spectral output of the phosphor. Figure 13-9, Parts 1 and 2, gives the characteristics of some commonly used phosphors as well as typical films recommended for recording.

CRT Exposure Index — The film speed needed to produce a useful density on the film to record the spot intensity and writing speed of the CRT is another important consideration. One system used to define film speeds for CRT recording is the CRT Exposure Index (see reference 99). This system is based on exposures in units of ergs/cm^2 rather than meter-candle-seconds. The values required to produce net densities of 0.10, 1.00, and 2.00 with a given phosphor stimulation, film, and process are expressed as the reciprocal of the exposure in ergs/cm^2 . The values represent the conversion of a phosphor's radiant energy output into film density and can be used to compare speeds of various films when used with the same phosphors.

JEDEC Designation	JEDEC Persistence Class	Decay Time	Color of Fluorescence and Phosphorescence	Wavelength of Peak Radiant Energy nm	SPECTRAL OUTPUT Wavelength - nm
P1	Medium	24.5ms	Yellowish-green	525	
P2	Medium-short	35 to 70μs	Yellowish-green	535	
P4 (for aluminized screens)	Medium-short	22μs	Violet	455	
P4 (for nonaluminized screens)	Medium-short	60μs	Greenish-yellow	565	
P7	Medium-short	22μs	Violet	457	
			Greenish-yellow	565	
P11	Medium-short	25 to 75μs	Violet	435	
		400 ms	Yellowish-green	555	
P14	Medium-short	34μs	Blue	460	
		27μs	Violet	435	
P16	Medium	5ms	Yellowish-orange	600	
		0.12μs	Near Ultraviolet	383	
P20	Medium to Medium-short	60μs	Yellowish-green	560	
		22μs	Violet	450	
P22	Medium-short	60μs	Green	515	
		0.7ms	Red	680	
P31	Short	1.5μs	Green	510	
		38μs	Green	522	

Fig. 1 3-9 Phosphor characteristics (Adapted from Reference 99, with permission). (Part 1 of 2)

JEDEC Designation	Usual Applications	Remarks	Types of Film for Recording	Suitable for Single-Frame Recording	Suitable for Moving-Film Recording
P1	General-purpose oscilloscopes for visual observation of recurrent phenomena		Ortho & Pan	Yes	No
P2	Oscilloscopes for visual observation of low-speed nonrecurrent phenomena	Low-level yellowish phosphorescence may last for over a minute	Ortho & Pan	Yes	No
P4 (for aluminized screens)	Direct-view black-and-white television picture tubes		Pan	Yes	No
P4 (for nonaluminized screens)	Projection black-and-white kinescopes		Pan	Yes	No
P7	Radar indicators and pulse-modulated applications	Yellowish-green phosphorescence lasts several minutes	Pan	Yes	Yes ^A
P11	Special oscilloscopes for photographic recording, transcriber kinescopes, and image-converter cameras	Has highest photographic efficiency	Blue, Ortho & Pan	Yes	Yes
P14	Oscilloscopes for observing high-frequency pulse-modulated phenomena	Yellowish-orange phosphorescence lasts for about a minute	Pan	Yes	Yes ^A
P16	Flying-spot scanners	Has very high resolution	Blue, Ortho & Pan	Yes	Yes
P20	Direct-view display storage tubes		Pan	Yes	Yes
P22	Direct-view color television picture tubes		Pan	Yes	No
P24	Color flying-spot scanners		Ortho & Pan	Yes	Yes
P31	Oscilloscopes for visual observation of low-speed nonrecurrent phenomena	Greenish phosphorescence may last for about a minute	Ortho & Pan	Yes	No

A - Blue filter should be used to remove long-persistence longer-wavelength component. Without a filter, a blue-sensitive film should be used.

Fig. 13-9 Phosphor characteristics (Adapted from Reference 99, with permission). (Part 2 of 2)

13.3 PHOTOGRAPHING CATHODE-RAY TUBE IMAGES

Camera Arrangement — Figure 13-10 illustrates a typical camera arrangement for single-frame recording. The CRT should be adjusted to provide a sharp trace at an intensity that is compatible with the application. For example, moving film recordings normally require very high intensity settings. It is helpful to take trial exposures at different intensities to determine an optimum setting.

Writing Speed — This function records how fast the image of a spot on the CRT moves across the surface of the photographic emulsion. Writing speed should be considered in CRT moving-film recordings to assure that the combination of CRT, lens aperture, magnification, and film is capable of recording the signals. For example, assume that a sine wave is displayed on the CRT in one dimension with a frequency (f) and an amplitude of A (1/2 peak to peak). The maximum writing speed (v_s) can then be calculated as follows:

$$v_s = [(2 \pi f A M)^2 + v_x^2]^{1/2} \quad (13-7)$$

where M = photographic magnification
 v_x = film speed perpendicular to the motion of the CRT spot image.

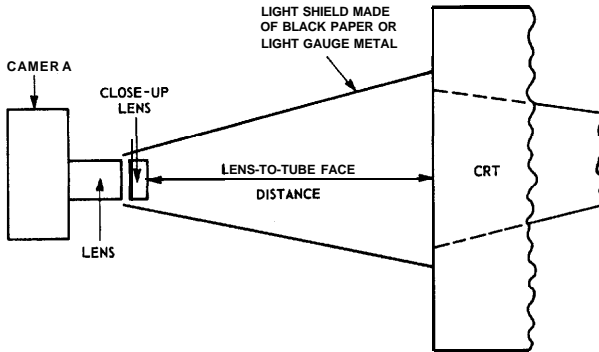
If the **film** speed \ll speed of the image

$$v_s = 2 \pi f A M. \quad (13-8)$$

To test the maximum writing speed that can be photographed with a given combination of CRT, lens aperture, magnification, and film, record a damped sine wave and compute the writing speed where part of the waveform does not record.

13.4 LENS-APERTURE AND EXPOSURE-METER-SETTING FORMULAE

Lens Aperture — The ratio of the focal length of a lens f to the diameter of the lens D is defined as the F/number of the lens, i.e., $F = f/D$. The F/number is a measure of the light-collecting ability of the lens. For a given scene luminance, the illuminance on the film is inversely proportional to the square of the F/number. Cameras are usually provided with a lens-stop indicator and an adjustment control for setting the lens opening. Each stop provides a change in film illuminance by a factor of 2. Thus for a lens stop, or F/number of 2.0, the illuminance is twice that of an F/number of 2.8.



Size of CRT Face (inches)	Use Close-Up Lens	Focus-Scale Setting (feet)	Front of Lens to Tube Face Distance (inches)
35mm Camera and 50mm Lens (24 x 36mm format)			
3	3+ plus 2+	15	7 3/4
5	3+	15	12 1/4
7	2-f	6	15 1/4
10	1+	6	25 1/2
16	1+	10	30

2 1/4 x 2 1/4-inch Roll-Film Camera and 80mm **Lens**

3	3+ plus 3+	3 1/2	5 3/4
5	3+ plus 2+	4	7
7	3+ plus 1+	inf	9 3/4
10	2+	4	14
16	1+	3	22

Fig. 13-10 Camera setup for single-frame recording (Adapted from Reference 99, with permission).

The numerical aperture (NA) which is another method of lens-aperture measurement is given as

$$NA = n \sin \theta \quad (13-9)$$

where n = index of refraction in object space (generally air)
 θ = maximum possible angle value between the optical axis and a ray originating on the axial point and passing through the lens.

The numerical aperture is approximately equal to $\frac{1}{2F}$

when the object is at infinity, i.e. $NA \approx \frac{1}{2F}$.

Exposure Meter Setting – Exposure meters should be adjusted so that the average scene luminance produces an exposure on the film corresponding to the mid-range of the density-log exposure characteristic. For color film, this exposure is approximately the value of E_m as given in Equation 13-6. For photographic negative film an equivalent value would be one log E unit above the E_m shown in Figure 13-5. Accordingly, in both cases the proper mid-range exposure is approximately:

$$E_{\text{mid-range}} = 8/S_x \quad (\text{in m cd s}) \quad (13-10)$$

where S_x is the ASA speed number.

If the average scene luminance is L in candles per meter², the transmission of the camera lens is T , the F /number of the camera lens is F , the image magnification is M , and the exposure time in seconds is t , the exposure on the film becomes

$$\frac{\pi L T t}{4 F^2 (1 + M)^2} = \frac{8}{S_x} \quad (13-11)$$

If the magnification $\ll 1$ and the lens transmission is assumed to be 0.8, then

$$\frac{F^2}{t} = 0.079 L S_x \quad (13-12)$$

If L is measured in footlamberts, equation 13-12 then becomes

$$\frac{F^2}{t} = 0.27LS_x \quad (13-13)$$

References

93. Levi, L., APPLIED OPTICS, A GUIDE TO MODERN OPTICAL SYSTEM DESIGN, Vol. 1, John Wiley & Sons Inc., New York, N.Y., 1968.
95. KODAK PROFESSIONAL BLACK-AND-WHITE FILMS, Kodak Professional Data Book, F-5, 1973.
96. BASIC PHOTOGRAPHIC SENSITOMETRY WORKBOOK, Kodak Publication Z-22-ED, 2nd edition, 1971.
97. "Method for Determining Speed of Photographic Negative Materials (Monochrome, Continuous-Tone), "AMERICAN NATIONAL STANDARD, ANSI PH2.5 - 1972.
98. "Sensitometric Exposure and Evaluation Method for Determining Speed of Color Reversal Films for Still Photography," AMERICAN NATIONAL STANDARD, ANSI PH2.21 - 1972.
99. KODAK FILMS FOR CATHODE-RAY TUBE RECORDING, Kodak Publication P-37, 1969.
100. TECHNIQUES OF PHOTO-RECORDING FROM CATHODE-RAY TUBES, Dumont Division of Fairchild Camera and Instrument Corporation, 1964.
101. Carroll, J.S., Editor, PHOTO-LAB-INDEX, Morgan & Morgan, Inc., Hastings-on-Hudson, N.Y., 1966.

Section 14

Contributors

Following is a list of people who have made contributions to the technical contents of this edition.

D.A. DeWolf
A.J. DiStasio
T. Doyle
R.D. Faulkner
R.W. Fitts
P.D. Huston
G.D. Kissinger
T.T. Lewis
W.D. Lindley
C.A. Meyer
A.G. Nekut
R.G. Neuhauser
R.C. Park
D.E. Persyk
G.A. Robinson
R.M. Shaffer
H. A. Weakliem

Index

Aberration, chromatic213
Aberration, lens212
Aberration, spherical212
Absorptance	12
Aerosol scattering	82
Airy disk214
Albedo	64
American national standard for letter symbols	26
American national standard speed, film231
Angle conversion factors	23, 25
Angular threshold of eye	120
Anode pulse, characteristics168
Fall time169
Rise time169
Apostilb	19, 20
Argon arc lamp	78
Array, corner reflectors222
ASA speed scale, film231
ASA speed, film229
Astigmatism213
Atmospheric backscatter	97
Atmospheric effects on sensor performance	93
Atmospheric transmittance	81
Factor (TA)101
In 0.4 to 4 μm region	87
In 8 to 14 μm infrared region	91

Attenuation coefficient	82
Aurora light	67
Avalanche diodes	165
Average gradient, film	227
Avogadro's number	24
Black and white film reversal processing	230
Blackbody radiation	15, 35
Curves	37
Equations	35
References	42, 43
Boltzmann's constant	24
Brightness	18
Brightness range, film	228
Camera arrangement for CRT image photography	237
Camera tube	173, 180
Contrast transfer function (CTF)	193
Lag characteristic	191
Low-light-level performance data	207
Modulation transfer function (MTF)	193
Performance characteristics	189
Performance data	207
Resolution characteristics	205
Tube responsivity	185
Signal-to-noise ratio	190
Trade names	186
Transfer characteristic	185
Transfer characteristics	190
Candela	15-20
Candle	15
Capacitive lag, camera tube	192
Carbon arc lamp	78
Cathode-ray tube recording	233
Cavity dumping	128
CCD (charge-coupled device)	184
Certainty coefficient	197
Characteristic curve, film negative	227
Characteristics of image tube	176
Characteristics of thick lens	212
Charge-coupled device (CCD)	184
Chroma	48
Chromatic aberration	213
Chromaticity diagrams	51, 52
Circuit noise	165
Close-confinement lasers	137
Coherent radiation	127

Color:

- And human eye 47
- Matching 48
- Mixture curves 50
- Reversal film speed 230,232

Colorimetry 48

Coma 212

Commercial retroreflector characteristics 224

Cone vision 45

Cones 45

Contrast transfer function (CTF) 114

Contrast transfer function, camera tube 193

Convergent lens 209

Conversion factors:

- For illuminance quantities 18
- For luminance quantities 20
- For luminous exitance quantities 19

Corner reflector array 222

Corner reflectors 217

Coupled image and camera tube resolution characteristics 205

CRT exposure index 233

CRT image photographing 236

Crystalline lasers 128, 129

CTF (contrast transfer function) 114

CTF, camera tube 193

D* (specific detectivity) 159

Darkcurrent 147,149

Dark-adapted eye 200

Dark-adapted eye response 45

Density-exposure characteristic 226

Detection 109

- Parameters 202
- Probability 110, 122,202
- Probability factors 123

Detectivity 147,150

Detector characteristics 145

Detector parameters, symbols, and units 147

Development time, film 227

Diffraction limits 214

Display interpretation 119

Distortion 213

Divergent lens 209

Double heterojunction laser 138

Dye lasers 132

Electroluminescent diodes 143

- Systems 141

Electromagnetic spectrum	13, 14
Electron charge	24
Electrostatic-type image tube	173
Emissivity	12
EN1 (equivalent noise input)	147, 150
Equivalent luminous flux	147
Equivalent noise input (ENI)	147, 150
Exposure:	
Index, CRT recording	233
Latitude, film	228
Meter setting, CRT image photography	238
Photographic	226
Extinction coefficient	82
Eye :	
Angular threshold	120
Dark-adapted	200
Quantum efficiency	200
Receptors	45
Response	45
Search time	121
Spectral responsivity	46
Time constant	199
F/number	211
Fabray-Perot cavity	136
Fall time, anode pulse	169
False alarm rate	110
Far infrared response, solid-state devices	156
Field curvature	213
Film:	
Average gradient	227
Brightness range	228
Characteristics curve	227
Development time	227
Exposure latitude	228
For CRT recording	233
Gross fog	228
Negative density	226
Negative transmittance	226
Opacity	225
Spectral characteristics	233
Speed	229
Speed, ASA scale	231
Transmittance	225
First radiation constant ($8\pi hc$)	24
Fluorescent daylight lamp	79

Focal length, F	209
Thin lens	210
Thick lens	212
Footcandle	18
Footlambert	19, 20
Formulae for thin lenses	209
Fovea	4 5
Gain, image tube	179
Galactic irradiance	71
Gamma (γ)	226
Gaslasers	128, 130
Gas-filled phototubes	145
Glass lasers	128
Glass properties, optical	217
Gross fog, film	228
Harmonic-generator laser	134
Homojunction type laser	138
Horizontal visibility	87
Horizontal-path transmittance	82
Hue	48, 51
Human eye response	45
Illuminance	16, 17
Illuminance formula, lens	216
Illumination	17
Image converter tube	173
Image dissector	184
Image intensifier tube	173
Image isocon	182
Image magnification (M)	211
Image orthicon	181
Image tube:	
Characteristics	176
Electrostatic type	173
Inverter design	176
Low-light-level performance data	207
Magnetic focus type	174
Modulation transfer function (MTF)	177
Output phosphor	180
Performance data	207
Proximity focus type	174
Resolution	176
Spectral response	180
Wafer design	176

Incident flux	. 146
Index of refraction (N)	. 210, 212
Opticalglass	. 218, 219
Infrared transmittance, optical material	. 220
Injection laser sources	. 142
Inverter design image tube	. 176
Irradiance	. 10
Irradiance formula, lens	. 216
JEDEC phosphor designation	. 234
Lag, camera tube	. 191
Lambert	. 19, 20
Lamp sources	. 72
Large optical cavity (LOC) laser	. 137, 138, 143
Laser :	
Action	. 127
Safety procedures	. 128
Lasers, crystalline	. 128, 129
Dye	. 132
Gas	. 128, 130
Glass	. 128
P-N junction	. 135
LED	. 135, 139, 143
LED sources	. 142
Lens:	
Aberration	. 212
Limitations	. 199
Modulation transfer function (MTF)	. 213
Power	. 211
Requirements	. 209
Resolving power	. 215
Speed	. 211
Transmittance	. 211
Light sources, p-n junction	. 135
Light-adapted eye response	. 45
Light-emitting diode (LED)	. 135, 139, 143
Limitations to low-light-level viewing	. 195
Limiting resolution	. 119, 201
Limits of lens diffraction	. 214
Line resolution	. 120
LOC (large optical cavity)	. 137, 143
Longitudinal chromatic aberration	. 213
Low-light-level performance data, image and camera tubes	. 207
Low-light-level image intensifier system nomograph	. 203

Low-light-level viewing, camera tube 195

Lumen 15, 16

Luminance 16, 17, 18, 48

 Gain, image tube 179

 Units 18

Luminous density 16

 Efficacy 16, 45, 55

 Efficacy calculations 55

 Efficiency. 16, 55

 Energy 16, 17

 Exitance 18

 Flux 16

 Flux density 16

 Intensity 15, 16

 Intensity standard

Lunar illuminance. 63, 64, 65

Lux 16, 17, 18

Magnetic focus image tube 174

MCP (microchannel plate) 175

Measurement error probability 197

Mercury short arc lamp 76

Mesopic eye response 46

Metric system units. 23, 26

 Prefixes and symbols. 33

Microchannel plate (MCP) 175

MIE scattering 82

Mode locking 128

Modulation transfer analyzer 177

Modulation transfer function 114

 Camera tube 193

 Image tube. 177

 Lens 213

Moon illuminance 63

MTF 114

 Camera tube 193

 Characteristic of lens 215

 Degradation by image motion. 117

 Image tube. 177

 Lens. 213

Natural illuminance levels 72, 74, 75

Natural scene illuminance 70

Near-infrared spectral response for photoemissive devices151
NEP (noise equivalent power)150
Night sky irradiance	71, 72, 73
NIT	16, 19, 20
Noise	109, 147, 160
Current150
Equivalent power	147, 150
Nomograph for low-light level image intensifier system203
Numerical aperture (NA)2
Opacity of film225
Optical density, film225
Optical glass index of refraction218, 219
Optical glass properties217
Optical material infrared transmittance220
Optics209
Output phosphor, image tube180
Ozone absorption82
P-N junction lasers135
P-N junction light sources135
Parametric down-conversion133
Performance characteristics of camera tubes189
Performance data, camera and image tubes207
Permittivity of free space24
Phosphor designations, JEDEC234
Phosphor spectral characteristics233
Phot18
Photocathode cooling158
Photocathode responsivity17
Photoconductive detectors145
Photoconductive lag, camera tube192
Photodetector145
Relationships and definitions146
Spectral response15
Time characteristics167
Time response characteristics168
With internal amplification164, 165
Photodiode noise160
Photoemissive devices145
Temperature effects155
Photoemitter characteristics, near infrared-visible157
Photoemitter characteristics, visible156
Photographic exposure226

Photographic paper	233
Photographing CRT images	236
Electro-optical displays	225
Photometric quantities	9, 15
Photometry units	26
Photomultiplier	145, 146, 164
Time response characteristics	167
Photopic eye response	45
Photopic vision	53
Photovoltaic detectors	145
Physical constants	23, 24
Planck's constant	24
Planck's equation for spectral radiant exitance	35
Planetary spectral irradiance	68
Principal planes, thick lens	212
Principal points, thick lens	212
Probability of detection	110, 202
Probability of recognition	202
Properties of optical glasses	217
Proximity focus image tube	174
Pulse counting	166
Pulse detection in quantum noise	113
Pulse detection in white noise	109
Quantum efficiency	147, 148
Quantum efficiency of eye	200
Quantum noise	109
Radiance	10
Radiant density	10
Emittance	10
Energy	10
Exitance	10
Flux	10
Intensity	10
Radiation conversion chart	13
Equation constants	37
Sources	61
Radiometric quantities	9, 12
Radiometry units	26
Rayleigh scattering	82
Receptors of the human eye	45
Recognition	109
Parameters	202
Probability	202
Statistics	197

Reflectance	12
Relationship between quanta and radiant flux units	147
Relative spectral luminous efficiency	54
Resolution	109
Resolution characteristics, camera tubes	205
Image tubes and camera tubes	205
Image tubes	176
Resolving power of lens	215
Responsivity	147, 148
Camera tube	185
Retinal receptors	45
Retroreflector characteristics, commercial	224
Retroreflectors	217
Reversal processing, black and white film	230
Rise time, anode pulse	169
Rod vision	45
Rods	45
S/N (signal-to-noise ratio)	150
S/N camera tube	190
Saturation	48, 51
Scotopic vision	53
Scotopic eye response	45
SEC camera tube	183
Second generation image tube	175
Second harmonic generation	133
Second radiation constant (hc/k)	24
Secondary electron conduction camera tube	183
Sensitometry	225
Sensor limitations	199
SH-CC laser (single heterojunction, close confined)	137, 143
SI units9
Signal current	148
Signal response	147
Signal-to-noise ratio	147, 150
Camera tube	190
Silicon intensifier target camera tube	183
Silicon photovoltaic cells	146
Sine-wave spatial frequency amplitude response	114
Single-heterojunction close-confined (SH-CC)	138, 143
SIT camera tube	183
Sky illuminance	68
Light spectral distribution	7 1
Luminance	70
Solar illuminance	61, 63
Solar irradiance	6 1

Solid state:	
Devices, far infrared spectral response	.156
Imager	.184
Photodetectors	.146
Photodetector time response characteristics	.168
Source-detector matching	.170
Sources of radiation	61
Specific detectivity (D^*)	147, 151, 159
Crystal detectors	.162
Thin-film detectors	.161
Variation with frequency	.159
Variation with temperature	.159
Vs frequency	.163
Vs temperature	.163
Specific spectral detectivity	.151
Spectral characteristics, film	.233
Phosphor	.233
Spectral irradiance	11
Spectral luminous efficacy	53
Spectral luminous efficiency	16, 53
Spectral radiance	11
Spectral radiant exitance	11, 35
Spectral radiant flux	11
Spectral radiant intensity	11
Spectral response:	
CdS and CdSe cells	.159
Designations and characteristics	.153
Far infrared	.156
Image tube	.180
Near-infrared	.151
P-I-N silicon and germanium photodetectors	.159
Photoconductive cells	.159
Photodetectors	.151
Photovoltaic cells	.159
Se and n-on-p silicon cells	.159
UV-visible	.151
Visible and near-infrared	.155
Visible light	.151
Spectral responsivity	.151
Of eye	46
Spectral transmittance, materials	.217
Window materials	.220
Spectroradiometric quantities	11
Speed:	
ASA	.229
Color reversal film	230, 232

(Continued on page 254)

Speed: (Continued)	
Film	229
Lens	211
Light	24
Spherical aberration	212
Square-wave spatial frequency amplitude response	114
SS devices, visible and near-infrared spectral response	155
Standard color mixture curves	50, 51
Standard unit symbols	26
Star illuminance	65
Stefan-Boltzmann constant	24
Stellar illuminance	65, 66
Stellar spectral irradiance	67, 69
Stilb	19, 20
Sun's irradiance	61
Sun's spectral radiance	62
Symbols	23
T/number	211
Talbot	16
Target detection	121
Detection/recognition model	121
Recognition	121
Television camera tube	180
Thermal noise	166
Thick-lens characteristics	212
Thin-lens characteristics	209
Formulae	209, 210
Types	210
Thin lenses in contact	211
Threshold detection process	110
Threshold of human eye response	46
Time constant of eye	199
Time response characteristics, photomultiplier	167
Time response characteristics, solid-state photodetector	168
Trade names, camera tubes	186
Transfer characteristic camera tube	185, 190
Transference (T)	94
Transference factor (τ_c)	101
Transmittance	12
Film	225
Optical material, infrared	220
Through gaseous atmosphere	81
Trichromatic response theory of human eye	47
Tungsten lamp	78
Standard	19

TV camera tube	180
Typical electroluminescent systems	141
Typical lamp parameters	76
UV-visible photoemitter characteristics	155
UV-visible spectral response for photoemissive devices	151
Vacuum photodiodes	145
Vidicon	180
Visible and near-infrared response, solid-state devices	155
Visible light spectral response for photoemissive devices	151
Visual search time	121
Wafer-design image tube	176
Wavelength	10
Wavelength of maximum spectral power	36
White noise	109
Wien's displacement law	36
Window material spectral transmittance	2 17, 220
Xenon short arc lamp	77
Zirconium concentrated-arc lamp	77
Zodiacal irradiance	71
Zodiacal light	67